

**Highly Accelerated Cardiovascular Magnetic  
Resonance Myocardial Perfusion Imaging**

**Studies in Spatial Resolution, Spatial Coverage and Cardiac Phase**

Manish Motwani

Submitted in accordance with the requirements for the degree of

Doctor of Philosophy (PhD)

The University of Leeds

Faculty of Medicine and Health

Leeds Institute of Genetics, Health and Therapeutics

December 2015

## **Intellectual Property and Publication Statements**

The candidate confirms that the work submitted is his/her own, except where work which has formed part of jointly-authored publications has been included. The contribution of the candidate and the other authors to this work has been explicitly indicated below. The candidate confirms that appropriate credit has been given within the thesis where reference has been made to the work of others.

This copy has been supplied on the understanding that it is copyright material and that no quotation from the thesis may be published without proper acknowledgement.

The right of Manish Motwani to be identified as Author of this work has been asserted by him in accordance with the Copyright, Designs and Patents Act 1988.

© 2014 The University of Leeds and Dr. Manish Motwani

## Chapter 1

Chapter 1 has been modified from the following peer-reviewed publications:

***i) Accelerated, high spatial resolution cardiovascular magnetic resonance myocardial perfusion imaging. Motwani M, Lockie T, Greenwood JP, Plein S. J Nucl Cardiol. 2011;18(5):952-8.***

Author contributions: MM - primary authorship, drafting and revision of manuscript; TL - critical review and revision of manuscript; JPG - critical review and revision of manuscript; SP - critical review and revision of manuscript.

***ii) Advances in cardiovascular magnetic resonance in ischaemic heart disease and non-ischaemic cardiomyopathies. Motwani M, Kidambi A, Greenwood JP, Plein S. Heart. 2014;100(21):1722-33***

Author contributions: MM - primary authorship, manuscript preparation and revision of manuscript; AK - manuscript preparation and revision; JPG - critical review and revision of manuscript; SP - critical review and revision of manuscript.

***iii) Advanced cardiovascular magnetic resonance myocardial perfusion imaging: high-spatial resolution versus 3-dimensional whole-heart coverage. Motwani M, Jogiya R, Kozerke S, Greenwood JP, Plein S. Circ Cardiovasc Imaging. 2013;6(2):339-48***

Author contributions: MM - primary authorship, review proposal, patient recruitment and manuscript preparation; RJ - critical review and revision of manuscript; SK - technical support, critical review and revision of manuscript; JPG -

critical review and revision of manuscript; SP - critical review and revision of manuscript

## **Chapter 2**

Chapter 2 has been peer-reviewed and published as below:

***High-resolution versus standard-resolution cardiovascular MR myocardial perfusion imaging for the detection of coronary artery disease. Motwani M, Maredia N, Fairbairn TA, Kozerke S, Radjenovic A, Greenwood JP, Plein S. Circ Cardiovasc Imaging. 2012;5(3):306-13.***

Author contributions: MM - primary authorship, study design, patient recruitment, data-collection, data analysis and manuscript preparation. NM - patient recruitment and revision of manuscript; TAF - patient recruitment and revision of manuscript; SK – technical support; AR - critical review and revision of manuscript; JPG - study design, critical review and revision of manuscript; SP - study design, critical review and revision of manuscript.

## **Chapter 3**

Chapter 3 has been peer-reviewed and published as below:

***Assessment of ischemic burden in angiographic three-vessel coronary artery disease with high-resolution myocardial perfusion cardiovascular magnetic resonance imaging. Motwani M, Maredia N, Fairbairn TA, Kozerke S, Greenwood JP, Plein S. Eur Heart J Cardiovasc Imaging. 2014;15(6):701-8***

Author contributions: MM - primary authorship, study design, patient recruitment, data-collection, data analysis and manuscript preparation. NM - study design, patient recruitment and revision of manuscript; TAF - patient recruitment and revision of manuscript; SK - technical support; JPG - study design, critical review and revision of manuscript; SP - study design, critical review and revision of manuscript.

## **Chapter 4**

Chapter 4 has been peer-reviewed and published as below:

***Three-Dimensional versus High-Resolution Perfusion CMR – A Pilot Study***

***Comparing Myocardial Ischemic Burden Estimates. McDiarmid A, Ripley DP,***

***Mohee K, Kozerke S, Greenwood JP, Plein S, Motwani M. Eur Heart J Cardiovasc***

***Imaging. 2015 Oct 7. pii: jev231. [Epub ahead of print]***

Authors' contributions: AKM - acquisition, analysis and interpretation of data, drafting of manuscript DR: acquisition, analysis and interpretation of data, critical and intellectual revision of manuscript; KM - acquisition and analysis of data, critical and intellectual revision of manuscript; SK - technical support, critical and intellectual revision of manuscript; JPG - interpretation of data, critical and intellectual revision of manuscript; SP - conception and design, interpretation of data, critical and intellectual revision of manuscript; MM - conception and design, acquisition, analysis and interpretation of data, drafting of manuscript, critical and intellectual revision of manuscript. All authors read and approved the final manuscript.

## Chapter 5

Chapter 5 has been peer-reviewed and published as below:

***Systolic versus diastolic acquisition in myocardial perfusion MR imaging. Motwani M, Fairbairn TA, Larghat A, Mather AN, Biglands JD, Radjenovic A, Greenwood JP, Plein S. Radiology. 2012;262(3):816-23.***

Author contributions: MM - primary authorship, study design, patient recruitment, data-collection, data analysis, manuscript preparation and revision. TAF - patient recruitment, critical review and manuscript revision; AL - technical support; ANM - patient recruitment, critical review and manuscript revision; JB - technical support and critical review of manuscript; AR - study design, technical support, critical review and manuscript revision; JPG - study design, critical review and manuscript revision; SP - study design, critical review and manuscript revision.

## Chapter 6

Chapter 6 has been peer-reviewed and published as below:

***Quantitative three-dimensional cardiovascular magnetic resonance myocardial perfusion imaging in systole and diastole. Motwani M, Kidambi A, Sourbron S, Fairbairn TA, Uddin A, Kozerke S, Greenwood JP, Plein S. J Cardiovasc Magn Reson. 2014;16:19***

Author contributions: MM - primary authorship, study design, patient recruitment, data-collection, data analysis, manuscript preparation and revision; AK - data analysis, critical review and manuscript revision; SS - technical support, critical

review and manuscript revision; TAF - critical review and manuscript revision; AU - patient recruitment, critical review and manuscript revision; SK - technical support and critical review of manuscript; JPG - study design, critical review and manuscript revision; SP - study design, critical review and manuscript revision.

## **Chapter 7**

Chapter 7 has been peer-reviewed and published as below:

***Quantification of Myocardial Blood Flow with Cardiovascular Magnetic Resonance throughout the Cardiac Cycle. Motwani M, Kidambi A, Uddin A, Sourbron S, Greenwood JP, Plein S. J Cardiovasc Magn Reson. 2015;17:4***

Author contributions: MM - primary authorship, study design, patient recruitment, data-collection, data analysis, manuscript preparation and revision; AK - data analysis, critical review and manuscript revision; AU - patient recruitment, critical review and manuscript revision; SS - technical support, critical review and manuscript revision; JPG - critical review and manuscript revision; SP - study design, critical review and manuscript revision.

## Publications arising from this work

### Papers

1. McDiarmid AK, Ripley DP, Mohee K, Kozerke S, Greenwood JP, Plein S, **Motwani M**. Three-dimensional whole-heart vs. two-dimensional high-resolution perfusion-CMR: a pilot study comparing myocardial ischaemic burden. *Eur Heart J Cardiovasc Imaging*. 2015 Oct 7. pii: jev231. [Epub ahead of print]
2. **Motwani M**, Kidambi A, Uddin A, Sourbron S, Greenwood JP, Plein S. Quantification of myocardial blood flow with cardiovascular magnetic resonance throughout the cardiac cycle. *J Cardiovasc Magn Reson*. 2015;29;17:4
3. **Motwani M**, Kidambi A, Greenwood JP, Plein S. Advances in cardiovascular magnetic resonance in ischaemic heart disease and non-ischaemic cardiomyopathies. *Heart*. 2014; 100:1722-33
4. **Motwani M**, Kidambi A, Sourbron S, Fairbairn TA, Uddin A, Kozerke S, Greenwood JP, Plein S. Quantitative three-dimensional cardiovascular magnetic resonance myocardial perfusion imaging in systole and diastole. *J Cardiovasc Magn Reson*. 2014; 16:19.
5. **Motwani M**, Maredia N, Fairbairn TA, Kozerke S, Greenwood JP, Plein S. Assessment of ischaemic burden in angiographic three-vessel coronary artery disease with high-resolution myocardial perfusion cardiovascular magnetic resonance imaging. *Eur Heart J Cardiovasc Imaging*. 2014; 15:701-8

6. **Motwani M**, Jogiya R, Kozerke S, Greenwood JP, Plein S. Advanced cardiovascular magnetic resonance myocardial perfusion imaging: high-spatial resolution versus 3-dimensional whole-heart coverage. *Circ Cardiovasc Imaging*. 2013; 6:339-48.
7. **Motwani M**, Maredia N, Fairbairn TA, Kozerke S, Radjenovic A, Greenwood JP, Plein S. High-Resolution Versus Standard-Resolution Cardiovascular Magnetic Resonance Myocardial Perfusion Imaging for the Detection of Coronary Artery Disease. *Circ Cardiovasc Imaging*. 2012; 5:306-13.
8. **Motwani M**, Fairbairn TA, Larghat A, Mather AN, Biglands JD. Systolic Versus Diastolic Acquisition in Myocardial Perfusion MR Imaging. *Radiology*. 2012; 262:816-23.
9. **Motwani M**, Lockie T, Greenwood JP, Plein S. Accelerated, high spatial resolution cardiovascular magnetic resonance myocardial perfusion imaging. *J Nucl Cardiol*. 2011; 18:952-8.

## **Abstracts**

1. **Motwani M**, Dobson L, Smith C, Maredia N, Sourbron S, Biglands J, Plein S, Greenwood J. Regional variation in myocardial blood flow in patients with left bundle branch block evaluated with quantitative perfusion CMR. *J Cardiovasc Magn Reson*. 2013; 15:P205.
2. Manka R, Gebker R, Wissmann L, Jogiya R, **Motwani M**, Frick M, Reinartz S, Schnackenburg B, Nagel E, Plein S, Kozerke S. Multicenter evaluation of dynamic three-dimensional whole-heart myocardial perfusion imaging for the

- detection of coronary artery disease defined by fractional flow reserve. *J Cardiovasc Magn Reson*. 2013; 15:O103.
3. **Motwani** M, Kidambi A, Fairbairn T, Uddin A, Kozerke S, Sourbron S, Greenwood J, Plein S. Quantitative whole-heart three-dimensional magnetic resonance myocardial perfusion imaging in systole and diastole at 3.0T. *J Cardiovasc Magn Reson*. 2013; 15:P206.
  4. **Motwani M**, Dobson L, Smith C, Maredia N, Sourbron S, Biglands JD, Plein S, Greenwood JP. 089 Regional Variation in Myocardial Blood Flow in Patients with Left Bundle Branch Block: A Quantitative Perfusion CMR Study. *Heart*. 2013; 99:A55-A56.
  5. **Motwani M**, Kidambi A, Sourbron S, Fairbairn TA, Uddin A, Kozerke S, Greenwood JP, Plein S. 091 Quantitative Three-Dimensional Cardiovascular Magnetic Resonance Myocardial Perfusion Imaging In Systole And Diastole at 3.0 T. *Heart*. 2013; 99:A56-A57.
  6. **Motwani** M, Fairbairn T, Larghat A, Mather A, Biglands J, Radjenovic A, Greenwood J, Plein S. Systolic versus diastolic myocardial blood flow in patients with suspected coronary artery disease - a cardiovascular magnetic resonance study. *J Cardiovasc Magn Reson*. 2012; 14:P17.
  10. **Motwani** M, Maredia N, Fairbairn T, Kozerke S, Radjenovic A, Greenwood J, Plein S. High-resolution versus standard-resolution cardiovascular magnetic resonance perfusion imaging for the detection of coronary artery disease. *J Cardiovasc Magn Reson*. 2012; 14:O89.

11. **Motwani** M, Fairbairn TA, Larghat A, Mather AN, Biglands JD, Radjenovic A, Greenwood JP, Plein S. 085 Systolic vs diastolic acquisition in cardiovascular magnetic resonance myocardial perfusion imaging. *Heart*. 2012; 98:A48-A49.
12. **Motwani** M, Fairbairn TA, Maredia N, Kozerke S, Greenwood JP, Plein S. 086 Assessment of ischaemic burden in patients with three-vessel coronary artery disease using high-resolution myocardial perfusion cardiovascular MRI. *Heart*. 2012; 98:A49-A49.
13. **Motwani** M, Fairbairn TA, Maredia N, Kozerke S, Greenwood JP, Plein S. Abstract 11418: Incremental Value of High-Resolution Myocardial Perfusion Cardiovascular Magnetic Resonance Imaging in Patients with Three-Vessel Coronary Artery Disease. *Circulation*. 2011; 124:A11418.

## **Acknowledgements**

I am greatly indebted to my supervisors, Professor Sven Plein and Professor John Greenwood for their support, encouragement and teaching. Without their ideas, enthusiasm and assistance this project would not exist.

The CMR department at Leeds is a team of dedicated professionals. They provided the environment and guidance to succeed, and I am grateful to them all for their individual contributions. Specifically, I thank Petra and Fiona for their tireless assistance with patient recruitment. Petra deserves an additional mention for her assistance with ethics approval submissions, as well as her ability to instil organisation into the occasional chaos. I thank Gavin, Margaret and Caroline for their scanning and technical expertise - and thank Gavin again for his frequent percolation of coffee. I am also grateful to my co-fellows: Tim, Ananth, Akki, Bernhard, Neil, Dave and Adam for their good-spirited, positive and friendly approach to team work.

Most importantly, I am truly grateful to the patients of West Yorkshire for their willingness to participate in research studies despite their ongoing ailments and the required time commitment. Without their goodwill, this thesis would not have been possible.

Final acknowledgements go to my parents for their endless support and encouragement.

## **Abstract**

### **Background**

Myocardial perfusion imaging with cardiovascular magnetic resonance (CMR) is bound by spatio-temporal constraints. Standard perfusion CMR techniques permit the acquisition of 3-4 myocardial slices with a spatial resolution of 2-3mm. However, acceleration techniques can be applied to achieve higher spatial resolution (<2mm) or 3-dimensional (3D) acquisitions with increased spatial coverage (12-16 slices). Acceleration can also be used to simultaneously acquire perfusion data at different time-points in the cardiac cycle. Accordingly, this thesis includes studies that modify the standard approach to perfusion CMR in order to investigate the impact of spatial resolution, spatial coverage and cardiac phase of acquisition.

### **Methods and Results**

Study 1 and 2 compared high-resolution and standard-resolution perfusion CMR in patients with suspected coronary artery disease (CAD). Study 1 found high-resolution acquisition had greater diagnostic accuracy compared to standard-resolution for detecting CAD (area under curve [AUC]: 0.93 vs. 0.83;  $p < 0.001$ ); and study 2 found it also had greater diagnostic accuracy for specifically identifying 3-vessel CAD (AUC: 0.90 vs. 0.69;  $p < 0.0001$ ). Study 3 compared high-resolution and 3D perfusion CMR in patients with CAD and found limited agreement between myocardial ischaemic burden estimates (95% limits of agreement: -8.68%, 9.82%). Study 4 and 5 compared systolic and diastolic acquisitions using standard perfusion CMR (limited to 1 slice) and 3D perfusion CMR respectively. Both studies found

higher estimates of myocardial blood flow (MBF) in diastole compared to systole at stress ( $p < 0.05$ ). Study 6 utilised accelerated perfusion CMR to compare MBF estimates at 5 different time-points in the cardiac cycle in healthy volunteers. Estimates of stress MBF peaked at end-diastole and fell steadily to end-systole ( $p < 0.0001$ ).

## **Conclusion**

By altering the spatial resolution, spatial coverage and cardiac phase of acquisition of perfusion CMR, we have gained valuable insights into the relative impact of these parameters on both qualitative and quantitative assessment of ischaemia.

# Table of Contents

<b>Intellectual Property and Publication Statements .....</b>	<b>2</b>
<b>Publications arising from this work .....</b>	<b>8</b>
<b>Acknowledgements .....</b>	<b>12</b>
<b>Abstract.....</b>	<b>13</b>
<b>Table of Contents.....</b>	<b>15</b>
<b>List of Figures.....</b>	<b>22</b>
<b>Abbreviations .....</b>	<b>27</b>
<b>1 Introduction .....</b>	<b>29</b>
1.1 Background.....	29
1.2 Perfusion CMR .....	30
1.2.1 Myocardial Ischaemia .....	30
1.2.2 Perfusion CMR Technique .....	31
1.2.3 Clinical Validation of Perfusion CMR .....	32
1.2.4 Challenges of Perfusion CMR.....	36
1.3 Basic Principles of MRI.....	37
1.4 Acceleration Techniques.....	39
1.4.1 Basic Acceleration Methods .....	40
1.4.2 Advanced Acceleration Methods.....	43
1.5 High-resolution Perfusion CMR .....	46
1.6 Three-Dimensional Perfusion CMR.....	53
1.7 Limitations of Highly Accelerated Perfusion CMR .....	59
1.8 High Spatial Resolution or Full Cardiac Coverage? .....	60
1.9 Other Advances in Perfusion CMR.....	67
1.9.1 Perfusion CMR at 3-Tesla.....	67

1.9.2	Quantitative Perfusion CMR .....	68
1.10	Implications of Cardiac Phase on Perfusion CMR.....	69
1.11	Aims of Thesis .....	71
<b>2</b>	<b>Study 1 - High-resolution Versus Standard-resolution Perfusion CMR for the Detection of Coronary Artery Disease .....</b>	<b>73</b>
2.1	Abstract.....	73
2.2	Introduction .....	75
2.3	Methods.....	76
2.3.1	Population.....	76
2.3.2	CMR protocol .....	76
2.3.3	CMR analysis.....	78
2.3.4	Quantitative coronary angiography.....	79
2.3.5	Statistical analysis .....	79
2.4	Results.....	80
2.4.1	Study population.....	80
2.4.2	Detection of CAD .....	82
2.4.3	Detection of anatomic location of CAD .....	85
2.4.4	Subendocardial ischaemia .....	86
2.4.5	Image quality .....	86
2.5	Discussion .....	87
2.6	Study limitations .....	91
2.7	Conclusions .....	93
<b>3</b>	<b>Study 2 - Assessment of Myocardial Ischaemic Burden in Angiographic Three-Vessel Coronary Artery Disease Using High-Resolution Perfusion CMR .....</b>	<b>94</b>
3.1	Abstract.....	94

- 3.2 Introduction ..... 96
- 3.3 Methods..... 97
  - 3.3.1 Study population..... 97
  - 3.3.2 CMR protocol ..... 98
  - 3.3.3 CMR analysis ..... 99
  - 3.3.4 Quantitative coronary angiography..... 101
  - 3.3.5 Statistical analysis ..... 102
- 3.4 Results..... 104
  - 3.4.1 Study population..... 104
  - 3.4.2 Image quality and artefacts ..... 104
  - 3.4.3 Detection of 3VD pattern ..... 105
  - 3.4.4 Detection of CAD in each territory ..... 105
  - 3.4.5 Detection of subendocardial ischaemia ..... 107
  - 3.4.6 Detection of ischaemic burden..... 108
- 3.5 Discussion ..... 111
  - 3.5.1 Detection of subendocardial ischaemia ..... 112
  - 3.5.2 Detection of 3VD pattern ..... 113
  - 3.5.3 Estimation of ischaemic burden ..... 115
- 3.6 Study Limitations ..... 116
- 3.7 Conclusions ..... 118
- 4 Study 3 - Three-Dimensional versus High-Resolution Perfusion CMR: A Pilot Study Comparing Myocardial Ischaemic Burden Estimates ..... 119**
  - 4.1 Abstract..... 119
  - 4.2 Introduction ..... 121
  - 4.3 Methods..... 122
    - 4.3.1 Patient Population ..... 122

4.3.2	CMR Protocol.....	122
4.3.3	CMR Analysis.....	124
4.3.4	Quantitative coronary angiography.....	126
4.3.5	Statistical Analysis.....	126
4.4	Results.....	128
4.4.1	Study population.....	128
4.4.2	Diagnostic Confidence and Image Quality.....	128
4.4.3	Total Perfusion Defect .....	130
4.4.4	Myocardial Ischaemic Burden .....	130
4.4.5	Reproducibility.....	131
4.5	Discussion .....	135
4.5.1	Study Limitations .....	139
4.6	Conclusion.....	140
<b>5</b>	<b>Study 4 - Systolic versus Diastolic Acquisition in Myocardial Perfusion Imaging with CMR .....</b>	<b>141</b>
5.1	Abstract.....	141
5.2	Introduction .....	143
5.3	Methods.....	144
5.3.1	Study Population.....	144
5.3.2	CMR Imaging.....	144
5.3.3	Image Quality.....	145
5.3.4	Quantitative Image Analysis .....	146
5.3.5	Coronary Angiography Analysis .....	146
5.3.6	Statistical Analysis.....	147
5.4	Results.....	148
5.4.1	Study Population.....	148

- 5.4.2 Image Quality..... 151
- 5.4.3 Quantitative Image Analysis ..... 152
- 5.4.4 Diagnostic Performance..... 153
- 5.4.5 Intra-observer and Inter-observer Variability..... 156
- 5.5 Discussion ..... 156
- 5.6 Limitations ..... 159
- 5.7 Conclusion..... 160
  
- 6 Study 5 - Quantitative Three-Dimensional Perfusion CMR in Systole and Diastole..... 162**
- 6.1 Abstract..... 162
- 6.2 Background..... 164
- 6.3 Methods..... 165
  - 6.3.1 Population..... 165
  - 6.3.2 CMR protocol..... 165
  - 6.3.3 Image quality ..... 167
  - 6.3.4 Myocardial blood flow estimation..... 168
  - 6.3.5 Quantitative coronary angiography..... 169
  - 6.3.6 Statistical analysis ..... 169
- 6.4 Results..... 170
  - 6.4.1 Study population..... 170
  - 6.4.2 Image quality ..... 173
  - 6.4.3 Myocardial blood flow estimation..... 173
  - 6.4.4 Diagnostic performance ..... 176
  - 6.4.5 Reproducibility..... 181
- 6.5 Discussion ..... 181
- 6.6 Study Limitations ..... 186

6.7	Conclusions.....	187
<b>7</b>	<b>Study 6 - Quantification of Myocardial Blood Flow with Cardiovascular Magnetic Resonance throughout the Cardiac Cycle .....</b>	<b>188</b>
7.1	Abstract.....	188
7.2	Introduction .....	190
7.3	Methods.....	191
7.3.1	Study Population.....	191
7.3.2	CMR protocol .....	192
7.3.3	MBF estimation.....	194
7.3.4	Statistical analysis .....	195
7.4	Results.....	196
7.4.1	Study population.....	196
7.4.2	Myocardial blood flow estimation.....	197
7.5	Discussion .....	203
7.6	Study Limitations .....	207
7.7	Conclusions.....	208
<b>8</b>	<b>Final Conclusions .....</b>	<b>209</b>
8.1	Spatial Resolution .....	210
8.2	Spatial coverage.....	210
8.3	Cardiac Phase.....	211
<b>9</b>	<b>References .....</b>	<b>212</b>
<b>10</b>	<b>Appendix.....</b>	<b>230</b>
10.1	Ethics Approval Form: Study 1 and 2.....	230
10.2	Ethics Approval Form: Study 3.....	232
10.3	Ethics Approval Form: Study 4 and 6.....	235

10.4 Ethics Approval Form: Study 5..... 238

## List of Figures

<b>Figure 1.1</b> CMR Techniques .....	30
<b>Figure 1.2</b> k-t acceleration techniques .....	45
<b>Figure 1.3</b> Dark Rim Artefact: Standard-resolution vs. High-resolution.....	46
<b>Figure 1.4</b> Dark Rim Artefact.....	48
<b>Figure 1.5</b> Standard-resolution vs. high-resolution stress perfusion CMR.....	49
<b>Figure 1.6</b> High-resolution Perfusion CMR in Multi-vessel CAD.....	51
<b>Figure 1.7</b> Example of 3D Perfusion CMR .....	53
<b>Figure 1.8</b> Pulse Sequence Diagrams for 2D and 3D Perfusion CMR.....	55
<b>Figure 1.9</b> MIB Quantification with 3D Perfusion CMR .....	58
<b>Figure 1.10</b> 3D versus High-resolution Perfusion CMR - Case 1 .....	63
<b>Figure 1.11</b> 3D versus High-resolution Perfusion CMR - Case 2 .....	64
<b>Figure 1.12</b> 3D versus High-resolution Perfusion CMR - Case 3 .....	65
<b>Figure 1.13</b> 3D versus High-resolution Perfusion CMR - Case 4.....	66
<b>Figure 2.1</b> Case Example: Standard vs. High-Resolution Perfusion CMR .....	83
<b>Figure 2.2</b> ROC Curves: Standard-resolution vs High-resolution Perfusion CMR.....	84
<b>Figure 2.3</b> Distribution of Transmural Ischaemia Index.....	87
<b>Figure 3.1</b> Case Example: Standard vs. High-resolution Perfusion CMR .....	101
<b>Figure 3.2</b> Distribution of Ischaemia Detected by Perfusion CMR .....	106

<b>Figure 3.3</b> Distribution of Transmural Ischaemia Index.....	108
<b>Figure 3.4</b> MIB: Standard-resolution vs High-resolution Perfusion CMR .....	110
<b>Figure 3.5</b> Diagnostic accuracy of MIB to detect 3VD .....	111
<b>Figure 4.1</b> 3D versus High-resolution Perfusion CMR – Case 5 .....	127
<b>Figure 4.2</b> TPD (%): 2D High-resolution vs. 3D Perfusion CMR.....	132
<b>Figure 4.3</b> Correlation between High-resolution and 3D estimates of MIB .....	133
<b>Figure 4.4</b> MIB (%): 2D High-resolution vs. 3D Perfusion CMR .....	134
<b>Figure 5.1</b> Case Example: Systolic vs. Diastolic Acquisition.....	150
<b>Figure 5.2</b> Dark rim artefact: Systole vs Diastole .....	151
<b>Figure 5.3</b> MPR: Systole versus Diastole.....	153
<b>Figure 5.4</b> MPR for CAD detection - Systolic and Diastolic Boxplots.....	154
<b>Figure 5.5</b> ROC curve of quantitative perfusion CMR using MPR. ....	155
<b>Figure 6.1</b> 3D Acquisition Planning for Systole and Diastole.....	167
<b>Figure 6.2</b> Case Example: 3D-Perfusion CMR in Systole and Diastole.....	172
<b>Figure 6.3</b> Diagnostic Accuracy of Quantitative 3D-Perfusion CMR.....	178
<b>Figure 6.4</b> Myocardial Perfusion Reserve Threshold .....	179
<b>Figure 6.5</b> Diastolic/Systolic Stress Myocardial Blood Flow Ratio .....	180
<b>Figure 7.1</b> Quantitative Perfusion CMR throughout the Cardiac Cycle .....	193
<b>Figure 7.2</b> Cyclic Variation in Stress MBF .....	199
<b>Figure 7.3</b> Cyclic Variation in MPR .....	200

**Figure 7.4** Individual Stress MBF estimates in Healthy Volunteers ..... 201

**Figure 7.5** Correlation between MCV and Peak Heart Rate at Stress ..... 202

## List of Tables

<b>Table 1-1</b> Large Scale Clinical Validation of Perfusion CMR .....	34
<b>Table 1-2</b> ESC and AHA Recommendations for Perfusion CMR in Stable CAD.....	35
<b>Table 1-3</b> Diagnostic Performance of Advanced Perfusion CMR .....	52
<b>Table 1-4</b> Relative Merits of High-Resolution and 3D Perfusion CMR.....	62
<b>Table 2-1</b> Patient Characteristics .....	81
<b>Table 2-2</b> Diagnostic Accuracy of Standard-resolution and High-resolution perfusion CMR for the Detection of CAD .....	84
<b>Table 2-3</b> Sensitivity, Specificity and Predictive values for Standard-resolution and High-resolution perfusion CMR for the detection of CAD .....	85
<b>Table 3-1</b> Patient Clinical Characteristics.....	103
<b>Table 3-2</b> Diagnostic Performance of Perfusion CMR in Each Territory in Patients with 3VD.....	107
<b>Table 3-3</b> Ischaemic Burden Using Perfusion CMR in Patients with 3VD.....	109
<b>Table 4-1</b> Patient Characteristics .....	128
<b>Table 5-1</b> Baseline Patient Characteristics.....	149
<b>Table 5-2</b> Coronary Angiography Findings.....	150
<b>Table 5-3</b> Diagnostic Performance of Perfusion CMR: Systole vs. Diastole .....	156
<b>Table 6-1</b> Patient Characteristics .....	171

<b>Table 6-2</b> Estimates of MBF and MPR from 3-Dimensional Perfusion CMR - Per Patient Analysis .....	174
<b>Table 6-3</b> Estimates of MBF and MPR from 3-Dimensional Perfusion CMR - Per Territory Analysis .....	174
<b>Table 6-4</b> Regional Estimates of MBF and MPR - Per Territory .....	175
<b>Table 6-5</b> Comparison of Regional MBF and MPR Estimates – in Normal Patients .....	176
<b>Table 6-6</b> Diagnostic Accuracy of Quantitative 3D-perfusion CMR – Per Territory .....	179
<b>Table 7-1</b> Healthy Volunteer Demographics.....	196
<b>Table 7-2</b> Estimates of MBF and MPR throughout the Cardiac Cycle .....	198

## Abbreviations

AHA = American Heart Association

AIF = arterial input function

AUC = area under curve

BLAST = broad linear acquisition speed-up technique

CABG = coronary artery bypass grafting

CAD = coronary artery disease

CMR = cardiovascular magnetic resonance

CoV = coefficient of variation

CT = computed tomography

EPI = echo planar imaging

ESC = European Society of Cardiology

FFR = fractional flow reserve

FOV = field of view

$k-t$  =  $k$ -space and time

LAD – left anterior descending

LCX = left circumflex

LGE= late-gadolinium enhancement

LV = left ventricle

LVEF = left ventricular ejection fraction

LVEDV = left ventricular end-diastolic volume

LVESV = left ventricular end-systolic volume

MBF = myocardial blood flow

MCV = maximal cyclic variation

MI = myocardial infarction

MIB = myocardial ischaemic burden

MPR = myocardial perfusion reserve

MRI = magnetic resonance imaging

PET = positron emission tomography

PCA = principal component analysis

PCI = percutaneous coronary intervention

QCA = quantitative coronary angiography

RCA = right coronary artery

ROC = receiver operating characteristic

ROI = region of interest

SENSE = sensitivity encoding

SPECT = single photon emission computed tomography

SNR = signal to noise ratio

SSFP = steady state free precession

T = Tesla

TE = Echo Time

TR = Repetition Time

2D = 2-dimensional

3D = 3-dimensional

1VD = 1-vessel coronary artery disease

2VD = 2-vessel coronary artery disease

# 1 Introduction

## 1.1 Background

Coronary artery disease (CAD) is a leading cause of death and disability worldwide. In the United Kingdom (UK) alone there are an estimated 2 million people with angina costing the UK economy £9.0 billion/year (British Heart Foundation, 2010). National and international guidelines recommend a variety of investigative strategies in those presenting with chest pain to inform diagnosis, risk stratify and determine the need for revascularisation (Fihn et al., 2012; Montalescot et al., 2013). These may involve anatomical imaging of the coronary arterial tree with computed tomography (CT) or invasive X-ray coronary angiography; or assessment for functionally significant coronary artery stenosis with single photon emission computed tomography (SPECT), positron emission tomography (PET), stress echocardiography or cardiovascular magnetic resonance (CMR).

CMR produces high resolution images which can be acquired in any plane and allows assessment of global and regional cardiac function, myocardial perfusion, myocardial viability, tissue characterisation and proximal coronary anatomy - all within a single study and without the use of ionising radiation. This unique multi-parametric approach leads to a high diagnostic accuracy for the detection of CAD and the assessment of myocardial ischaemia to guide appropriate therapy (Figure 1.1).

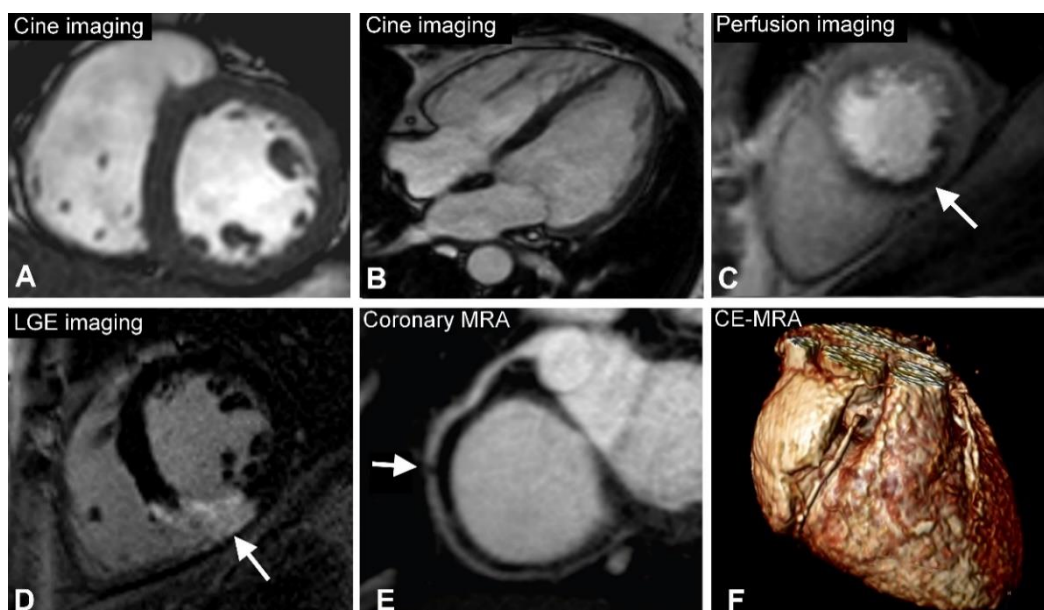


**Figure 1.1 CMR Techniques**

*Panels A and B are cine images (short-axis and 4-chamber views respectively) which give anatomical and functional information. Panel C is a stress perfusion image showing an inferior perfusion defect (white arrow) in the mid-ventricular slice. Panel D is late gadolinium enhancement (LGE) imaging showing inferior wall transmural myocardial infarction (white arrow). Panel E shows coronary magnetic resonance angiography (MRA) demonstrating a mid right coronary artery stenosis. Panel F is an example of three-dimensional volume rendered contrast enhanced MRA showing the right coronary artery.*

## **1.2 Perfusion CMR**

### **1.2.1 Myocardial Ischaemia**

The detection of reversible myocardial ischaemia is a cornerstone in the investigation and treatment of patients with stable CAD. Large scale studies have shown that in the absence of inducible ischaemia, patients with CAD have an excellent prognosis with an adverse event rate of less than 1% per annum (Hachamovitch et al., 2003b; Klocke et al., 2003). Large perfusion defects and defects

in multiple coronary territories, however, suggest a poor prognosis (Iskandrian et al., 1993; Klocke et al., 2003; Hachamovitch et al., 1998). In addition, those with a low burden of ischaemia have been found to gain little benefit from coronary revascularisation compared to optimal medical therapy (Shaw et al., 2008).

### **1.2.2 Perfusion CMR Technique**

The feasibility of myocardial perfusion imaging with CMR was first reported in 1990 and since then the technique has undergone continuous technical development, experimental validation, and clinical evaluation (Atkinson et al., 1990). In contrast to nuclear imaging techniques, perfusion CMR is a *dynamic* contrast technique, which monitors the first-pass of a T1-shortening contrast agent bolus through the myocardium during a hyperaemic state. In territories supplied by significantly stenosed coronary arteries, the dynamic wash-in of contrast media (CM) and thus signal enhancement is diminished. Several different magnetic resonance imaging (MRI) pulse sequences have been used for perfusion CMR, such as spoiled gradient echo, balanced steady state free precession (SSFP) and segmented echo planar imaging (EPI) (Kellman & Arai, 2007; Gebker et al., 2007a). All of these pulse sequences are T1-sensitive and are thus suitable to track the T1-shortening effect of the CM. Importantly, in the multi-centre, multi-vendor MR-IMPACT study, several different pulse sequences were used with similar performance (Schwitter et al., 2008).

The T1-shortening CM agents currently used for perfusion CMR are gadolinium-based and diffuse partly into the extracellular space unlike the potassium analogues used in SPECT imaging that are taken up by perfused myocardium. Hyperaemia is

typically induced with an adenosine infusion via a brachial vein (140mcg/kg/min) over 3 min. During the first-pass, the patient is instructed to hold their breath to eliminate respiratory motion artefacts. Stress induced images can be compared to an acquisition at rest after 10-15 min, when most of the CM has washed out of the myocardium. Although absolute quantification of regional myocardial blood flow is possible, analysis of perfusion images in clinical practice is most commonly qualitative (visual).

Most perfusion CMR studies also include late gadolinium enhancement (LGE) imaging, acquired 10-15 min after the completion of perfusion CMR to detect areas of infarction and provide a morphological assessment of viability. Unlike nuclear techniques, the assessment of scar in CMR is thus not based on a matched stress-rest perfusion defect, but on direct morphological assessment. Provided the transmural extent of infarction on LGE imaging is <50% there remains a good likelihood of contractile recovery after revascularisation with either percutaneous coronary intervention or coronary artery bypass grafting (Gerber, 2008; Kim et al., 2000).

As well as the lack of exposure to ionising radiation, the major advantage of CMR versus SPECT perfusion imaging is considered to be its higher spatial resolution (typically 2-3mm versus 5-10mm), which allows the detection of smaller perfusion defects and the recognition of subendocardial ischaemia (Panting et al., 2002).

### **1.2.3 Clinical Validation of Perfusion CMR**

The use of perfusion CMR as a first line diagnostic tool in patients with suspected CAD has been the subject of several recent clinical studies and meta-analyses

(Greenwood et al., 2012; Schwitter et al., 2013; Jaarsma et al., 2012; Hamon et al., 2010). The most recent meta-analysis of 37 studies demonstrated a pooled sensitivity of 89% (95%CI: 88%-91%) and pooled specificity of 76% (95%CI: 73%-78%) of CMR for the detection of angiographically-defined IHD (Jaarsma et al., 2012). In the large single centre CE-MARC study (n=752), CMR had higher sensitivity (87% vs. 67%,  $p<0.0001$ ), similar specificity (83% vs. 83%  $p=0.916$ ) and greater overall diagnostic accuracy (area under curve [AUC]:0.89 vs. 0.74,  $p<0.0001$ ) compared with SPECT (Greenwood et al., 2012). The subsequent multi-centre, multi-vendor MR-IMPACT II trial also confirmed a greater overall diagnostic accuracy for CMR compared to SPECT (AUC: 0.75 vs. 0.6,  $p=0.018$ ) with a higher sensitivity, but lower specificity (Table 1.1) (Schwitter et al., 2013, 2012). Health economic analyses have demonstrated that diagnostic pathways integrating stress perfusion CMR can be more cost effective than other strategies including the most common practice of exercise treadmill testing (ETT) (Walker et al., 2013). In addition, the prognostic value of a negative stress CMR (perfusion or dobutamine) has been further confirmed with corresponding annualised event rates for myocardial infarction (MI) and death of  $\leq 1\%$ /year over a 2 year follow-up period (Table 1.1)(Lipinski et al., 2013; Gargiulo et al., 2013; Bingham & Hachamovitch, 2011).

The 2013 European Society of Cardiology (ESC) guidelines on the management of stable CAD recommend non-invasive stress imaging as the first-line strategy for investigating suspected angina in patients with a pre-test probability of 15-85% (Class I recommendation) with stress perfusion CMR as one of the suggested options (Table 1.2) (Montalescot et al., 2013). The 2012 ACCF/AHA chest pain guidelines

reserve Class I recommendations for exercise ECG, nuclear perfusion imaging and stress echocardiography based on their more extensive historical data and the option for non-pharmacological stress, but do allocate a Class IIa recommendation to stress perfusion CMR for several scenarios, reflecting its growing evidence-base (Table 1.2)(Fihn et al., 2012).

**Table 1-1 Large Scale Clinical Validation of Perfusion CMR**

<b>Authors</b>	<b>Year</b>	<b>Study design</b>	<b>n</b>	<b>Results</b>
<b>Diagnostic accuracy</b>				
Hamon et al	2010	Meta-analysis 35 studies	2154	Sensitivity = 89% Specificity = 80%
Greenwood et al	2011	Prospective Single-centre	752	Sensitivity = 87% Specificity = 83%
Schwitter et al	2012	Retrospective Multi-centre	515	Sensitivity = 67% Specificity = 61%
Jaarsma et al	2012	Meta-analysis 37 studies	2841	Sensitivity = 89% Specificity = 76%
<b>Prognostic data</b>				
Bingham et al	2011	Retrospective Single-centre	908	AER for negative stress CMR <1%/year
Lipinski et al	2013	Meta-analysis 19 studies*	11636	AER for negative stress CMR <1%/year
Gargiulo et al	2013	Meta-analysis 14 studies†	12178	AER for negative stress CMR = 1%/year

\* including 4 studies using dobutamine stress for inducible wall-motion abnormality

† including 6 studies using dobutamine stress for inducible wall-motion abnormality

AER = combined annualised event rate (cardiac death or myocardial infarction)

**Table 1-2** ESC and AHA Recommendations for Perfusion CMR in Stable CAD

Recommendation	Class
<b>ESC Guidelines (2013)</b>	
CMR is a recommended initial test to diagnose CAD in patients with intermediate PTP (15-85%)	I
CMR used for diagnosis of CAD may be combined with clinical assessment for event risk-stratification	I
CMR is a recommended test for patients with known CAD for new or recurrent symptoms (once instability excluded)	I
CMR is a recommended test after MI (before or after discharge) to detect ischaemia from bystander lesions if further revascularisation is considered[w5]	I
<b>ACCF/AHA Guidelines (2012)</b>	
CMR is reasonable as the initial test to diagnose CAD in patients with intermediate (10-90%) or high (>90%) PTP and unable to exercise	IIa
CMR can be useful as the initial test to diagnose CAD in patients with intermediate (10-90%) or high (>90%) PTP, able to exercise but with an uninterpretable resting ECG.	IIa
It is reasonable to use CMR in patients with known CAD, requiring prognostic risk assessment and who are unable to exercise	IIa
CMR is reasonable to assess patients with known CAD who have new or worsening symptoms (but not unstable) and who are unable to exercise	IIa

ESC = European Society of Cardiology; ACCF = American College of Cardiology Foundation; AHA = American Heart Association; CMR = cardiovascular magnetic resonance; CAD = coronary artery disease. PTP = Pre-test probability. Note that CMR in this table refers specifically to stress perfusion CMR.

### **1.2.4 Challenges of Perfusion CMR**

Combined with the assessment of ventricular function by cine imaging, and viability by LGE imaging, perfusion CMR allows for the comprehensive assessment of CAD (Plein et al., 2004; Bodi et al., 2005). However, standard perfusion CMR (despite having higher spatial resolution than SPECT and PET) still yields a lower spatial resolution than cine or LGE imaging CMR techniques (Greenwood et al., 2012; Schwitter et al., 2008; Wolff et al., 2004; Keijer et al., 2000a, 2000b; Sakuma et al., 2005; Gerber, 2008; Kim et al., 2000; Jahnke et al., 2007; Panting et al., 2002; Atkinson et al., 1990). The main reason for this limitation is that perfusion CMR is bound by spatio-temporal constraints as data acquisition is limited to short windows in each cardiac cycle in order to limit the effects of cardiac motion and track the rapid myocardial passage of contrast. Standard perfusion CMR techniques therefore permit the acquisition of 3-4 myocardial slices with a spatial resolution of only 2-3mm. Acquisition of cine and LGE CMR data on the other hand is typically segmented and acquired over several heartbeats to boost spatial resolution (typically 1.5-1.8 mm) and/or signal-to-noise ratio (SNR).

For this reason, there has been a high demand for development of perfusion CMR methods that can boost spatial resolution to match that of other CMR methods. Several such techniques are now available which 'accelerate' the data acquisition to improve spatial resolution <2mm (high-resolution perfusion CMR) without sacrificing temporal resolution or spatial coverage. Alternatively, the speed-up afforded by acceleration techniques can be used to achieve 3-dimensional (3D) acquisitions with

increased spatial coverage (12-16 slices) - in order to overcome the assumptions of the standard 3-4 slice approach.

### **1.3 Basic Principles of MRI**

Prior to discussing acceleration techniques applicable to CMR, it is necessary to review our understanding of how MRI signals are generated and of the spatial encoding scheme used - which is inherently responsible for the relatively low imaging speed of MRI. When a subject is placed in the magnetic field, it causes millions of protons or 'spins' in the body to either align themselves with the magnetic field (low-energy spins) or against it (high-energy spins). The small difference in energy between the two spin populations constitutes the magnetisation used for imaging and is proportional to the field strength of the scanner. Short excitation pulses of radio-frequency (RF) energy (preparation pulse) are applied to disrupt the magnetisation equilibrium – 'magnetisation preparation'. This causes some spins to move to a higher energy state (align against the field) and some to move to a lower energy state (align with the field). After the excitation preparation pulse, magnetisation returns to its equilibrium and a small RF signal is emitted which is then detected by sensitive receiver coils and used to form an image after amplification and processing.

A slice selection gradient (Gs) or magnetic field is applied at the same time as the preparation pulse to direct the excitation effect to the image slice of interest. Additionally, once the slice selection process has created resonance within the selected slice, two further gradients are applied at right angles to each other within

the imaging plane. Firstly, the phase encoding gradient ( $G_p$ ) is applied for a specified time such that when it is switched off, the protons will have changed their relative phase by a prescribed amount depending on their position along the gradient - which therefore leaves the signal 'phase-encoded'. Secondly, the frequency encoding gradient ( $G_f$ ) is applied to encode the frequency of the signal and the signal is simultaneously sampled. This sequence of slice selection, phase encoding, frequency encoding and signal sampling is repeated many times with a repetition interval known as the 'repetition time' (TR).

The final signals are therefore quite complex and contain frequency-encoded and phase-encoded data which is then stored in a virtual grid or matrix known as  $k$ -space. A single data point in  $k$ -space contributes to the whole image and conversely a single pixel in the image may have contributions from all of the MRI signals collected. The data in the centre of  $k$ -space holds most of the signal content and therefore provides the image contrast. If only the centre of  $k$ -space is obtained, the image formed is high in signal but of low resolution. The data at the edges of  $k$ -space hold fine detail of the image and therefore define its spatial resolution. A sophisticated mathematical process (Fourier transformation) is required to extract the individual components from each dimension of  $k$ -space and reconstruct the image. However powerful, data acquisition in  $k$ -space is very time consuming as conventionally only one data point can be sampled at a time and consequently MRI is not a real-time technique. For example, acquisition of a typical image of 128 x 128 pixels would take 400 ms, thus allowing acquisition of only 2 slices per heart-beat. Doubling the resolution to 256 x 256 pixels would at least double the acquisition time and allow

imaging of only one slice. Therefore, imaging speed-up techniques are required if a sufficient number of slices are to be imaged with an increased spatial resolution.

## 1.4 Acceleration Techniques

There are essentially two ways to accelerate data acquisition with MRI: either  $k$ -space is sampled faster, or fewer points in  $k$ -space and/or time are sampled (spatio-temporal undersampling). Previously, advances in accelerated imaging have come from developments in gradient hardware and gradient encoding such as EPI and spiral imaging that allow faster sampling of  $k$ -space (Mansfield, 1984; Meyer et al., 1992). However, it seems unlikely that there will be further advances in speed from these areas, since physiological limits for peripheral nerve stimulation and radiofrequency deposition have been reached (Schaefer, 1998). Any further reduction in scan time or data acquisition is therefore only possible by reducing the amount of acquired  $k$ -space data by a given factor (acceleration factor). This is not a simple strategy however, as undersampling of  $k$ -space causes signal aliasing in the reconstructed image if the Nyquist sampling limits are exceeded. Imaging speed-up techniques are able to avoid or resolve this aliasing without significantly compromising image quality because image series often exhibit a high degree of spatio-temporal correlations and image redundancy.

Although several methods of accelerated imaging have now been described and this continues to be an area of active research, we will only discuss the most notable examples and those relevant to perfusion CMR here (Kozerke & Plein, 2008). We will also pay preferential attention to advanced acceleration techniques where speed-up

can be invested into spatial resolution or spatial coverage to facilitate high-resolution and 3D perfusion CMR respectively.

### **1.4.1 Basic Acceleration Methods**

The basic methods of acceleration below are commonly used to reduce the acquisition time per slice per cardiac cycle in perfusion CMR. Whilst this is helpful in reducing breath-hold durations and motion artefact during stress imaging with high heart rates, coverage is still limited to 3-4 slices with a relatively standard in-plane spatial resolution of 2-3 mm. More advanced acceleration is required to afford sufficient investment of speed-up in spatial-resolution or coverage without compromising SNR.

#### ***1.4.1.1 Echo Planar Imaging***

Although a number of pulse sequences are used for perfusion imaging, one of the most common is EPI and this is because it is one of the fastest techniques available. Conventional imaging sequences acquire only one line of  $k$ -space per heart beat and are therefore slow to acquire a full dataset. In EPI pulse sequences, several lines of  $k$ -space lines are acquired together following one single RF excitation. This pulse design has been validated in larger trials with good results and therefore is frequently used in perfusion CMR (Wolff et al., 2004; Schwitter et al., 2001, 2008).

The initial part is very similar to a standard sequence but the frequency encoding gradient is successively re-applied with alternating direction which generates multiple gradient echoes (signals) all from a single RF excitation. In order to rapidly sample the multiple echoes before they decay, a wide receiver bandwidth is used.

To ensure that each echo fills a different line of  $k$ -space, a small phase encoding gradient is applied prior to each sampling.

The benefits of the fast imaging time are not without cost. EPI is relatively demanding on the scanner hardware, in particular on gradient strengths, gradient switching times, and receiver bandwidth. In addition, the decay of multiple echoes and the high receiver bandwidth result in a low SNR and therefore EPI can be vulnerable to image artefacts and distortions.

#### ***1.4.1.2 Interleaved Notched Saturation***

In all pulse sequences, the magnetisation recovery time (TI) plays a major role in determining contrast, SNR and the maximum number of sections that can be acquired. A preparation pulse with a long TI provides higher SNR and better contrast, but the consequent delay inserted between preparation and acquisition reduces spatial coverage.

The 'interleaved notched saturation' technique has two major differences from conventional pulse sequences used in multi-section perfusion CMR (Slavin et al., 2001). Firstly, there is no insertion of physical dead time into the sequence to allow relaxation between preparation and acquisition of each section. Secondly, the consecutive preparation and acquisition pulses do not affect the same section – instead any given section is prepared before acquisition of the preceding section. This is achieved by an alternative method of magnetization preparation using a preparation pulse with a notched profile. Saturation bands are created on both sides of the 'notch', which is centred such that spins in the subsequently imaged section are unaffected by the preparation pulse. The presence of the notch essentially

decouples the preparation-acquisition combination and enables the most time efficient implementation of long T1 recovery without sacrificing section coverage.

#### **1.4.1.3 Parallel Imaging**

Among all the different parallel imaging techniques presented to date, sensitivity encoding (SENSE) and generalized autocalibrating partial parallel acquisition (GRAPPA) have been the most successful and are now widely available on commercial MRI systems (Pruessmann et al., 2001; Griswold et al., 2002). Central to parallel imaging is the availability of dedicated receiver coils. The speed-up is achieved by undersampling  $k$ -space (skipping phase encoding steps) during the acquisition. For example, in two-fold undersampling, only every other line of  $k$ -space is filled which would ordinarily lead to significant image aliasing. However, the missing information is re-populated, based on differences in perception of the signal by multiple receiver coils positioned around the object. This reconstruction process therefore requires knowledge of the coil sensitivity map - a 3D plot of how the signal varies with distance from each receiver coil. Coil sensitivity maps are formed from the central lines of  $k$ -space and can either be acquired as a separate low-resolution reference scan (SENSE); or as part of the acquisition with a few profiles of fully encoded data for coil calibration (GRAPPA). By comparing the signal from each receiver coil and with reference to the coil sensitivity map, there is sufficient data to reconstruct the image without aliasing.

In dynamic imaging applications such as perfusion CMR, the undersampling pattern can be shifted as a function of time, such that coil sensitivity maps can be estimated from a time-average image. This therefore removes the need for separate calibration

data. The use of interleaved sampling for calibration purposes in combination with SENSE reconstruction is known as temporal sensitivity encoding (TSENSE) (Kellman et al., 2001).

Theoretically, in parallel imaging the unaliasing is possible as long as the acceleration factor (undersampling factor) does not exceed the number of receive coils. In practice however it is difficult to achieve acceleration greater than 2-3-fold without SNR penalties and unresolved aliasing. Nonetheless, the significant reduction in acquisition time that can be achieved means that parallel imaging techniques are a well-established method of accelerating perfusion CMR and almost any MRI application (Kozerke & Plein, 2008).

#### **1.4.2 Advanced Acceleration Methods**

Accelerating data acquisition with parallel imaging or EPI methods has been standard practice in perfusion CMR for over a decade, but trade-offs in SNR and artefacts limit the achievable acceleration to 2-3 fold. In a typical stress perfusion study, these methods still only permit the acquisition of 3-4 myocardial slices with an in-plane spatial resolution of 2-3mm. More recently proposed 'prior-knowledge' based techniques allow much higher acceleration factors for data acquisition (Kozerke & Plein, 2008; Tsao & Kozerke, 2012). The 'prior-knowledge' principle is not limited to CMR or even MRI per se and has also been applied to CT and PET (Chen et al., 2008; Christian et al., 2010). Prior-knowledge methods are based on the observation that image data sets exhibit considerable correlation in space and time. Perfusion CMR datasets in particular contain a high degree of temporal redundancy, because data are acquired at a single time point in the cardiac cycle using ECG-gating and during

breath-holding, so that most of the image is static and the predominant change between neighbouring time frames is related to the relatively slow contrast passage. This image redundancy can be exploited by undersampling data in the time ( $t$ ) domain in addition to the more conventional undersampling in the spatial ( $k$ -space) domain (Kozerke & Plein, 2008; Motwani et al., 2011; Tsao & Kozerke, 2012).

Examples of these spatiotemporal (or  $k$ - $t$ ) undersampling techniques are  $k$ - $t$  broad linear acquisition speed up technique ( $k$ - $t$  BLAST),  $k$ - $t$  sensitivity encoding ( $k$ - $t$  SENSE) and  $k$ - $t$  principal component analysis ( $k$ - $t$  PCA). In  $k$ - $t$  BLAST,  $k$ - $t$  SENSE and  $k$ - $t$  PCA perfusion CMR sequences, under-sampling is applied along  $k$ -space and time whilst a low spatial resolution image ('training data') is obtained in an interleaved fashion during the acquisition (Plein et al., 2007). A non-aliased, full image series is then reconstructed using prior knowledge derived from the training data (Figure 1.2). In  $k$ - $t$  SENSE and  $k$ - $t$  PCA receiver coil sensitivity information is additionally employed to facilitate image reconstruction. Further technical details beyond the scope of this introduction can be found in recent technical reviews (Tsao & Kozerke, 2012; Kozerke & Plein, 2008).

Other related methods have also been proposed such as the highly constrained back-projection reconstruction (HYPR) method, in which spatial and temporal redundancy are exploited serially (Kozerke & Plein, 2008; Tsao et al., 2003; Ge et al., 2009). In HYPR and its variants  $k$ -space data is acquired with undersampled radial projections and overall rotation of the undersampling pattern at different time points (Ge et al., 2009; Mistretta et al., 2006; Ma et al., 2012). In image reconstruction, a fully sampled composite image is formed by populating missing data from neighbouring time

frames. This very low temporal resolution composite is then used to constrain back-projection of the undersampled data acquired for each individual time frame (Ge et al., 2009; Ma et al., 2012). Other promising acceleration techniques such as spiral imaging are in early development but their clinical utility has yet to be assessed (Salerno et al., 2011; Shin et al., 2013; Chen et al., 2012).

With the techniques listed above, it is possible to accelerate image acquisition up to a factor of 10 times or more. This speed-up has been utilised to improve spatial resolution (high-resolution perfusion CMR) or to acquire 3D myocardial perfusion data within a single acquisition shot facilitating greater spatial coverage (Maredia et al., 2010; Shin et al., 2008; Plein et al., 2008a; Manka et al., 2010, 2012; Jogiya et al., 2012).

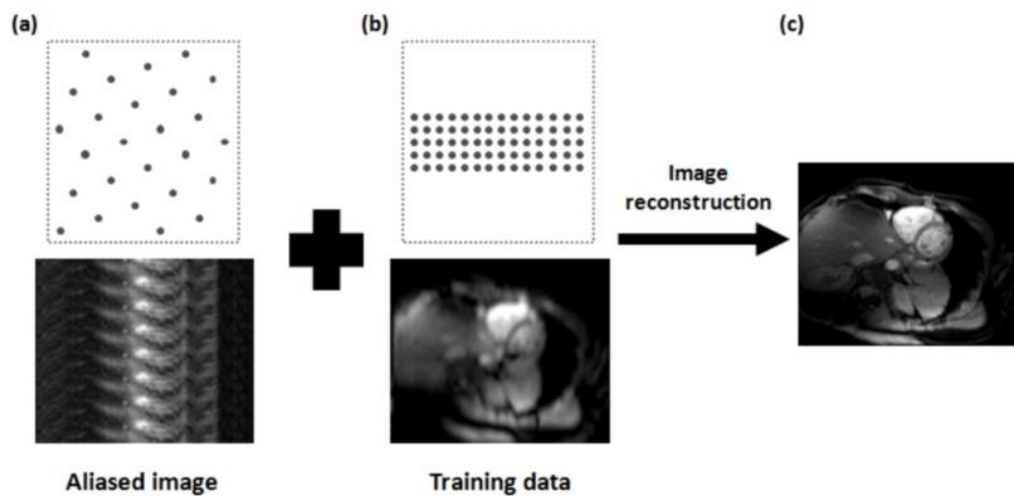


**Figure 1.2 k-t acceleration techniques**

(a) In *k-t BLAST* and *k-t SENSE*, data acquisition is accelerated by under-sampling along the spatial encoding (*k*) and time (*t*) axes which leads to an aliased image. (b) Low resolution ‘training data’ is also obtained to determine data correlations i.e. ‘prior-knowledge’. (c) Finally, a non-aliased full image series is reconstructed using a statistical model derived from the training data. *BLAST*= broad linear speed-up technique; *SENSE*=sensitivity encoding.

## 1.5 High-resolution Perfusion CMR

Although no accepted definition exists, perfusion CMR is considered as “high spatial resolution” when the in-plane resolution is better than 2mm, making the resolution comparable to that of other common CMR methods. The first feasibility study of high-resolution perfusion CMR used 5-fold *k-t* SENSE to achieve an in-plane spatial resolution of 1.5mm in a group of 10 volunteers (Plein et al., 2007). Image quality was similar to that from a standard-resolution sequence (in-plane spatial resolution of 2.6mm) but there was a significant reduction in the extent of dark rim artefact (mean thickness: 1.7 vs. 2.4mm;  $p < 0.01$ ) (Figure 1.3).

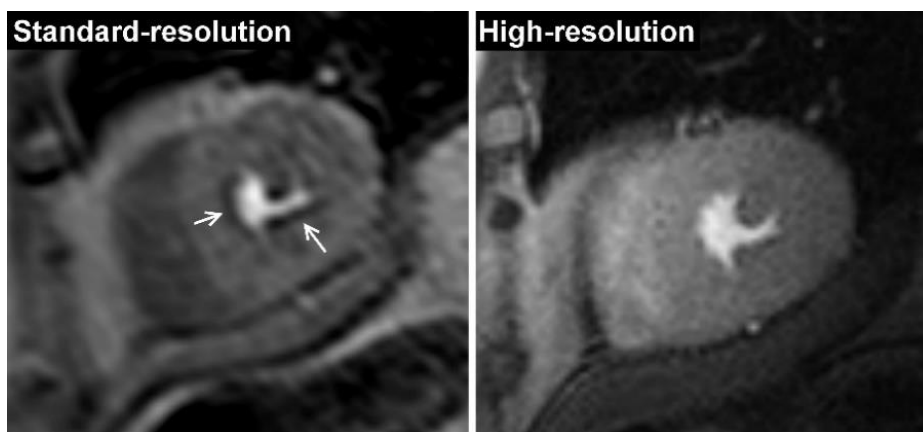


**Figure 1.3 Dark Rim Artefact: Standard-resolution vs. High-resolution**

*A 60-year-old man with suspected angina underwent stress perfusion CMR at 1.5T with both standard-resolution (2.5mm in-plane) and high-resolution (1.5mm in-plane) acquisition. High-resolution acquisition was facilitated by 8-fold *k-t* BLAST acceleration). There were no significant stress-induced perfusion defects seen with either acquisition (mid-ventricular slices shown) but there was significant dark-rim artefact on the standard-resolution images (arrows). Subsequent X-ray angiography confirmed normal coronary arteries*

Images acquired at high-resolution also displayed an increased SNR compared to standard-resolution when corrected for pixel size – facilitated by constraining the reconstruction with the low resolution, high SNR training data. In 3 of the volunteers, higher *k-t* SENSE acceleration factors of 8 and 10 were successfully used, without compromise in image quality or temporal signal intensity profiles.

The reduction of dark rim artefact with high-resolution acquisition was confirmed in another volunteer study (n=10) (Maredia et al., 2010). In this study, mean artefact thickness was 3.4 mm with standard-resolution, compared to only 1.1mm with a *k-t* SENSE high-resolution acquisition ( $p < 0.001$ ). Dark rim artefacts are a common finding in conventional perfusion CMR and are thought to be caused by magnetic susceptibility effects, Gibbs ringing and cardiac motion during acquisition (Di Bella et al., 2005). As these artefacts are directly proportional to voxel size, the use of high-resolution perfusion CMR offers a significant advantage (Figures 1.3 and 1.4).

Following the feasibility studies in volunteers, high-resolution perfusion CMR has been validated in several patient studies (Table 1.3)(Maredia et al., 2010; Plein et al., 2008a, 2008b; Manka et al., 2010). In the first of these, Plein et al used an identical sequence to their previous volunteer study (1.5T, 5-fold *k-t* SENSE, in-plane resolution 1.4mm) in 51 patients with known or suspected CAD (Plein et al., 2008a). High-resolution acquisition was found to have a high image quality and high diagnostic accuracy (area under the curve [AUC] = 0.85) against quantitative coronary angiography (QCA). Notably, the diagnostic accuracy in single-vessel disease and multi-vessel disease was similar (AUC: 0.87 vs. 0.82 respectively) suggesting that sufficient spatial resolution to resolve a transmural ischaemic

gradient can overcome one of the major limitations of perfusion imaging in multi-vessel disease i.e. its dependence on a reference area of normal perfusion (Figures 1.5 and 1.6). Other benefits of high-resolution acquisition noted in the study were better integration with cine and LGE data and minimal dark rim artefact. A subsequent study demonstrated the clinical feasibility of high-resolution perfusion CMR at 3.0T and confirmed the expected improvement in image quality and SNR compared to 1.5T (Table 1.3)(Plein et al., 2008b).

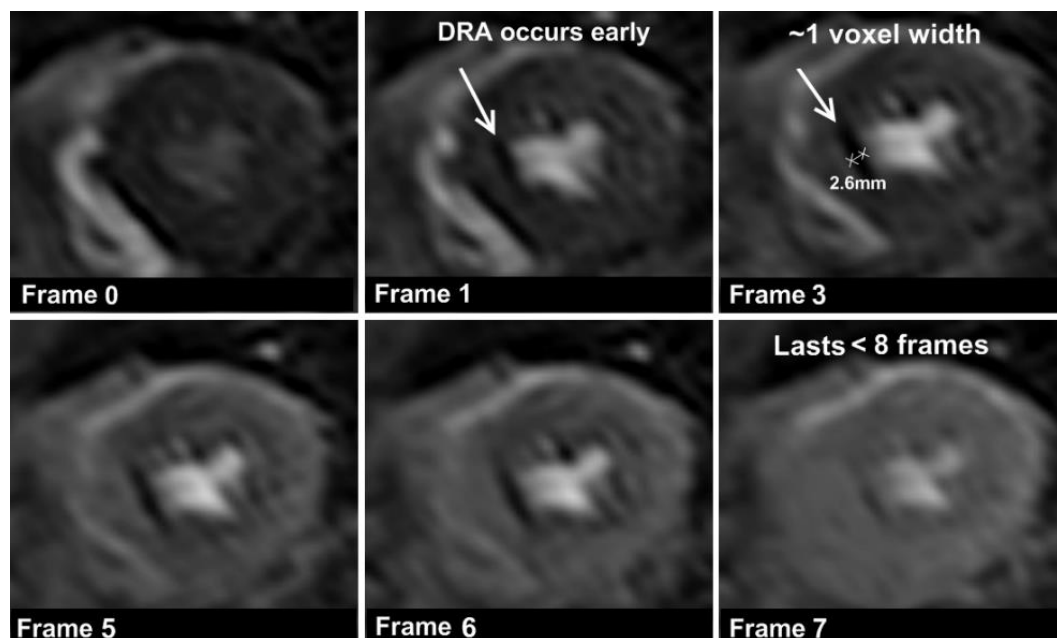


**Figure 1.4 Dark Rim Artefact**

*This example shows a midventricular slice during standard-resolution perfusion-CMR. Dark rim artefact (arrows) is a frequent finding and relates to several factors including cardiac motion, Gibb's ringing, susceptibility, and partial volume cancellation between the myocardium and blood pool. Although dark rim artefacts may mimic perfusion defects, they can be distinguished by characteristic features: they occur at the arrival of contrast in the left ventricular cavity and before its arrival in the myocardium (Frame 1); they tend to disappear within 8 to 10 frames (Frame 7); their location is usually typical for a particular pulse sequence; and their width roughly equates to the in-plane spatial resolution, which was 2.5 mm in this example (Frame 3). DRA = dark rim artefact*

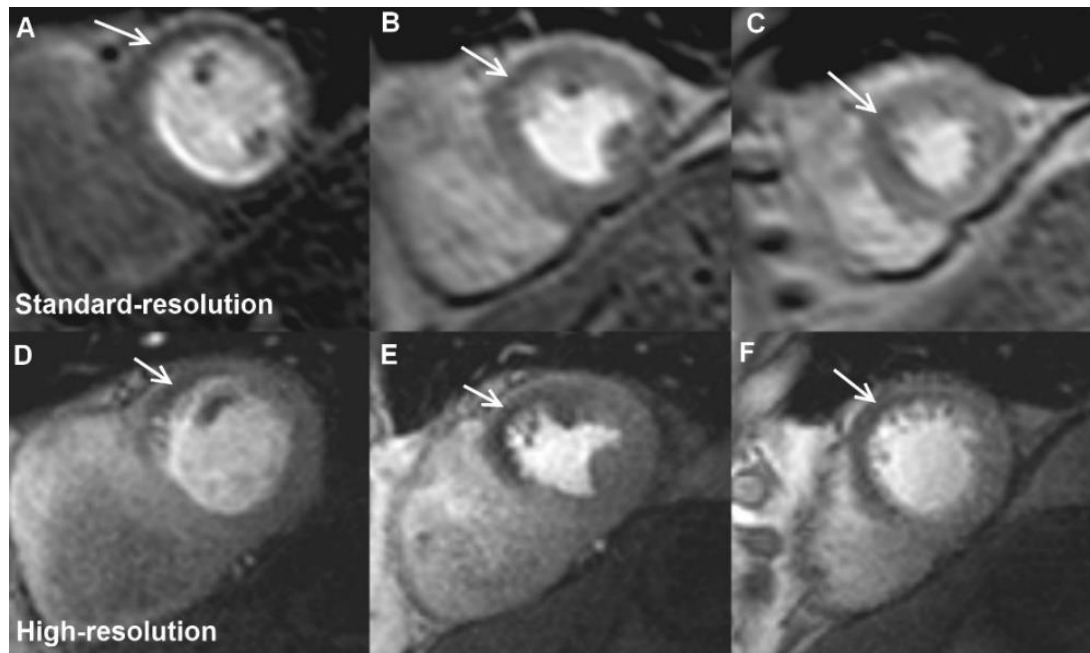


**Figure 1.5 Standard-resolution vs. high-resolution stress perfusion CMR**

A 53 yr old man had proximal LAD 80% stenosis on x-ray angiography. Standard-resolution acquisition at 1.5T shows a subtle anterior wall perfusion defect (white arrows) at the basal (A), mid-ventricular (B) and apical (C) level. With high-resolution acquisition (using 8-fold *k-t* BLAST) the anterior defect is much better defined (D-F) and the presence of a

Manka et al followed with an extension of the *k-t* SENSE technique at 3.0T to achieve 8-fold acceleration and an in-plane spatial resolution of 1.1 mm which was then evaluated in 20 patients with suspected CAD. The combined benefits of higher field strength and greater acceleration led to an incremental improvement in spatial resolution and an even greater AUC of 0.94 (95% CI: 0.74-0.99)(Manka et al., 2010).

Most recently, in the only study to offer a direct comparison (and which forms part of the current thesis), high-resolution perfusion CMR (8-fold *k-t* BLAST, in-plane spatial resolution 1.6mm) was found to have a significantly greater overall diagnostic accuracy compared to standard-resolution in 100 patients with suspected CAD (AUC 0.93 vs. 0.83;  $p < 0.001$ ). The improved diagnostic performance was attributed to

better detection of subendocardial ischaemia (Figures 1.5 and 1.6)(Motwani et al., 2012a) As the endocardial layer is the most vulnerable to ischaemia, the ability to confidently detect subendocardial perfusion deficits can be expected to improve the detection of CAD in a perfusion study (Bache & Schwartz, 1982). Furthermore, a recent study by Hautvast *et al* showed that high-resolution perfusion CMR data can be used to accurately quantify transmural perfusion gradients and these new measurements may serve as diagnostic markers for the detection and characterisation of epicardial coronary disease as well as microvascular disease (Hautvast et al., 2011).

The HYPR method was used in one recent single-centre study, in a variant known as sliding-window conjugate-gradient HYPR (6 contiguous slices, 1.6mm in plane spatial resolution). The study demonstrated clinical feasibility and a high diagnostic accuracy in 50 patients with suspected CAD (Ma et al., 2012). Whereas the previous studies have all used QCA as their reference standard, Lockie *et al* validated high-resolution perfusion CMR against invasive pressure-wire derived fractional flow reserve (FFR)(2011). In the 42 patients studied, high-resolution perfusion CMR (5-fold *k-t* BLAST, in-plane resolution 1.2mm) had a high diagnostic accuracy (AUC=0.92) for the detection of hemodynamically significant lesions (FFR<0.75)(Lockie et al., 2011). To have a non-invasive method that so closely correlates with FFR is highly attractive and more widespread use could have a significant impact on clinical pathways - especially in patients with anatomically complex and multi-vessel disease (Tonino et al., 2010). However, whether high-resolution perfusion CMR conveys a diagnostic increment against FFR is not certain and notably in a previous study using

FFR<0.75 as the reference standard, Watkins et al found a high level of diagnostic performance with a standard-resolution acquisition (sensitivity 91%, specificity 94%), comparable to the high-resolution method used by Lockie et al (Watkins et al., 2009).

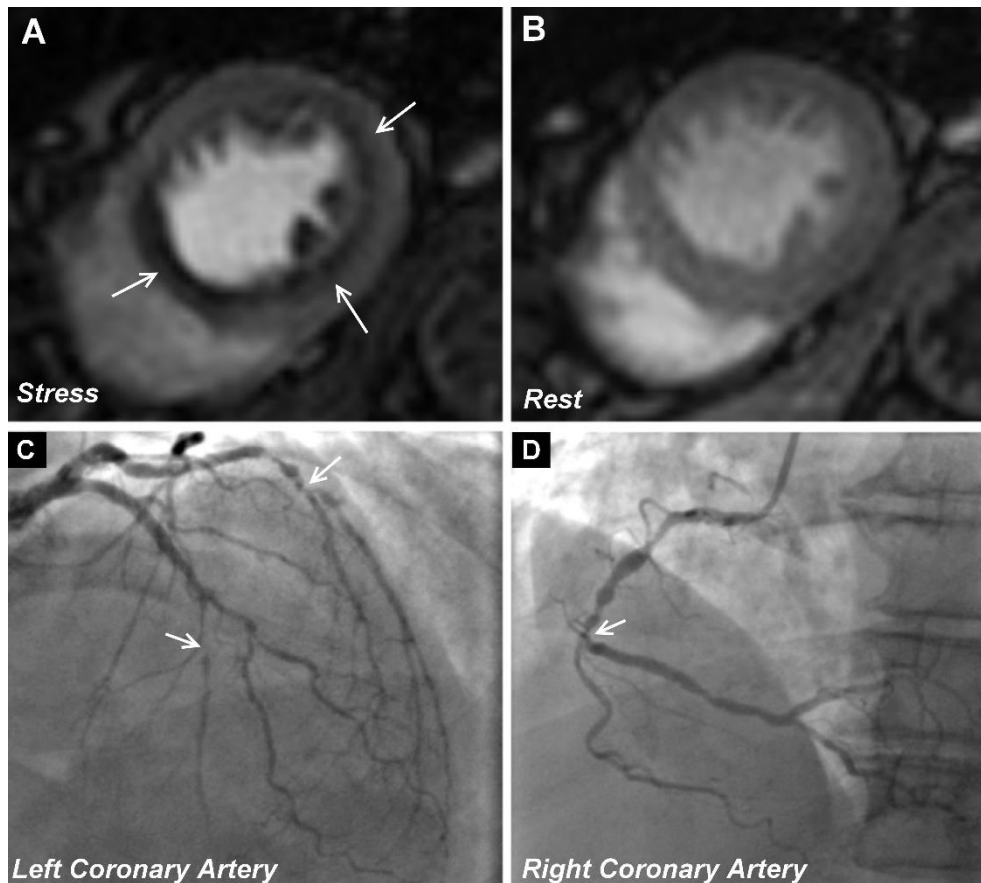


**Figure 1.6 High-resolution Perfusion CMR in Multi-vessel CAD**

A 48yr old lady with suspected angina underwent stress perfusion CMR at 1.5-T using a high-resolution (1.4mm in-plane) technique facilitated by 5-fold k-t-BLAST. Stress-induced perfusion defects were seen in all three territories (arrows, A, B) and are clearly demarcated as subendocardial. Subsequent X-ray angiography revealed significant three-vessel disease (arrows, C, D). This case highlights the ability of high-resolution acquisition to overcome the potential effects of balanced ischaemia in multi-vessel disease by detecting transmural perfusion gradients and subendocardial ischaemia.

**Table 1-3 Diagnostic Performance of Advanced Perfusion CMR**

	n	Field Strength & Acceleration		Spatial Resolution & Spatial Coverage		Reference standard & Diagnostic Accuracy	
<b>High-Field Strength</b>							
<i>Cheng 2007</i>	61	3.0T	-	2.6mm	4 slices (NC)	QCA>50%	0.87
<i>Ebersberger 2013</i>	116	3.0T	-	3.0mm	3 slices (NC)	QCA> 75% or FFR≤0.8*	0.93
<b>High-Resolution</b>							
<i>Plein 2008</i>	51	1.5-T	5 x k-t-SENSE	1.4mm	4 slices (NC)†	QCA>50%	0.85‡
<i>Plein 2008</i>	33	1.5-T	5 x k-t SENSE	1.5mm	4 slices (NC)†	QCA>50%	0.80‡
<i>Plein 2008</i>	33	3.0-T	5 x k-t SENSE	1.3mm	4 slices (NC)†	QCA>50%	0.89‡
<i>Manka 2010</i>	20	3.0-T	8 x k-t SENSE	1.1mm	3 slices (NC)	QCA>50%	0.94‡
<i>Motwani 2012</i>	100	1.5-T	8 x k-t BLAST	1.6mm	3 slices (NC)	QCA ≥50%	0.93‡
<i>Lockie 2011</i>	42	3.0-T	5 x k-t BLAST	1.2mm	3 slices (NC)	FFR<0.75	0.92‡
<b>3-D</b>							
<i>Manka 2011</i>	146	3.0-T	6 x k-t SENSE	2.3mm	16 slices (WH)	QCA ≥50%	0.83§
<i>Manka 2012</i>	120	1.5-T	10 x k-t PCA	2.0mm	16 slices (WH)	FFR<0.75	0.87§
<i>Jogiya 2012</i>	53	3.0-T	10 x k-t PCA	2.3mm	12 slices (WH)	FFR<0.75	0.91§
<b>HYPR</b>							
<i>Ma 2012</i>	50	3.0-T	SW-CG-HYPR	1.6mm	6 slices (WH)	QCA ≥50%	0.90§

†In these studies, temporal resolution was 2 R-R intervals whereas in all others it was 1 R-R interval.

‡In these studies, diagnostic accuracy was calculated by receiver-operating characteristic analysis and expressed as area under the curve. §In these studies, diagnostic accuracy was expressed as the proportion of correctly classified subjects (true positives + true negatives) among all subjects. FFR = fractional flow reserve; HYPR = highly constrained back-projection reconstruction; SENSE = sensitivity encoding; BLAST = broad linear speed-up technique; PCA = principal component analysis; SW-CG-HYPR= sliding-window conjugate-gradient HYPR; NC = non-contiguous; WH= whole-heart; QCA = quantitative coronary angiography.

## 1.6 Three-Dimensional Perfusion CMR

Conventionally, cardiac coverage with perfusion CMR is limited to 3-4 non-contiguous slices through the left ventricle (LV). However, nuclear perfusion studies have demonstrated that the extent of hypoperfusion and overall myocardial ischaemic burden (MIB) is a strong marker of clinical outcome (Brown et al., 1983; Hachamovitch et al., 1998). It is unknown how accurately MIB can be measured from non-contiguous image sections. Therefore, despite the demonstrated high diagnostic accuracy of conventional 2-dimensional (2D) perfusion CMR, the lack of complete myocardial coverage remains a potential limitation of the method.

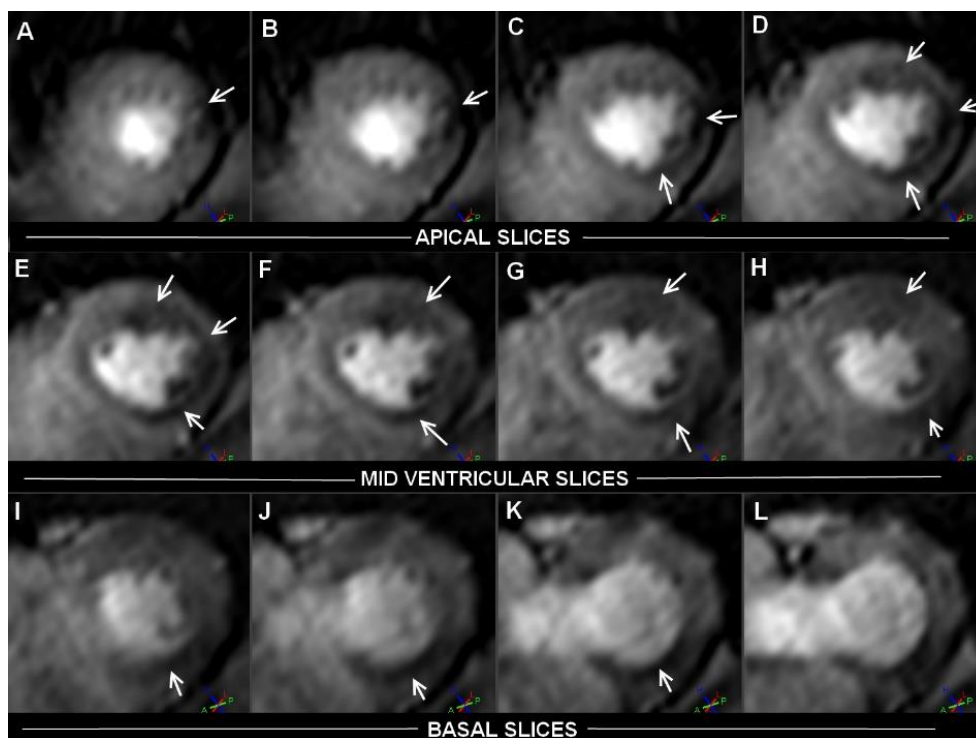


**Figure 1.7 Example of 3D Perfusion CMR**

12 short-axis slices are covered rather than the conventional 3 slices seen in standard imaging. Perfusion defects (arrows) are seen in the inferior segments from base to apex (A-L), mid anterolateral segments (E-H), and lateral segments from mid-ventricle to apex (A-H) – consistent with the severe RCA and 1st -diagonal disease seen at coronary angiography

The same speed-up methods that permit high-resolution myocardial perfusion CMR can also be used to acquire a single 3D stack covering all or a large proportion of the heart whilst preserving adequate temporal and spatial resolution (Figures 1.2 and 1.8)(Schwitter et al., 2008). Advanced acceleration methods allow the acquisition of 3D data covering the whole heart in up to 16 contiguous slices within an acquisition duration of less than 200ms (Manka et al., 2011). The most significant advantage of 3D acquisition is that contiguous spatial coverage allows the true extent of perfusion defects to be visualised (Shin et al., 2008). Additionally, although data in the literature regarding the incidence of pure apical ischaemia is lacking and it is presumed to be rare, the inability of 2D perfusion CMR to image the apical cap is sometimes stated as a limitation – and this is overcome by 3D acquisition (Elkington et al., 2004; Schwitter et al., 2008). Another limitation of conventional 2D perfusion CMR is that each slice is acquired in a different phase of the cardiac cycle (Figure 1.8). In practice this means that the acquisition cannot be optimised for all slices and may coincide with rapid cardiac motion in some slices, leading to motion artefacts in the images. In 3D acquisition all data are acquired in the same cardiac phase and the time-point for acquisition in the cardiac cycle can be optimised to minimise artefact. Furthermore, the cardiac phase can be matched with other acquired data such as LGE imaging for improved co-registration. As a related benefit, 3D acquisition also permits the optimal choice of the saturation recovery time and the ability to scan at high heart rates because only one preparation pulse and one readout per heart beat is applied (Shin et al., 2008, 2010). The optimal phase within the cardiac cycle for 3D

acquisition is the subject of ongoing research, with end-systole and mid-diastole the favoured options (Shin et al., 2010).

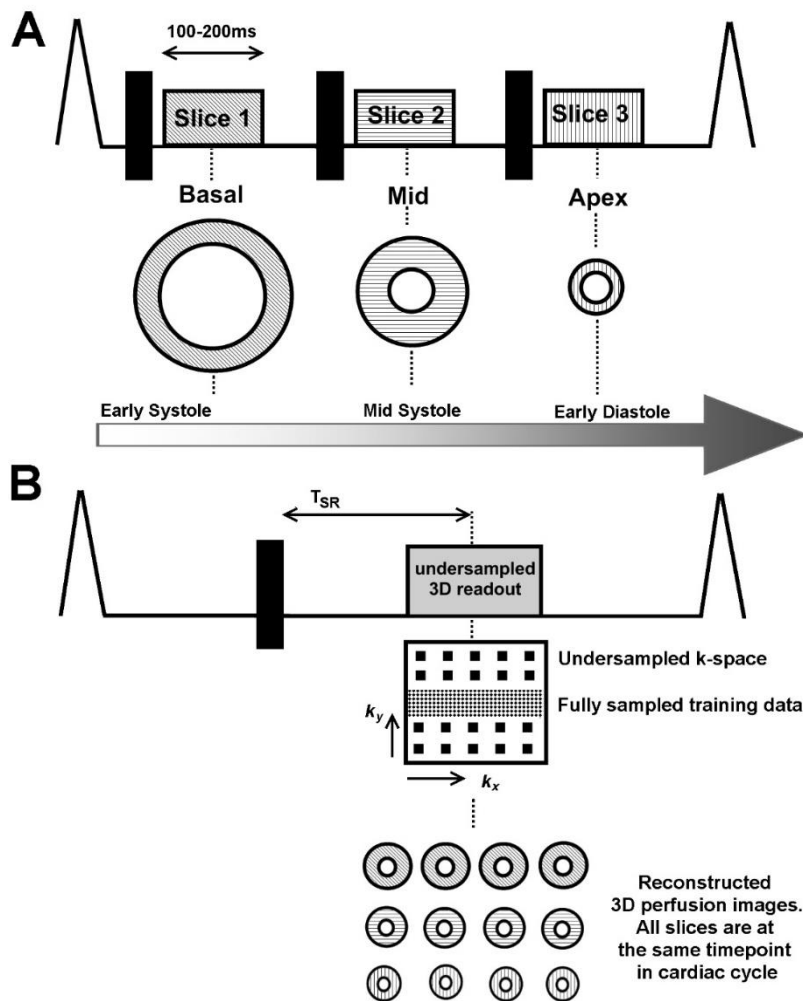


**Figure 1.8 Pulse Sequence Diagrams for 2D and 3D Perfusion CMR**

In 2D perfusion CMR (A), 3-4 non-contiguous slices are acquired in different phases of the cardiac cycle in order to maximise spatial coverage. Each slice is acquired after a saturation pre-pulse (black bar). A shared pre-pulse can be used to save time but results in different contrast characteristics for each slice. In 3D-perfusion CMR (B), a single saturation pre-pulse is followed by a saturation recovery time ( $T_{SR}$ ) and undersampled 3D perfusion data readout. The use of advanced spatiotemporal undersampling allows sufficient data acquisition to reconstruct 12-16 contiguous slices i.e. whole-heart coverage. The ‘training data’ is acquired with the undersampled data in an interleaved fashion. As all perfusion data in the 3D technique are acquired at the same point in the cardiac cycle, the reconstructed slices all appear in the same cardiac phase.

In mid-diastole, the heart is usually at its most stationary, but the relatively thin myocardium can compound the effect of dark-rim artefact and limit the assessment of the transmural perfusion defects. End-systole, on the other hand, has a shorter quiescent period but the thicker myocardium reduces the effect of dark rim artefact and facilitates the grading of defect transmural. Systolic acquisition is also less sensitive to R-R variability and arrhythmia, which is relevant to the increasing burden of patients with atrial fibrillation (Shin et al., 2010). Notably, recent studies have found significant differences between systolic and diastolic myocardial blood flow estimates with perfusion CMR (Motwani et al., 2012b; Radjenovic et al., 2010) and the choice of either cardiac phase for 3D myocardial perfusion may therefore be of physiological interest or relevant to certain disease processes such as hypertrophic cardiomyopathy (Rakowski & Carasso, 2007; Shin et al., 2010).

3D myocardial perfusion CMR is therefore a highly promising development and recent studies have shown it to be clinically feasible, highly accurate and to have a potential role in the assessment and follow-up of MIB (Manka et al., 2011; Shin et al., 2008; Manka et al., 2012; Jogiya et al., 2012). In the first clinical study of 3D perfusion CMR, Manka et al evaluated 146 patients with suspected CAD using *k-t* acceleration to achieve 16-slice coverage and an in-plane spatial resolution of 2.3mm (Manka et al., 2011). Image quality was consistently high and the overall sensitivity, specificity, and diagnostic accuracy to detect significant CAD (QCA  $\geq$  50%) were 92%, 74% and 83% respectively, comparable to conventional 2D perfusion CMR (Manka et al., 2011; Greenwood et al., 2012). Furthermore, MIB (expressed as a percentage of LV myocardial hypo-enhancement to total LV myocardium) was calculated from

3D perfusion CMR data (Figure 1.9). In 48 patients that had a repeat scan after PCI, there was a relative reduction in MIB of  $79 \pm 25\%$ , highlighting the potential role of 3D perfusion CMR to serially monitor the response to anti-ischaemic therapies (Manka et al., 2011). In addition, the quantification of ischaemic burden using myocardial hypo-enhancement volumetry (with an arbitrary signal intensity threshold of 2 standard deviations below remote myocardium) was found to be highly reproducible on intra-reader and inter-reader assessment.

While the previous study used  $QCA \geq 50\%$  as the reference standard for CAD, two recent studies (one at 1.5T and one at 3.0T) have validated 3D perfusion CMR against FFR and shown high diagnostic accuracy of the method (Manka et al., 2012; Jogiya et al., 2012). In a study by Manka et al, 3D perfusion CMR at 1.5T was found to have a sensitivity, specificity and diagnostic accuracy of 90%, 82% and 87% respectively (2012). At 3.0T, a study by Jogiya et al found similar figures of 91%, 90% and 91% respectively (Jogiya et al., 2012). Both of these studies further verified the feasibility and reproducibility of ischaemic burden quantification using volumetry of myocardial hypo-enhancement. Additionally, Manka et al also found that the quantified MIB had a high diagnostic accuracy (AUC=0.90) for identifying FFR-defined CAD - with an optimal cut-off value of  $>4.4\%$  (2012).

Although FFR is widely considered the invasive reference standard for determining the hemodynamic significance of a coronary stenosis, it does not provide any information about the magnitude of consequent ischaemia. This deficiency highlights a potential role for 3D perfusion CMR - and in both of the validation studies against FFR, it demonstrated a higher ischaemic burden with proximal lesions

compared to distal lesions (Manka et al., 2012; Jogiya et al., 2012). Furthermore, Jogiya et al, found a strong correlation ( $r = 0.82$ ; 95% CI: 0.70 to 0.89;  $p < 0.0001$ ) between the MIB on 3D perfusion CMR and the Duke Jeopardy score - which is a validated invasive assessment of ischaemic burden based on lesion severity and location (2012).

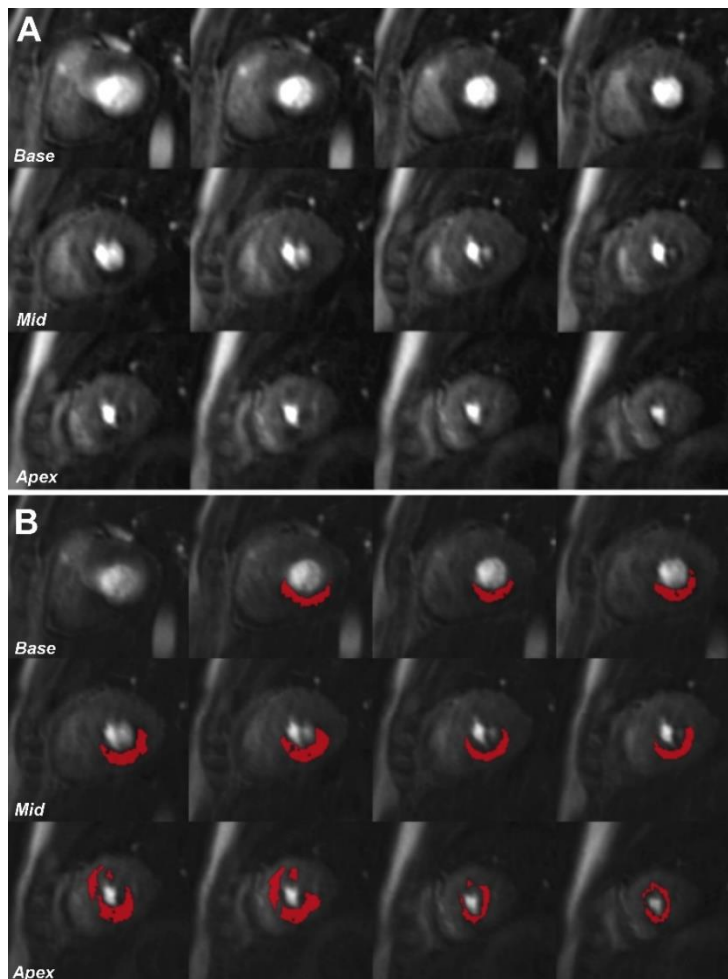


**Figure 1.9 MIB Quantification with 3D Perfusion CMR**

*Panel (A) shows consecutive slices of a 3D perfusion CMR scan during adenosine stress in a patient with significant stenoses in the proximal right coronary artery and distal left anterior descending coronary artery. Panel (B) shows identical images illustrating volumetry of myocardial hypo-enhancement using a signal intensity threshold of 2 standard deviations below remote myocardium (red areas). The volume of myocardial hypo-enhancement was 30.4% of total myocardium. 3D = 3-dimensional; CMR = cardiovascular magnetic resonance*

## 1.7 Limitations of Highly Accelerated Perfusion CMR

*k-t* techniques add complexity to the acquisition of perfusion CMR and they are sensitive to respiratory motion and cardiac arrhythmias. In order to reduce respiration-related artefacts when using these techniques, fewer dynamic images tend to be acquired compared with conventional methods and more emphasis is placed on respiratory coaching (Plein et al., 2008a). The acquisition of fewer dynamic images does however confer a risk of inadequate temporal sampling of myocardial contrast passage, particularly if there is significant arrhythmia - and therefore patients with arrhythmia may not be ideal for these techniques. In practice, the breath-hold capacity of patients can be maximised by clear breathing instructions, trial runs and acquisition in inspiration. Alternative strategies are shallow respiration throughout the acquisition or a more focused breath-hold during myocardial contrast passage (Manka et al., 2010). Previous studies have shown that in compliant patients, respiratory artefacts are rare and tend to occur at the end of a breath-hold; if the timing of the acquisition is correctly synchronised to the breath-hold command, such artefacts rarely interfere with image interpretation (Motwani et al., 2012a). Furthermore, recent improvements such as *k-t* PCA are less sensitive to respiratory motion and improve temporal fidelity (compared to *k-t* SENSE and *k-t* BLAST reconstructions which can suffer from temporal blurring) because image reconstruction is constrained using temporal basis functions derived from the low-resolution training data acquired in every heartbeat (Pedersen et al., 2009). Advanced motion correction techniques that allow free-breathing throughout acquisition are also in development (Pedersen & Kelle, 2008).

A further limitation is that the described reconstruction techniques all assume the heart remains entirely static but there are of course small movements throughout the cardiac cycle which can cause motion-related artefacts including DRA. 3D acquisition is more vulnerable to motion-related artefact than 2D acquisition, as well as respiratory artefact, because of its larger temporal footprint (length of acquisition is approximately 200ms for 3D vs. <100ms for most 2D acquisitions).

Finally, and this applies to all undersampling methods, reducing the number of sampled data points leads to an SNR reduction that is proportional to  $1/\sqrt{R}$  where  $R$  is the acceleration factor (Kozerke & Plein, 2008). In  $k-t$  methods, the actual SNR reduction may, however, be much less if the dynamics of the object are highly correlated in successive time-frames (Gebker et al., 2007b).

## **1.8 High Spatial Resolution or Full Cardiac Coverage?**

Whether the benefits of high spatial resolution such as detection of subendocardial ischaemia and reduction of dark rim artefact outweigh the potential benefits of whole-heart coverage including more reliable ischaemia quantification is a complex and as yet unanswered question. Initial studies albeit in selected and small patient populations, suggest that the diagnostic accuracy of the two approaches is similar - but there has not yet been a direct head-to-head comparison and further large-scale studies are required (Motwani et al., 2012a; Manka et al., 2010, 2012; Jogiya et al., 2012). In clinical practice, the two different approaches may have specific benefits for individual patients. In a patient with a de-novo suspicion of CAD, the available limited data on diagnostic accuracy suggest that either technique – or indeed

conventional 2D perfusion CMR would be appropriate choices. However, in a patient who has already undergone angiography and is found to have diffuse multi-vessel disease with possible PCI targets, high-resolution acquisition might be favourable on account of its ability to detect subendocardial ischaemia in the presence of balanced ischaemia (Figure 1.6). In patients with a history of myocardial infarction and suspected peri-infarct ischaemia, a 3D perfusion scan may better allow matching of LGE and perfusion images over the entire heart with more reliable quantification of peri-infarct ischaemia - rather than an assumption based on three sparse slices. Figures 1.10 - 1.13, show examples of patients undergoing both acquisitions and the relative merits (Table 1.4) of both techniques are discussed in each case.

An alternative strategy to either high-resolution or whole-heart coverage would be to divide the speed-up afforded by acceleration techniques between spatial resolution and cardiac coverage. However, at present there is insufficient data to adequately define the optimal compromise between these parameters. The subendocardial layer is the most vulnerable to ischaemia and therefore sufficient spatial resolution to resolve a transmural perfusion gradient is preferable - and this remains a significant advantage of CMR over SPECT (Greenwood et al., 2012). However, it is unclear how far this notion needs to be taken or whether the spatial resolution used in recent large-scale studies is sufficient - particularly given the high levels of diagnostic performance. Only a large-scale clinical study comparing acquisitions of varying spatial resolution and differing degrees of cardiac coverage can answer this question. Furthermore, whether an optimal compromise is best acquired throughout the cardiac cycle with a multi-slice 2D approach, en-bloc with a

3D approach or with newer techniques such as HYPR would also have to be determined. Finally, beyond studies of diagnostic accuracy we also need to evaluate whether the various approaches differ in their quantification of ischaemic burden, particularly given the increasing use of CMR for this purpose in clinical studies and for accurate prognostic information (Bingham & Hachamovitch, 2011).

**Table 1-4 Relative Merits of High-Resolution and 3D Perfusion CMR**

High-Resolution Perfusion CMR	3D-Whole Heart Perfusion CMR
Greater detection of subendocardial ischaemia	Assesses true extent of perfusion defects
Less dark rim artefact	High SNR
Similar spatial resolution to LGE imaging	Single selected phase for all slices
Quantitative analysis of TPG	Quantitative assessment of MIB

3D = 3-dimensional; CMR =cardiovascular magnetic resonance; SNR= signal-to-noise ratio; LGE= late-gadolinium enhancement; TPG= transmural perfusion gradient; MIB= myocardial ischaemic burden.

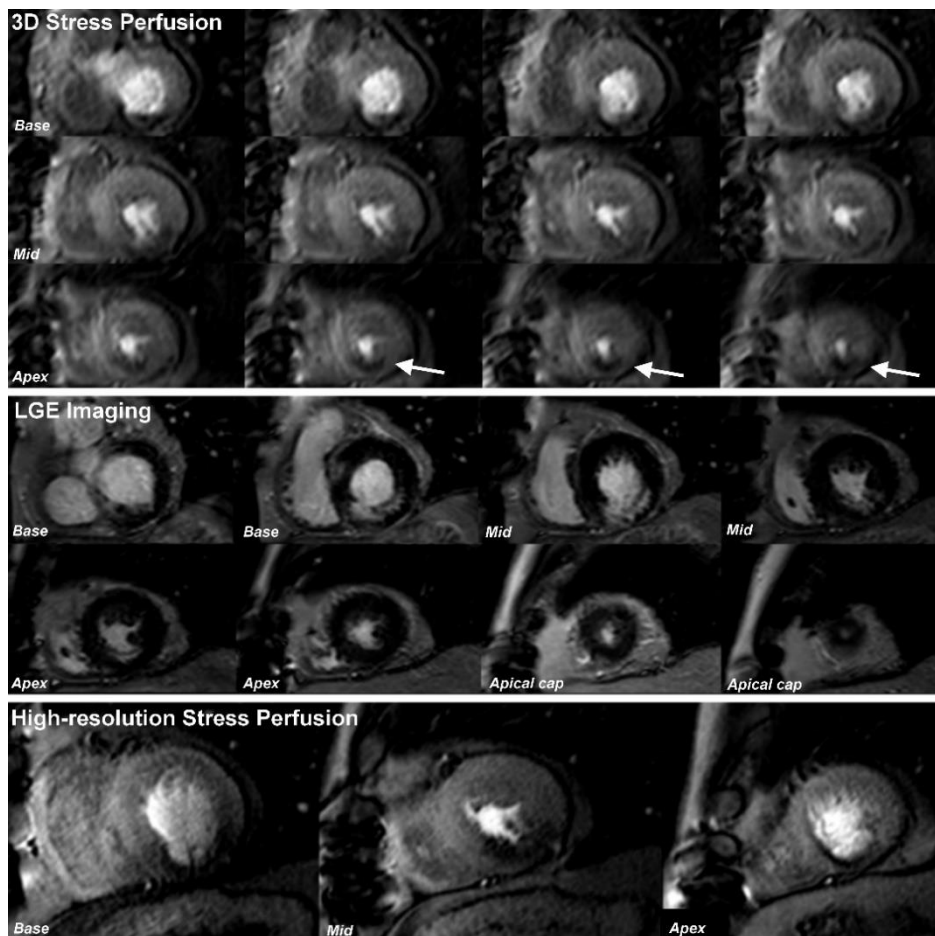


**Figure 1.10 3D versus High-resolution Perfusion CMR - Case 1**

A 62-year-old man with a history of previous bypass surgery 10 years ago, re-presented with increasing angina. The top panel dimensional shows 3D perfusion CMR at stress (2.5mm in-plane resolution, 12 slices); the middle panel shows LGE imaging (1.5mm in-plane resolution) and the bottom panel shows high-resolution stress perfusion CMR (1.1mm in-plane resolution, 3 slices) - all performed on the same patient at 3.0-T. Both 3D perfusion and high-resolution techniques show inferior perfusion defects from base to apex. The benefit of whole-heart coverage with the 3D technique is demonstrated in this case, as hypoperfusion is seen to extend beyond the scar into the apical cap (top panel, arrows) which is not covered by the three-slice high-resolution technique. On the other hand, the perfusion defects and their transmural extent are better delineated with the high-resolution technique particularly at the mid-ventricular level. By virtue of their similar in-plane spatial resolution, it is easier to correlate LGE images with high-resolution perfusion CMR on a per slice basis, compared to the 3D technique.

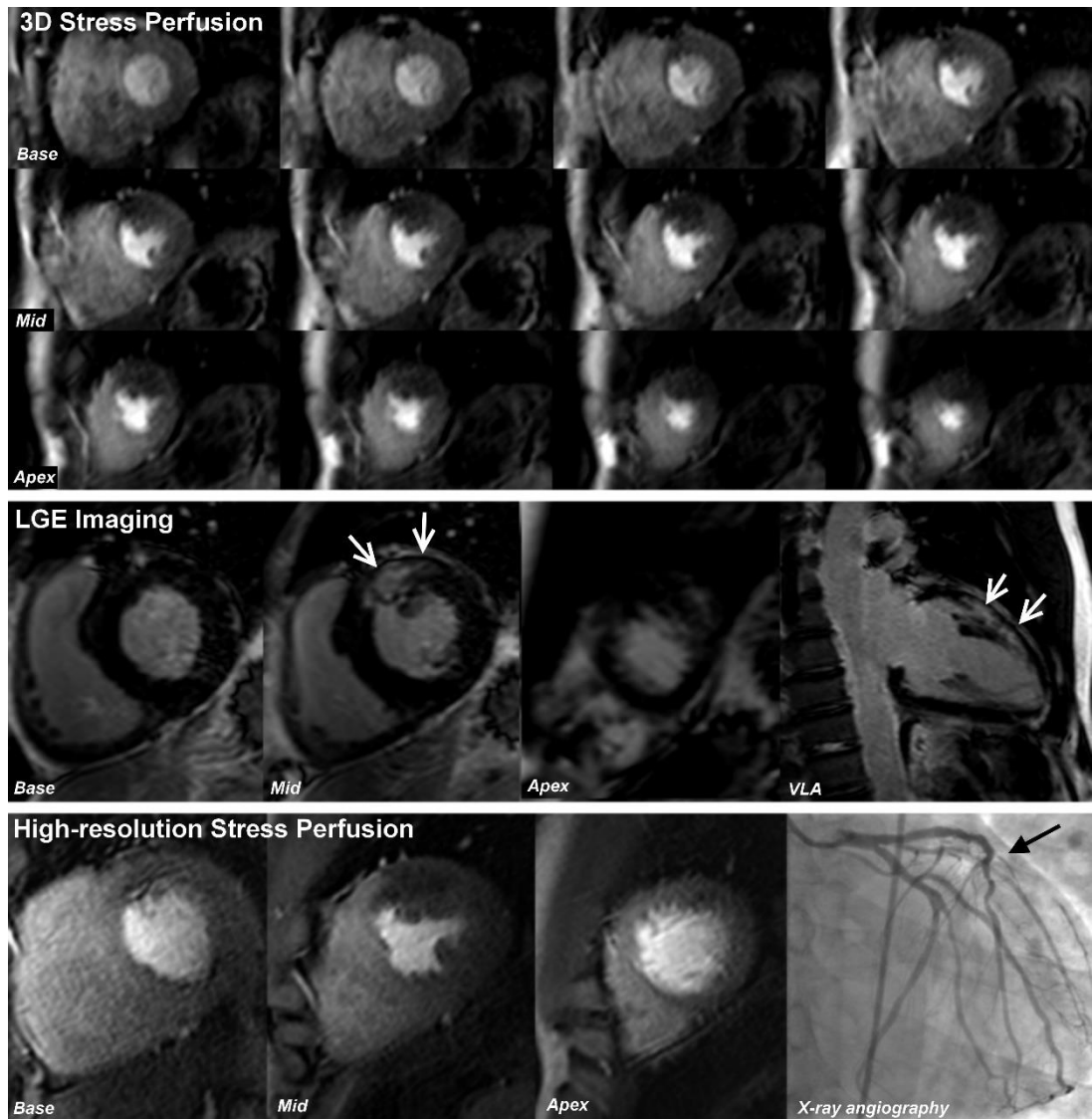


**Figure 1.11 3D versus High-resolution Perfusion CMR - Case 2**

A 45-year-old man with previous PCI to the LAD re-presented with significant angina. The top panel dimensional shows 3D perfusion CMR (12 slices) at stress; the middle panel shows LGE imaging and the bottom panel shows high-resolution (1.1mm in-plane) stress perfusion CMR - all performed at 3.0-T. 3D perfusion CMR shows stress-induced hypo-perfusion throughout the anterior wall from base to apex – i.e. well beyond the area of scar seen in the mid-anterior wall on LGE imaging. This example shows the benefit of whole-heart coverage with the 3D acquisition, as the 3-slice high-resolution techniques did not demonstrate any significant ischaemia beyond the established scar in the mid-ventricle. X-ray angiography confirmed a sub-total occlusion of a large diagonal branch, accounting for the anterior ischaemia (black arrow). VLA=vertical long axis.

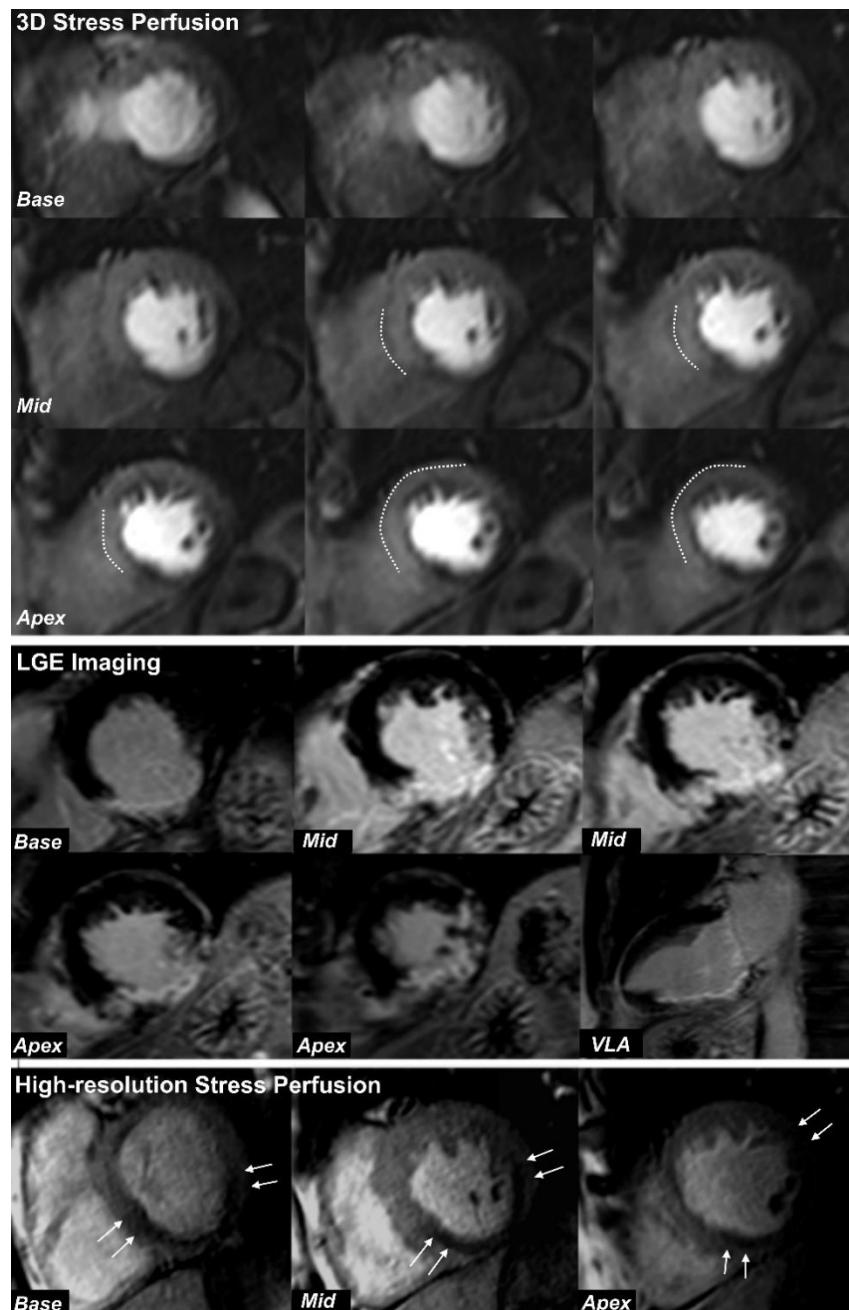


**Figure 1.12 3D versus High-resolution Perfusion CMR - Case 3**

A 57-year-old man presented with worsening angina after a myocardial infarction 6 months ago. The top panel dimensional shows stress 3D perfusion CMR (12 slices); the middle panel shows LGE imaging; and the bottom panel shows high-resolution (1.1mm in-plane) stress perfusion CMR - all performed at 3.0-T. Both 3D perfusion and high-resolution perfusion techniques show an inferior perfusion defect from base to apex consistent with the infarction seen on LGE imaging. However, the perfusion defects are better delineated at high-resolution and a small amount of peri-infarct ischaemia can be seen in each of the 3 slices (arrows) beyond the established scar on corresponding LGE images. With 3D acquisition, the lower spatial resolution (2.5mm in-plane) means that the borders of the perfusion defect within each slice are less distinct and are more difficult to distinguish from dark-rim artefact in the mid to apical anteroseptal regions (endocardial border opposite dashed lines).

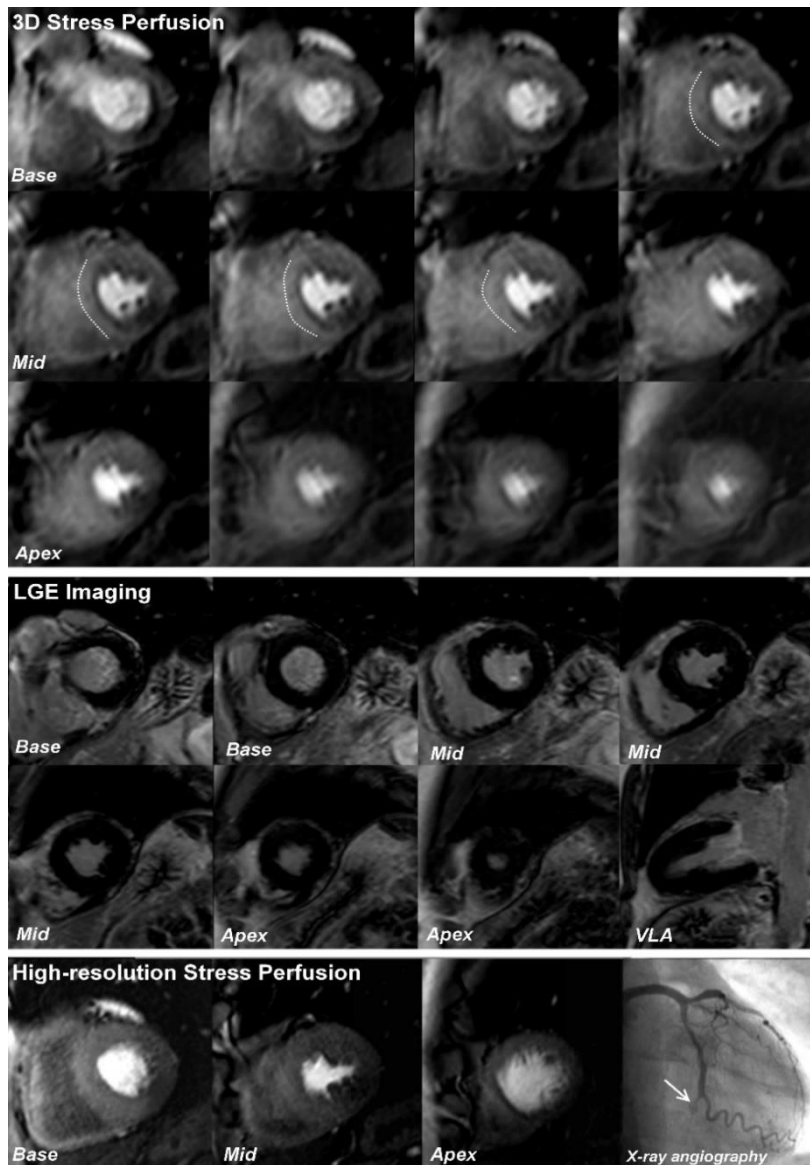


**Figure 1.13 3D versus High-resolution Perfusion CMR - Case 4**

The top panel dimensional shows stress 3D perfusion CMR; the middle panel shows LGE imaging; and the bottom panel shows high-resolution (1.1mm in-plane) stress perfusion CMR - all performed at 3.0T. The 3D technique demonstrated significant stress-induced hypoperfusion in the inferior wall from base to apex and extending into the basal inferolateral segments; but there was also significant dark-rim artefact in the septum (endocardial border opposite dashed lines). X-ray angiography confirmed total occlusion of the mid left circumflex artery (arrow). Due to the sparsity of coverage, the 3-slice high-resolution technique only detected a significant perfusion defect at the mid-ventricular level and therefore significantly underestimated the ischaemic burden in this case, compared to the 3D technique. Additionally, interpretation of the apical high-resolution slice is difficult as it is significantly more diastolic than the other slices, which is a disadvantage of all 2-dimensional acquisitions which employ a single-shot technique. By comparison, with 3D perfusion CMR all slices are acquired at the same point in the cardiac cycle which makes it easier to determine the extent of perfusion defects across different myocardial sections.

## 1.9 Other Advances in Perfusion CMR

### 1.9.1 Perfusion CMR at 3-Tesla

CMR imaging at 3T offers an increased SNR and increased contrast enhancement (Araoz et al., 2005; Gutberlet et al., 2006). Several studies have demonstrated the clinical feasibility of myocardial perfusion CMR at 3T and one direct comparison to 1.5T by Cheng *et al* (n=61) found that 3T perfusion imaging provided a superior diagnostic accuracy in single-vessel (AUC: 0.89 vs. 0.70;  $p < 0.05$ ) and in multi-vessel disease (AUC: 0.95 vs. 0.82;  $p < 0.05$ ) (2007)(Table 1.3).

More recently, a study by Ebersberger *et al* (n=116), compared perfusion CMR at 3T to a clinical routine algorithm in which coronary stenoses exceeding 75% on coronary angiography were deemed pathological and FFR measurements were performed in intermediate lesions (50-75%) (2013). In this study, 3T perfusion CMR provided a consistently high image quality and an excellent diagnostic performance for detecting significant CAD (AUC = 0.93).

In clinical practice, CMR at 3T has in the past been hampered by artefacts related to magnetic field inhomogeneities and dielectric shading as well as restrictions related to local energy deposition (Bernstein et al., 2006). These challenges are largely overcome today, for example with the introduction of multi-transmit radiofrequency magnetic resonance imaging (MRI) techniques which reduce dielectric shading and improve homogeneity of the MRI signal (Willinek et al., 2010).

### **1.9.2 Quantitative Perfusion CMR**

One of the limitations of myocardial perfusion imaging and standard visual interpretation is the dependence on a reference area of normal perfusion. This can be a particular impediment in diffuse or balanced multi-vessel disease, although the high resolution of CMR usually allows the detection of endo-epicardial perfusion gradients as a marker of widespread ischaemia in such instances. The limitations of visual analysis can also be avoided by using absolute quantification of myocardial blood flow (MBF)(Patel et al., 2010). The current clinical reference standard to quantify MBF noninvasively is PET (Knuuti et al., 2009; Uren et al., 1994). Quantitative analysis of myocardial perfusion CMR follows similar principles as quantitative PET, but without exposure to ionizing radiation and with higher in-plane spatial resolution. Following earlier validation in animal models and volunteers, recent clinical studies have demonstrated high diagnostic accuracy of CMR derived estimates of absolute MBF and myocardial perfusion reserve (MPR) against both QCA and FFR (Costa et al., 2007; Lockie et al., 2011; Motwani et al., 2012b; Patel et al., 2010; Futamatsu et al., 2007). A direct comparison of quantitative CMR and PET demonstrated good agreement between the two methods for the measurement of MPR but agreement for absolute MBF values at rest and stress was weaker (Morton et al., 2012).

The scope for quantitative perfusion CMR in clinical practice and cardiovascular research is immense but there remain a number of limitations that currently constrain this advance. The most important of these is a lack of standardisation in image acquisition, contrast dosing protocols, post-processing and mathematical

modelling - but efforts to standardise these are under way. There is also no widely available, validated software for quantitative analysis and therefore research groups generally use different in-house solutions. Recently, several studies have used a dual-bolus method of contrast administration to improve accuracy of the analysis, and there have also been improvements in post-processing using non-rigid registration techniques that allow pixel-by-pixel quantification (Utz et al., 2008; Hsu et al., 2012; Salerno & Kramer, 2013)

### **1.10 Implications of Cardiac Phase on Perfusion CMR**

MBF follows a phasic pattern due to the interaction between myocardium and coronary vessels. As early as 1695, Scaramucci was the first to speculate that cardiac contraction causes a phasic impediment to MBF - and since then micro-angiography techniques have directly observed the compression of intramyocardial vessels confirming this hypothesis (Yada et al., 1993; Hiramatsu et al., 1998; Kassab et al., 1993). In contrast to other organs, coronary arterial inflow is predominantly diastolic when myocardial tension is low, and venous outflow is systolic when myocardial tension is high (Sabsiton Jr & Gregg, 1957). It has been shown that even in distal extramural coronary arteries, virtually no forward flow occurs during systole under physiological conditions (Chilian & Marcus, 1982, 1985; Carew & Covell, 1976; Eckstein et al., 1963; Kajiya et al., 1985). This phasic nature of MBF raises a number of important considerations for perfusion CMR.

Firstly, in perfusion CMR, data acquisition is limited to short windows in the cardiac cycle (typically ~100ms) in order to limit the effects of cardiac motion. As a result,

each of the 3-4 slices obtained with standard 2D perfusion CMR are acquired at different time-points in the cardiac cycle in order to preserve spatial coverage. However, given that MBF is not uniform throughout the cardiac cycle, the impact of a variable phase of acquisition is speculated to affect quantitative estimates of MBF using CMR. This is particularly important given the desire to develop and better standardise quantitative perfusion CMR analysis as discussed above. Notably, a previous volunteer study demonstrated significantly greater stress MBF estimates in diastole than systole (Radjenovic et al., 2010). However, whether these findings exist in disease and whether they have potential diagnostic consequences has not been studied before.

Secondly, the development of 3D perfusion CMR, facilitated by advanced acceleration, now allows for contiguous whole-heart coverage - all in a single cardiac phase which can be freely chosen. However, the optimal cardiac phase for acquisition has yet to be determined or standardised (Shin et al., 2008). Most previous 3D perfusion CMR studies have acquired data in systole but to date it is unknown whether systolic or diastolic acquisition leads to better image quality or diagnostic yield. Mid-diastole is an attractive window for data acquisition as the heart is at its most stationary, but has the disadvantage of being more prone to dark-rim artefact due to partial volume effects (Plein et al., 2007, 2008b) (Kellman & Arai, 2007). End-systole has a shorter quiescent period but on the other hand is less sensitive to R-R variability and arrhythmia (Gharib et al., 2007). Finally, as with 2D perfusion CMR it is unknown whether quantitative estimates of MBF from 3D data demonstrate significant phasic differences and whether these are clinically relevant.

As part of this thesis, we investigate the impact from variable phase of acquisition by utilising novel 2D and 3D pulse sequences to directly compare simultaneous acquisitions of systolic and diastolic perfusion data.

## **1.11 Aims of Thesis**

Perfusion CMR is a highly accurate method for detecting CAD, but is hindered by spatial-temporal constraints. Advanced acceleration techniques have been used to improve spatial resolution, or alternatively achieve 3D whole-heart coverage – but it is not clear which of these alternative strategies offers greater benefit. Acceleration can also be used to simultaneously acquire perfusion data at different time-points in the cardiac cycle. The latter is particularly important as the impact of a variable cardiac phase of acquisition on quantitative estimates of MBF is poorly understood. Accordingly, this thesis includes studies that modify the standard approach to perfusion CMR in order to investigate the relative impact of spatial resolution, spatial coverage and cardiac phase of acquisition on both qualitative and quantitative assessment of ischaemia. We have specifically focused on the following aims and each is dealt with in the subsequent chapters with an appropriate introduction, methods, results and discussion section:

1. To compare the diagnostic accuracy of 2D high-resolution and standard-resolution perfusion CMR in patients with suspected CAD – **[Chapter 2]**.
2. To compare estimates of MIB in patients with angiographic three-vessel CAD using 2D high-resolution and standard-resolution perfusion CMR – **[Chapter 3]**

3. To compare image quality, diagnostic confidence and estimates of MIB by 2D high-resolution and 3D perfusion CMR – **[Chapter 4]**
4. To compare estimates of MBF from quantitative 2D perfusion CMR acquired in systole and diastole; and determine the diagnostic accuracy of both cardiac phases in patients with suspected CAD – **[Chapter 5]**
5. To establish the feasibility of quantitative 3D perfusion CMR for the detection of CAD and to compare systolic and diastolic estimates of MBF – **[Chapter 6]**
6. To determine if quantitative perfusion CMR can accurately track physiological variations in MBF throughout the cardiac cycle – **[Chapter 7]**

## 2 Study 1 - High-resolution Versus Standard-resolution

### Perfusion CMR for the Detection of Coronary Artery Disease

#### 2.1 Abstract

**Background:** Although accelerated high-spatial-resolution perfusion CMR has been shown to be clinically feasible, there has not yet been a direct comparison with standard-resolution methods. We hypothesised that higher spatial resolution detects more subendocardial ischaemia and leads to greater diagnostic accuracy for the detection of CAD. This study compared the diagnostic accuracy of high-resolution and standard-resolution perfusion CMR in patients with suspected CAD.

**Methods and Results:** One-hundred and eleven patients were recruited to undergo two separate perfusion CMR studies at 1.5T, one with standard-resolution (2.5 x 2.5mm in-plane) and one with high-resolution (1.6 x 1.6 mm in-plane) acquisition. High-resolution acquisition was facilitated by eight-fold *k-t* BLAST acceleration. Two observers visually graded perfusion in each myocardial segment on a 4-point scale. Segmental scores were summed to produce a perfusion score for each patient. All patients underwent invasive coronary angiography and CAD was defined as stenosis  $\geq$  50% luminal diameter (quantitative coronary angiography). CMR data were successfully obtained in 100 patients. In patients with CAD ( $n=70$ ), more segments were determined to have subendocardial ischaemia with high-resolution than with standard-resolution acquisition (279 vs.108;  $p<0.001$ ). High-resolution acquisition had a greater diagnostic accuracy than standard-resolution for identifying single-

vessel disease (area under the curve [AUC]: 0.88 vs. 0.73;  $p < 0.001$ ) or multi-vessel disease (AUC: 0.98 vs. 0.91;  $p = 0.002$ ) and overall (AUC: 0.93 vs. 0.83;  $p < 0.001$ ).

**Conclusions:** High-resolution perfusion CMR has greater overall diagnostic accuracy than standard-resolution acquisition for the detection of CAD in both single and multi-vessel disease and detects more subendocardial ischaemia.

## 2.2 Introduction

Myocardial perfusion imaging with CMR is a highly accurate method of detecting significant CAD in single and multi-vessel disease (Schwitter et al., 2008; Sakuma et al., 2005; Greenwood et al., 2012). Recent comparative studies have suggested a higher diagnostic accuracy of CMR compared with SPECT (Greenwood et al., 2012). This increase in accuracy is thought to relate in part to the higher spatial resolution of CMR (typically 2-3 mm versus 5-10 mm).

With recently developed spatio-temporal undersampling methods such as *k-t* BLAST and *k-t* SENSE, the in-plane spatial resolution of perfusion CMR can be improved further, from 2-3 mm to 1-2 mm (Tsao et al., 2003). The feasibility and clinical applicability of high-resolution perfusion CMR has been demonstrated in a number of studies (Gebker et al., 2007b; Plein et al., 2008a, 2008b; Maredia et al., 2010); but to date only one small-scale study in volunteers has directly compared high-resolution and standard-resolution acquisition. In their study, Maredia et al demonstrated a reduction in endocardial dark rim artefact and improved image quality of high-resolution perfusion images (Maredia et al., 2010).

We hypothesised that in patients with CAD, high-spatial-resolution perfusion CMR would improve detection of subendocardial ischaemia and thus the overall diagnostic accuracy compared with standard-resolution perfusion CMR.

## **2.3 Methods**

### **2.3.1 Population**

A total of 111 patients with suspected CAD were recruited. Each patient's pre-test probability of CAD was calculated based on their age, sex and symptoms (Diamond & Forrester, 1979). All had undergone or were scheduled to undergo diagnostic coronary angiography within the previous/next 30 days as part of routine clinical care. No coronary intervention or clinical events occurred between angiography and recruitment. Exclusion criteria were contra-indications to CMR, adenosine or gadolinium contrast agents; a history of recent (within 6 months) myocardial infarction or unstable angina; or poorly controlled arrhythmias. Patients were instructed to refrain from caffeine for 24hrs prior to their CMR study but continue cardiac medications as normal. All patients gave written consent to participate and the study was approved by the regional ethics committee.

### **2.3.2 CMR protocol**

Studies were carried out on a 1.5T CMR system (Philips Healthcare, Best, The Netherlands) using a five-element cardiac phased array receiver coil for signal reception. All patients underwent two CMR studies on separate days within 4 weeks. For each patient, both scans were performed before or after coronary angiography. On one occasion, a 'standard' perfusion pulse sequence was used, and on the other a high-resolution method accelerated with *k-t* BLAST was employed. The order of methods was randomly chosen.

For both techniques, perfusion data was acquired in 3 short-axis slices (basal, mid and apical) in each R-R interval. The standard pulse sequence was a saturation recovery gradient echo method accelerated with SENSE (acceleration factor 2, half Fourier sampling, partial echo, repetition time (TR) 2.7 ms, echo time (TE) 1.0 ms, flip angle 15°, image acquisition time per slice 136 ms, single saturation pre-pulse per R-R interval shared over three slices, matrix 144 x 144, median field of view (FOV) 360 mm, 2.5 x 2.5 mm in-plane spatial resolution). The high-resolution pulse sequence used a similar saturation recovery gradient echo method, but was accelerated with *k-t* BLAST (acceleration factor 8 with 11 training profiles, no partial Fourier or partial echo acquisition, TR 3.4 ms, TE 1.7ms, flip angle 15°, one saturation pre-pulse per slice, image acquisition time per slice 103 ms, matrix 192 x 192, median FOV 310 mm, and 1.6 x 1.6 mm in-plane spatial resolution).

For both studies, stress perfusion commenced after 4 minutes of an intravenous adenosine infusion (140 mcg/kg/min), during an intravenous bolus injection of dimeglumine gadopentetate (Magnevist®, Schering AG, West Sussex, UK) and a 15ml saline flush delivered at 5ml/s while the patient held their breath in end-expiration. For the standard-resolution method, a contrast agent dose of 0.05mmol/kg bodyweight was used during perfusion data acquisition as in previous studies with this pulse sequence (Greenwood et al., 2012). In order to compensate for the lower signal-to-noise ratio associated with the smaller voxel size, a contrast agent dose of 0.1mmol/kg bodyweight was used for the high-resolution method, consistent with previous reports (Plein et al., 2008b, 2007; Manka et al., 2010). Rest perfusion imaging was performed 15mins later using identical imaging parameters.

Late gadolinium enhanced imaging (LGE) was performed in all patients on their first visit using conventional methods (1.6 x 1.6 mm in-plane spatial resolution) with a cumulative contrast agent dose of 0.2mmol/kg bodyweight (the same for both protocols) (Kramer et al., 2008). During standard-resolution perfusion CMR scans, this cumulative dose was achieved by administration of an additional bolus of 0.1mmol/kg bodyweight of contrast agent immediately following rest perfusion.

### **2.3.3 CMR analysis**

CMR images were interpreted in random order by 2 observers (S.P., M.M; 10 years and 1 year experience in CMR) acting in consensus and blinded to all clinical information (QMASS 6.1.6 , Medis, Leiden, The Netherlands). Visual analysis used a 16-segment American Heart Association (AHA) model (Cerqueira et al., 2002). Perfusion in a segment was considered abnormal if signal intensity was reduced compared with remote myocardial segments or an endocardial to epicardial perfusion gradient within a segment was present (Plein et al., 2008a). Additionally, any perfusion defect was required to persist longer than the contrast media first-pass to distinguish it from artefact. Corresponding LGE images were reviewed side-by-side with the perfusion data. Perfusion defects present at stress but not rest and occurring outside any hyperenhanced myocardial tissue on LGE images were considered as inducible defects according to the Duke algorithm (Klem et al., 2006). Perfusion in each myocardial segment was graded on a 4-point scale (transmural ischaemia index) from 0-3 (0 = normal, 1 = inconclusive, 2 = subendocardial defect, 3 = transmural defect). All segmental scores were summed to produce a perfusion score (0-48) for each patient. In addition, perfusion scores were calculated for the

left anterior descending (LAD), left circumflex (LCX) and right coronary artery (RCA) territories according to the 16-segment AHA model adjusted for arterial dominance (Cerqueira et al., 2002; Marie et al., 1993). Image quality was graded 1-4 (1 = unusable, 2 = poor, 3 = adequate, 4 = excellent) by consensus of the two observers. Occurrence of artefacts related to *k-t* reconstruction, respiratory motion, electrocardiographic gating, and endocardial dark rim artefact was scored between 0 and 3 (0 = none, 1 = minor, 2 = moderate, 3 = severe). Dark rim artefacts were recorded if an endocardial dark rim appeared at the arrival of contrast in the left ventricular (LV) cavity and prior to contrast arrival in the myocardium (Figure 1.4). Where present, the maximum width of dark rim artefact was measured with electronic callipers at standardized window settings.

### **2.3.4 Quantitative coronary angiography**

Quantitative coronary angiography (QCA) was performed (QCAPlus, Sanders Data Systems, Palo Alto, California, USA) on all X-ray angiography images by an experienced observer blinded to clinical and CMR data (M.M.; 6 years of experience in coronary angiography). Each myocardial segment was ascribed a coronary artery territory according to the standard AHA 16-segment model adjusted for arterial dominance (Cerqueira et al., 2002; Marie et al., 1993). Significant CAD was defined angiographically as stenosis  $\geq 50\%$  diameter in any of the main epicardial coronary arteries or their branches with a diameter of  $\geq 2\text{mm}$ .

### **2.3.5 Statistical analysis**

Analysis was performed using SPSS 17.0 (SPSS, Chicago, IL, USA). Data are presented as mean  $\pm$  SD. Group means were compared using the paired Student *t* test. Ordinal

data were compared using Chi-square or Wilcoxon signed-rank tests as appropriate. All statistical tests were two-tailed and a p value <0.05 was considered significant. Receiver operating characteristic (ROC) analysis was performed on a per patient basis using summed perfusion scores to determine the diagnostic accuracies of standard and high-resolution acquisition to detect coronary stenosis of  $\geq 50\%$  on QCA. A secondary analysis, using a stenosis severity of  $\geq 70\%$  was also performed. Optimal perfusion score cut-off values were determined as the values that maximized the sum of sensitivity and specificity. Diagnostic accuracies are presented as areas under the curve (AUCs) and compared using the methods described by DeLong and DeLong (DeLong et al., 1988). The study was designed to have a statistical power of 80% to detect a 10% difference in AUC with an alpha level of 0.05. Sensitivity, specificity and positive/negative predictor values were also calculated for each technique but these values were not directly compared as the study was not statistically powered for such analyses (Eng, 2003).

## **2.4 Results**

### **2.4.1 Study population**

A total of 111 patients were enrolled in the study. In 5 patients, both standard and high-resolution CMR scans could not be completed (3 patients were claustrophobic and 2 patients declined to return for a second visit). Three patients successfully completed both scans but X-ray angiography was cancelled for clinical reasons unrelated to the CMR findings. Three patients had to be excluded due to technical problems on either one of their visits. Therefore, 100 patients (90% of the cohort)

were included in the final analysis and all images were of analysable quality. Clinical details of the 100 study patients (74% men, mean age  $61 \pm 7$  yrs) are summarised in Table 2.1.

**Table 2-1 Patient Characteristics**

\*Pre-test likelihood of CAD is expressed as median % (interquartile range);

<b>Parameter</b>	<b>Data (n=100)</b>
<b>Age (yrs <math>\pm</math> SD)</b>	<b>61 <math>\pm</math> 7</b>
<b>Male, n (%)</b>	74 (74)
<b>Medical history, n (%)</b>	
Hypertension	67 (67)
Hypercholesterolemia	65 (65)
Diabetes Mellitus	18 (18)
Smoking	42 (42)
Family history of CAD	37 (37)
Previous MI	12 (12)
Previous PCI	8 (8)
Atrial Fibrillation	2 (2)
<b>LV Ejection Fraction , %</b>	58 $\pm$ 9
<b>Pre-test likelihood of CAD,% (IQR)*</b>	51 (31-65)
<b>Presenting cardiac symptoms, n (%)</b>	
Non-anginal chest pain	22 (22)
Atypical angina	37 (37)
Typical angina	32 (32)
Dyspnoea	9 (9)
<b>Angiography findings, n (%) **</b>	
No significant disease	30 (30)
One-vessel disease	32 (32)
Two-vessel disease	14 (14)
Three -vessel disease	24 (24)
LAD disease	46 (46)
LCX disease	42 (42)
RCA disease	43 (43)

\*\*Significant CAD defined as coronary stenosis  $\geq 50\%$  on QCA.

CAD = coronary artery disease; IQR = interquartile range; MI = myocardial infarction; PCI = percutaneous coronary intervention

QCA confirmed significant CAD in 70 patients (70%). Thirty-two patients (32%) had single-vessel disease and 38 patients (38%) had multi-vessel disease (two or three vessel disease) (Table 2.1). In terms of anatomic location of coronary artery stenoses, 46 patients (46%) had significant LAD stenoses, 42 patients (42%) had significant LCX stenoses and 43 patients (43%) had significant RCA stenoses. Typical examples of patients with ischaemia are shown in Figures 1.5 and 2.1. The hemodynamic stress response achieved with adenosine during standard and high-resolution imaging was similar (rate-pressure product, mmHg x beats/min:  $10262 \pm 2491$  vs.  $10247 \pm 2279$ ;  $p=0.90$ ). All patients were in sinus rhythm and heart rate allowed acquisition at each R-R interval in all. All 12 patients with a clinical history of MI but no additional patients had evidence of hyperenhancement on LGE imaging.

#### **2.4.2 Detection of CAD**

The diagnostic accuracy (AUC) of standard-resolution perfusion CMR for the detection of CAD  $\geq 50\%$  was 0.83 (Table 2.2, Figure 2.2). The optimal perfusion score cut-off value was determined as  $\geq 4$ , which resulted in a sensitivity and specificity of 84% and 73% respectively (Table 2.3).

The diagnostic accuracy of high-resolution perfusion CMR to detect CAD  $\geq 50\%$  was significantly higher with an AUC of 0.93 ( $p<0.001$ ) (Table 2.2, Figure 2.2). The optimal perfusion score cut-off value was also  $\geq 4$  with this technique, which resulted in a sensitivity and specificity of 91% and 80% respectively (Table 2.3). Similar diagnostic performance was seen using a CAD threshold  $\geq 70\%$  and the diagnostic accuracy of high-resolution perfusion CMR remained significantly higher than standard-resolution acquisition (AUC:0.92, 95% CI 0.87-0.97 vs 0.83, 95% CI 0.75-91;  $p<0.001$ ).

The statistical power for the comparison of AUCs was 0.93 (alpha 0.05, beta 0.07) (Hanley & McNeil, 1983).

The diagnostic performance of high-resolution acquisition to detect CAD  $\geq$  50% was significantly greater than standard-resolution for both single-vessel disease (AUC: 0.88 vs. 0.73;  $p < 0.001$ ) and multi-vessel disease (AUC: 0.98 vs. 0.91;  $p = 0.002$ ) (Table 2.2).

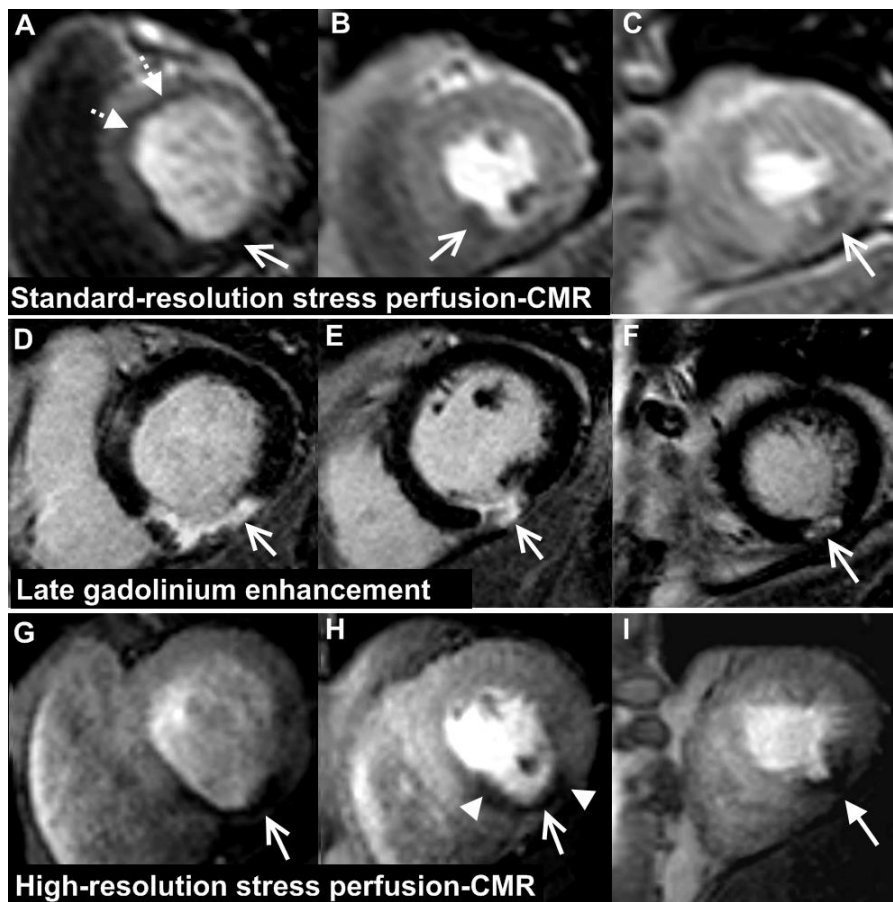


**Figure 2.1 Case Example: Standard vs. High-Resolution Perfusion CMR**

An inferior scar with thinning of the myocardium is seen in all images (open arrows, A-I). Dark-rim artifact seen on the basal slice (dashed arrows, A) at standard-resolution (2.5mm in-plane spatial resolution) is not present at high-resolution (G). By virtue of their identical spatial-resolution, LGE imaging and high-resolution perfusion-CMR allow for a better correlation between scar and perfusion than LGE imaging and standard resolution perfusion-CMR. An area of peri-infarct ischemia (small arrows, H) is therefore more clearly identified at high-resolution. In this patient, coronary angiography showed a chronic total occlusion of the right coronary artery and the patient's symptoms were relieved by subsequent PCI.

**Table 2-2 Diagnostic Accuracy of Standard-resolution and High-resolution perfusion CMR for the Detection of CAD**

Area Under Receiver-Operator Characteristic Curve			
	Standard-resolution	High-resolution	p value
<b>Overall</b>	0.83 (0.75-0.91)	0.93 (0.88-0.98)	<0.001
<b>Single-vessel disease</b>	0.73 (0.60-0.86)	0.88 (0.79-0.97)	<0.001
<b>Multi-vessel disease</b>	0.91 (0.83-0.99)	0.98 (0.95-1.00)	0.002
<b>LAD disease</b>	0.81 (0.71-0.90)	0.92 (0.86-0.97)	<0.001
<b>LCX disease</b>	0.73 (0.64-0.83)	0.87 (0.79-0.94)	<0.001
<b>RCA disease</b>	0.81 (0.72-0.90)	0.88 (0.81-0.95)	0.08

Values expressed as mean (95% confidence interval). CAD defined as stenosis  $\geq 50\%$ .

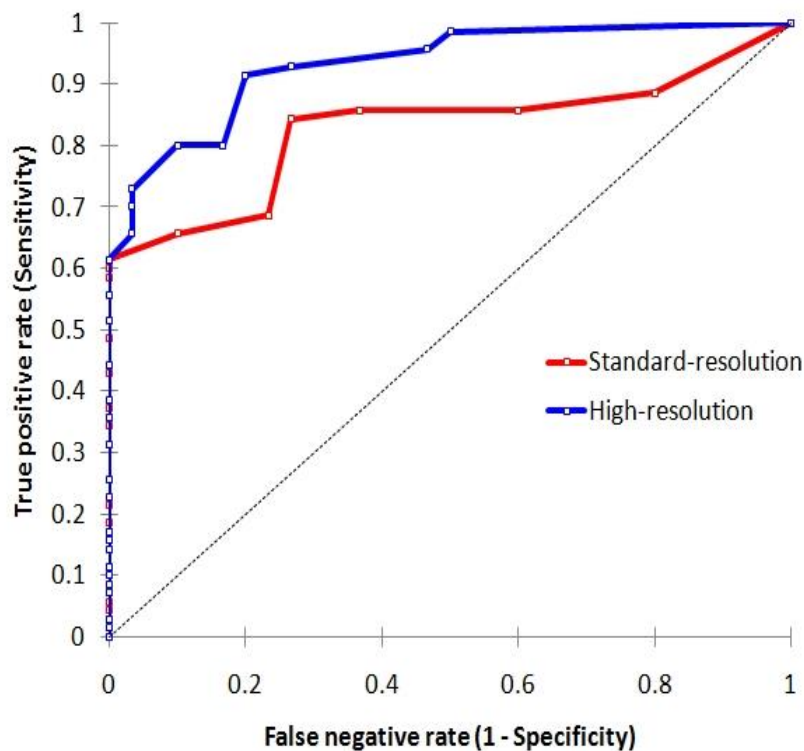


**Figure 2.2 ROC Curves: Standard-resolution vs High-resolution Perfusion CMR**

Standard and high-resolution perfusion CMR both had a high diagnostic accuracy for the detection of CAD ( $\geq 50\%$  stenosis) but the high-resolution technique was superior. The areas under the curve were 0.83 for standard-resolution and 0.93 for high-resolution ( $p < 0.001$ ).

**Table 2-3 Sensitivity, Specificity and Predictive values for Standard-resolution and High-resolution perfusion CMR for the detection of CAD**

	Standard-resolution	High-resolution
<b>Overall</b>		
Sensitivity, %	84 (74-91)	91 (82-96)
Specificity, %	73 (55-86)	80 (62-91)
PPV, %	88 (77-94)	91 (82-96)
NPV, %	67 (48-82)	80 (61-92)
<b>Single-vessel disease</b>		
Sensitivity, %	78 (61-89)	88 (71-96)
Specificity, %	73 (55-86)	80 (62-91)
PPV, %	76 (57-88)	82 (65-93)
NPV, %	76 (56-89)	86 (67-95)
<b>Multi-vessel disease</b>		
Sensitivity, %	84 (69-93)	95 (82-99)
Specificity, %	93 (73-97)	97 (82-100)
PPV, %	91 (76-98)	97 (85-99)
NPV, %	82 (64-93)	94 (78-99)

Values are expressed as percentage (95% confidence interval) and are quoted at optimal perfusion score cut-off thresholds (determined by receiver-operator curve analysis). Coronary artery disease defined as  $\geq 50\%$  stenosis. PPV = positive predictive value; NPV = negative predictive value.

### 2.4.3 Detection of anatomic location of CAD

High-resolution acquisition had a significantly higher diagnostic accuracy than standard-resolution in the LAD and LCX territories for the detection of CAD  $\geq 50\%$  (AUC: LAD 0.92 vs. 0.81, LCX 0.87 vs. 0.73; both p values  $< 0.001$ ). Differences for the

RCA territory did not reach statistical significance (AUC: 0.88 vs. 0.80;  $p=0.08$ ) (Table 2.2).

In single-vessel disease ( $n=32$ ), both standard and high-resolution imaging identified perfusion defects in only one territory in a similar number of patients (25 [78%] vs. 27 [84%];  $p=0.75$ ). However, in multi-vessel disease, high-resolution imaging identified perfusion defects in more than one territory in significantly more patients than standard resolution (32 [84%] vs. 23 [61%];  $p = 0.04$ ).

#### **2.4.4 Subendocardial ischaemia**

Using the 16-segment model, 1120 myocardial segments were available from the 70 patients with CAD for further analysis. With high-resolution acquisition, significantly more segments were determined as having subendocardial ischaemia (transmural index score of 2) than with standard-resolution (279 vs. 108;  $p<0.001$ ); and there was a significant reduction in the number of segments determined as being normal (692 vs. 831;  $p<0.001$ ) or inconclusive (47 vs. 70;  $p= 0.04$ ) (Figure 2.3). By contrast, the number of segments assessed as having transmural ischaemia was similar with both techniques (102 vs. 111;  $p =0.56$ ).

#### **2.4.5 Image quality**

Overall image quality (median score = 3 for both;  $p =0.58$ ) and artefact score (median score = 0 for both;  $p = 0.10$ ) were similar for both standard and high-resolution techniques. However, dark rim artefact was significantly less frequent with high-resolution (8% vs. 30 %;  $p<0.001$ ) and when it did occur it was less marked than with standard-resolution ( $1.7 \pm 0.3$  vs.  $3.3 \pm 0.8$  mm;  $p<0.001$ ). Fifteen high-resolution

data sets (15%) were affected by *k-t* reconstruction artefacts at stress and/or rest due to respiratory motion – but this did not affect myocardial contrast passage and generally occurred at the end of a breath-hold.

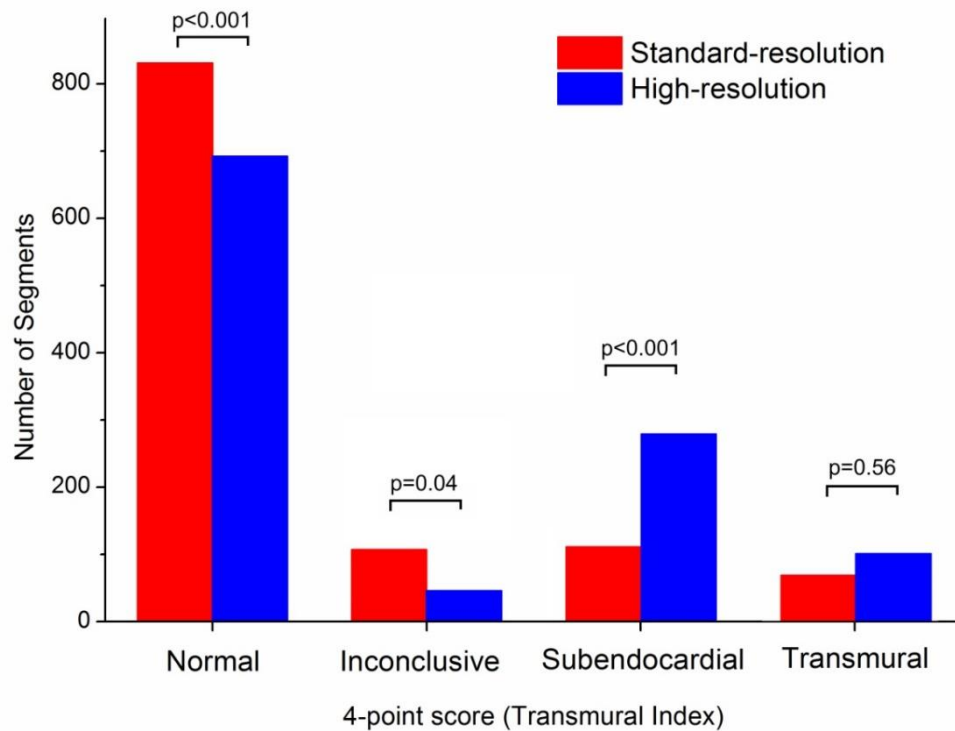


**Figure 2.3 Distribution of Transmural Ischaemia Index**

*In patients with coronary artery disease (≥50% stenosis), high-resolution perfusion CMR determined significantly more segments as having subendocardial ischaemia than the standard resolution technique; and fewer as normal or inconclusive.*

## 2.5 Discussion

This study has demonstrated a high diagnostic accuracy for both standard and high-resolution perfusion CMR. However, the high-resolution technique outperformed the standard-resolution technique with greater diagnostic accuracy in single-vessel

disease, multi-vessel disease and overall. In particular, high-resolution acquisition was better at distinguishing a multi-vessel pattern of disease. These benefits are likely to be derived from better detection of subendocardial ischaemia at greater spatial resolution. Our findings may therefore have important implications for the non-invasive assessment of myocardial ischaemia and for defining the role of high-resolution perfusion CMR in current clinical practice.

CMR perfusion imaging requires rapid data acquisition, which necessitates a trade-off between spatial resolution, temporal resolution, SNR and spatial coverage. *k-t* BLAST exploits correlations in time and space to accelerate data acquisition and the speed-up afforded can be used to improve spatial resolution with relatively preserved SNR (Motwani et al., 2011; Kozerke & Plein, 2008; Plein et al., 2008a). Although the clinical feasibility of *k-t* BLAST and similar acceleration techniques such as *k-t* SENSE have been demonstrated, their advantages over commonly used standard-resolution methods has not been defined in a clinical setting (Gebker et al., 2007b; Plein et al., 2008a, 2008b; Maredia et al., 2010). In particular there has been no previous direct comparison between standard and high-resolution techniques in a patient population.

In this study, the overall diagnostic accuracy of standard-resolution perfusion CMR for detecting angiographically defined CAD was within the range of previous studies with an AUC of 0.83 compared to 0.86 by Schwitter et al, 0.78 by Cheng et al and 0.89 in the perfusion analysis of the CE-MARC study (2008; 2007; Greenwood et al., 2012). Similarly, the overall diagnostic accuracy of high-resolution perfusion CMR

was within the range of previous studies using *k-t* SENSE or *k-t* BLAST with an AUC of 0.93 compared to 0.94 by Manka et al and 0.85 by Plein et al (2010; 2008a).

We speculate that the demonstrated superiority of high-resolution acquisition relates to a better specificity due to reduction in subendocardial dark rim artefacts and a greater sensitivity due to better detection of subendocardial ischaemia (Table 2.3). Previous work investigating dark rim image artefacts has shown the prominent role of spatial resolution on the occurrence and extent of this artefact (Plein et al., 2007; Di Bella et al., 2005). The significant reduction in both frequency and severity of dark rim artefact with high-resolution acquisition seen in this study confirms similar findings in a previous volunteer study (Maredia et al., 2010).

In this study, high-resolution perfusion CMR detected more segments with subendocardial ischaemia than the standard-resolution method. The two possible explanations for this observation are that standard-resolution acquisition failed to detect subendocardial ischaemia in some patients or that high-resolution acquisition over-estimated ischaemia in normal segments. Without an available reference standard for determining subendocardial ischaemia this question cannot be conclusively resolved. However, given that the overall diagnostic accuracy for detection of CAD was significantly better with high-resolution than standard-resolution, the more plausible explanation is that high-resolution acquisition leads to better detection of subendocardial ischaemia. As well as the benefits this provides in typical CAD detection, high-resolution perfusion CMR could potentially provide an improved tool for the evaluation of conditions where there are microvascular perfusion abnormalities at the subendocardial level, such as

syndrome X, hypertensive heart disease or hypertrophic cardiomyopathy (Stanton & Marwick, 2010).

In this study, contrast agent dose was optimised for visual analysis. However, quantitative methods for the estimation of myocardial blood flow (MBF) based on myocardial perfusion CMR data have been validated in animal models and applied to clinical studies (Christian et al., 2004; Costa et al., 2007; Patel et al., 2010). High-resolution perfusion CMR offers further intriguing opportunities for quantitative analysis such sharper delineation of transmural perfusion gradients (Hautvast et al., 2011). However, the algorithms applied for the reconstruction of high-resolution perfusion CMR data acquired with spatio-temporal undersampling methods give rise to a degree of low-pass temporal filtering, posing additional challenges to quantitative assessment. Recent developments such as *k-t* Principal Component Analysis are likely to overcome some of these challenges and will require evaluation in future studies (Pedersen et al., 2009).

One of the limitations of myocardial perfusion imaging and visual analysis is the dependence on a reference area of normal perfusion. This is a particular impediment in diffuse or multi-vessel disease –the group of patients who are at greatest risk and would benefit most from accurate diagnosis and correct risk-stratification (Emond et al., 1994). The ability of high-resolution perfusion CMR to adequately resolve subendocardial ischaemia and transmural perfusion gradients should therefore be a major advantage as it reduces the need for an intra-patient comparison. Our study demonstrated this advantage as 84% of patients with multi-vessel disease were correctly identified as having perfusion defects in more than one territory compared

to only 61% with standard-resolution. This finding is of considerable significance as the assessment of multi-vessel disease has long been recognised as a weakness of myocardial perfusion imaging. With SPECT, as few as 29% of patients with known angiographic three-vessel disease (3VD) are recognised as having inducible perfusion abnormalities in all three coronary artery territories (Christian et al., 1992). Similarly, in the only study that has evaluated standard-resolution perfusion CMR specifically in the setting of angiographic 3VD, the detection of a 3VD pattern was only 57% (Chung et al., 2010). Therefore, the demonstrated ability of high-resolution acquisition to more accurately identify the extent of ischaemia in multi-vessel disease may represent a significant step-forward in non-invasive imaging with potential implications for correctly stratifying and managing this high-risk group.

## **2.6 Study limitations**

*k-t* BLAST adds complexity to the acquisition of perfusion data. In particular, the method is sensitive to respiratory motion and cardiac arrhythmia. In our study, respiratory artefacts affected 15% of high-resolution studies which is similar to previous studies (Plein et al., 2008b, 2008a). For this reason image quality and artefact scores for both techniques were similar, despite the significant reduction of dark rim artefact seen at high-resolution. Newer spatio-temporal undersampling methods for high-resolution acquisition are less susceptible to respiratory motion but were not available at the time of this study (Pedersen et al., 2009). Potentially these techniques could offer the demonstrated benefits of high-resolution

acquisition without the respiratory artefact trade-off - but this is yet to be investigated.

This study was powered to detect a difference in overall diagnostic performance as defined by the AUC of ROC analysis, but not to compare individual sensitivity or specificity values in a dichotomous model as this would have required a very large sample size (Eng, 2003). Such large comparative studies pose considerable logistic challenges and are unlikely to be conducted for incremental optimisations of an established imaging test such as perfusion CMR. The presented diagnostic accuracies must also be interpreted within the context of referral bias as all patients had been clinically preselected for coronary angiography. We also acknowledge that because transmural ischaemic index can only be assessed at a segmental level, data clustering may affect the analysis of its distribution - but as each patient contributed the same number of segments, the presented estimates remain valid.

Finally, similar to the majority of previous perfusion CMR studies, another limitation was the use of X-ray coronary angiography to determine the presence of significant CAD as this only provides an anatomical rather than functional assessment of a coronary artery stenosis. However, X-ray coronary angiography remains the most widespread investigation in clinical-decision making and thus relates this study to real-world practice.

## **2.7 Conclusions**

This study showed that accelerated, high-resolution perfusion CMR imaging has higher diagnostic accuracy than standard-resolution acquisition for the detection of CAD in both single and multi-vessel disease. Dark rim artefact is reduced and the extent of multi-vessel disease is better identified at high-resolution. High-spatial-resolution perfusion CMR may also provide an improved tool for identifying subendocardial ischaemia.

### 3 Study 2 - Assessment of Myocardial Ischaemic Burden in Angiographic Three-Vessel Coronary Artery Disease Using High-Resolution Perfusion CMR

#### 3.1 Abstract

**Aims:** This study compared the myocardial ischaemic burden (MIB) in patients with angiographic three-vessel CAD (3VD) using high-resolution and standard-resolution perfusion CMR imaging.

**Methods:** 105 patients undergoing coronary angiography had two separate stress/rest perfusion CMR studies, one with standard-resolution (2.5 mm in-plane) and one with high-resolution (1.6 mm in-plane). Quantitative coronary angiography (QCA) was used to define patients with angiographic 3VD. Perfusion CMR images were anonymised, randomly ordered and visually reported by 2 observers acting in consensus and blinded to all clinical and angiographic data. Perfusion was graded in each segment on a 4-point scale and summed to produce a perfusion score and estimate of MIB for each patient.

**Results:** In patients with angiographic 3VD (n=35), high-resolution acquisition identified more abnormal segments ( $7.2 \pm 3.8$  vs.  $5.3 \pm 4.0$ ;  $p=0.004$ ) and territories ( $2.4 \pm 0.9$  vs.  $1.6 \pm 1.1$ ;  $p=0.002$ ) and a higher overall perfusion score ( $20.1 \pm 7.7$  vs.  $11.9 \pm 9.4$ ;  $p<0.0001$ ) per patient compared to standard-resolution. The number of segments with subendocardial ischaemia was greater with high-resolution acquisition (195 vs. 101;  $p<0.0001$ ). Hypoperfusion in all three territories was

identified in 57% of 3VD patients by high-resolution compared to only 29% by standard-resolution ( $p=0.04$ ). The area-under-curve (AUC) for detecting angiographic 3VD using the estimated MIB was significantly greater with high-resolution than standard-resolution acquisition (AUC=0.90 vs. 0.69;  $p<0.0001$ ).

**Conclusion:** In patients with angiographic 3VD, the ischaemic burden detected by perfusion CMR was greater with high-resolution acquisition due to better detection of subendocardial ischaemia. High-resolution perfusion CMR may therefore be preferred for risk stratification and management of this high-risk patient group.

## 3.2 Introduction

Three-vessel CAD (3VD) is found in approximately 9% of patients undergoing elective coronary angiography and these patients have a considerably poorer prognosis than those with less extensive disease (Emond et al., 1994). Detection of 3VD with non-invasive imaging can be challenging due to the effects of balanced ischaemia leading to false-negative results in up to 20% of cases (Christian et al., 1992; Martin et al., 1992). This limitation has been well-documented with SPECT, and although its overall sensitivity for detecting CAD in multi-vessel disease is 80-95%, it often only detects perfusion defects in one territory (Christian et al., 1992; Mahmorian et al., 1990; DePasquale et al., 1988). In one SPECT study, inducible perfusion abnormalities in all three territories were identified in only 12% of patients with known angiographic 3VD (Chung et al., 2010).

Myocardial perfusion imaging with CMR is a highly accurate method for the detection of significant CAD (Schwitter et al., 2008; Sakuma et al., 2005; Greenwood et al., 2012). One of the major advantages of perfusion CMR compared to SPECT is its higher spatial resolution (typically 2-3mm versus 8-10mm). Balanced ischaemia can lead to diffuse subendocardial hypoperfusion and although there are few comparisons between perfusion CMR and SPECT in 3VD, it is expected that the higher resolution of CMR can better resolve the transmural perfusion gradient in balanced ischaemia and thereby potentially improve the detection of 3VD (Bache & Schwartz, 1982). With recently developed spatio-temporal undersampling methods such as *k-t* BLAST, the spatial resolution of perfusion CMR can be improved further to under 2 mm (Tsao et al., 2003).

Several studies have demonstrated the feasibility and accuracy of high-resolution perfusion CMR (Plein et al., 2008a, 2008b; Manka et al., 2010; Lockie et al., 2011; Motwani et al., 2012a). In a direct comparison, we have previously shown that high-resolution perfusion CMR has a higher overall diagnostic accuracy compared to standard-resolution imaging in patients with suspected CAD. This previous study included a small subset of patients with multi-vessel disease (Motwani et al., 2012a). The present study aims to compare the distribution of and extent of ischaemia in patients with 3VD detected by both techniques and tests the hypothesis that improved performance of high resolution CMR is due to better detection of subendocardial ischaemia in 3VD.

### **3.3 Methods**

#### **3.3.1 Study population**

One-hundred-and-five patients were included in this analysis. All had undergone coronary angiography for suspected angina within the last 30 days. Seventy patients were prospectively recruited; 35 had 3VD on quantitative coronary angiography and 35 normal coronary arteries on angiography and served as a control group. Data from 24 of the patients with angiographic 3VD have been previously reported with different end-points (diagnostic accuracy rather than pattern of ischaemia or ischaemic burden) (16). Additionally, we selected 35 consecutive patients with angiographic 1VD or 2VD from this previous study to prevent a spectrum bias for the secondary analyses relating to myocardial ischaemic burden (Motwani et al., 2012a). Exclusion criteria for all patients were contra-indications to CMR, adenosine or

gadolinium; or a history of recent (within 6 months) myocardial infarction, unstable angina or revascularisation. Additionally, patients with angiographic 1VD or 2VD and co-existing moderate coronary artery stenoses (i.e. 40-69%) in other territories were not included. All patients gave written consent and the study was approved by the regional ethics committee.

### **3.3.2 CMR protocol**

All patients underwent a standard-resolution and a high-resolution perfusion scan on separate days (within 4 weeks) using a 1.5-T scanner (Intera, Philips Healthcare, Best, The Netherlands).

The standard pulse sequence was a saturation recovery gradient-echo method accelerated with SENSE (acceleration factor 2, repetition time (TR) 2.7ms, echo time (TE) 1.0ms, flip-angle = 15°, acquisition time per slice = 136ms, single-saturation pre-pulse per R-R interval shared over three slices, matrix=144 x 144, median field-of-view (FOV) = 360 mm, in-plane spatial resolution = 2.5 mm). The high-resolution pulse sequence used a similar saturation recovery gradient-echo method, but was accelerated with *k-t* BLAST (acceleration factor 8 with 11 training profiles, TR = 3.4ms, TE = 1.7ms, flip-angle = 15°, one saturation pre-pulse per slice, acquisition time per slice = 103ms, matrix=192x192, median FOV = 310 mm, in-plane spatial resolution = 1.6 mm). For both techniques, perfusion data were acquired in 3 short-axis slices in each R-R interval. For both studies, stress perfusion started after 4minutes of an intravenous adenosine infusion (140g/kg/min) during an intravenous bolus injection of dimeglumine gadopentetate (Magnevist; Schering AG, West Sussex, UK) and a 15mL saline flush delivered at 5mL/s. Contrast dose and

administration protocols for both studies were chosen to optimise their visual analysis performance based on experience with both pulse sequence and their use in previous studies. For the standard-resolution method, a contrast dose of 0.05 mmol/kg body weight was used during perfusion acquisition, identical to previous studies with this pulse sequence (Greenwood et al., 2012; Motwani et al., 2012a). To compensate for the lower SNR associated with smaller voxel size, a contrast dose of 0.1mmol/kg body weight was used for the high-resolution method, consistent with previous reports (Motwani et al., 2012a; Plein et al., 2008b, 2007; Manka et al., 2010).

Rest perfusion imaging was performed 15minutes later. LGE imaging was performed in all patients on their first visit using conventional methods (1.6mm in-plane spatial resolution) and a cumulative contrast dose of 0.2mmol/kg body weight (the same for both protocols). During standard-resolution perfusion CMR scans, this cumulative dose was achieved by administration of an additional contrast bolus of 0.1mmol/kg body weight immediately after rest perfusion.

### **3.3.3 CMR analysis**

CMR images were anonymised, randomly ordered and visually reported by 2 observers (S.P., M.M; 10 and 2 years experience respectively) acting in consensus and blinded to all clinical and angiographic data (QMASS 6.1.6, Medis, Leiden, The Netherlands). In case of disagreement, arbitration from a third observer was sought (JPG, 10 years experience). Using a 16-segment model, perfusion in a segment was considered abnormal if signal intensity was reduced compared with remote myocardium or an endocardial-to-epicardial perfusion gradient was present (Plein et

al., 2008a)(Cerqueira et al., 2002). Additionally, any perfusion defect was required to persist longer than the contrast first-pass to distinguish it from artefact. Corresponding LGE images were reviewed side-by-side with the perfusion data. Perfusion defects present at stress but not rest and occurring outside any hyperenhanced myocardial tissue on LGE images were considered as inducible defects. Perfusion in each segment was graded on a 4-point scale (transmural ischaemia index: 0 = normal, 1 = inconclusive, 2 = subendocardial defect, 3 = transmural defect). A typical example of perfusion images is seen in Figure 3.1. All segmental scores were summed to produce a perfusion score (0-48) for each patient. Myocardial ischaemic burden as a percentage of the total myocardium (MIB%) was estimated by dividing the perfusion score by 48 and multiplying by 100 (Hachamovitch et al., 2003a). In patients with 3VD, perfusion scores were also calculated for the left anterior descending (LAD), left circumflex (LCX) and right coronary artery (RCA) territories according to AHA segmentation adjusted for arterial dominance (Cerqueira et al., 2002).

Image quality was graded 1-4 (1 = unusable, 2 = poor, 3 = adequate, 4 = excellent). Occurrence of artefacts related to *k-t* reconstruction, respiratory motion, electrocardiographic gating, and endocardial dark rim was scored 0-3 (0 = none, 1 = minor, 2 = moderate, 3 = severe). Where present, the width of dark rim artefact (a frequent finding in perfusion CMR at the myocardial-blood pool interface relating to cardiac motion, Gibb's ringing, susceptibility, and partial volume cancellation) was measured with electronic callipers (Motwani et al., 2012a; Di Bella et al., 2005).

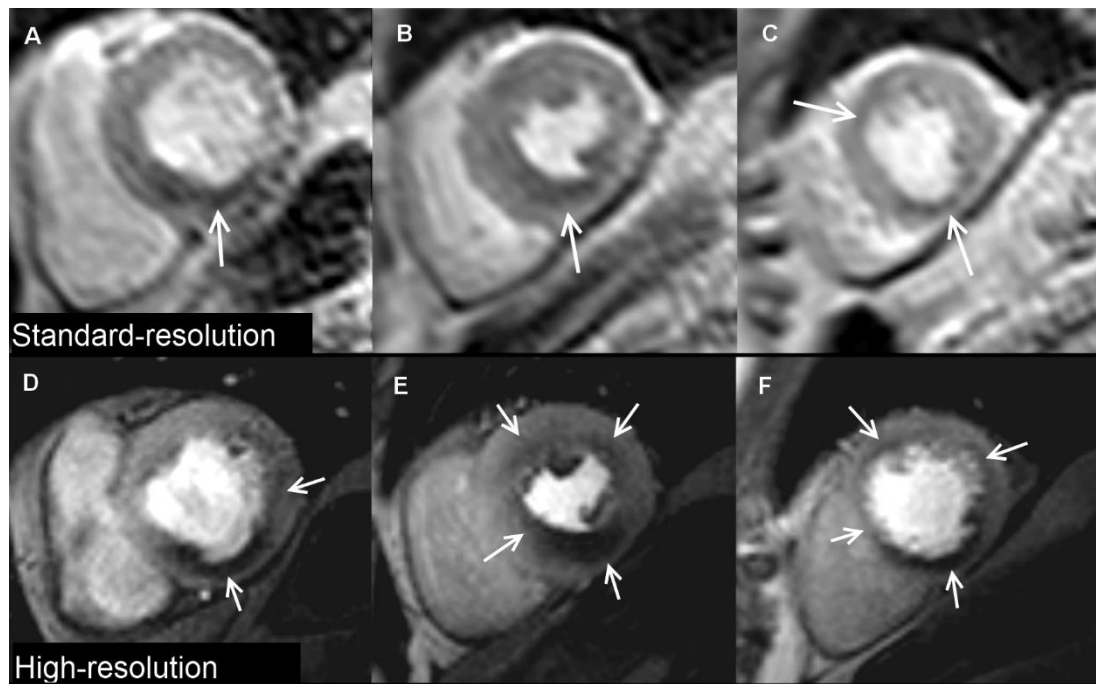


**Figure 3.1 Case Example: Standard vs. High-resolution Perfusion CMR**

Standard and high-resolution stress perfusion CMR in a patient with three-vessel coronary artery disease. Standard-resolution shows perfusion defects (arrows) in the basal-inferior (A), mid-inferior, mid-inferoseptal (B), apical-anterior and apical-inferior segments (C). High-resolution shows a similar distribution of perfusion defects but demonstrates additional ischaemia in the basal-lateral (D), mid-anterior and mid-anterotlateral segments (E) with a circumferential defect in the apical slice (F). Perfusion defects are also better delineated at high-resolution and the transmural extent of ischaemia more clearly seen.

### 3.3.4 Quantitative coronary angiography

Quantitative coronary angiography (QCA) was performed (QCAPlus, Sanders Data Systems, Palo Alto, California, USA) by an experienced observer blinded to CMR data (M.M.; 7 years of experience in coronary angiography). Stenoses were assigned to the appropriate myocardial segments of an AHA 16-segment model using standard criteria adjusted for arterial dominance and lesion location (Patel et al., 2010; Cerqueira et al., 2002). As per convention, significant CAD was defined as luminal

stenosis  $\geq 70\%$  in any of the major epicardial coronary arteries or first-order branches  $\geq 2$  mm. Angiographic 3VD was defined as stenosis  $\geq 70\%$  in all three coronary arteries; or the presence of  $\geq 50\%$  stenosis in the left main stem (LMS) with  $\geq 70\%$  in the RCA. Normal coronary arteries were defined as an absence of any stenosis  $\geq 40\%$ . Collateral circulation was graded according to the Rentrop classification (RC) depending on the angiographic findings of the occluded artery using the best injection: 0 = no collateral circulation; 1 = collateral filling of side branches without visualization of any epicardial segments; 2 = collateral partially filling the epicardial segment; 3 = collateral completely filling the epicardial segment (Rentrop et al., 1985).

### **3.3.5 Statistical analysis**

Analysis was performed using SPSS 17.0 (SPSS, Chicago, IL, USA). Mean values were compared using paired Student *t*-tests. Ordinal data were compared using Chi-square or Wilcoxon signed-rank tests as appropriate. Paired proportions were compared using McNemar's exact test. The pattern of ischaemia determined by both techniques for patients with angiographic 3VD was compared using Cohen's kappa statistic. MIB% was compared across 1VD, 2VD and 3VD groups using one-way analysis of variance and Tukey's post-hoc test. Receiver-operator characteristic (ROC) curve analyses were performed on summed perfusion scores for individual territories and on MIB% per patient. Area-under-the-curve (AUC) for both imaging techniques were compared using methods described by DeLong and DeLong. All tests were two-tailed and  $p < 0.05$  was considered statistically significant.

**Table 3-1 Patient Clinical Characteristics**

<b>Parameter</b>	<b>Data (n=105)</b>
<b>Age, yrs</b>	68 ± 10
<b>Males</b>	75 (71)
<b>Medical history</b>	
Hypertension	65 (62)
Hypercholesterolemia	62 (59)
Diabetes Mellitus	18 (17)
Smoking	43 (41)
Family history of CAD	39 (37)
Previous MI	14 (13)
Previous PCI	10 (9)
Atrial Fibrillation	1 (1)
<b>LV Ejection Fraction, %</b>	55 ± 11
<b>Angiography findings <sup>a</sup></b>	
No significant disease	35 (33)
One-vessel disease	25 (24)
Two-vessel disease	10 (9)
Three-vessel disease	35 (33)
LAD disease	51 (49)
LCX disease	50 (48)
RCA disease	49 (47)
Significant lesions per patient	1.4 ± 1.2
Total significant lesions	150
70-90% stenoses	109 (73)
90-99% stenoses	35 (23)
Chronic total occlusions	6 (4)

Values are mean ±SD or n (%). <sup>a</sup>Significant CAD defined as ≥70% QCA.

## **3.4 Results**

### **3.4.1 Study population**

105 patients were enrolled in the study, including 35 with 3VD by QCA. Of these 35 patients, 32 qualified as angiographic 3VD on the basis of significant stenoses in the proximal coronary segments; and no patients qualified as angiographic 3VD on the basis of distal coronary segment disease. Further demographics are given in Table 3.1. All 14 patients with a clinical history of MI (but no additional patients) had evidence of hyperenhancement on LGE imaging. A chronic total occlusion (CTO) was seen in 6 patients (all in the group with prior MI) and 2 of these patients were in the 3VD group. There were no patients with more than one CTO. In 2 cases of CTO (neither in the 3VD group) there was mild collateral flow (RC=2), but in the remaining 4 cases there was no or minimal collateralization (RC ≤1).

### **3.4.2 Image quality and artefacts**

There was no significant difference in the haemodynamic stress response during standard and high-resolution imaging (rate-pressure-product, mmHg x beats/min:  $10251 \pm 2321$  vs.  $10201 \pm 2109$ ;  $p=0.92$ ). No images were graded as unusable and therefore there were no exclusions from the image analysis for either technique. Image quality (median score=3 for both;  $p=0.67$ ) and artefact scores (median=0 for both;  $p=0.06$ ) were similar for both standard and high-resolution imaging across the full spectrum of patients ( $n=105$ ). Dark rim artefact was significantly less frequent with high-resolution (7% vs. 26%;  $p=0.03$ ) and when it did occur, it was less marked than with standard-resolution ( $1.6 \pm 0.2$  vs.  $3.2 \pm 0.8$  mm;  $p=0.004$ ). Seven high-

resolution data sets (10%) were affected by *k-t* reconstruction artefacts at stress and/or rest due to respiratory motion, but this did not affect myocardial contrast passage and generally occurred at the end of a breath hold.

### **3.4.3 Detection of 3VD pattern**

In patients with angiographic 3VD (n=35), perfusion defects in all three territories were detected in 29% of patients (10 of 35) by standard-resolution and in 57% of patients (20 of 35) by high-resolution imaging ( $p=0.04$ ) (Figure 3.2). Overall, there was poor agreement between the two techniques in determining the pattern of ischaemia in patients with angiographic 3VD ( $\kappa=0.09$ , 95% CI: -0.10 to 0.29) (Figure 3.2).

### **3.4.4 Detection of CAD in each territory**

In patients with angiographic 3VD (n=35), separate ROC analyses of perfusion scores for each of the 3 coronary territories were performed. The AUC for each territory in patients with angiographic 3VD was greater with high-resolution than with standard-resolution imaging, but reached statistical significance only for the LCX territory (Table 3.2). With standard-resolution imaging, diagnostic accuracy was significantly lower for the LCX than for the LAD (0.62 vs. 0.82;  $p < 0.01$ ) or RCA territory (0.62 vs. 0.83;  $p=0.02$ ). With high-resolution, diagnostic accuracies were more homogenous between territories (although still lowest in the LCX territory) with no statistical difference between them (LAD: 0.85 vs. LCX: 0.83 vs. RCA: 0.90; all  $p$  values  $> 0.05$ ).

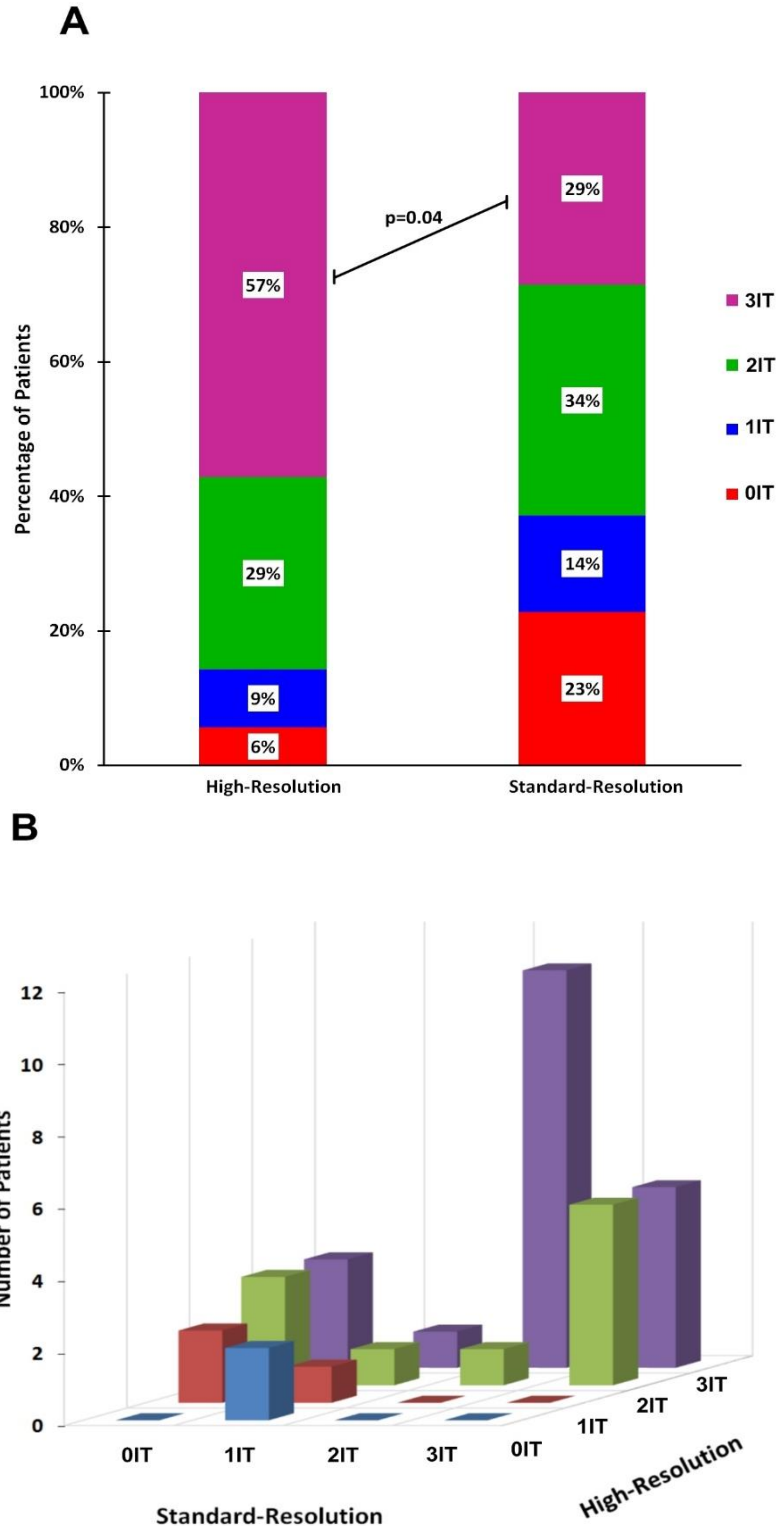


**Figure 3.2 Distribution of Ischaemia Detected by Perfusion CMR**

(A) In patients with 3VD ( $n=35$ ), hypoperfusion in all three territories was detected in 57% using high-resolution imaging but in only 29% using standard-resolution ( $p=0.04$ ). (B) There was also poor agreement between high-resolution and standard-resolution imaging in determining the distribution of ischaemia in patients with 3VD ( $kappa=0.09$ , 95% CI:  $-0.10-0.29$ ). IT = ischaemic territories.

**Table 3-2 Diagnostic Performance of Perfusion CMR in Each Territory in Patients with 3VD**

Area Under ROC Curve (95% CI)			
	Standard Resolution	High Resolution	P value
LAD	0.82 (0.69-0.95)	0.85 (0.73-0.97)	0.62
LCX	0.62 (0.46-0.79)	0.83 (0.70-0.95)	0.02
RCA	0.83 (0.70-0.95)	0.90 (0.80-1.00)	0.27

### 3.4.5 Detection of subendocardial ischaemia

560 myocardial segments were available from the 35 patients with angiographic 3VD. Of these, 420 were determined as angiographically hypoperfused and used for further analysis. With high-resolution acquisition, significantly more of these hypoperfused segments were determined as having subendocardial ischaemia than with standard-resolution (195 vs. 101;  $p < 0.0001$ ); and there was a significant reduction in the number of segments determined as being normal (135 vs. 212;  $p < 0.001$ ) or inconclusive (15 vs. 40;  $p < 0.001$ ). The number of segments assessed as having transmural ischaemia was similar with both techniques (75 vs. 67;  $p = 0.25$ ) (Figure 3.3).

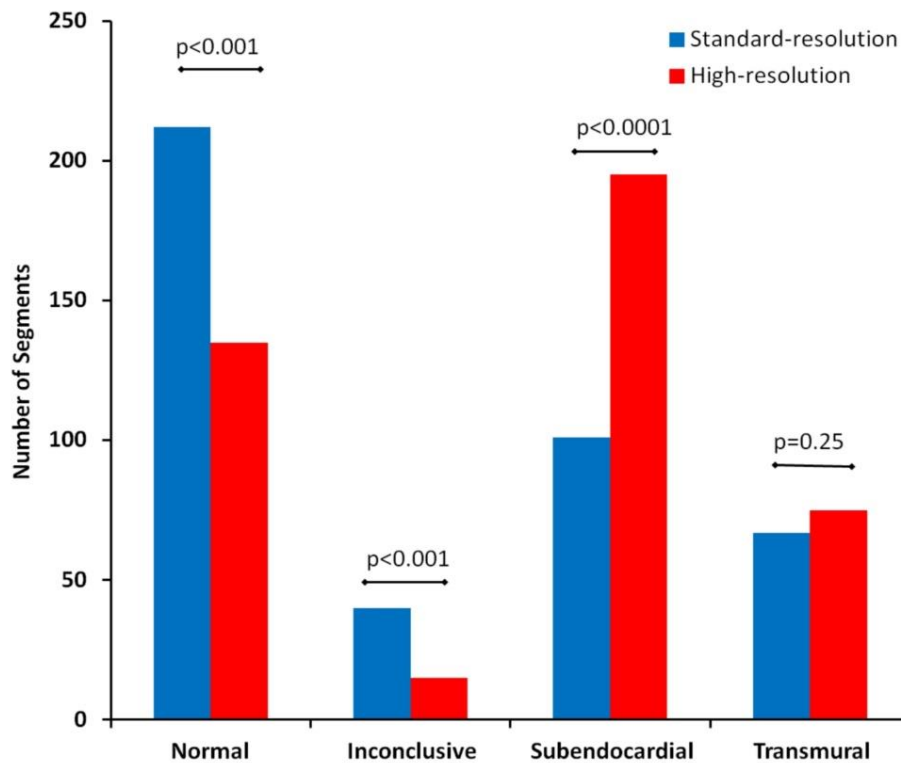


**Figure 3.3 Distribution of Transmural Ischaemia Index**

*In patients with three-vessel disease (n=35), high-resolution perfusion CMR determined significantly more segments as having subendocardial ischaemia and fewer as normal or inconclusive compared with standard-resolution imaging.*

### 3.4.6 Detection of ischaemic burden

In patients with angiographic 3VD (n=35), the overall extent of myocardial ischaemia detected was significantly greater with high-resolution than standard-resolution imaging, with more abnormal segments per patient ( $7.2 \pm 3.8$  vs.  $5.3 \pm 4.0$ ;  $p=0.004$ ), more abnormal territories per patient ( $2.4 \pm 0.9$  vs.  $1.6 \pm 1.1$ ;  $p=0.002$ ), a higher perfusion score per territory ( $5.9 \pm 4.3$  vs.  $4.7 \pm 5.0$ ;  $p=0.01$ ) and a higher overall perfusion score per patient ( $20.1 \pm 7.7$  vs.  $11.9 \pm 9.4$ ;  $p<0.0001$ ) (Figure 3.1, Table 3.3).

**Table 3-3 Ischaemic Burden Using Perfusion CMR in Patients with 3VD**

	Standard-resolution	High-resolution	P value
<b>Mean abnormal segments per patient</b>	5.3 ± 4.0	7.2 ± 3.8	0.004
<b>Mean abnormal territories per patient</b>	1.6 ± 1.0	2.4 ± 0.9	0.002
<b>Mean perfusion score per patient</b>	11.9 ± 9.4	20.1 ± 7.7	<0.0001
<b>Mean perfusion score per territory</b>	4.7 ± 5.0	5.9 ± 4.3	0.01

When the full spectrum of 105 patients were assessed, high-resolution found a significant upward trend in estimated MIB% in those with significant CAD (n=70) across advancing disease groups (1VD: 12 ± 7% vs. 2VD: 39 ± 15% vs. 3VD: 42 ± 16%; p<0.0001)(Motwani et al., 2012a). However, with standard-resolution, there was no discriminate difference in estimated MIB% across the disease groups (1VD: 21 ± 11% vs. 2VD: 25 ± 6% vs. 3VD: 25 ± 19%; p=0.53) (Figure 3.4).

Accordingly, on ROC analysis, the AUC for detecting angiographic 3VD using the estimated MIB% was significantly greater with high-resolution (AUC=0.90, 95% CI: 0.84-0.96) than standard-resolution (AUC=0.69, 95% CI: 0.62-0.76; p<0.0001) (Figure 3.5). For high-resolution the optimal MIB% threshold to detect angiographic 3VD was 31% which resulted in a sensitivity and specificity of 80% (95% CI: 64-90%) and 90% (95% CI: 80-95%) respectively. For standard-resolution, the optimal threshold was 23%, which resulted in a sensitivity and specificity of 51% (95% CI: 36-67%) and 78% (95% CI: 66-86%), respectively (Figure 3.5).

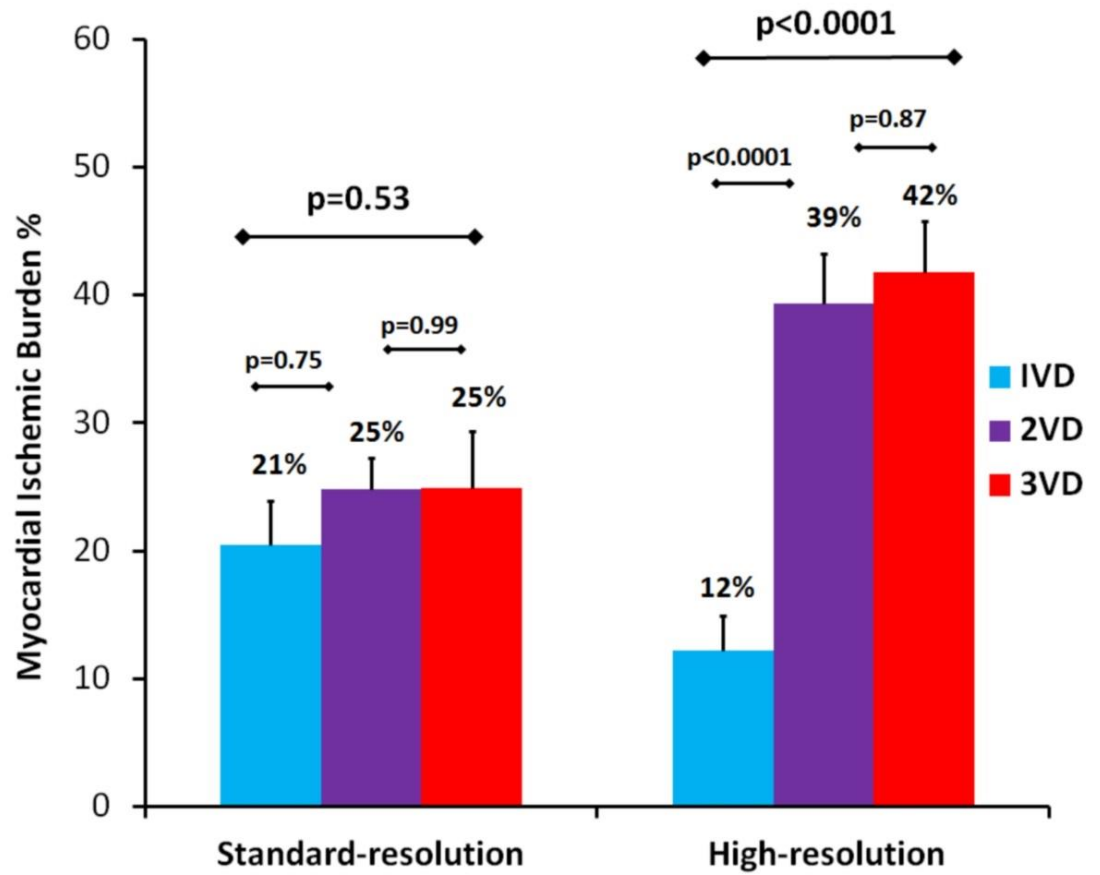


**Figure 3.4 MIB: Standard-resolution vs High-resolution Perfusion CMR**

*In patients with significant coronary artery disease (n=70), high-resolution perfusion CMR was able to detect significant differences in myocardial ischaemic burden (MIB) across disease categories unlike standard-resolution imaging (error bars=SEM).*

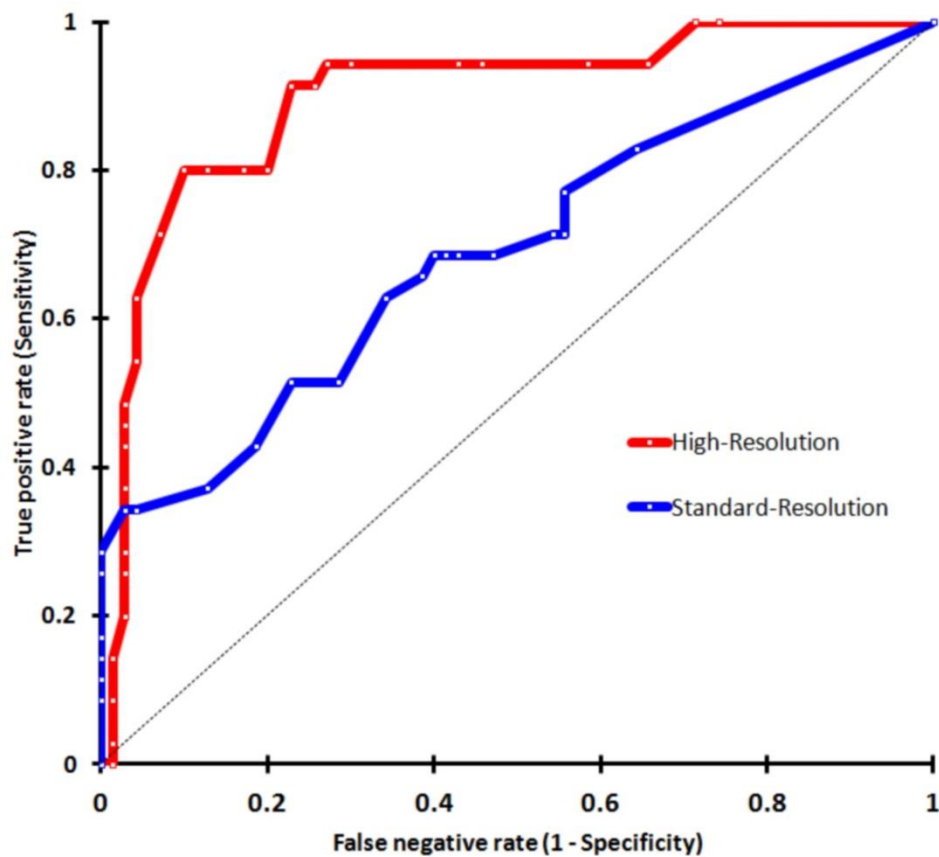


**Figure 3.5 Diagnostic accuracy of MIB to detect 3VD**

(B) The area under curve (AUC) for detecting 3VD using MIB amongst patients with suspected angina ( $n=105$ ) was significantly greater with high-resolution than standard-resolution (AUC= 0.90 vs.0.69;  $p<0.0001$ ).VD= vessel disease.

### 3.5 Discussion

This study shows that in patients with angiographic 3VD, high-resolution perfusion CMR detects a greater ischaemic burden than standard-resolution and more frequently identifies a 3VD pattern of ischaemia due to a higher detection rate of subendocardial ischaemia.

The evidence for using perfusion CMR in patients with 3VD is limited. Although previous studies evaluating perfusion CMR have included patients with 3VD, they have rarely reported separate results for this specific patient population. In the published data, the incidence of patients with 3VD was only 2% (2 patients) in the study by Sakuma et al, 15% (8 patients) in the study by Ishida et al, and 19% (7 patients) in the study by Schwitter et al (2005; 2003; 2001). Although other studies may contain larger numbers, patients with 3VD are rarely analysed separately and they are usually grouped together with patients found to have 2VD (Schwitter et al., 2008; Greenwood et al., 2012; Schwitter et al., 2013). Only one study to date has been specifically designed to evaluate standard-resolution perfusion CMR in patients with 3VD (n=78) and it demonstrated a sensitivity of 85% for CAD detection and superiority of perfusion CMR compared with SPECT (Chung et al., 2010). Data on the use of high-resolution perfusion CMR in the specific 3VD population is even scarcer. However, in a recent related analysis, we reported on 38 patients with angiographic multi-vessel disease (24 had 3VD) and found a greater diagnostic accuracy for the detection of CAD (any perfusion defect) with high-resolution perfusion CMR compared to standard-resolution imaging (AUC, 0.98 vs.0.91;  $p<0.002$ ); but the pattern of perfusion defects detected and the ischaemic burden were not assessed (Motwani et al., 2012a).

### **3.5.1 Detection of subendocardial ischaemia**

The finding in the present study that high-resolution acquisition identified significantly more ischaemic segments and in particular more segments with subendocardial ischaemia in angiographic 3VD is consistent with the expected

improvement in subendocardial definition with higher spatial resolution. Although we have previously demonstrated this finding across the full spectrum of CAD, it was important to confirm that this advantage is maintained in the 3VD population, against the competing challenge of balanced ischaemia (Motwani et al., 2012a). It means that one of the major limitations of myocardial perfusion imaging and visual analysis in 3VD i.e. its dependence on a reference area of normal perfusion, can be overcome to some extent with high-resolution techniques that are able to resolve subendocardial ischaemia and transmural perfusion gradients, reducing the need for intra-patient comparison. An alternative approach is *quantitative* analysis of standard perfusion CMR and although this has been shown to identify patients with 3VD better than visual analysis, it remains a time-consuming research tool until technical developments lead to greater automation (Patel et al., 2010). The significant reduction of dark rim artefact with high-resolution may also partially account for its improved detection of subendocardial ischaemia and notably there were fewer inconclusive segments with high-resolution acquisition compared to standard-resolution (Figure 3.3). Previous work investigating dark rim artefact has shown the prominent role of spatial resolution on the occurrence and extent of this artefact (Plein et al., 2007; Di Bella et al., 2005).

### **3.5.2 Detection of 3VD pattern**

Standard-resolution perfusion CMR identified defects in all three perfusion territories in only 29% of patients with angiographic 3VD (10 of 35) (Figure 3.2). In the published CMR literature there is only one study that investigates the same question and it found a significantly greater figure of over 50% using standard-

resolution techniques (Chung et al., 2010). However, this previous retrospective study only analysed patients with 3VD, without a control group; and additionally did not use LGE imaging to exclude areas of infarction from inducible ischaemia, both of which are likely to have led to a positive bias. In the comparative SPECT literature, we see the ability to detect a 3VD pattern is similarly only 29% in one series and as low as 12% in another (Christian et al., 1992; Chung et al., 2010).

With the high-resolution perfusion CMR method, twice as many patients with angiographic 3VD i.e. 57% (20 of 35) were correctly classified as having a 3VD pattern of ischaemia (Figure 3.2). The improved detection of a 3VD pattern of ischaemia with high-resolution compared to standard-resolution acquisition was due to better detection of ischaemia in the LCX territory and more subendocardial ischaemia detection. Disease of the LCX territory can be difficult to detect because this territory is farthest from the radiofrequency coil and because visual, unlike quantitative assessment analysis, cannot correct signal intensity for distance from the coil (Cheng et al., 2007; Chung et al., 2010). In keeping with previous studies, high-resolution acquisition used a higher contrast dose (in order to compensate for the lower SNR associated with smaller voxel size) and arguably this may have contributed to its superior performance in the LCX territory (Motwani et al., 2012a; Plein et al., 2008b, 2007; Manka et al., 2010).

Rather than inadequacy of the perfusion analysis, the low detection rate of ischaemia in multiple territories by different imaging modalities may reflect at least in part the inadequacy of the angiographic endpoint in these studies including our own. In a sub-analysis of the FAME study, only 14% of patients with angiographic

3VD (n=115), had concordant 3-vessel functional disease determined by fractional flow reserve (FFR) (i.e.  $FFR < 0.80$  in all 3 vessels)(Tonino et al., 2010).

### **3.5.3 Estimation of ischaemic burden**

It can be argued that in clinical practice, it is less relevant whether a functional scan depicts a typical three-vessel pattern if there is myocardial ischaemia involving a significant proportion of total myocardium. An accurate assessment of ischaemic burden is important because the extent of ischaemia is a marker of patient prognosis – and a large ischaemic burden supports aggressive medical treatment and angiography with a view to revascularization regardless of the territorial pattern of perfusion defect (Hachamovitch et al., 1998, 2003a; Wijns et al., 2010; Shaw et al., 2008). When MIB% was estimated using high-resolution CMR, it was found to reliably discriminate angiographic 3VD from less extensive disease and normal controls (AUC=0.89) (Figure 3.5). This was not the case for standard-resolution CMR, for which MIB% had a significantly poorer diagnostic accuracy (AUC=0.69;  $p < 0.0001$ ) and was not able to reliably differentiate between patients with 1VD, 2VD or 3VD (Figure 3.4). The latter observation regarding standard-resolution perfusion CMR, has been previously noted by Patel et al who found similar estimates of ischaemic burden in patients with angiographic single-vessel disease and 3VD with visual assessment (21% vs. 31%;  $p=0.26$ ); but a significant difference if quantified with myocardial perfusion reserve analysis (25% vs. 60%;  $p=0.02$ )(Patel et al., 2010). A similar phenomenon has been described with PET (Parkash et al., 2004). The higher spatial resolution of *k-t* BLAST perfusion CMR acquisition appears to overcome this limitation seen with lower spatial resolution imaging methods.

Although there is no agreed reference standard for MIB% the current data suggest that standard-resolution imaging underestimates MIB% - and this should be considered in the interpretation of future perfusion CMR studies that may use a particular threshold of ischaemic burden as a defined end-point or inclusion criteria. In the nuclear sub-study of COURAGE, patients with a MIB% >10% had a lower risk of death or MI if they underwent revascularization rather than optimal medical therapy alone (Shaw et al., 2008). Notably, there has been no direct comparison of CMR and SPECT for MIB% assessment - but if the threshold defined for SPECT is applied to the CMR data in this study, 24 of 35 patients with angiographic 3VD had a MIB% >10% using standard-resolution perfusion CMR, compared to 33 patients with the high-resolution technique. Thus, high-resolution perfusion CMR may offer an improved non-invasive assessment of ischaemic burden and help identify the optimal therapeutic approach.

### **3.6 Study Limitations**

We accept our findings are mainly technical and further studies with clinical outcome data would be required to support the proposed incremental value of high-resolution perfusion CMR. We also accept that although we hypothesise the superior performance of high-resolution perfusion CMR relates to greater spatial resolution and better detection of subendocardial ischaemia, we cannot exclude the influence of other factors such as differences in SNR between scans and the difference in contrast protocols used as compensation.

A functional endpoint such as FFR would have been preferable - but this is not easily achievable given the logistics of performing multiple FFR assessments on serial and complex stenoses in three diffusely diseased arteries to define each subject. However, our findings predominantly relate to comparative differences in ischaemic burden assessment between the two techniques rather than their absolute ability to detect any ischaemia.

Because the visual CMR analysis was performed by two observers acting in consensus, inter-observer and intra-observer variability for perfusion scoring were not tested; however, arbitration from a third reader was only required in 5 out of the 210 analyses (3 with standard and 2 with high-resolution).

Finally, quantitative methods for the estimation of MBF based on perfusion CMR data have been validated in animal models and applied to clinical studies (Patel et al., 2010). However, in this study, contrast agent dose and administration (single-bolus technique) were optimised for visual analysis and therefore quantitative analysis was not performed. Although, high-resolution perfusion CMR offers further intriguing opportunities for quantitative analysis such as quantitation of transmural perfusion gradients, the algorithms applied for the reconstruction of high-resolution perfusion CMR data acquired with temporo-spatial undersampling methods give rise to a degree of low-pass temporal filtering, posing additional challenges to quantitation of MBF including an underestimation bias (Hautvast et al., 2011; Jerosch-Herold, 2010). Recent developments such as *k-t* Principal Component Analysis are likely to overcome some of these challenges but will require evaluation in future studies (Pedersen et al., 2009).

### **3.7 Conclusions**

High-resolution perfusion CMR increases the observed ischaemic burden and distribution of ischaemia detected in angiographic 3VD. The incremental value of high-resolution acquisition for correctly identifying, stratifying and management of this high-risk group has to be determined in further clinical studies.

## 4 Study 3 - Three-Dimensional versus High-Resolution Perfusion CMR: A Pilot Study Comparing Myocardial Ischaemic Burden Estimates

### 4.1 Abstract

**Background:** Typically, myocardial perfusion imaging with 2-dimensional (2D) cardiovascular magnetic resonance (CMR) acquires data in 3-4 myocardial slices at a spatial resolution of 2-3mm. However, accelerated data acquisition can facilitate higher spatial resolution (<2mm) or 3D whole-heart coverage (up to 16 slices). This study aims to compare image quality, diagnostic confidence and quantitation of myocardial ischemic burden (MIB) between 2D high-resolution and 3D whole-heart perfusion CMR.

**Methods and results:** 27 patients with stable angina underwent both high-resolution 2D and whole-heart 3D perfusion CMR. Total perfusion defect (TPD) and total scar burden (TSB) areas were contoured and expressed as percentage myocardium. MIB was calculated by subtracting TSB from TPD. Image quality, artefact and diagnostic confidence scores were similar for both techniques ( $p > 0.05$ ). The mean MIB from high-resolution and 3D acquisition was similar ( $4.3 \pm 5.2\%$  vs  $4.1 \pm 4.9\%$ ;  $p = 0.81$ ), with a strong correlation between techniques ( $r = 0.72$ ;  $p < 0.001$ ). There was no systematic bias for estimates of MIB between techniques (mean bias =  $-0.17\%$ , 95% CI:  $-1.7$  to  $1.3\%$ ) and the 95% limits of agreement were  $-7.5\%$  to  $7.2\%$ . When used to

categorize MIB as >10% or <10%, there was only fair agreement between the two techniques (kappa = 0.29, 95% CI: -0.12-0.70).

**Conclusions:** There is strong correlation and broad agreement between estimates of MIB from both techniques. However, the 95% limits of agreement are relatively wide and therefore a larger comparative study is needed before they can be considered interchangeable - particularly around the clinically relevant 10% threshold.

## 4.2 Introduction

Myocardial perfusion imaging with CMR is a highly accurate method for diagnosing CAD, but its role in quantifying myocardial ischaemic burden (MIB) is less certain (Greenwood et al., 2012; Hamon et al., 2010). The lack of complete myocardial coverage with standard 2D perfusion CMR (3-4 short axis slices only) means that any assessment of MIB is an extrapolation. MIB measured by SPECT, which has the advantage of whole-heart coverage, has been shown to be an important prognostic marker and can help identify patients most likely to benefit from revascularisation compared to medical therapy alone (Hachamovitch et al., 1998; Shaw et al., 2008).

However, the introduction of accelerated data acquisition using spatio-temporal undersampling methods, has led to the option of 3D whole-heart perfusion CMR, or alternatively 2D perfusion CMR with higher spatial resolution (<2mm) (Motwani et al., 2013). Potentially, 3D perfusion CMR presents a direct alternative to SPECT for the measurement of MIB - without any inter-slice assumptions (Jogiya et al., 2014). On the other hand, higher spatial resolution acquisition has been shown to have several other benefits such as reduced dark rim artefact, greater detection of subendocardial ischaemia and particular diagnostic strength in patients with multi-vessel disease (Plein et al., 2008a; Manka et al., 2010; Motwani et al., 2012a, 2014a). Although both of these methods have been shown to have high diagnostic accuracy and have been validated against FFR, it is not known how their estimates of MIB compare (Lockie et al., 2011; Jogiya et al., 2012; Manka et al., 2012). The decision whether to invest acceleration into 3D coverage for the purpose of MIB assessment, or into higher spatial resolution, partly depends on the question of whether MIB

estimates differ between the two methods. Therefore, this pilot study directly compares image quality, diagnostic confidence and quantification of MIB between 2D high-resolution and 3D whole-heart perfusion CMR.

## **4.3 Methods**

### **4.3.1 Patient Population**

Thirty patients with stable angina and scheduled for coronary angiography on a clinical basis were recruited to undergo both a high-resolution 2D and a 3D perfusion CMR scan on two separate days within 8 weeks. The order of methods was randomly chosen. No coronary intervention or clinical events occurred between the two scans. The presence or absence of significant CAD in patients was defined by quantitative coronary angiography (QCA) as detailed below. Exclusion criteria were contraindications to CMR, adenosine or gadolinium contrast agents; a history of recent (within 6 months) myocardial infarction or unstable angina; or poorly controlled arrhythmias. Patients were instructed to refrain from caffeine for 24hrs prior to their CMR study but continue cardiac medications as normal. All patients gave written consent to participate and the study was approved by the regional ethics committee.

### **4.3.2 CMR Protocol**

All studies were performed on a 3.0T scanner (Achieva TX, Philips Healthcare, Best, The Netherlands) equipped with dual-source parallel radiofrequency transmission technology and a 32-channel cardiac receiver coil.

High-resolution and 3D perfusion CMR acquisitions used the optimal imaging parameters derived from previously published studies (Motwani et al., 2012a; Jogiya et al., 2012; Manka et al., 2012, 2011). For high-resolution perfusion imaging, a spoiled saturation recovery fast gradient echo sequence was used (TR/TE/flip angle: 2.7ms/1.0ms/20°; saturation pre-pulse delay 120ms, 1 saturation prepulse per slice, image acquisition time per slice 134ms; no partial Fourier or partial echo acquisition; typical field of view 340 x340 mm; 5 fold *k-t* BLAST [broad-use linear acquisition speed-up technique] acceleration with 11 interleaved training profiles; 3 short-axis slices [basal, mid ventricle and apical] with 10mm thickness and 1.2 x 1.2mm acquired in-plane spatial resolution). For 3D perfusion imaging, a spoiled fast saturation recovery gradient-echo sequence was used (TR/TE/flip angle 1.8ms/0.7ms/15°; saturation prepulse delay 150ms; linear *k*-space encoding; 70% partial Fourier acquisition in two dimensions; typical field of view 350 x 350mm; 10 fold *k-t* acceleration and 11 training profiles leading to a net acceleration of 7.0; typical acquisition duration 192ms, *k-t* BLAST reconstruction; reconstructed to 12 contiguous short-axis slices with voxel size 2.3 x 2.3 x 5mm<sup>3</sup>). Stress perfusion images were acquired during intravenous adenosine-induced hyperaemia administered for 4min at 140mcg/kg/min. Consistent with previous *k-t* BLAST facilitated perfusion CMR studies, an intravenous bolus of 0.075mmol/kg of gadobutrol (Gadovist, Bayer Schering Pharma, Berlin, Germany) was administered at a rate of 4.0ml/s followed by a 20ml saline flush. Stress perfusion CMR was followed by cine imaging covering the left ventricle in 10-12 short-axis sections. Rest perfusion CMR was performed 15min after stress, using identical imaging parameters. Late gadolinium

enhancement (LGE) imaging was performed in all patients on their first visit only, after an additional 10-15min using a 2D T1 weighted segmented inversion recovery gradient echo method (TR/TE/flip angle 4.9ms/1.9ms/15°; inversion time individually adjusted according to Look-Locker scan; spatial resolution 1.35 x 1.35 x 10 mm; contiguous short-axis slices to cover LV). Case examples of both acquisitions are shown in Figures 1.10-1.13 and Figure 4.1.

### **4.3.3 CMR Analysis**

#### ***4.3.3.1 Visual Analysis***

Perfusion CMR images were anonymised, randomly ordered and visually reported by 2 observers (SP, AKM; >10yrs and 2yrs experience respectively) (Qmass MR 7.5, Medis, Leiden, The Netherlands). The presence or absence of a perfusion defect was recorded by both observers acting independently. In case of disagreement, arbitration from a third observer was sought (JPG, >10yrs experience). A perfusion defect was defined as an area of reduced signal intensity on stress perfusion images compared to remote myocardium or the presence of an endocardial-to-epicardial perfusion gradient (Plein et al., 2008a). Additionally, any perfusion defect was required to persist longer than the contrast first-pass to distinguish it from artefact. Corresponding LGE images were reviewed side-by-side with the perfusion data. Perfusion defects present at stress but not rest and occurring outside any hyper-enhanced myocardial tissue on LGE images were considered as inducible defects (ischaemia) (Motwani et al., 2012a). Image quality and diagnostic confidence were graded by both observers in consensus. Image quality was graded 0 to 3 (0 = uninterpretable, 1 = poor, 2 = adequate, 3 = high). Occurrence of artefacts related to *k*-

*t* reconstruction, respiratory motion, electrocardiographic gating, and endocardial dark rim artefact was scored between 0 and 3 (0 = none, 1 = minor, 2 = moderate, 3 = severe). Using the AHA 16 segment model, diagnostic confidence was recorded for each perfusion territory (0 = uncertain, 1 = low confidence, 2 = high confidence)(Cerqueira et al., 2002) .

#### **4.3.3.2 Myocardial Ischaemic Burden**

For both high-resolution and 3D acquisitions, the total perfusion defect (TPD) as percentage myocardium was determined by dividing the area of any perfusion defect by the area of total myocardium (both contoured on stress perfusion images) and multiplying by 100. All perfusion defects were contoured by an experienced observer (AKM, 2yrs experience) at the frame of maximal myocardial signal intensity determined by a region of interest drawn in remote myocardium. Contiguous perfusion defects across different perfusion territories were contoured as a whole; non-contiguous perfusion defects were contoured separately and summed. Total scar burden (TSB) in percentage myocardium was determined by dividing the total area of any hyperenhancement by the area of total myocardium (both contoured on LGE images) and multiplying by 100. Myocardial hyperenhancement for LGE images were defined as areas with signal intensity  $\geq 2$  SD above the mean signal intensity of remote myocardium(Kidambi et al., 2013). For each acquisition, MIB as percentage myocardium was calculated as by subtracting TSB from TPD. Any negative values for MIB were normalised to zero (i.e. no ischaemia). To determine the reproducibility of MIB assessment, the analysis was repeated in 10 randomly selected patients 1

month later by the same observer (AKM), and by a second observer (DPR, >3 years of experience) blinded to the results of all previous analyses.

#### **4.3.4 Quantitative coronary angiography**

Quantitative coronary angiography (QCA) was performed (QCAPlus, Sanders Data Systems, Palo Alto, CA, USA) on all anonymised X-ray angiography images (M.M. 8 years experience in coronary angiography). Significant CAD was defined angiographically as luminal stenosis  $\geq 70\%$  diameter in any of the main epicardial coronary arteries or their branches with a diameter of  $\geq 2\text{mm}$ .

#### **4.3.5 Statistical Analysis**

Analysis was performed using SPSS version 21.0 (SPSS Inc, Chicago, Illinois, USA). All data are presented as mean  $\pm$  SD unless otherwise stated. Group means were compared using paired Student t-tests. Ordinal data were compared using the Wilcoxon signed-rank test. Linear correlations were assessed using Pearson correlation coefficients. All statistical tests were 2-tailed and a p value  $< 0.05$  was considered significant. Agreement between high-resolution and 3D perfusion CMR measurements for TPD and MIB were assessed using Bland-Altman analysis; and the degree of agreement was determined as mean absolute difference (bias)  $\pm 2$  SDs of the mean difference (95% limits of agreement). The categorisation of MIB as  $< 10\%$  or  $> 10\%$  by both techniques was compared using Cohen's kappa statistic. To assess reproducibility, the coefficients of variation (CoV) for intra- and inter-observer measurements were calculated.

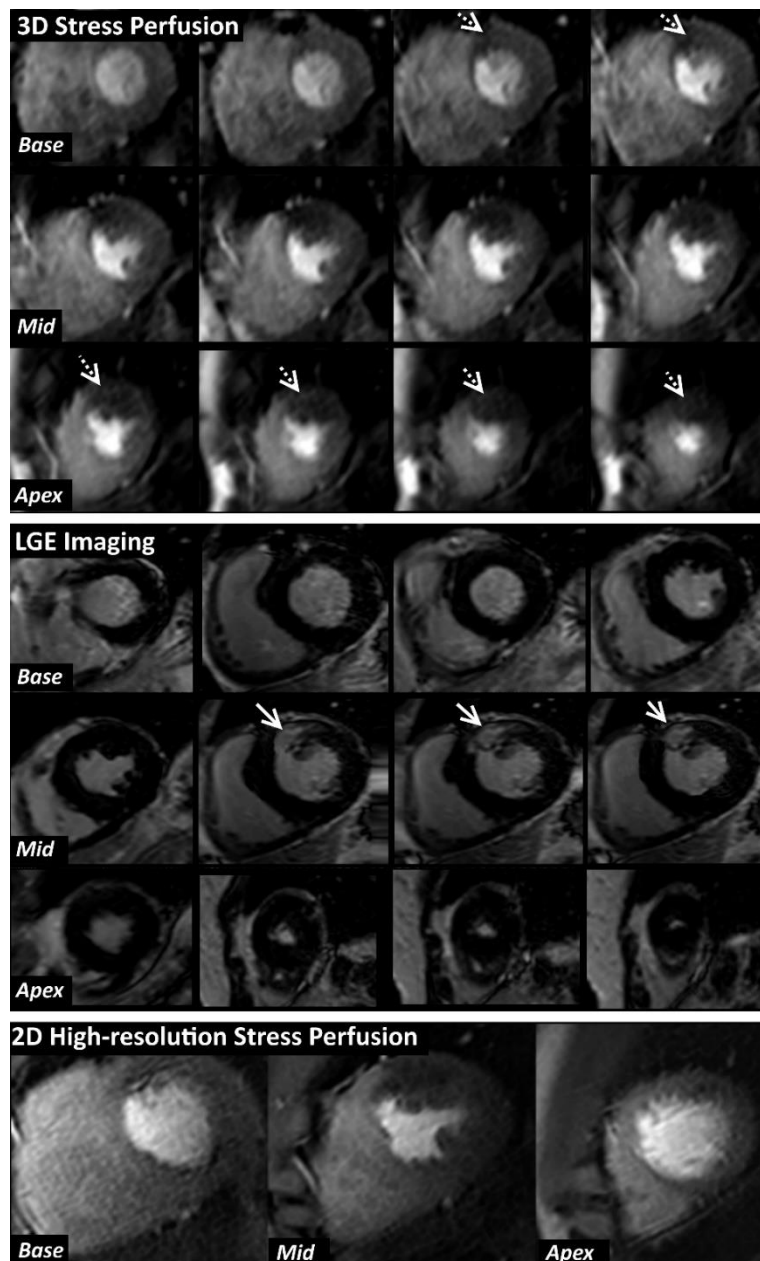


**Figure 4.1 3D versus High-resolution Perfusion CMR – Case 5**

A 45-year-old man with previous PCI to the LAD presented with significant angina. The top panel shows 3D perfusion CMR (12 slices) at stress; the middle panel shows LGE imaging; and the bottom panel shows 2D high-resolution (1.1 mm in-plane) perfusion CMR at stress, all performed at 3.0 T. 3D perfusion CMR shows stress-induced hypoperfusion throughout the anterior wall from base to apex, well beyond the area of scar seen in the mid-anterior wall on LGE imaging (solid arrows = scar; dashed arrows = ischaemia beyond scar). The 3-slice 2D high-resolution technique did not demonstrate any significant ischaemia beyond the established scar in the mid-ventricle. X-ray angiography confirmed a subtotal occlusion of a large diagonal branch, accounting for the anterior ischaemia.

## **4.4 Results**

### **4.4.1 Study population**

Of the 30 recruited patients, 28 completed both perfusion CMR acquisitions (2 patients did not return for a second scan due to claustrophobia). Data from one patient was excluded due to a mistimed contrast injection during their high-resolution perfusion acquisition. Therefore, paired perfusion CMR scan data from 27 patients were available for the final analysis. All of these 27 patients underwent coronary angiography within 6 weeks of their second CMR scan (8 patients before CMR; and 19 patients after CMR), and all had evidence of significant CAD as defined by QCA. Further clinical details of the 27 patients are summarised in Table 4.1. The mean interval between perfusion CMR scans was  $17 \pm 38$  days. There was no significant difference in the haemodynamic stress response during 2D high-resolution and 3D whole-heart perfusion CMR imaging (rate–pressure product, mmHg  $\times$  beats/min:  $10274 \pm 2246$  vs.  $10219 \pm 2259$ ;  $p=0.89$ ).

### **4.4.2 Diagnostic Confidence and Image Quality**

No images were graded as unusable and therefore there were no further exclusions from the image analysis for either technique. Image quality (median score = 2 for both;  $p=0.52$ ) and artefact scores (median = 1 for both;  $p=0.87$ ) were similar for both techniques. Diagnostic confidence was high for both techniques in all three perfusion territories (all median scores = 2; all  $p$  values between methods were  $> 0.05$ ).

**Table 4-1 Patient Characteristics**

<b>Parameter</b>	<b>Data (n=27)</b>
<b>Age (yrs ± SD)</b>	64 ± 11
<b>Sex, n (%)</b>	
Male	23 (85)
Female	4 (15)
<b>Clinical history, n (%)</b>	
Hypertension	11 (41)
Hypercholesterolemia	15 (56)
Diabetes Mellitus	4 (15)
Smoking	9 (33)
Previous MI	16 (59)
Previous PCI	8 (30)
<b>CCS Angina Scale, n (%)</b>	
No angina or atypical symptoms	1 (4)
Class 1	11 (41)
Class 2	11 (41)
Class 3	4 (15)
Class 4	0 (0)
<b>CMR Imaging data</b>	
LV EDVi (ml/m <sup>2</sup> )	90 ± 21
LV ESVi (ml/m <sup>2</sup> )	40 ± 14
LV SVi (ml/m <sup>2</sup> )	49 ± 10
LV mass index (g)	48 ± 11
LV EF (%)	54 ± 8
<b>Angiographic data</b>	
No significant CAD	0 (0)
1VD	17 (63)
2VD	5 (19)
3VD	5(19)
LAD disease	19(70)
LCX disease	11 (41)
RCA disease	12 (44)

CCS = Canadian Cardiovascular Society Angina Grading Scale; LV = left ventricular; EDV= end-diastolic volume; ESV = end-systolic volume; EF = ejection fraction; CAD = coronary artery disease (defined as stenosis ≥70%); VD = vessel disease

#### **4.4.3 Total Perfusion Defect**

All 27 patients (100%) were found to have perfusion defects by both observers. TPD by 2D high-resolution and 3D whole-heart acquisition showed strong positive correlation ( $r = 0.75$ ;  $p < 0.001$ ) and there was no significant difference in mean TPD values ( $9.1 \pm 5.7\%$  vs  $7.8 \pm 5.8\%$  respectively;  $p = 0.12$ ). There was no systematic bias for estimates of TPD between techniques (mean bias =  $-1.26\%$ , bias 95% CI:  $-2.8$  to  $0.4\%$ ) and the 95% limits of agreement were  $-9.3\%$  to  $6.8\%$  (Figure 4.2).

#### **4.4.4 Myocardial Ischaemic Burden**

MIB by 2D high-resolution and 3D whole-heart acquisition showed strong positive correlation ( $r = 0.72$ ;  $p < 0.001$ ) and there was no significant difference in mean MIB values ( $4.3 \pm 5.2\%$  vs  $4.1 \pm 4.9\%$  respectively;  $p = 0.81$ ) (Figure 4.3). There was no systematic bias for estimates of MIB between techniques (mean bias =  $-0.17\%$ , bias 95% CI:  $-1.7$  to  $1.3\%$ ) and the 95% limits of agreement were  $-7.5\%$  to  $7.2\%$  (Figure 4.4).

Out of the 27 patients, MIB was found to be  $>10\%$  by both methods in 3 patients; and  $<10\%$  by both methods in 17 patients (including 4 patients with an MIB of  $0\%$  by both methods). In 7 of the 27 patients the two methods disagreed at the  $10\%$  threshold: in 3 patients, the high-resolution method estimated MIB as  $> 10\%$  but 3D acquisition estimated it as  $<10\%$  (MIB difference =  $4.1 \pm 2.6\%$ ); and in 4 patients, the high-resolution method estimated MIB as  $<10\%$  but 3D acquisition estimated it  $> 10\%$  (MIB difference =  $9.3 \pm 1.2\%$ ). Overall, when used to categorise MIB as  $>10\%$  or  $<10\%$ , there was only fair agreement between the two techniques ( $\kappa = 0.29$ , 95% CI:  $-0.12-0.70$ ) (Figure 4.3).

All 16 patients with a prior history of MI had evidence of hyperenhancement on LGE imaging. There were no cases of LGE hyperenhancement without a clinical history of MI. In 8 out of the 16 patients (50%) with prior MI, a negative MIB value was determined with both 2D and 3D methods (normalized to zero for subsequent agreement analyses). There were no cases where only one of the techniques determined a negative MIB value.

After categorising patients into prior MI (n=16) or no MI (n=11), there were no significant differences in mean MIB values between 2D and 3D methods for either group (MI:  $1.9 \pm 3.9\%$  vs  $1.4 \pm 3.3\%$ ,  $p = 0.55$ ; No MI:  $8.4 \pm 4.7\%$  vs  $8.6 \pm 3.7\%$ ,  $p = 0.93$ ). Similarly, there was no systematic bias for estimates of MIB between techniques for either the MI group (mean bias =  $-0.41\%$ , bias 95% CI:  $-1.8$  to  $1.0\%$ , 95% limits of agreement:  $-5.7\%$  to  $5.0\%$ ) or the no MI group (mean bias =  $0.23\%$ , bias 95% CI:  $-3.5$  to  $4.0\%$ , 95% limits of agreement:  $-10.0\%$  to  $10.5\%$ ).

#### **4.4.5 Reproducibility**

The intra-observer CoV for MIB estimates from high-resolution and 3D perfusion CMR were 9% and 12% respectively. Corresponding CoV for inter-observer reproducibility were 14% and 15%, respectively.

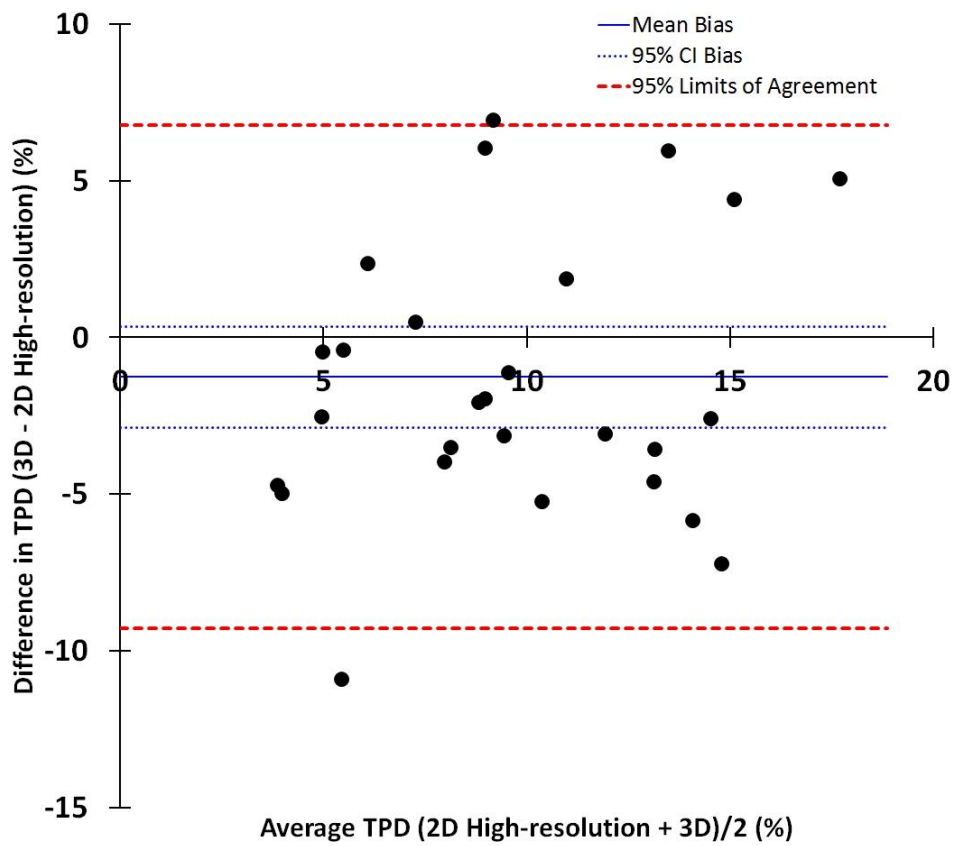


**Figure 4.2 TPD (%): 2D High-resolution vs. 3D Perfusion CMR**

The Bland-Altman plot shows no systematic bias for estimates of TPD between 2D high-resolution and 3D techniques (mean bias = -1.26%, bias 95% CI: -2.8 to 0.4%) and the 95% limits of agreement were -9.3% to 6.8%. TPD = total perfusion defect as percentage myocardium

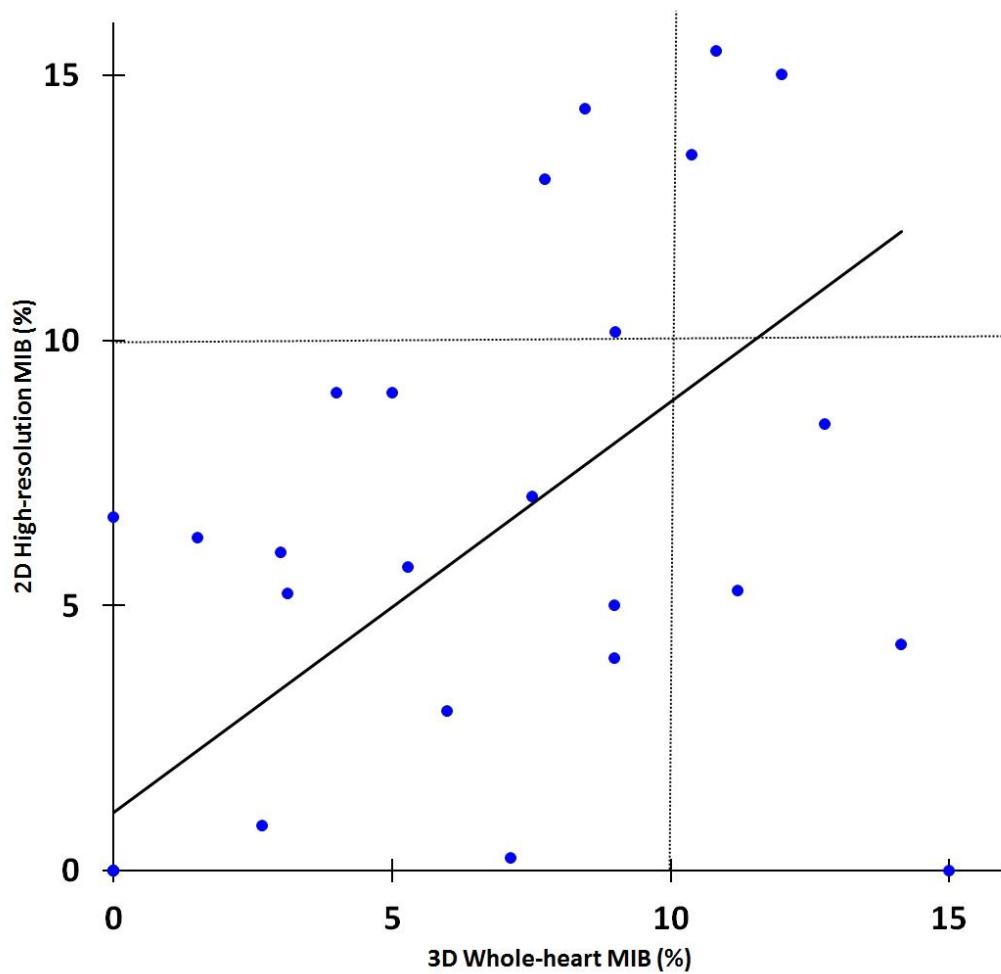


**Figure 4.3 Correlation between High-resolution and 3D estimates of MIB**

There was strong positive correlation between estimates of MIB from high-resolution 2D perfusion CMR and from 3D perfusion CMR ( $r = 0.72$ ;  $p < 0.001$ ). The dotted line indicates the 10% MIB threshold. MIB = myocardial ischaemic burden

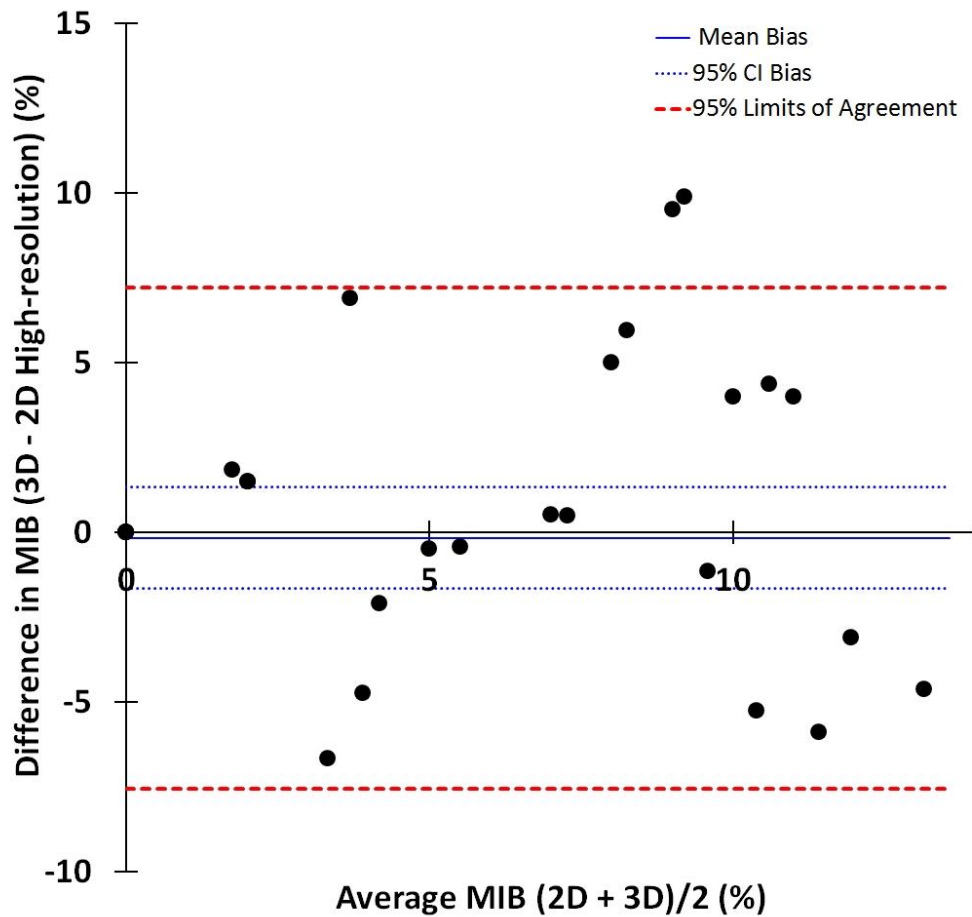


**Figure 4.4 MIB (%): 2D High-resolution vs. 3D Perfusion CMR**

The Bland-Altman plot shows no systematic bias for estimates of MIB between 2D high-resolution and 3D perfusion CMR techniques (mean bias = -0.17%, bias 95% CI: -1.7 to 1.3%) and the 95% limits of agreement were -7.5% to 7.2%. MIB = myocardial ischaemic burden as percentage myocardium

## 4.5 Discussion

The main findings of this study are: 1) image quality and diagnostic confidence scores are similar for both 2D high-resolution and 3D whole-heart perfusion CMR; and 2) although there is strong correlation and broad agreement between estimates of MIB from both techniques, the 95% limits of agreement are relatively wide and therefore a larger comparative study is needed before they can be considered interchangeable - particularly when categorising MIB as either side of 10%.

An accurate assessment of MIB is important because the extent of ischaemia is a marker of patient prognosis. In the nuclear imaging sub-study of COURAGE, patients with a MIB >10% had a lower risk of death or MI if they underwent revascularisation rather than optimal medical therapy alone (Shaw et al., 2008). Most data on MIB have been derived from SPECT studies, but with advances in accelerated data acquisition, 3D whole-heart perfusion CMR has become feasible and its role in assessing MIB has also been evaluated in a number of recent studies (Shin et al., 2008; Jogiya et al., 2012; Manka et al., 2012; Jogiya et al., 2014; Manka et al., 2011). In the first study, 3D perfusion CMR was shown to perform better than conventional 2D acquisition in estimating the size of perfusion defects in phantoms (Shin et al., 2008). Since then, several clinical studies have demonstrated its feasibility and high level of reproducibility for measuring MIB in patients (Jogiya et al., 2012; Manka et al., 2012, 2011). In particular, estimates of MIB from 3D perfusion CMR have been used to confirm a reduction in ischaemic volume following PCI, have shown strong correlation with the Duke Jeopardy Score (an invasive index of ischaemic burden)

and have also been validated against FFR for the detection of significant CAD (Manka et al., 2011; Jogiya et al., 2012; Manka et al., 2012).

A recent study by Jogiya *et al* found strong correlation between 3D perfusion CMR and SPECT estimates of MIB in 38 patients with confirmed perfusion defects on both modalities (2014). Although the latter study found no systematic bias between 3D perfusion CMR and SPECT estimates of MIB, and therefore suggested potential interchangeability, the 95% limits of agreement were relatively wide (-14.3% to 13.1%). Considering that a 10% MIB threshold is often used to direct clinical management, this caution is particularly relevant at the lower end of the MIB spectrum given the clinical impact of even a 5-10% absolute difference. Nonetheless, disagreement between 3D perfusion CMR and SPECT estimates of MIB at the 10% threshold only occurred in 3 out of 38 cases in the latter study (Jogiya et al., 2014).

On the other hand, investing acceleration into high-resolution 2D perfusion CMR rather than 3D whole-heart coverage, also has potential benefits for MIB estimation compared to standard 2D acquisition. As well as being less-susceptible to dark rim artefact and having better in-slice correlation with LGE (which is acquired at a similar spatial resolution), high-resolution perfusion CMR has also been shown to detect greater amounts of subendocardial ischaemia compared to standard-resolution 2D acquisitions - with particular benefit in patients with multi-vessel disease (Motwani et al., 2012a, 2014a). In one direct comparison, in 35 patients with angiographically confirmed 3-vessel CAD, only 24 patients were found to have a MIB >10% with a 2D standard-resolution perfusion CMR method compared to 33 with the high-resolution technique (Motwani et al., 2014a). However, unlike 3D whole-heart perfusion CMR,

the 2D high-resolution method has not yet been compared to SPECT or angiographic scores for MIB estimation.

As both 3D and high-resolution 2D perfusion CMR offer competing benefits in MIB estimation, their comparison in the current study is well justified. Although there has been no previous direct comparison of 3D whole-heart and 2D high-resolution perfusion CMR, the study by Jogiya *et al* did compare MIB estimates from 3D acquisition with estimates from 3 slices selected from the same 3D whole-heart dataset (2014). The authors explicitly acknowledged the limitations of such an extrapolation, including the impact of resolution and timing of acquisition in the cardiac cycle, but the data offer some insight into the impact of three-slice versus whole heart estimates of MIB. Although MIB estimates in Jogiya *et al.*'s study were smaller from the three-slice analysis compared to whole-heart analysis (5.7% vs 6.8%  $p=0.03$ ), there was no difference in assigning patients to either medical or revascularisation therapy when using a clinical threshold of 10% MIB (Jogiya *et al.*, 2014).

In our study, which is the first direct comparison of high-resolution 2D and whole-heart 3D perfusion CMR acquisition, there was only fair agreement across the 10% MIB threshold ( $\kappa = 0.29$ ). In 4 of 27 cases, 3D perfusion CMR identified a MIB>10%, but estimates with 2D high-resolution perfusion CMR were <10%; and conversely there were 3 cases where MIB was > 10% with 2D high-resolution perfusion CMR but not with 3D acquisition. These differences with potential clinical impact likely relate to the competing merits of both techniques, i.e. complete spatial coverage for ischemia detection including the apical cap with 3D acquisition, versus

better detection of subendocardial ischemia with high-resolution acquisition. As these factors are likely to affect individual patients differently according to their specific distribution of CAD, a single-best approach is difficult to define. Furthermore, with similar image quality, artefact and diagnostic confidence scores for both 3D and high-resolution perfusion CMR, it remains difficult to conclude on the preferred approach for MIB estimation – particularly in the absence of a true reference standard.

An additional finding in this study was a negative MIB value, with both techniques. This was seen in 50% of patients with prior MI and for the purpose of analysis was considered to represent inducible ischemia. A potential reason for the occurrence of negative MIB values may be an issue of inadequate co-registration between perfusion and LGE imaging slices. Such misregistration would be expected to have most impact on the 2D perfusion technique in which only 3 perfusion slices must be related to 12 LGE imaging slices. However, whilst 3D perfusion CMR may offer better slice-to-slice registration with LGE imaging by virtue of greater spatial coverage, the 2D high-resolution perfusion technique offers better intra-slice registration by virtue of the similar spatial resolution as LGE (1.2 vs 1.3 mm). Which of these effects is the most important in an individual patient, for an individual perfusion defect, cannot be predicted, and depends on the precise intra-slice and inter-slice extent of any perfusion defect, as well as the relative contributions of scar and ischemia. However, both effects clearly have the potential to lead to the scenario where quantified TSB from LGE imaging is larger than the TPD from either the 2D high-resolution or 3D whole-heart perfusion sequence. Furthermore, it is recognized that an infarct

detected on LGE imaging may sometimes be underestimated or not seen on perfusion imaging as a result of small size, heterogeneous infarct tissue characteristics, or recanalization of the culprit vessel (Klem et al., 2006). The findings in this study highlight the difficulties in reliably assessing peri-infarct ischemia which ideally requires intimate registration of perfusion and LGE images in terms of both spatial coverage and spatial resolution – and not just one variable in isolation.

Finally, the relatively wide 95% limits of agreement between 3D and high-resolution estimates of MIB in this study, suggest that estimates of MIB may not be used interchangeably at present – particularly when categorising patients either side of the 10% threshold. We would also apply the same argument to previous comparisons of MIB by SPECT and 3D perfusion CMR. Instead, there is a need to define the optimal prognostic MIB threshold for each of these techniques separately in future studies.

#### **4.5.1 Study Limitations**

We acknowledge this is a pilot study and only a larger study with prognostic outcomes will determine whether the differences seen in MIB between techniques are clinically meaningful. Nonetheless, the findings from this exploratory data are a reminder of the heterogeneity of available perfusion CMR methods and the need for greater standardisation given the potential influence of factors such as spatial resolution, temporal resolution and spatial coverage (Nagel & Shaw, 2014).

This study investigated a population with a relatively high prevalence of previous MI (n=16), but we were primarily interested in the assessment of inducible ischaemia.

In some cases, the presence of scar may have limited the detection of superimposed inducible ischaemia, and it is possible that the assessment of ischaemia may have been more accurate in populations without previous MI. Similarly, although a population with a broader spectrum of MIB would have been more comprehensive, our focus at the lower end around the 10% threshold is the most clinically relevant.

We acknowledge the use of QCA is an imperfect reference standard for ischemia. However, our main aim was to compare the size of perfusion defects in patients with CAD between techniques, rather than re-examine their diagnostic accuracy which has been done previously. Although FFR is clearly a better endpoint for perfusion studies, we considered QCA an adequate end-point for this purpose. Following this initial pilot study, a larger study with an FFR end-point is planned.

## **4.6 Conclusion**

This study adds to the ongoing debate about the comparative benefits of either higher spatial resolution or greater spatial coverage in perfusion CMR - and where the optimal trade-off lies. Although estimates of MIB from high-resolution and 3D perfusion CMR are strongly correlated, the 95% limits of agreement are relatively wide and therefore a larger comparative study is needed to determine if they can be considered freely interchangeable – particularly around the clinically relevant 10% threshold. Moreover, there is a need to define the optimal prognostic MIB threshold for each of these techniques separately.

## 5 Study 4 - Systolic versus Diastolic Acquisition in Myocardial Perfusion Imaging with CMR

### 5.1 Abstract

**Aim:** The aim of this study was to compare myocardial blood flow (MBF) between systole and diastole and determine the diagnostic accuracy of both phases in patients with suspected CAD.

**Methods:** All patients gave written consent and the study was approved by the regional ethics committee. Following coronary angiography, 40 patients (27 men,  $64 \pm 8$  yrs) underwent stress/rest perfusion CMR at 1.5T, acquired at end-systole and mid-diastole simultaneously. Based on angiographic stenosis  $>70\%$ , patients were classified as having 'CAD' or 'no significant CAD'. In patients with CAD, myocardial segments were grouped as 'stenosis-dependent' (downstream of significant stenosis) or 'remote'. MBF and myocardial perfusion reserve (MPR) were calculated for each segment; and mean values in each phase were compared with paired t tests. The diagnostic accuracy of each phase was determined with receiver-operator characteristic analysis.

**Results:** Twenty-one patients (53%) had CAD. Resting MBF was similar in both phases for normal and CAD patients ( $p>0.05$ ). Stress MBF was greater in diastole than systole in normal, remote and stenosis-dependent segments ( $3.75 \pm 1.50$  vs.  $3.15 \pm 1.10$  ml/g/min;  $2.75 \pm 1.20$  vs.  $2.38 \pm 0.99$  ml/g/min;  $2.49 \pm 1.07$  vs.  $2.23 \pm 0.90$  ml/g/min;  $p<0.01$ ). MPR was greater in diastole than systole in all segment groups

( $p < 0.05$ ). The diagnostic accuracy of diastole and systole were similar (area under curve 0.79 vs. 0.82;  $p = 0.30$ ).

**Conclusion:** Perfusion CMR estimates of stress MBF and MPR were greater in diastole than systole in patients with and without CAD. However, both phases had similar diagnostic accuracy. These observations may be relevant to other dynamic perfusion methods, including CT and echocardiography.

## 5.2 Introduction

The mechanical interaction between the myocardium and intramyocardial vessels yields a unique coronary blood flow profile. Left coronary artery (LCA) blood flow is predominantly diastolic when myocardial tension is low. Cardiac contraction in systole causes compression of intramyocardial vessels with virtually no forward or even retrograde systolic flow in the LCA (Yada et al., 1993; Hiramatsu et al., 1998; Chilian & Marcus, 1982; Kajiya et al., 1985; Sabsiton Jr & Gregg, 1957). Blood flow in the right coronary artery (RCA) shows less phasic variation with a small systolic preponderance because right ventricular peak systolic pressure is much lower than aortic peak systolic pressure and because the right ventricular wall offers less mechanical compressive resistance. The distal RCA segments which supply part of the left ventricle are however subject to the same haemodynamic conditions as the LCA (Heller et al., 1994).

In dynamic myocardial perfusion imaging by CMR, CT, or contrast echocardiography, myocardial blood flow (MBF) is estimated by tracing the myocardial passage of a contrast agent. In order to limit the effects of cardiac motion, data acquisition needs to be limited to short windows in the cardiac cycle. 2D acquisition methods, which prevail in CMR, typically acquire several sections of the heart in different phases of the cardiac cycle in order to maximise spatial coverage, while in 3D methods, such as CT or recent 3D CMR methods, one cardiac phase is typically pre-determined for data read-out. In particular in view of the technical constraints, the potential effects of cardiac phase on the acquired data and on estimates of MBF are generally not considered in 2D CMR methods. However, given the variability of coronary arterial

inflow throughout the cardiac cycle, the impact of the cardiac phase on estimates of MBF may be substantial.

A recent volunteer study has demonstrated significantly greater perfusion CMR-estimates of MBF during hyperaemic stress and myocardial perfusion reserve (MPR) in diastole than systole (Radjenovic et al., 2010). Whether these relationships exist in disease and whether there are potential diagnostic consequences of varying estimates of MBF between cardiac phases has not been investigated before.

The aim of this study was to compare MBF between systole and diastole and determine the diagnostic accuracy of both phases in patients with suspected CAD.

## **5.3 Methods**

### **5.3.1 Study Population**

Forty patients who had undergone clinically indicated diagnostic coronary angiography within the previous 30 days were recruited. All patients gave written consent and the study was approved by the regional ethics committee. No coronary intervention or clinical events occurred between angiography and recruitment. Exclusion criteria were contra-indications to CMR imaging, adenosine or gadolinium contrast agents or acute coronary syndrome within 6 months. Patients refrained from caffeine for 24hrs prior to CMR. Cardiac medications were continued as normal.

### **5.3.2 CMR Imaging**

CMR imaging was performed on a 1.5-T Intera CV system (Philips Healthcare, Best, the Netherlands) with a five-element cardiac phased array receiver coil. Stress

perfusion imaging was performed after 4 minutes of intravenous adenosine (140 mcg/kg/min) infusion. A bolus of 0.05 mmol/kg dimeglumine gadopentetate (Gd-DTPA) (Magnevist, Schering, Berlin, Germany) followed by 15 mls of saline flush were injected into an antecubital vein at 5 ml/s (Spectris®, Medrad, Indianola, PA). Rest perfusion images were acquired 15 minutes later followed by LGE imaging using a standard protocol (Kramer et al., 2008).

Perfusion data were acquired in the same 2D mid-ventricular slice in both end-systole and mid-diastole using identical preparation and readout settings (Radjenovic et al., 2010). Pulse sequence details were as follows: saturation recovery gradient-echo, 150ms preparation pulse delay, repetition time (TR) 2.7ms, echo time (TE) 1.0ms, flip angle 15°, acquisition duration 135ms, two-fold parallel imaging (SENSE), field of view 320mm, matrix 160 x 160mm, spatial resolution 2 x 2 x 10 mm<sup>3</sup>.

### **5.3.3 Image Quality**

Image quality was graded as (1 = poor, 2 = adequate, 3 = excellent) by consensus of two observers (S.P., M.M., 10 years and 1 year experience in perfusion CMR imaging). The occurrence of endocardial dark rim artefacts was scored as (0 = none, 1 = mild, 2 = moderate, 3 = severe). The width of any artefacts was measured using electronic callipers with standardized window settings. All systolic and diastolic images were analysed in separate reporting sessions and randomly ordered by readers blinded to the results for the other phase.

### **5.3.4 Quantitative Image Analysis**

Myocardial contours excluding any dark rim artefact were outlined in QMass 6.1.6 (Medis, Leiden, the Netherlands) and segmented into 6 equiangular segments (Cerqueira et al., 2002). The systolic arterial input function (AIF) was used for both systolic and diastolic analysis to avoid potential variations in the AIF between phases (Radjenovic et al., 2010). Signal intensity/time data were converted to concentration/time data and MBF at stress and rest estimated with Fermi-constrained deconvolution in MATLAB (The Mathworks Inc., Natick, MA) (Jerosch-Herold et al., 1998; Biglands et al., 2011). MPR was calculated by dividing hyperaemic by resting MBF.

Ten random studies (60 segments) were re-analysed one month later by the same observer (M.M.) and by a second observer (A.L.) blinded to all previous analyses (one and 5 years' experience, respectively).

### **5.3.5 Coronary Angiography Analysis**

X-ray angiography images were analysed by an experienced observer (M.M, 6 years experience) blinded to CMR and clinical data. Quantitative coronary angiography (QCA) was performed with QCAPlus (Sanders Data Systems, Palo Alto, California, USA). 'Significant CAD' was defined as at least 1 stenosis of >70% (luminal diameter reduction) in vessels with a diameter of >2mm. Stenoses were assigned to myocardial segments adjusted for arterial dominance and lesion location (Patel et al., 2010; Cerqueira et al., 2002; Marie et al., 1993). In patients with significant CAD, myocardial segments were classified as either 'stenosis-dependent' (i.e. considered downstream of a significant stenosis) or 'remote' (i.e. supplied by a non-obstructed

coronary vessel or considered upstream of any significant stenosis) - and these two groups were analysed separately. This distinction was undertaken as MBF and MPR is reduced in remote segments in patients with CAD. Segments from patients without any significant stenoses were considered the 'normal' control group.

### **5.3.6 Statistical Analysis**

Analysis was performed using SPSS version 17.0 (SPSS, Chicago, IL, USA). Data are presented as mean  $\pm$  SD. Group means were compared using paired and unpaired Student *t* test as appropriate. Discrete data were compared using Fisher's exact test or Wilcoxon signed-rank tests as appropriate. All tests were two-tailed and a *p* value  $<0.05$  was considered statistically significant.

Receiver operating characteristic (ROC) analyses were used to determine the diagnostic accuracy of quantitative CMR analysis in systole and diastole and to determine the MPR with the greatest sensitivity and specificity to detect significant CAD. Areas under the curve (AUC) were determined from the ROC analyses for systole and diastole and then compared using validated methods described by DeLong and DeLong (DeLong et al., 1988).

A repeated measures one-way analysis of variance test for within-subject difference (with Greenhouse–Geisser correction for multi-sample sphericity and Bonferroni adjustment for post-hoc analysis) was used to compare the relationship (and any trends) between MPR and severity of disease. Sensitivity and specificity were compared between systole and diastole using the McNemar test. Intra- and inter-observer variabilities for MPR quantification were calculated as the absolute

difference between two measurements in percent of their mean and according to the methods of Bland and Altman (Martin Bland & Altman, 1986)

## **5.4 Results**

### **5.4.1 Study Population**

The patient characteristics of the 40 study patients (27 men, mean age  $64 \pm 8$  yrs) are outlined in Table 5.1. QCA confirmed significant CAD in 21 patients (53%). Thirteen patients (33%) had one vessel disease, seven (18%) had two-vessel disease and one (3%) had three-vessel disease (Table 5.2).

All CMR scans and data analyses were completed. A typical example of a patient with ischaemia is shown in Figure 5.1. A total of 240 segments in 40 patients were therefore available for analysis in both systole and diastole. From the 19 patients with no significant CAD on QCA, 114 'normal' segments were derived. From the 21 patients with significant CAD on QCA, 126 segments were derived and these were further divided into 38 'stenosis-dependent' segments (downstream of a significant stenosis) and 88 'remote' segments (supplied by a non-obstructed vessel or upstream of significant stenosis). Only 5 patients had evidence of myocardial infarction on LGE imaging (the same 5 patients with a clinical history) and this involved only 4 of the 240 segments in the perfusion analysis (bearing in mind that only the mid-ventricular slice was analysed).

**Table 5-1 Baseline Patient Characteristics**

	All (n=40)	CAD (n=21)	No CAD (n=19)	p Value
<b>Demographics</b>				
Male, n (%)	27 (68)	16 (76)	11 (58)	0.37
Age, yrs	64 ± 8	65 ± 8	63 ± 8	0.49
<b>Risk Factors for CAD, n (%)</b>				
Smoking	9 (23)	8 (38)	1 (5)	0.02
Hypertension	22 (55)	16 (76)	6 (30)	0.01
Diabetes	5 (13)	5 (24)	0 (0)	0.05
Previous PCI	4 (10)	4 (19)	0 (0)	0.11
Previous MI	5 (13)	5 (24)	0 (0)	0.05
<b>Medications, n (%)</b>				
Aspirin	32 (80)	21 (100)	11 (58)	<0.01
Beta-Blocker	25 (63)	19 (90)	6 (32)	<0.01
ACE-Inhibitor	23 (58)	19 (90)	4 (21)	<0.01
Statin	25 (63)	20 (95)	5 (26)	<0.01
Nitrate	6 (15)	6 (29)	0 (0)	0.02
Calcium Channel blocker	12 (30)	6 (29)	6 (32)	1.00
<b>CMR imaging data</b>				
LVEF %	60 ± 6	61 ± 7	59 ± 5	0.42
LVEDV, ml	150 ± 22	153 ± 16	147 ± 27	0.44
LVESV, ml	63 ± 14	66 ± 14	60 ± 14	0.19
LV Mass, g/m <sup>2</sup>	93 ± 25	100 ± 25	87 ± 24	0.11
Stress Heart Rate (beats/min)	80 ± 15	79 ± 12	82 ± 13	0.65

**Table 5-2 Coronary Angiography Findings**

QCA findings	Patients, n (%)
No significant stenoses	19 (48)
Any stenoses >70%	21 (53)
1-vessel disease	13 (33)
2-vessel disease	7 (18)
3-vessel disease	1 (3)
LMS disease	3 (8)
LAD disease	9 (23)
LCX disease	4 (10)
RCA disease	6 (15)

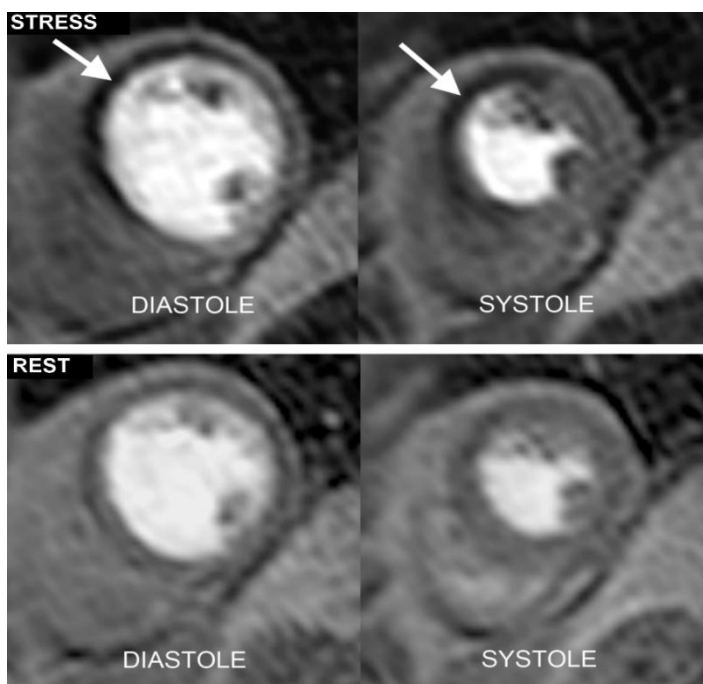


**Figure 5.1 Case Example: Systolic vs. Diastolic Acquisition**

Example perfusion CMR images with acquisition in diastole and systole. This patient had a subtotal occlusion of the left anterior descending artery. Corresponding stress perfusion defects (white arrows) are seen in the anterior, anteroseptal and inferoseptal segments of a mid-ventricular slice acquired in both diastole and systole

### 5.4.2 Image Quality

On per patient analysis (n=40), overall image quality was better for systole than diastole (mean score  $2.73 \pm 0.51$  vs.  $2.25 \pm 0.74$  respectively;  $p=0.002$ ) with a greater incidence of dark rim artefact in diastolic images (n=10 [25%] vs. n=1 [3%]) (Figure. 5.2). The corresponding mean artefact scores were  $0.53 \pm 1.01$  for diastole and  $0.03 \pm 0.16$  for systole ( $p=0.008$ ). The mean artefact width was 2.4 mm for diastole; and the single dark rim artefact in systole had a width of 2.2 mm and was graded as only mild. Four of the 10 artefacts in diastole were graded as severe, 3 as moderate and 3 as mild.

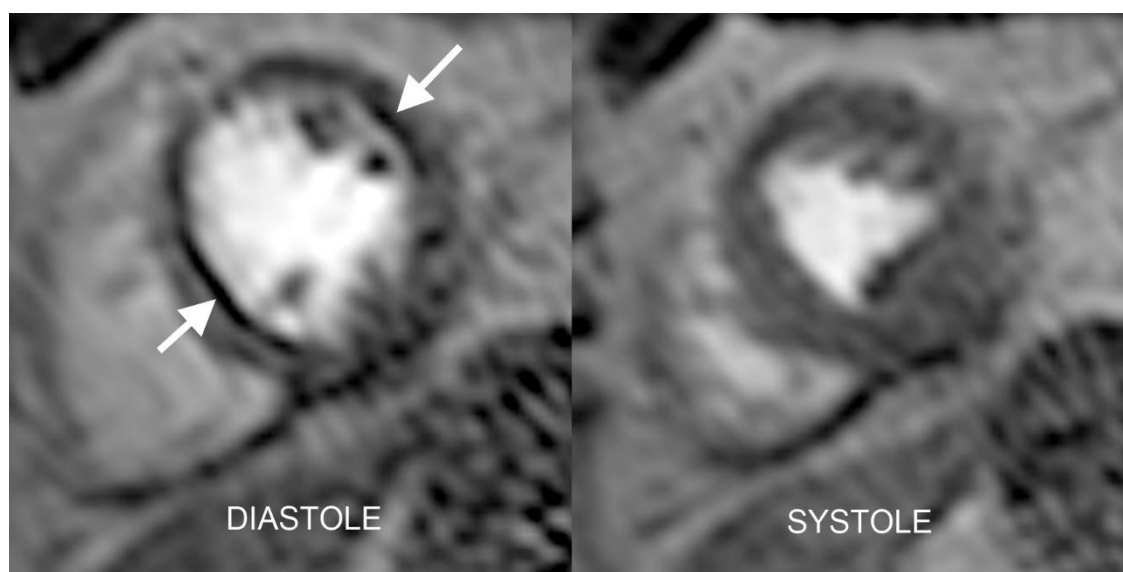


**Figure 5.2 Dark rim artefact: Systole vs Diastole**

*In this example, dark rim artefacts (white arrows) are seen on the diastolic CMR perfusion image (mid-ventricular level) in the septal and lateral segments during adenosine stress but are not seen on the corresponding systolic image.*

### **5.4.3 Quantitative Image Analysis**

#### **5.4.3.1 Per Patient Analysis**

In the patients with CAD (n=21), the mean resting MBF was similar between phases ( $1.13 \pm 0.46$  ml/g/min in systole vs.  $1.14 \pm 0.47$  ml/g/min in diastole;  $p=0.40$ ). Stress MBF however was greater in diastole than systole ( $2.49 \pm 1.07$  ml/g/min vs.  $2.23 \pm 0.90$  ml/g/min;  $p=0.004$ ) and so was the MPR ( $2.26 \pm 0.77$  vs.  $2.03 \pm 0.56$ ;  $p=0.02$ ). The same relationship was found in patients with no significant CAD (n=19). The mean resting MBF was similar between systole and diastole ( $1.12 \pm 0.32$  ml/g/min vs.  $1.12 \pm 0.31$  ml/g/min;  $p=0.5$ ). Stress MBF was greater in diastole than systole ( $3.57 \pm 1.22$  ml/g/min vs.  $3.18 \pm 1.07$  ml/g/min;  $p=0.02$ ) and so was the MPR ( $3.44 \pm 1.78$  vs.  $3.05 \pm 1.61$ ;  $p=0.10$ ).

#### **5.4.3.2 Per Segment Analysis**

The above relationships remained present on segmental analysis (n=240) in each of the three groups of segments (Figures 5.3 and 5.4) i.e. MBF was not different between phases at rest, but both stress MBF and MPR were significantly greater in diastole than systole in 'stenosis-dependent' (n=38), 'remote' (n=88) and 'normal' control segments (n=114) ( $p$  values < 0.01). There was a good correlation between systolic MPR and diastolic MPR ( $r=0.78$ ;  $p<0.0001$ ) between all segments.

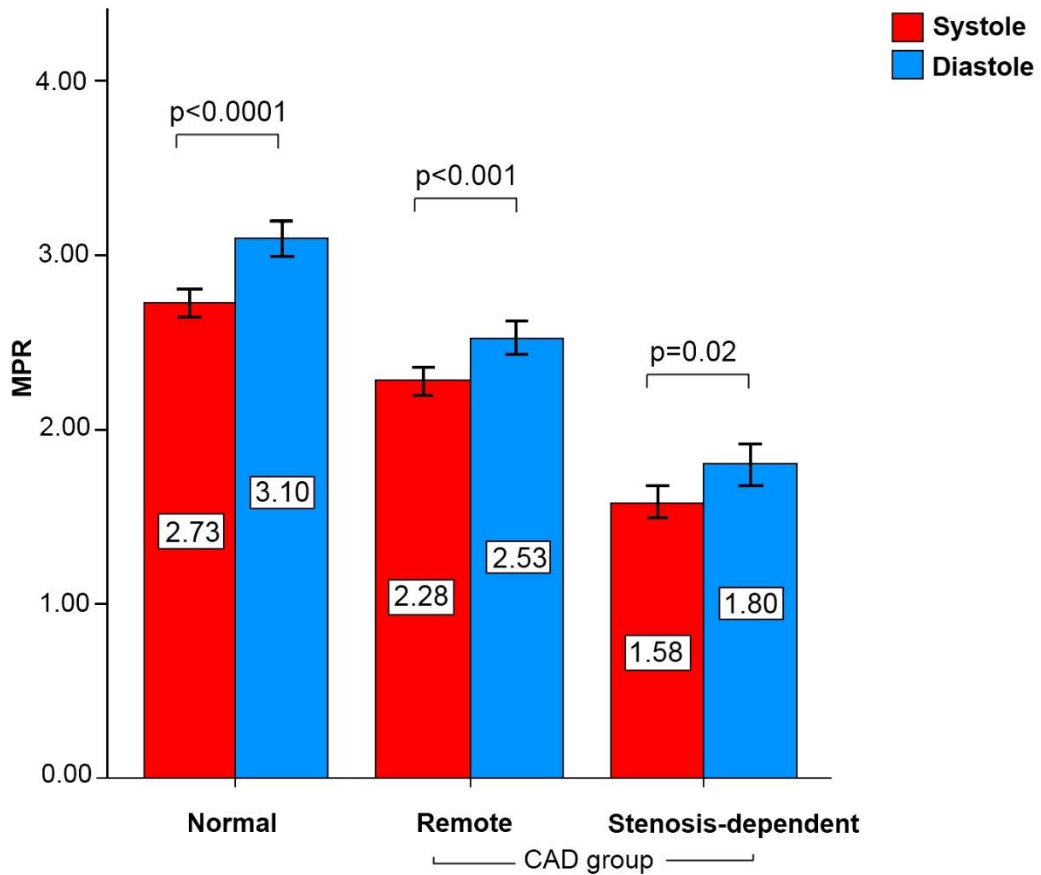


**Figure 5.3 MPR: Systole versus Diastole**

A comparison of MPR between systole and diastole. Segmental MPR (mean ± SEM) is shown for normal segments, remote CAD segments and stenosis-dependent CAD segments.

#### 5.4.4 Diagnostic Performance

In both systole and diastole, the mean MPR was highest in the ‘normal’ control segments (systole  $2.73 \pm 0.75$ , diastole  $3.10 \pm 1.11$ ), intermediate in the ‘remote’ CAD segments (systole  $2.28 \pm 0.69$ , diastole  $2.52 \pm 0.89$ ) and lowest in the ‘stenosis-dependent’ CAD segments (systole  $1.58 \pm 0.57$ , diastole  $1.80 \pm 0.75$ ) with a significant difference between all segment categories ( $p$  values  $< 0.05$ ) and for the trend ( $p < 0.001$ ) (Figures 5.3 and 5.4).

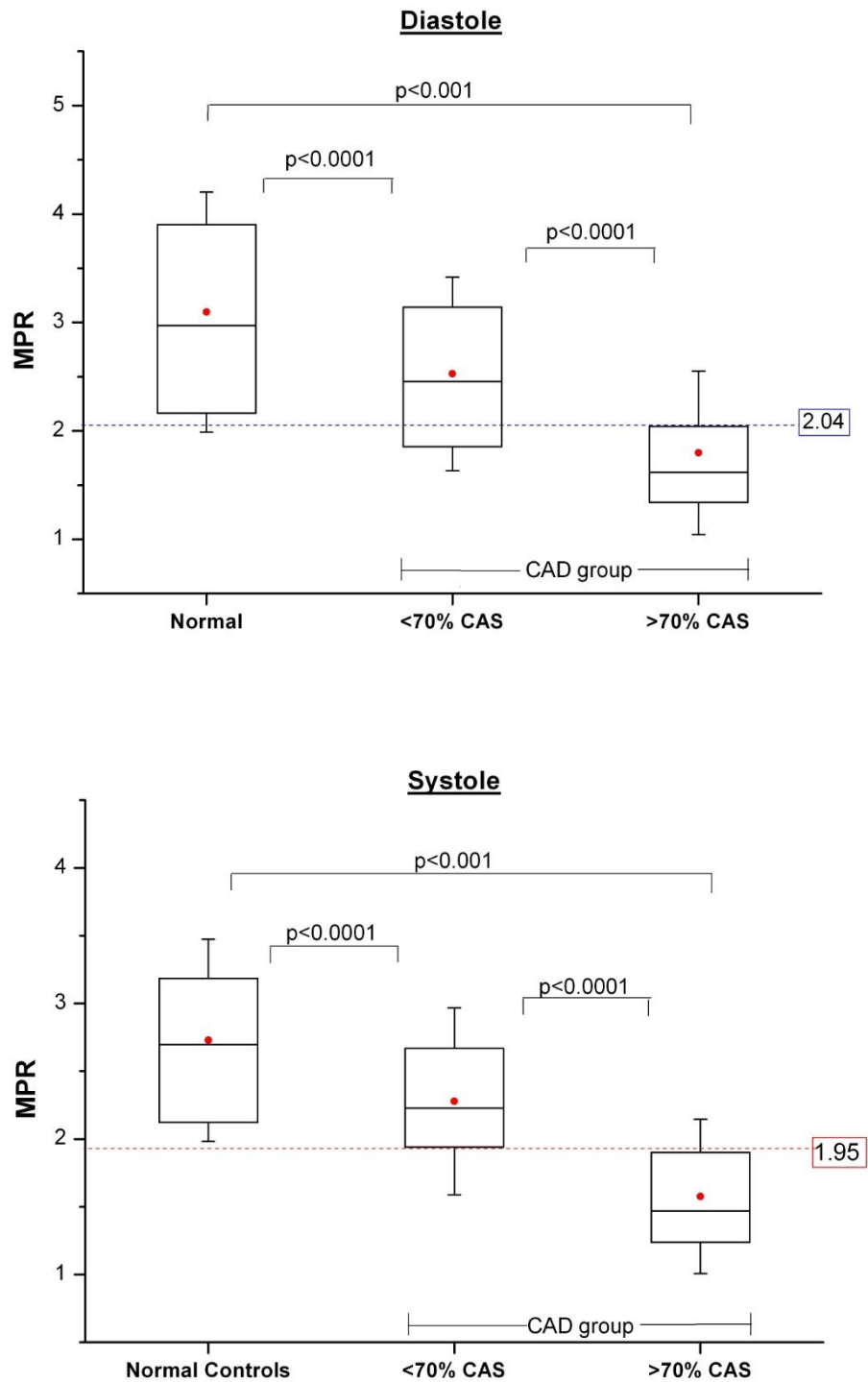


**Figure 5.4 MPR for CAD detection - Systolic and Diastolic Boxplots**

Systolic and diastolic MPR by disease category. Boxplots show mean (dot), median, quartile and standard deviation values for each category. Optimal diagnostic MPR cut-offs are plotted as dashed line (1.95 in systole, 2.04 in diastole).

ROC analysis (using all 240 segments) for distinguishing angiographically significant stenosis from non-significant stenosis (combining remote CAD and normal control segments), revealed similar diagnostic accuracies for the MPR in both systole and diastole (AUC of 0.82 and 0.79 respectively;  $p=0.30$ ). The optimal MPR cut-off value, defined as the value with optimal sensitivity and specificity, was 1.95 for systole and 2.04 for diastole. At these thresholds the sensitivity and specificity were 79% and 76% respectively for systole and 77% and 73% for diastole. There was no significant difference between systole and diastole for diagnostic accuracy (AUC), sensitivity or specificity ( $p$  values  $>0.05$ ) (Figure 5.5, Table 5.3).

There was no significant difference between the ratio of diastolic stress MBF to systolic stress MBF across the three groups of segments ('normal'  $1.20 \pm 0.36$ , 'remote CAD'  $1.17 \pm 0.25$ , 'stenosis-dependent'  $1.21 \pm 0.34$ ;  $p=0.40$ ).

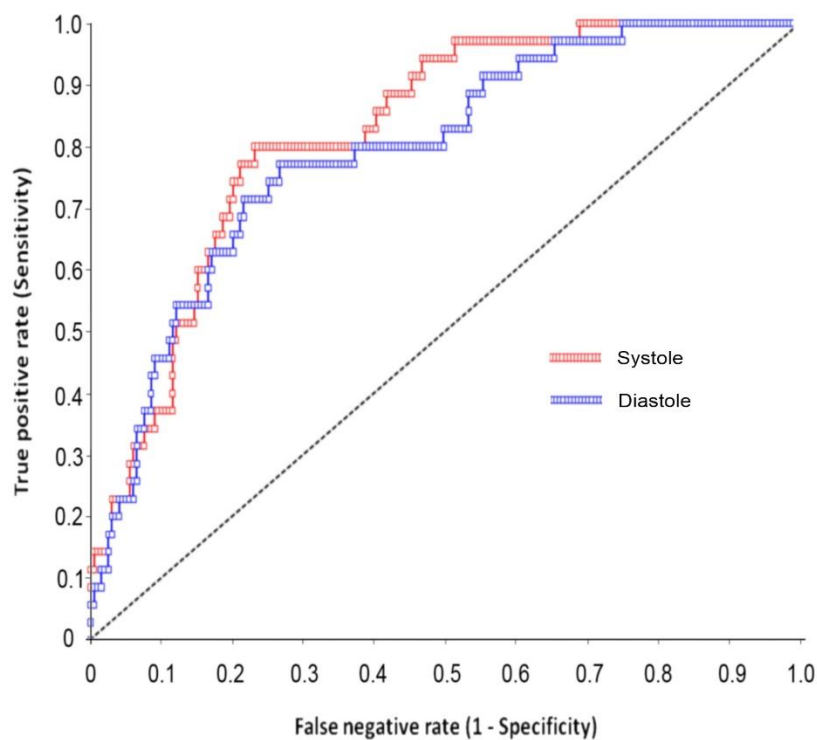


**Figure 5.5 ROC curve of quantitative perfusion CMR using MPR.**

*The area under the curve was 0.82 for systole and 0.79 for diastole ( $p=0.30$ ).*

**Table 5-3 Diagnostic Performance of Perfusion CMR: Systole vs. Diastole**

	<b>Systole</b>	<b>Diastole</b>	<b>p Value</b>
<b>AUC</b>	0.82 (0.76-0.89)	0.79 (0.72-0.87)	0.30
<b>Sensitivity</b>	79% [30/38](64-90)	76% [29/38] (60-88)	0.99
<b>Specificity</b>	77% [155/202] (71-82)	73% [147/202] (67-79)	0.31

\*(95% CI given in brackets). Sensitivity and specificity expressed as % [fraction]

### **5.4.5 Intra-observer and Inter-observer Variability**

Intra-observer variability of MPR measurement was similar in systole and diastole ( $2.0 \pm 12.6\%$  vs.  $2.1 \pm 16.7\%$ ;  $p=0.96$ ); as was inter-observer variability ( $4.8 \pm 17.9\%$  vs.  $4.9 \pm 19.1\%$ ;  $p=0.98$ ). On Bland-Altman analysis the intra- and inter-observer bias was similar for both phases (intra-observer bias:  $-0.04 \pm 0.49$  vs.  $-0.10 \pm 0.71$ ; inter-observer bias:  $0.07 \pm 0.72$  vs.  $0.16 \pm 0.81$ , for systole vs. diastole, respectively).

## **5.5 Discussion**

This study has shown that in patients with suspected and confirmed CAD, estimates of MBF by CMR imaging are similar in systole and diastole at rest, but are significantly higher in diastole during maximal hyperaemic stress. Accordingly, the MPR is greater in diastole. Diagnostic accuracy is similar between the two phases.

The differences in hyperaemic MBF between systole and diastole in this study are consistent with the reduced effects of adenosine-mediated vasodilatation in systole when myocardial contraction compresses intramyocardial vessels (Hiramatsu et al., 1998; Yada et al., 1993). Our data are also consistent with the sparse existing

literature. A study of 5 healthy subjects with a dual-phase 3D perfusion CMR method showed no differences between the two phases with semi-quantitative analysis of resting perfusion (Shin et al., 2010). A study in 17 healthy volunteers using a 2D perfusion CMR method confirmed similar MBF values at rest but higher estimates of diastolic MBF at stress (Radjenovic et al., 2010). One small animal study using real-time myocardial contrast echocardiography demonstrated higher estimates of MBF using end-diastolic frames than with end-systolic frames under hyperaemic stress (Leongpoi et al., 2001). Our results show that the differences between systolic and diastolic MBF seen in animal and volunteer studies are also found in patients with CAD and in the presence of myocardial ischaemia.

The optimal MPR cut-off values to detect significant CAD (1.95 for systole and 2.04 for diastole) were within the range (1.5-2.06) reported in previous studies (Rieber et al., 2006; Futamatsu et al., 2007; Al-Saadi et al., 2000; Watkins et al., 2009; Costa et al., 2007). Quantitative analysis with MPR yielded high diagnostic accuracies in both systole and diastole (AUC 0.82 and 0.79 respectively). Importantly, due to study design and the limitations of 2D acquisition, these results were obtained from only a single mid-ventricular section. Sensitivity in particular may be higher if more sections are acquired, for example in future 3D perfusion CMR imaging studies.

Dark rim artefact is a frequent finding in myocardial perfusion CMR imaging and it is thought to relate to several factors including cardiac motion, Gibb's ringing caused by truncation of *k*-space, non-uniformity of *k*-space weighting due to saturation recovery and readout, and partial volume cancellation between the myocardium and blood pool (Kellman & Arai, 2007). Although dark rim artefacts may mimic perfusion

defects, they can usually be distinguished by characteristic features i.e. they are most intense at peak signal intensity in the left ventricle cavity, are transient (persist for less than 10 dynamic images) and their location is usually typical for a particular pulse sequence. Our study found dark rim artefact was significantly more abundant in diastole (only 1 mild artefact in systole) and this is consistent with previous studies (Plein et al., 2007, 2008b). Dark rim artefact may be more pronounced in diastole because the myocardium is thinner, making it more prone to partial volume effects at a given spatial resolution (Kellman & Arai, 2007).

In conventional 2D myocardial perfusion CMR methods, cardiac phase cannot be freely chosen as multiple 2D sections of the heart are acquired successively throughout the entire cardiac cycle. Thus, the impact of phase on estimates of MBF in 2D myocardial perfusion CMR imaging may be difficult to consider and potentially even complicate data analysis. However, the advent of 3D CMR and CT imaging allows for contiguous coverage of the whole left ventricle in a single cardiac phase, which avoids misregistration problems - but the optimal phase has yet to be determined (Shin et al., 2008). In mid-diastole the heart is usually at its most stationary, but as shown, may be more affected by dark rim artefact. End-systole has a shorter quiescent period, but is less sensitive to R-R variability and arrhythmia, which is relevant to the increasing burden of patients with atrial fibrillation (Kellman & Arai, 2007). Systole is less affected by dark rim artefacts and contour delineation is easier because of the thicker myocardium. Given the comparable diagnostic performance between the two phases in this study, systole may thus be the favoured cardiac phase for data acquisition in CMR imaging, if a choice can be made.

In this study, MPR was greatest in segments of patients with no CAD, intermediate in remote segments of patients with CAD and smallest in segments downstream of a significant stenosis (Figure 5.3). This stepwise reduction in MPR related to the severity of CAD has been shown in previous studies using positron emission tomography and fractional flow reserve (Lockie et al., 2011; Watkins et al., 2009; Costa et al., 2007; Al-Saadi et al., 2000; Rieber et al., 2006; Patel et al., 2010). As shown in previous PET studies, coronary flow and myocardial perfusion reserve are impaired in patients with CAD even in the absence of flow-limiting stenosis due to endothelial dysfunction and alterations in the microcirculation associated with CAD and its risk factors (Beanlands et al., 1995; Muzik PhD & Duvernoy, 1998; Wang et al., 2006). In addition to existing literature, our data have shown that the ratio of diastolic to systolic stress MBF is similar in the absence of CAD, in the presence of significant coronary stenosis and in remote myocardium in CAD patients.

## **5.6 Limitations**

Like the majority of previous myocardial perfusion CMR studies, we used X-ray angiography to determine the presence of significant coronary stenosis. Although MPR performed well in our study, perfusion imaging is a measurement of the haemodynamic consequences of a stenosis rather than its anatomy so that QCA is an imperfect reference standard (Lockie et al., 2011). It is also important to acknowledge that myocardial segments and vessel territories do not always match; and that both remote and stenosis-dependent myocardium can be found in the same myocardial segments which are limitations of per segment analyses.

In order to obtain systolic and diastolic perfusion data in the same location and within the same acquisition using conventional 2D CMR imaging, this study was limited to the assessment of a single mid-ventricular slice. This was a technical necessity and only by compromising temporal resolution with consequent impact on the validity of MBF estimates could we have overcome this limitation. Clearly, only analysing a single slice will have led to an underestimation of diagnostic performance in both systole and diastole. Furthermore, this study could not assess differences between cardiac phases in apical and basal myocardial segments, which may behave differently to the mid-ventricular location. Future studies using 3D myocardial perfusion CMR will be needed to address these issues.

Qualitative visual analysis was not performed as the limitation to a single slice is not in keeping with clinical practice and it was felt this would be an inadequate endpoint to judge the difference between the two phases.

## **5.7 Conclusion**

In conclusion, systole and diastole provide similar estimates of MBF at rest in patients with suspected CAD; but measurements of MBF during stress are consistently greater in diastole - in normal, remote CAD and stenosis-dependent CAD segments. However, in this study the overall diagnostic accuracy of both phases was similar. If open to choice, systole may be the preferred phase as the thicker myocardium is less demanding on spatial resolution and is less prone to artefact. These results are relevant to any form of dynamic myocardial perfusion assessment and are of particular relevance to the promising developments in 3D CMR and CT

perfusion imaging where the cardiac phase for data acquisition can be specifically chosen.

## 6 Study 5 - Quantitative Three-Dimensional Perfusion

### CMR in Systole and Diastole

#### 6.1 Abstract

**Background:** 2D perfusion CMR remains limited by a lack of complete myocardial coverage. 3D perfusion CMR addresses this limitation and has recently been shown to be clinically feasible. However, the feasibility and potential clinical utility of *quantitative* 3D perfusion measurements, as already shown with 2D perfusion CMR and PET, has yet to be evaluated. The influence of systolic or diastolic acquisition on myocardial blood flow (MBF) estimates, diagnostic accuracy and image quality is also unknown for 3D perfusion CMR. The purpose of this study was to establish the feasibility of quantitative 3D perfusion CMR for the detection of CAD and to compare systolic and diastolic estimates of MBF.

**Methods:** Thirty-five patients underwent 3D perfusion CMR with data acquired at both end-systole and mid-diastole. MBF and myocardial perfusion reserve (MPR) were estimated on a per patient and per territory basis by Fermi-constrained deconvolution. Significant CAD was defined as stenosis  $\geq 70\%$  on quantitative coronary angiography.

**Results:** Twenty patients had significant CAD (involving 38 out of 105 territories). Stress MBF and MPR had a high diagnostic accuracy for the detection of CAD in both systole (area under curve [AUC]: 0.95 and 0.92, respectively) and diastole (AUC: 0.95 and 0.94). There were no significant differences in the AUCs between systole and

diastole (p values >0.05). At stress, diastolic MBF estimates were significantly greater than systolic estimates (no CAD:  $3.21 \pm 0.50$  vs.  $2.75 \pm 0.42$  ml/g/min,  $p < 0.0001$ ; CAD:  $2.13 \pm 0.45$  vs.  $1.98 \pm 0.41$  ml/g/min,  $p < 0.0001$ ); but at rest, there were no significant differences (p values >0.05). Image quality was higher in systole than diastole (median score 3 vs. 2,  $p = 0.002$ ).

**Conclusions:** Quantitative 3D perfusion CMR is feasible. Estimates of MBF are significantly different for systole and diastole at stress but diagnostic accuracy to detect CAD is high for both cardiac phases. Better image quality suggests that systolic data acquisition may be preferable.

## 6.2 Background

Myocardial perfusion imaging with CMR is a highly accurate technique for the detection of CAD (Greenwood et al., 2012). However, conventional acquisition with 2D methods covers only 3-4 non-contiguous slices of the LV at each R-R interval, and therefore incomplete myocardial coverage remains a significant limitation.

Recent technological advances have allowed unprecedented acceleration of dynamic CMR and the development of 3D myocardial perfusion CMR methods providing full LV coverage with preserved temporal and spatial resolution (Vitanis et al., 2011; Shin et al., 2013; Chen et al., 2012). Three recent studies have shown 3D-perfusion CMR to be clinically feasible and highly accurate for the detection of CAD with visual perfusion assessment (Manka et al., 2011, 2012; Jogiya et al., 2012). However, the feasibility and potential clinical application of deriving quantitative estimates of MBF from 3D perfusion CMR has not yet been studied.

A further limitation of conventional 2D perfusion CMR is that each slice is acquired in a different period of the cardiac cycle. Two recent quantitative studies have shown a significant difference in MBF estimates derived from the same mid-ventricular slice acquired in systole and diastole with 2D perfusion CMR (Radjenovic et al., 2010; Motwani et al., 2012b). As well as limiting quantitative comparisons between slices, these significant phasic differences impact on inter-study and longitudinal comparisons of MBF. Unlike 2D perfusion CMR, 3D acquisition allows acquisition of data from the entire myocardium in the same, optimised period of the cardiac cycle. Most previous 3D perfusion CMR studies have acquired data in systole but to date it is unknown whether systolic or diastolic acquisition leads to better image quality and

diagnostic yield. Furthermore, it is unknown whether quantitative estimates of MBF from 3D data demonstrate the same phasic differences previously reported for 2D techniques (Radjenovic et al., 2010; Motwani et al., 2012b).

The purpose of this study was therefore to establish the feasibility of quantitative 3D perfusion CMR for the detection of CAD and to compare systolic and diastolic estimates of MBF.

## **6.3 Methods**

### **6.3.1 Population**

Forty consecutive patients with known or suspected CAD were recruited. All patients were imaged within 30 days of clinically scheduled diagnostic coronary angiography. No revascularization or clinical events occurred between angiography and CMR. Exclusion criteria were contraindications to CMR, adenosine, or gadolinium contrast agents, recent myocardial infarction (MI) or unstable angina (within 6 months), or poorly controlled arrhythmias. Patients were instructed to refrain from caffeine for 24 hours before their CMR study but continue cardiac medications as normal. The study was approved by the regional ethics committee and all patients gave written consent.

### **6.3.2 CMR protocol**

All studies were performed on a 3.0T scanner (Achieva TX, Philips Healthcare, Best, The Netherlands) equipped with dual-source parallel radiofrequency transmission technology and a 32-channel cardiac coil. For perfusion imaging, a 3D spoiled turbo

gradient-echo sequence was used (TR/TE/flip angle 1.8ms/0.7ms/15°; saturation prepulse delay 150ms; linear *k*-space encoding; 70% partial Fourier acquisition in two dimensions; typical field of view 350 x 350mm; 10 fold *k*-*t* acceleration and 11 training profiles leading to a net acceleration of 7.0; typical acquisition duration 192ms, *k*-*t* principal component analysis (PCA) reconstruction; reconstructed to 12 contiguous slices with voxel size 2.3x2.3x5mm<sup>3</sup>)(Jogiya et al., 2012; Vitanis et al., 2011).

Two *k*-*t* undersampled 3D data sets were acquired in each R-R interval, each preceded by a non-selective saturation prepulse. Vertical and horizontal long-axis cine images were used to identify appropriate trigger delays for systolic and diastolic acquisition(Radjenovic et al., 2010; Shin et al., 2010; Motwani et al., 2012b). Additionally, because of the longitudinal lengthening of the heart from systole to diastole, the position of the end-systolic and mid-diastolic perfusion stacks (12 slices each) were individually planned from the chosen systolic and diastolic cine frames (Figure 6.1)(Radjenovic et al., 2010; Motwani et al., 2012b). The same trigger delays were used for stress and rest acquisitions.

Stress perfusion images were acquired during intravenous adenosine-induced hyperaemia administered for 4min at 140mcg/kg/min. Consistent with previous 3D-perfusion CMR studies, an intravenous bolus of 0.075mmol/kg of gadobutrol (Gadovist, Bayer Schering Pharma, Berlin, Germany) was administered at a rate of 4.0ml/s followed by a 20ml saline flush. Stress perfusion CMR was followed by cine imaging covering the left ventricle in 10-12 short-axis sections. Rest perfusion CMR was performed 15min after stress, using identical imaging parameters. LGE imaging

was acquired in the same short-axis geometry as perfusion imaging after an additional 10-15min using conventional 2D methods (T1 weighted segmented inversion recovery gradient echo; TR/TE/flip angle 4.9ms/1.9ms/15°; inversion time individually adjusted according to Look-Locker scan; spatial resolution 1.35 x 1.35 x 10 mm).

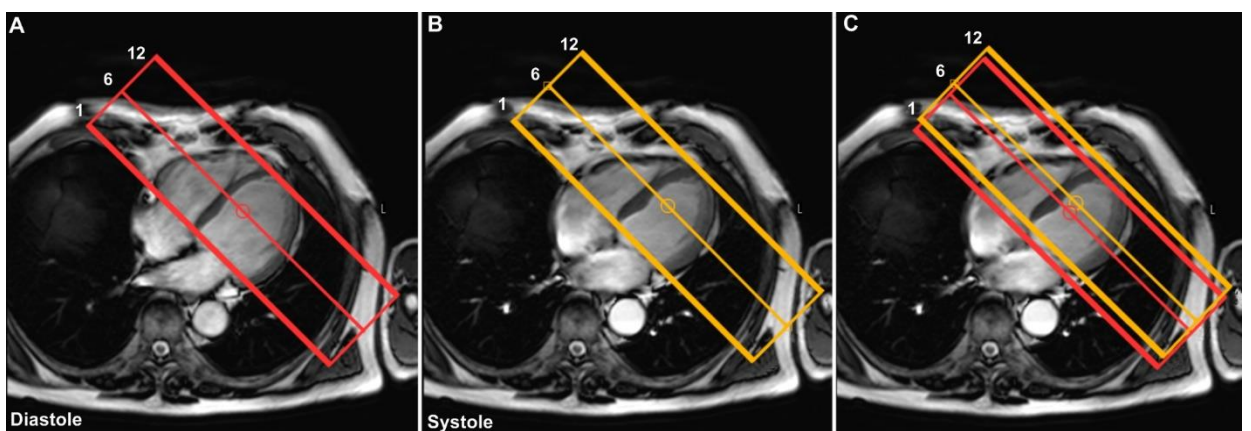


**Figure 6.1 3D Acquisition Planning for Systole and Diastole**

*Because of the longitudinal lengthening of the heart from systole to diastole, the position of the mid-diastolic (red) and end-systolic perfusion stacks (yellow) (12 slices each) were individually planned from the chosen diastolic (Panel A) and systolic (Panel B) 4-chamber cine frames. Panel C shows both stacks superimposed on the chosen end-systolic frame.*

### 6.3.3 Image quality

Systolic and diastolic perfusion images were analysed in separate reporting sessions in random order (MM, 2 years experience of perfusion CMR). Overall image quality was scored as follows: 0 = non-diagnostic, 1 = poor, 2 = adequate and 3 = excellent. The occurrence of artefact related to respiratory-motion, *k-t* reconstruction or dark rim artefact was scored as follows: 0 = none, 1 = mild, 2 = moderate and 3 = severe.

### **6.3.4 Myocardial blood flow estimation**

Perfusion images were processed offline using previously validated in-house software (PMI 0.4; written in IDL 6.4 (ITT Visual Information Systems, Boulder, CO)(Huber et al., 2012). All short-axis slices with clearly identifiable LV cavity enhancement during first-pass perfusion and with >75% circumferential LV myocardium were included in the analysis (Manka et al., 2011, 2012).

#### ***6.3.4.1 Per patient analysis***

Following manual rigid motion-correction, a circular region of interest (ROI) was drawn in the basal LV cavity in diastole, to derive the arterial input function (AIF). The same (diastolic) AIF was used for both systolic and diastolic estimates of MBF in order to avoid potential variations in the AIF between phases with subsequent effects on MBF estimation (Radjenovic et al., 2010).

A whole-heart myocardial region of interest (ROI) excluding any dark rim artefact was drawn for both systolic and diastolic perfusion images. Signal intensity–time data were converted to concentration–time data by subtracting the baseline signal, and global MBF was estimated at stress and rest using constrained deconvolution with a delayed Fermi-model applied to the first pass (Jerosch-Herold et al., 1998; Costa et al., 2007; Motwani et al., 2012b). MPR was calculated as stress MBF divided by rest MBF.

#### ***6.3.4.2 Per territory analysis***

The above analysis was repeated on a per territory basis using the 17-segment AHA model adjusted for coronary dominance (Cerqueira et al., 2002). All slices from an individual patient were first visually allocated to basal, mid or apical sections of the

model. For each perfusion territory, a myocardial ROI was then outlined including all segments pertaining to that territory across all slices according to the 17-segment AHA model. MBF and MPR estimates were obtained using the same algorithm as for the whole-heart ROI.

#### ***6.3.4.3 Intra-observer and inter-observer variability***

Thirty random territories were re-analysed 1 month later by the same observer (M.M.) and by a second observer A.K. (2yrs and 1yr experience respectively). A.K. was blinded to the results of all previous analyses.

#### **6.3.5 Quantitative coronary angiography**

Quantitative coronary angiography was performed (QCAPlus, Sanders Data Systems, Palo Alto, CA, USA) on anonymised X-ray angiography images (M.M. 6 years experience in coronary angiography). Significant CAD was defined as luminal stenosis  $\geq 70\%$  diameter in any of the main epicardial coronary arteries or their branches with a diameter of  $\geq 2\text{mm}$ .

#### **6.3.6 Statistical analysis**

Analysis was performed using SPSS 17.0 (SPSS, Chicago, IL). Data are presented as mean $\pm$ SD. Group means were compared using paired or unpaired Student t-tests; or within-subjects analysis of variance with Greenhouse-Geisser correction for multi-sample sphericity, as appropriate. Ordinal data were compared using the Wilcoxon signed-rank test. Receiver-operating characteristic (ROC) analysis was performed on a per territory basis, to determine the diagnostic accuracy of MPR to detect significant CAD. Diagnostic accuracies are presented as area under the ROC curve

(AUC); and were compared between systole and diastole using methods described by DeLong and DeLong. Optimal MPR cut-off values, for both cardiac phases, were defined as values that maximised the sum of sensitivity and specificity. A secondary ROC analysis was performed to evaluate the diagnostic accuracy of stress MBF diastolic/systolic ratio. To assess reproducibility, the coefficients of variation (CoV) for intra- and inter-observer measurements were calculated. Because three coronary territories were examined per patient, the intra-cluster correlation coefficient (ICC) was calculated for MPR estimates to determine the design effect and the need to adjust data for clustering. All statistical tests were 2-tailed and a p value <0.05 was considered significant.

## **6.4 Results**

### **6.4.1 Study population**

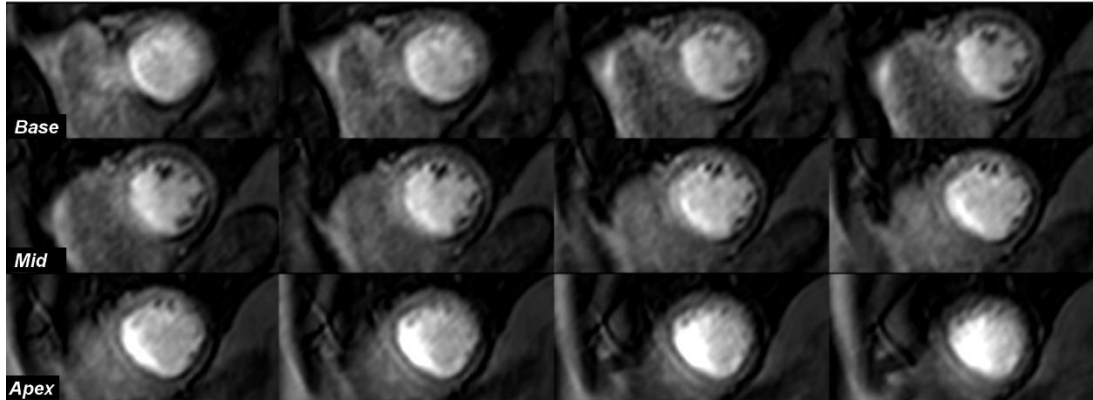
Five of the 40 recruited patients were excluded: 3 because of claustrophobia and 2 owing to technical problems (1 mistimed contrast injection; 1 significantly altered patient position between stress and rest scans). A total of 35 patients (105 coronary territories) were therefore available for analysis. Table 6.1 shows the baseline patient characteristics. QCA confirmed significant CAD in 20 patients (57%) and 38 coronary territories (36%). Only 3 patients had evidence of MI on LGE imaging (the same 3 patients with a clinical history of MI), and this involved only 3 of the 105 territories analysed. Figure 6.2 shows an example of the stress perfusion images acquired in a patient with significant CAD.

**Table 6-1 Patient Characteristics**

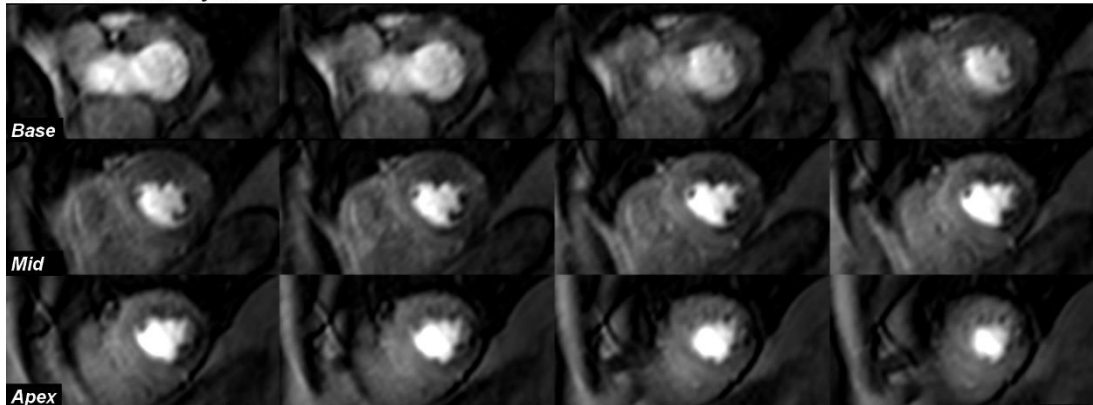
<b>Parameter</b>	<b>Data (n=35)</b>
<b>Age (yrs ± SD)</b>	62 ± 8
<b>Sex, n (%)</b>	
Male	26 (74)
Female	9 (26)
<b>Risk Factors, n (%)</b>	
Hypertension	18 (51)
Hypercholesterolemia	19 (54)
Diabetes Mellitus	6 (17)
Smoking	14 (40)
Previous MI	3 (9)
Previous PCI	3 (9)
<b>Angiography findings, n (%) *</b>	
No significant disease	15 (43)
One-vessel disease	6 (17)
Two-vessel disease	10 (29)
Three -vessel disease	4 (11)
LAD disease	17 (49)
LCX disease	10 (29)
RCA disease	11 (31)

\*Significant disease defined as coronary stenosis  $\geq 70\%$  on quantitative coronary analysis.

Stress Perfusion - Diastole



Stress Perfusion - Systole



LGE Imaging

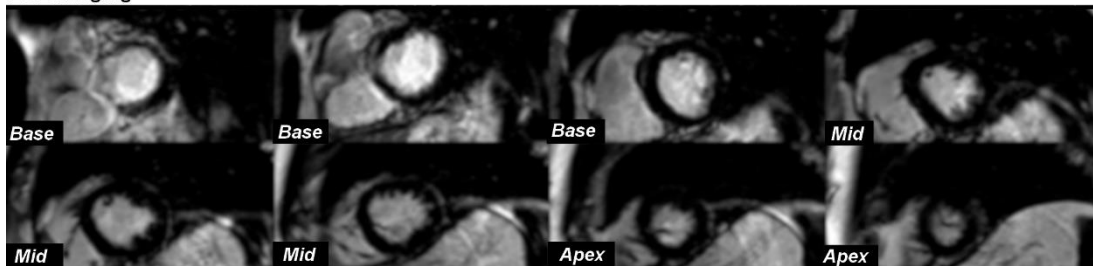


**Figure 6.2 Case Example: 3D-Perfusion CMR in Systole and Diastole**

*This example shows 3D-perfusion CMR in a 75-year-old man with angina. Stress-induced perfusion defects are seen infero-laterally from base to apex and antero-laterally from mid-ventricle to apex in both diastole and systole. However, perfusion defects are difficult to discern from dark rim artefact in diastole and are more clearly delineated with systolic acquisition. Late-gadolinium enhancement imaging did not reveal any myocardial infarction. X-ray coronary angiography revealed 80% stenosis of a large diagonal branch and significant proximal disease in a large dominant left circumflex artery.*

### **6.4.2 Image quality**

Overall image quality was better in systole than in diastole (median image quality score: 3 vs. 2 respectively;  $p=0.002$ ). In diastole, there was a greater frequency of dark rim artefact (19 patients [54%] vs. 9 patients [26%] and a higher overall artefact score compared to systole (median scores: 1 vs. 0 respectively;  $p<0.0001$ ). In 5 patients (14%), perfusion images (both cardiac phases) were affected by *k-t* reconstruction artefacts at stress and/or rest due to respiratory motion, but all of these artefacts occurred at the end of the breath-hold and did not affect analysis of the first-pass perfusion images.

### **6.4.3 Myocardial blood flow estimation**

Estimates of MBF and MPR for both cardiac phases are seen in Tables 6.2-6.4. On per patient ( $n=35$ ) and per territory analysis ( $n=105$ ), mean resting MBF was similar in both cardiac phases (all  $p$  values  $>0.05$ ); but mean stress MBF and MPR were significantly greater in diastole than systole (all  $p$  values  $<0.001$ ). These relationships existed in normal and CAD subgroups, as well as overall (all  $p$  values  $<0.01$ ) (Tables 6.2-6.4). In both cardiac phases, stress MBF and MPR were significantly lower in the presence of CAD than in normal patients (all  $p$  values  $<0.01$ ) or normal territories (all  $p$  values  $<0.0001$ ) (Tables 6.2-6.4).

Analysis of the normal patient group ( $n=15$ ) found no significant regional differences in stress MBF, rest MBF or MPR between the LAD, LCX or RCA perfusion territories in both phases (all  $p$  values  $<0.05$ ) (Table 6.5).

**Table 6-2 Estimates of MBF and MPR from 3-Dimensional Perfusion CMR - Per Patient Analysis**

	Stress MBF (ml/min/g)			Rest MBF (ml/min/g)			MPR		
	<i>Systole</i>	<i>Diastole</i>	<i>P</i>	<i>Systole</i>	<i>Diastole</i>	<i>p</i>	<i>Systole</i>	<i>Diastole</i>	<i>p</i>
<b>Normal (n=15)</b>	2.88 ± 0.32	3.47 ± 0.41	p<0.0001	1.28 ± 0.17	1.26 ± 0.15	p=0.45	2.27 ± 0.37	2.78 ± 0.40	p<0.0001
<b>CAD (n=20)</b>	2.32 ± 0.42	2.53 ± 0.47	p<0.0001	1.32 ± 0.19	1.28 ± 0.21	p=0.06	1.82 ± 0.54	2.08 ± 0.74	p<0.001
<b>Overall (n=35)</b>	2.56 ± 0.47	2.93 ± 0.65	p<0.0001	1.30 ± 0.18	1.27 ± 0.19	p=0.06	2.01 ± 0.08	2.38 ± 0.05	p<0.0001

**Table 6-3 Estimates of MBF and MPR from 3-Dimensional Perfusion CMR - Per Territory Analysis**

	Stress MBF (ml/min/g)			Rest MBF (ml/min/g)			MPR		
	<i>Systole</i>	<i>Diastole</i>	<i>p</i>	<i>Systole</i>	<i>Diastole</i>	<i>p</i>	<i>Systole</i>	<i>Diastole</i>	<i>p</i>
<b>Normal (n=67)</b>	2.75 ± 0.42	3.21 ± 0.50	p<0.0001	1.24 ± 0.15	1.25 ± 0.15	p=0.27	2.26 ± 0.43	2.59 ± 0.44	p<0.0001
<b>CAD (n=38)</b>	1.98 ± 0.41	2.13 ± 0.55	p<0.0001	1.24 ± 0.15	1.26 ± 0.14	p=0.20	1.63 ± 0.14	1.72 ± 0.19	p<0.01
<b>Overall (n=105)</b>	2.47 ± 0.55	2.82 ± 0.71	p<0.0001	1.24 ± 0.15	1.25 ± 0.15	p=0.10	2.03 ± 0.52	2.27 ± 0.61	p<0.0001

All values expressed as mean ± SD; MBF = myocardial blood flow; MPR = myocardial perfusion reserve

**Table 6-4 Regional Estimates of MBF and MPR - Per Territory (n=105)**

	Normal			CAD		
	<i>Systole</i>	<i>Diastole</i>	<i>p</i>	<i>Systole</i>	<i>Diastole</i>	<i>p</i>
<b>Stress MBF (ml/min/g)</b>						
<i>LAD</i>	2.91 ± 0.35	3.43 ± 0.46	p<0.0001	2.11 ± 0.46	2.28 ± 0.52	p<0.001
<i>LCX</i>	2.63 ± 0.33	3.10 ± 0.44	p<0.0001	1.90 ± 0.28	2.04 ± 0.28	p<0.01
<i>RCA</i>	2.77 ± 0.51	3.16 ± 0.55	p<0.0001	1.85 ± 0.39	1.97 ± 0.40	p<0.0001
<b>Rest MBF (ml/min/g)</b>						
<i>LAD</i>	1.26 ± 0.17	1.30 ± 0.17	p=0.10	1.21 ± 0.12	1.23 ± 0.12	p=0.52
<i>LCX</i>	1.26 ± 0.17	1.24 ± 0.13	p=0.56	1.22 ± 0.14	1.20 ± 0.10	p=0.27
<i>RCA</i>	1.20 ± 0.13	1.23 ± 0.15	p=0.28	1.28 ± 0.13	1.24 ± 0.16	p=0.26
<b>MPR</b>						
<i>LAD</i>	2.35 ± 0.42	2.68 ± 0.48	p<0.0001	1.75 ± 0.37	1.87 ± 0.51	p=0.02
<i>LCX</i>	2.12 ± 0.35	2.52 ± 0.38	p<0.0001	1.58 ± 0.32	1.72 ± 0.29	p<0.01
<i>RCA</i>	2.33 ± 0.51	2.59 ± 0.48	p<0.001	1.46 ± 0.34	1.60 ± 0.34	p<0.01

All values expressed as mean ± SD. MBF = myocardial blood flow; MPR = myocardial perfusion reserve; LAD = left anterior descending coronary artery; LCX = left circumflex coronary artery; RCA= right coronary artery.

Based on MPR estimates, the ICC for this study was low ( $r_1 = 0.09$  [95% CI: -0.25 to 0.41]) with a design effect of 1.18 where cluster size=3. This shows that the study design of using 3 'related' coronary territories per patient (n=35) to derive a sample size of 105 coronary territories does not significantly diminish statistical power.

**Table 6-5 Comparison of Regional MBF and MPR Estimates – in Normal Patients (n=15)**

	Perfusion Territory			<i>p</i>
	<i>LAD</i>	<i>LCX</i>	<i>RCA</i>	
<b>Stress MBF (ml/min/g)</b>				
Systole	2.95 ± 0.36	2.66 ± 0.29	2.88 ± 0.46	P=0.11
Diastole	3.51 ± 0.46	3.19 ± 0.27	3.27 ± 0.47	P=0.10
<b>Rest MBF (ml/min/g)</b>				
Systole	1.27 ± 0.17	1.29 ± 0.19	1.20 ± 0.13	p=0.25
Diastole	1.29 ± 0.17	1.27 ± 0.14	1.22 ± 0.15	p=0.47
<b>MPR</b>				
Systole	2.36 ± 0.42	2.10 ± 0.32	2.45 ± 0.53	P=0.06
Diastole	2.76 ± 0.45	2.54 ± 0.33	2.71 ± 0.48	P=0.27

All values expressed as mean ± SD. MBF = myocardial blood flow; MPR = myocardial perfusion reserve; LAD = left anterior descending coronary artery; LCX = left circumflex coronary artery; RCA= right coronary artery.

## 6.4.4 Diagnostic performance

### 6.4.4.1 Stress MBF

On a per territory analysis (n=105), the use of stress MBF alone had a high overall diagnostic accuracy for the detection of CAD - which was similar in both cardiac phases (AUC=0.95 for both; p=0.70). The optimal stress MBF cut-off value was

2.31ml/min/g for systole and 2.60ml/min/g for diastole. At these thresholds, the sensitivity and specificity were 92% and 93% respectively for systole; and 95% and 96% for diastole. There was no significant difference between the diagnostic accuracy of MPR or stress MBF alone for either cardiac phase (both p values >0.05) (Figure 6.3)

#### **6.4.4.2 MPR**

On per territory analysis (n=105), MPR also had a high overall diagnostic accuracy for the detection of significant CAD, and this was similar in both cardiac phases (AUC, systole: 0.92 vs. diastole: 0.94; p=0.41) (Figure 6.3). The optimal MPR cut-off value was 1.75 for systole and 2.02 for diastole (Figure 6.4). At these thresholds, the sensitivity and specificity were 82% and 93% respectively for systole; and 87% and 94% for diastole. The diagnostic accuracy of MPR to detect CAD in each of the 3 coronary territories is shown in Table 6.6 – and no significant differences were seen between cardiac phases.

#### **6.4.4.3 Diastolic/systolic stress MBF ratio**

The diastolic/systolic stress MBF ratio was significantly lower for territories with CAD than in normal territories ( $1.07 \pm 0.06$  vs.  $1.17 \pm 0.11$ ;  $p < 0.0001$ ). On ROC analysis, the diagnostic accuracy (AUC) of this ratio to detect significant CAD was 0.79. The optimal cut-off value for the ratio was 1.10 which gave a sensitivity of 82% and specificity of 76% (Figure 6.5).

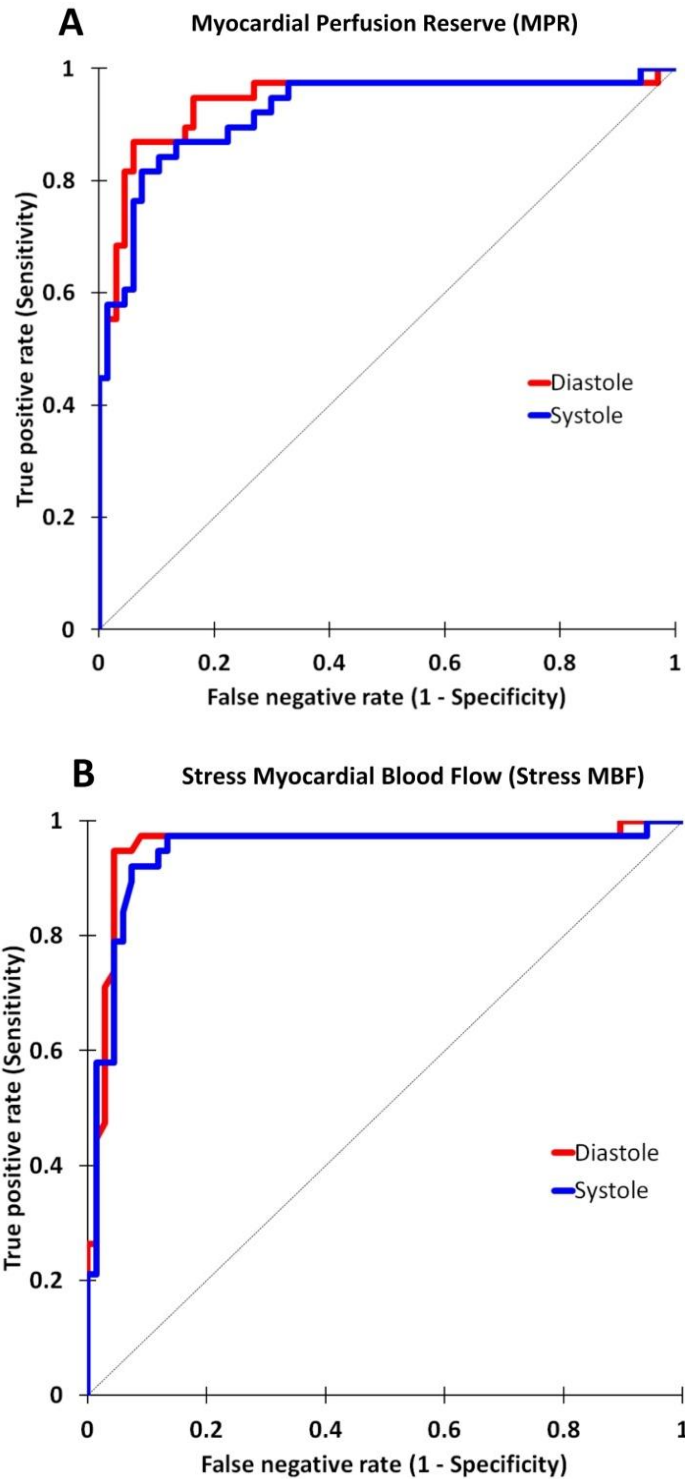


**Figure 6.3 Diagnostic Accuracy of Quantitative 3D-Perfusion CMR**

(A) Receiver-operator characteristic curves shows a high diagnostic accuracy in both systole and diastole for MPR (area under curve [AUC]: 0.92 vs. 0.94 respectively;  $p=0.41$ ). (B) Use of stress MBF alone also had a high diagnostic accuracy in both cardiac phases (AUC: 0.95 for both;  $p=0.70$ ) and in fact there was no significant difference compared to MPR ( $p>0.05$  for both cardiac phases).

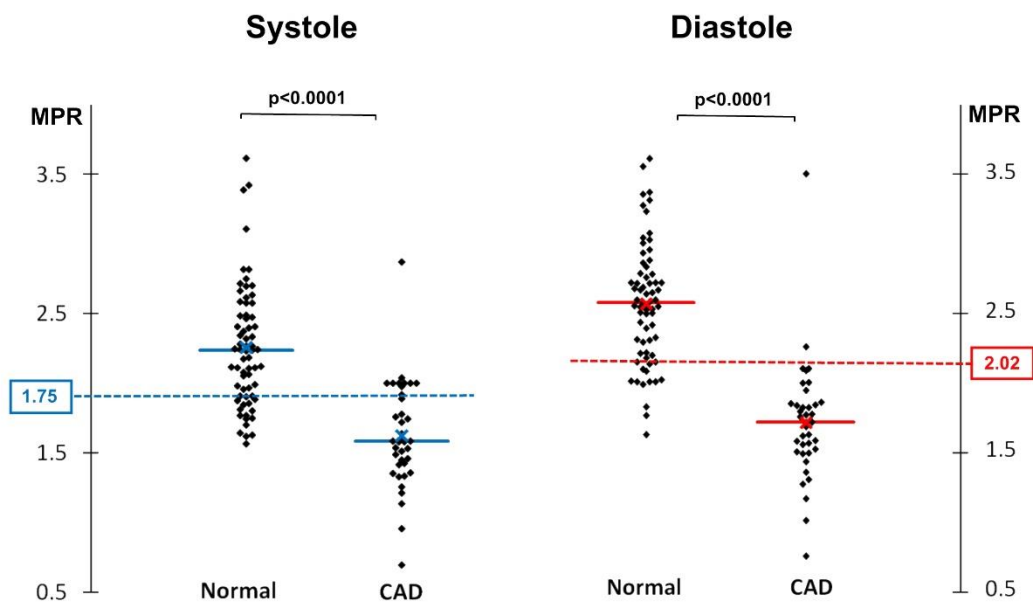


**Figure 6.4 Myocardial Perfusion Reserve Threshold**

The scatter-plots show myocardial perfusion reserve (MPR) values from normal and significantly diseased perfusion territories with both systolic and diastolic 3D-perfusion CMR ( $\bar{x}$ =mean value, solid line = median value). The optimal MPR cut-off values determined by receiver-operating characteristic analysis are also plotted (dashed lines, 1.75 for systole and 2.02 for diastole).

**Table 6-6 Diagnostic Accuracy of Quantitative 3D-perfusion CMR – Per Territory (n=105)**

AUC for MPR			
	<i>Systole</i>	<i>Diastole</i>	<i>P</i>
<b>All territories</b>	0.92 (0.87-0.98)	0.94 (0.88-0.99)	p=0.41
<b>LAD</b>	0.89 (0.78-0.99)	0.90 (0.79-1.00)	p=0.76
<b>LCX</b>	0.88 (0.77-0.99)	0.98 (0.93-1.00)	p=0.34
<b>RCA</b>	0.92 (0.86-0.99)	0.98 (0.93-1.00)	p=0.50

Area under the curve (AUC) and (95% confidence interval). LAD = left anterior descending coronary artery; LCX = left circumflex coronary artery; RCA= right coronary artery.

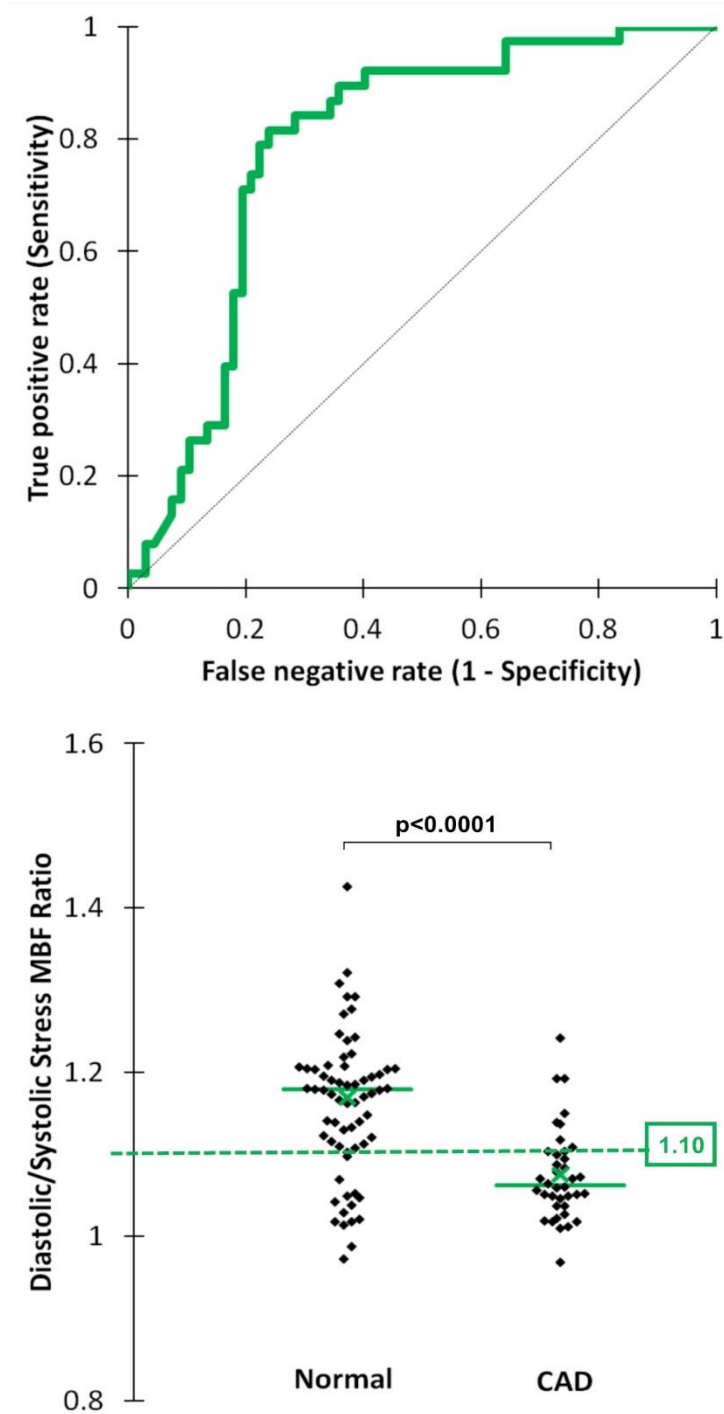


**Figure 6.5 Diastolic/Systolic Stress Myocardial Blood Flow Ratio**

The ratio of diastolic to systolic myocardial blood flow at stress was significantly lower for territories with coronary artery disease (CAD) than in normal territories ( $1.07 \pm 0.06$  vs.  $1.17 \pm 0.11$ ;  $p < 0.0001$ ). On receiver-operator characteristic analysis, the diagnostic accuracy (area under the curve) of this ratio to detect significant CAD was 0.79. The optimal cut-off value for the ratio was 1.10, which gave a sensitivity of 82% and specificity of 76%.

## **6.4.5 Reproducibility**

### **6.4.5.1 Stress MBF**

The mean absolute difference between intra-observer measurements of stress MBF was similar in systole and diastole ( $0.33 \pm 0.14$  vs.  $0.35 \pm 0.16$ ;  $p=0.18$ ); and the corresponding CoVs were 16% and 17% respectively. The mean absolute difference between inter-observer measurements of stress MBF was also similar in systole and diastole ( $0.41 \pm 0.22$  vs.  $0.45 \pm 0.20$ ;  $p=0.11$ ) with corresponding CoVs of 18% for both.

### **6.4.5.2 MPR**

The mean absolute difference between intra-observer measurements of MPR was similar in systole and diastole ( $0.30 \pm 0.15$  vs.  $0.36 \pm 0.13$ ;  $p=0.09$ ); and the corresponding CoVs were both 18%. The mean absolute difference between inter-observer measurements of MPR was also similar in systole and diastole ( $0.35 \pm 0.17$  vs.  $0.41 \pm 0.15$ ;  $p=0.07$ ) with corresponding CoVs of 20% and 21% respectively.

## **6.5 Discussion**

The main findings of this study are 1) quantitative 3D perfusion CMR is feasible and has a high diagnostic accuracy for the detection of CAD; 2) similar to 2D studies, estimates of stress MBF and MPR from 3D data are significantly greater in diastole than systole; and 3) the diastolic dominance of stress MBF estimates is reduced in ischaemia.

One of the limitations of myocardial perfusion imaging and standard visual interpretation is the dependence on a reference area of normal perfusion. This is a

particular impediment in diffuse or balanced multi-vessel disease. This limitation can be avoided by using absolute quantification of MBF (Patel et al., 2010). At present, the most robust technique to quantify MBF noninvasively is PET - but its wide-spread clinical application has been slowed by limited access (Kajander et al., 2011). PET imaging also involves exposure to ionizing radiation, and its spatial resolution limits evaluation of transmural flow differences in normal thickness myocardium.

Over the last decade, several animal, normal volunteer and patient studies have validated the use of CMR for absolute MBF quantification against microsphere and invasive coronary flow reserve measurements (Christian et al., 2004; Jerosch-Herold et al., 2002; Wilke et al., 1997). Furthermore, several clinical studies have demonstrated high diagnostic accuracy of CMR derived estimates of absolute MBF and MPR against both QCA and fractional flow reserve (Costa et al., 2007; Lockie et al., 2011; Motwani et al., 2012b; Patel et al., 2010; Futamatsu et al., 2007). Nonetheless, the lack of complete myocardial coverage has been a significant limitation of conventional 2D-perfusion CMR for this purpose.

This study has for the first time demonstrated the feasibility of quantitative whole-heart 3D perfusion CMR. Shin *et al* have previously reported semi-quantitative measures (time-intensity curve indices) of resting myocardial perfusion from a 3D acquisition in 3 healthy volunteers - but no stress acquisition or absolute MBF quantitation was performed (Shin et al., 2010). The MBF values derived with 3D perfusion CMR in normal patients in the present study are comparable to values from PET studies and the previous CMR literature (Sdringola et al., 2011; Chareonthaitawee et al., 2001). For example, in a large study of 160 healthy men and

women with PET, the mean resting MBF was  $0.98 \pm 0.23$  ml/min/g (range 0.59-2.05 ml/min/g) and the mean stress MBF was  $3.77 \pm 0.85$  ml/min/g (range 1.85-5.99 ml/min/g)(Chareonthaitawee et al., 2001). Intra- and inter-observer reproducibility for stress MBF and MPR in our study was also similar to that seen in 2D perfusion CMR and PET studies (Morton et al., 2012; Larghat et al., 2013).

The finding of lower estimates of stress MBF in systole compared to diastole is consistent with the expected physiology and a number of previous studies. Physiologically, one explanation is that during systole, the effect of adenosine-mediated vasodilatation is diminished by the compression of intramyocardial vessels (Hiramatsu et al., 1998). Two previous 2D-perfusion CMR studies have shown the same phasic differences with higher stress MBF estimates in diastole, but no difference between the phases at rest (Radjenovic et al., 2010; Motwani et al., 2012b). One previous 3D perfusion CMR study confirmed similar semi-quantitative measures of resting myocardial perfusion between systole and diastole - but no stress perfusion was performed (Shin et al., 2010). Our study has now demonstrated that these phasic differences are also seen with 3D perfusion CMR quantitation and underline the importance of stating the phase of acquisition in future studies to allow comparison in the literature.

Quantitative analysis with MPR yielded high diagnostic accuracies in both systole and diastole (AUC: 0.92 and 0.94 respectively). The optimal MPR cut-off values for detecting significant CAD (1.75 for systole and 2.02 for diastole) were within the range of 1.50–2.06 reported in previous 2D-perfusion CMR studies (Lockie et al., 2011; Rieber et al., 2006; Costa et al., 2007; Motwani et al., 2012b; Futamatsu et al.,

2007). Recently, in 2D-perfusion CMR, Huber *et al* (n=31) showed that the use of stress MBF alone had a similar diagnostic accuracy as MPR (AUC 0.92 vs. 0.84 respectively;  $p < 0.18$ ) (Huber et al., 2012). Our study has shown a similar finding in 3D perfusion CMR and the implication is that a rest perfusion sequence could potentially be omitted in quantitative studies, thus reducing both scanning and post-processing times without a loss in diagnostic yield (Figure 6.3).

The noted reduction in diastolic/systolic stress MBF ratio in territories with CAD is consistent with previous invasive studies measuring coronary flow velocity throughout the cardiac cycle (Segal et al., 1992). The loss of diastolic dominance has been explained by the increased influence of a significant stenosis on flow during periods of low vascular resistance and low intramyocardial tension (diastole); as compared with that during periods of high vascular resistance and high intramyocardial tension (systole) (Spaan et al., 1981). As such, the diastolic/systolic stress MBF ratio is a novel diagnostic index with moderate diagnostic accuracy (AUC=0.79) – and this may warrant further evaluation in future studies.

In our quantitative study, both phases had similar diagnostic performance and reproducibility. However, similar to previous 2D studies, diastole was more prone to dark rim artefact with an adverse effect on image quality; and this is thought to relate to the thinner myocardium, making it more prone to partial volume effects at a given spatial resolution (Motwani et al., 2012b). For this reason, as well as the fact that contour delineation is easier in systole because of the thicker myocardium, we would suggest systole as the preferred phase for 3D perfusion CMR acquisition - particularly for quantitative studies. Although analysis time was not specifically measured, each

3D perfusion dataset took approximately 20min to analyse on a per patient basis (including stress and rest analyses for either the systolic or diastolic cardiac phase). Quantifying 3D perfusion CMR can be simpler than quantifying conventional 2D datasets, because as in our study, fewer dynamic images are often acquired and there is a degree of temporal filtering due to the undersampling in the temporal domain which reduces the amount of time-consuming manual motion correction required.

Finally, there is considerable scope for quantitative perfusion CMR in clinical practice and therefore the feasibility of 3D whole-heart coverage and quantitation is an important step forward. Nonetheless, there still remain a number of other limitations that hold back the wider clinical adoption of quantitative perfusion CMR. The current lack of standardisation in image acquisition, contrast dosing protocols, post-processing, mathematical modelling and interpretation is addressed by an international standardisation task force (Kramer et al., 2013; Schulz-Menger et al., 2013). There is also no widely available and validated analysis software for quantitative analysis of perfusion CMR data and research groups generally use in-house solutions. Analysis can be time-consuming, precluding routine clinical application. Finally, the incremental value of quantitative analysis of myocardial perfusion CMR analysis needs to be shown in large clinical studies.

## 6.6 Study Limitations

The spatio-temporal undersampling methods required for 3D data acquisition are sensitive to respiratory motion, cardiac arrhythmia and low-pass temporal filtering - all of which pose additional challenges to quantitative assessment. Low-pass temporal filtering in particular may lead to underestimation of MBF. We reduced these limitations by use of the constrained  $k$ - $t$  PCA framework for image reconstruction, which has been shown to improve temporal fidelity, permitting robust measurements of MBF at very high acceleration factors (Pedersen et al., 2009). The latter is also less prone to respiratory artefact as temporal basis functions are derived based on the low-resolution training data acquired in every heartbeat (Vitanis et al., 2011).

Although MPR performed well in our study, perfusion imaging is a measurement of the haemodynamic consequences of a stenosis rather than its anatomy, and therefore our use of QCA is an imperfect reference standard. Following this initial feasibility study, future validation against fractional flow reserve is planned in a larger clinical population. Another limitation, common to many previous studies, is the potential effect of data clustering as three perfusion territories are examined per patient (Lockie et al., 2011; Rieber et al., 2006). However, the design effect of this was low (1.18) owing to a small ICC and cluster size.

Finally, the model used for estimating MBF assumes a linear relation between signal and contrast agent concentration i.e. ignoring saturation effects in the LV blood pool which can lead to underestimation of MBF (Sourbron, 2010). This is particularly relevant as we used a relatively high contrast agent dose of 0.075mmol/kg

bodyweight to be consistent with previous 3D perfusion CMR studies. Proposed solutions include the use of a non-linear signal model combined with precontrast T1-mapping and/or the use of a small pre-bolus to measure the AIF. However, such methods add further complexity to data acquisition and post-processing - and therefore neither was used in this study. Furthermore, there is currently no evidence that either of these potential solutions actually leads to improved diagnostic accuracy for the detection of CAD in the clinical setting. In fact the only study directly addressing this question came to the opposite conclusion i.e. the use of a pre-bolus AIF was found to reduce diagnostic accuracy compared to a single-bolus approach (Groothuis et al., 2010).

## **6.7 Conclusions**

We have shown that quantitative 3D perfusion CMR is feasible and can be used to detect CAD with high diagnostic accuracy. In addition, we have shown that there are significant differences in systolic and diastolic MBF estimates and therefore the phase of acquisition and AIF should always be stated in future 3D quantitative studies. Both cardiac phases provide comparable diagnostic yield, albeit at different thresholds. Because systolic images had fewer artefacts and higher image quality, systole may be the preferred phase for acquisition of 3D perfusion data.

## 7 Study 6 - Quantification of Myocardial Blood Flow with Cardiovascular Magnetic Resonance throughout the Cardiac Cycle

### 7.1 Abstract

**Background:** Myocardial blood flow (MBF) varies throughout the cardiac cycle in response to phasic changes in myocardial tension.

**Objectives:** This aim of this study was to determine if quantitative myocardial perfusion imaging with CMR can accurately track physiological variations in MBF throughout the cardiac cycle.

**Methods:** 30 healthy volunteers underwent a single stress/rest perfusion CMR study with data acquisition at 5 different time points in the cardiac cycle (early-systole, mid-systole, end-systole, early-diastole and end-diastole). MBF was estimated on a per-subject basis by Fermi-constrained deconvolution. Interval variations in MBF between successive time points were expressed as percentage change. Maximal cyclic variation (MCV) was calculated as the percentage difference between maximum and minimum MBF values in a cardiac cycle.

**Results:** At stress, there was significant variation in MBF across the cardiac cycle with successive reductions in MBF from end-diastole to early-, mid- and end-systole, and an increase from early- to end-diastole (end-diastole:  $4.50 \pm 0.91$  vs. early-systole:  $4.03 \pm 0.76$  vs. mid-systole:  $3.68 \pm 0.67$  vs. end-systole  $3.31 \pm 0.70$  vs. early-diastole:  $4.11 \pm 0.83$  ml/g/min; all p values <0.0001). In all cases, the maximum and minimum

stress MBF values occurred at end-diastole and end-systole respectively (mean MCV =  $26 \pm 5\%$ ). There was a strong negative correlation between MCV and peak heart rate at stress ( $r=-0.88$ ,  $p<0.001$ ). The largest interval variation in stress MBF occurred between end-systole and early-diastole ( $24 \pm 9\%$  increase). At rest, there was no significant cyclic variation in MBF (end-diastole:  $1.24 \pm 0.19$  vs. early-systole:  $1.28 \pm 0.17$  vs. mid-systole:  $1.28 \pm 0.17$  vs. end-systole:  $1.27 \pm 0.19$  vs. early-diastole:  $1.29 \pm 0.19$  ml/g/min;  $p=0.71$ ).

**Conclusion:** Quantitative perfusion CMR can be used to non-invasively assess cyclic variations in MBF throughout the cardiac cycle. In this study, estimates of stress MBF followed the expected physiological trend, peaking at end-diastole and falling steadily through to end-systole. This technique may be useful in future pathophysiological studies of coronary blood flow and microvascular function.

## 7.2 Introduction

Myocardial blood flow (MBF) varies throughout the cardiac cycle in response to changes in myocardial tension and phasic compression of the myocardial microcirculation (Sabsiton Jr & Gregg, 1957; Goto et al., 1991; Spaan et al., 1981; Matsumoto & Kajiya, 2005). The squeezing effect of myocardial contraction causes arterial blood inflow to peak during diastole when myocardial tension is low, and venous outflow to peak during systole when myocardial tension is high. Diseases such as diabetes, atherosclerosis, cardiomyopathies, and arterial hypertension result in functional and morphologic microvascular changes, which may precede clinical signs and symptoms. Quantitative assessment of MBF and characterization of cyclic myocardial perfusion variation in these diseases may offer valuable additional information relating to microvascular integrity and function.

Over the last decade, several animal, normal volunteer and patient studies have validated the use of CMR for absolute MBF quantification against microsphere and invasive coronary flow reserve measurements (Christian et al., 2004; Jerosch-Herold et al., 2002; Wilke et al., 1997). With conventional CMR methods perfusion data are acquired in a different cardiac phase for each slice. Previous volunteer and patient studies have now shown a significant difference in MBF quantified using CMR between acquisition in systole and diastole, suggesting that cardiac phase needs to be considered when interpreting CMR-derived MBF values (Radjenovic et al., 2010; Motwani et al., 2012b, 2014b). Although the development of 3D perfusion CMR, which allows the specific phase of data acquisition to be chosen, may overcome this concern in the future, these differences remain a challenge for CMR perfusion.

However, they also provide the opportunity to interrogate cyclic variations in perfusion as a unique diagnostic tool, not assessable by positron-emission tomography, which assess myocardial perfusion cumulatively.

So far, temporal and spatial constraints on dynamic CMR perfusion imaging have restricted previous volunteer and patient studies to assessing MBF between only two different time points in the cardiac cycle, and it is therefore unknown whether CMR has the capability to track changes in MBF *throughout* the cardiac cycle (Radjenovic et al., 2010; Motwani et al., 2012b, 2014b). Advanced acceleration techniques, based on spatiotemporal undersampling, which have mostly been employed to achieve higher spatial resolution, can also be used to improve temporal resolution in perfusion CMR studies. The purpose of the study was to capitalise on the dynamic aspect of CMR perfusion data acquisition and assess whether quantitative perfusion CMR can accurately follow the expected physiological variation in MBF *throughout* the cardiac cycle.

## **7.3 Methods**

### **7.3.1 Study Population**

Thirty-three healthy volunteers were recruited. Exclusion criteria included any history of cardiovascular disease, diabetes mellitus, hypertension, hyperlipidaemia, smoking or any contraindications to CMR, adenosine, or gadolinium-based contrast agents. The study protocol was approved by the local ethics committee, and written informed consent was obtained from all volunteers. All volunteers were instructed to refrain from caffeine for 24 hours before their CMR study.

### 7.3.2 CMR protocol

All volunteers underwent a single stress and rest perfusion CMR study performed on a 1.5T scanner (Intera, Philips Healthcare, Best, the Netherlands) equipped with a five-element cardiac phased array receiver coil. Perfusion data were acquired in a single mid-ventricular 2D slice at 5 different time points in each R-R interval (early-systole, mid-systole, end-systole, early-diastole and end-diastole) facilitated by *k-t* BLAST acceleration (Figure 7.1). Details of the perfusion pulse sequence were as follows: 2D saturation recovery gradient-echo sequence accelerated with 8-fold *k-t* BLAST and 11 interleaved training profiles, no partial Fourier or partial echo acquisition, TR 3.4ms, TE 1.7ms, flip angle 15°, one saturation pre-pulse per slice (i.e. per time point), image acquisition time per slice 103ms, matrix 192 x 192, median FOV 310 mm and in-plane spatial resolution 1.6 x 1.6 mm.

Vertical and horizontal long-axis cine images were used to identify appropriate trigger delays for each of the 5 time points (Radjenovic et al., 2010; Motwani et al., 2012b, 2014b; Shin et al., 2010). Additionally, because of the longitudinal lengthening of the heart from systole to diastole, the position of the mid-ventricular perfusion slice at each time point was individually planned from the chosen end-diastolic, early systolic, mid-systolic, end-systolic and early-diastolic cine frames (Radjenovic et al., 2010; Motwani et al., 2012b, 2014b).

Stress perfusion images were acquired during intravenous adenosine-induced hyperaemia (140mcg/kg/min administered for 4min). An intravenous bolus of 0.05 mmol/kg gadopentetate dimeglumine (Magnevist, Schering, Germany) was administered at a rate of 4.0ml/s followed by a 20ml saline flush. Stress perfusion

CMR was followed by cine imaging covering the left ventricle in short-axis sections. Rest perfusion CMR was performed 15min after stress, using identical imaging parameters. LGE imaging was not performed.

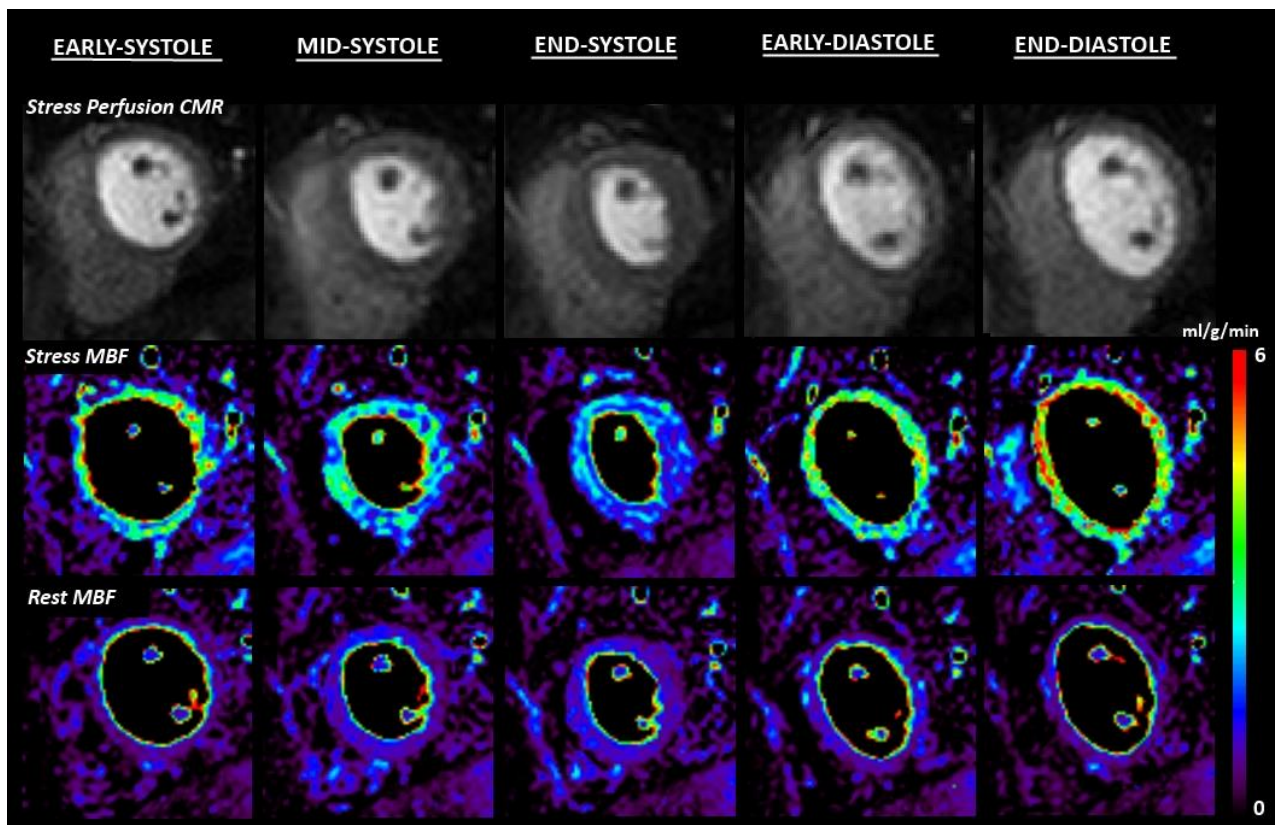


**Figure 7.1 Quantitative Perfusion CMR throughout the Cardiac Cycle**

*This example shows stress perfusion CMR (top row) in a healthy volunteer acquired at 5 different time points throughout the cardiac cycle in a single mid-ventricular slice facilitated by 8-fold k-t BLAST acceleration. Corresponding stress and rest MBF estimates are shown as myocardial maps (middle and bottom row respectively). Stress MBF shows significant cyclic variation peaking in end-diastole and steadily falling throughout systole. The maximal interval change in stress MBF is seen between end-systole and early-diastole. No significant cyclic variation was seen in rest MBF. CMR = cardiovascular magnetic resonance; BLAST = broad linear acquisition speed-up technique; MBF = myocardial blood flow*

### **7.3.3 MBF estimation**

Perfusion images were processed offline using previously validated in-house software (PMI 0.4; written in IDL 6.4 (ITT Visual Information Systems, Boulder, CO)(Motwani et al., 2014b; Huber et al., 2012).

#### ***7.3.3.1 Per-subject analysis***

Following manual rigid motion-correction, a circular region of interest (ROI) was drawn in the LV cavity at end-diastole, to derive the arterial input function (AIF). The same (end-diastolic) AIF was used for all estimates of MBF in order to avoid potential variations in the AIF between phases with subsequent effects on MBF estimation (Radjenovic et al., 2010; Motwani et al., 2012b, 2014b).

A whole-slice myocardial ROI excluding any dark-rim artifact was drawn on perfusion images for each of the 5 time points. Signal intensity–time data were converted to concentration–time data by subtracting the baseline signal. Global MBF was estimated at stress and rest using constrained deconvolution with a delayed Fermi-model applied to the first pass(Jerosch-Herold et al., 1998). Myocardial perfusion reserve (MPR) was calculated as stress MBF divided by rest MBF.

Interval variations in MBF or MPR between successive time points were expressed as percentage change. Maximal cyclical variation (MCV) in MBF was calculated as the percentage difference between maximum and minimum values in a cardiac cycle.

#### ***7.3.3.2 Per-territory analysis***

The above analysis was repeated on a per territory basis by segmenting the perfusion slices according to the 17-segment American Heart Association model(Cerqueira et

al., 2002). For each perfusion territory, a myocardial ROI including all segments pertaining to that territory was outlined. MBF and MPR estimates at each time point were obtained using the same algorithms as for the per subject analysis.

#### **7.3.3.3 Reproducibility**

Per-subject analysis was repeated on perfusion data from ten random volunteers 1 month later by the same observer (M.M.) and by a second observer A.K. (3yrs and 2yrs experience respectively). A.K. was blinded to the results of all previous analyses.

#### **7.3.4 Statistical analysis**

Analysis was performed using SPSS 17.0 (SPSS, Chicago, IL). Data are presented as mean $\pm$ SD. Mean perfusion values (MBF and MPR) were compared at the 5 different time points using one-way repeated measures analysis of variance (ANOVA) with Greenhouse-Geisser correction for multi-sample sphericity and Bonferonni adjustment for post-hoc analysis. Mean perfusion values at each time point were compared between perfusion territories using standard ANOVA. Intra- and inter-observer reproducibility for MBF, MPR and MCV were assessed by calculating coefficients of variation (CoVs): SD of the differences divided by the mean. All statistical tests were two-tailed and a p value <0.05 was considered significant.

## 7.4 Results

### 7.4.1 Study population

Thirty-three healthy volunteers were recruited. One volunteer could not complete the scan due to claustrophobia. Data from 2 other volunteers were excluded due to technical problems preventing analysis (1 excessive heart rate variability, 1 mistimed contrast injection). All remaining images were of analysable quality. Data from a total of 30 volunteers (90 perfusion territories) were therefore available for the final analysis. Clinical details of the 30 study volunteers (18 men; mean age 22±2yrs) are summarized in Table 7.1.

**Table 7-1 Healthy Volunteer Demographics**

Parameter	Data (n= 30)
Age (yrs)	22 ± 2
Sex, n (%)	
Male	18 (60)
Female	12 (40)
LV function	
EF %	61 ± 5
EDV, ml	140 ± 26
ESV, ml	59 ± 14
LV Mass, g/m <sup>2</sup>	82 ± 22
Hemodynamics at Peak Stress	
Heart Rate (beats/min)	81 ± 9
Systolic blood pressure (mmHg)	127 ± 20
RPP (mmHg x beats/min)	10226 ± 2319

Data n ± SD; EDV= end-diastolic volume; ESV = end-systolic volume; RPP = rate-pressure product

## **7.4.2 Myocardial blood flow estimation**

### **7.4.2.1 Per subject analysis**

Estimates of MBF and MPR at each of the 5 time points in the cardiac cycle are seen in Table 7.2. There was significant cyclic variation in stress MBF ( $p < 0.0001$ ) and MPR ( $p < 0.0001$ ) with successive reductions from end-diastole to early-, mid- and end-systole, followed by an increase from early- to end-diastole (all post-hoc  $p$  values  $< 0.01$ ) (Table 7.2, Figures 7.2-7.4). In all cases, the maximum and minimum stress MBF values occurred at end-diastole and end-systole respectively with a mean MCV of  $26 \pm 5\%$  (Figure 7.4). There was a strong negative correlation between MCV and peak heart rate at stress ( $r = -0.88$ ,  $p < 0.001$ ) (Figure 7.5). The largest interval variation in stress MBF occurred between end-systole and early-diastole ( $24 \pm 9\%$  increase) (Figure 7.2). The largest interval variation in MPR occurred between end-systole and early-diastole ( $31 \pm 20\%$  increase) (Figure 7.3). At rest, there were no significant cyclical variations in MBF ( $p = 0.71$ ) (Table 7.2) (Figure 7.1).

### **7.4.2.2 Per territory analysis**

Estimates of MBF and MPR in each perfusion territory at each of the 5 time points in the cardiac cycle are seen in Table 7.2. There were no significant differences in stress MBF, rest MBF or MPR between perfusion territories at each of the 5 cardiac phases assessed (all  $p$  values  $> 0.05$ ) (Table 7.2). There was significant cyclic variation in stress MBF and MPR in all 3 perfusion territories (all  $p$  values  $< 0.0001$ ) (Table 7.2). MCV for stress MBF was similar in all perfusion territories (left anterior descending [LAD]:  $27 \pm 8\%$  vs. left circumflex [LCX]:  $27 \pm 5\%$  vs. right coronary artery [RCA]:  $25 \pm 5\%$ ;  $p = 0.45$ ). The largest interval variation in the LAD, LCX and RCA perfusion

territories was the increase in stress MBF and MPR between end-systole and early-diastole and the magnitude was similar in all 3 territories (stress MBF:  $26 \pm 12\%$  vs.  $25 \pm 9\%$  vs.  $24 \pm 9\%$ ,  $p=0.62$ ; MPR:  $31 \pm 22\%$  vs.  $27 \pm 23\%$  vs.  $27 \pm 24\%$ ,  $p=0.79$  respectively). There was no significant cyclical variation in rest MBF in any territory (Table 7.2).

**Table 7-2 Estimates of MBF and MPR throughout the Cardiac Cycle**

	<i>End-diastole</i>	<i>Early-systole</i>	<i>Mid-systole</i>	<i>End-systole</i>	<i>Early-diastole</i>	<i>P</i>
<b>Global</b>						
<i>Stress MBF</i>	$4.50 \pm 0.91$	$4.03 \pm 0.76$	$3.68 \pm 0.67$	$3.31 \pm 0.69$	$4.11 \pm 0.83$	$p<0.0001$
<i>Rest MBF</i>	$1.24 \pm 0.19$	$1.28 \pm 0.17$	$1.28 \pm 0.17$	$1.27 \pm 0.19$	$1.29 \pm 0.19$	$p=0.71$
<i>MPR</i>	$3.63 \pm 0.95$	$3.19 \pm 0.66$	$2.92 \pm 0.66$	$2.62 \pm 0.63$	$3.40 \pm 0.92$	$p<0.0001$
<b>LAD perfusion territory*</b>						
<i>Stress MBF</i>	$4.38 \pm 0.87$	$3.88 \pm 0.78$	$3.59 \pm 0.64$	$3.19 \pm 0.67$	$3.99 \pm 0.80$	$p<0.0001$
<i>Rest MBF</i>	$1.25 \pm 0.16$	$1.30 \pm 0.14$	$1.24 \pm 0.11$	$1.25 \pm 0.13$	$1.21 \pm 0.13$	$p=0.14$
<i>MPR</i>	$3.54 \pm 0.74$	$3.01 \pm 0.60$	$2.91 \pm 0.53$	$2.58 \pm 0.58$	$3.35 \pm 0.80$	$p<0.0001$
<b>LCX perfusion territory*</b>						
<i>Stress MBF</i>	$4.40 \pm 0.94$	$3.93 \pm 0.70$	$3.58 \pm 0.67$	$3.21 \pm 0.69$	$4.01 \pm 0.85$	$p<0.0001$
<i>Rest MBF</i>	$1.25 \pm 0.08$	$1.28 \pm 0.17$	$1.24 \pm 0.14$	$1.24 \pm 0.14$	$1.23 \pm 0.12$	$p=0.60$
<i>MPR</i>	$3.52 \pm 0.73$	$3.12 \pm 0.65$	$2.93 \pm 0.63$	$2.60 \pm 0.56$	$3.29 \pm 0.85$	$p<0.0001$
<b>RCA perfusion territory*</b>						
<i>Stress MBF</i>	$4.55 \pm 0.90$	$4.13 \pm 0.76$	$3.78 \pm 0.67$	$3.41 \pm 0.69$	$4.21 \pm 0.85$	$p<0.0001$
<i>Rest MBF</i>	$1.33 \pm 0.15$	$1.38 \pm 0.17$	$1.38 \pm 0.20$	$1.39 \pm 0.19$	$1.33 \pm 0.19$	$p=0.50$
<i>MPR</i>	$3.46 \pm 0.78$	$3.03 \pm 0.60$	$2.78 \pm 0.60$	$2.49 \pm 0.57$	$3.24 \pm 0.83$	$p<0.0001$

\* Additionally there were no significant differences in mean perfusion values (MBF or MPR) between territories at any point in the cardiac cycle (all  $p$  values  $>0.05$ ). MBF = myocardial blood flow in ml/min/g; MPR = myocardial perfusion reserve; LAD = left anterior descending; LCX = left circumflex; RCA = right coronary artery

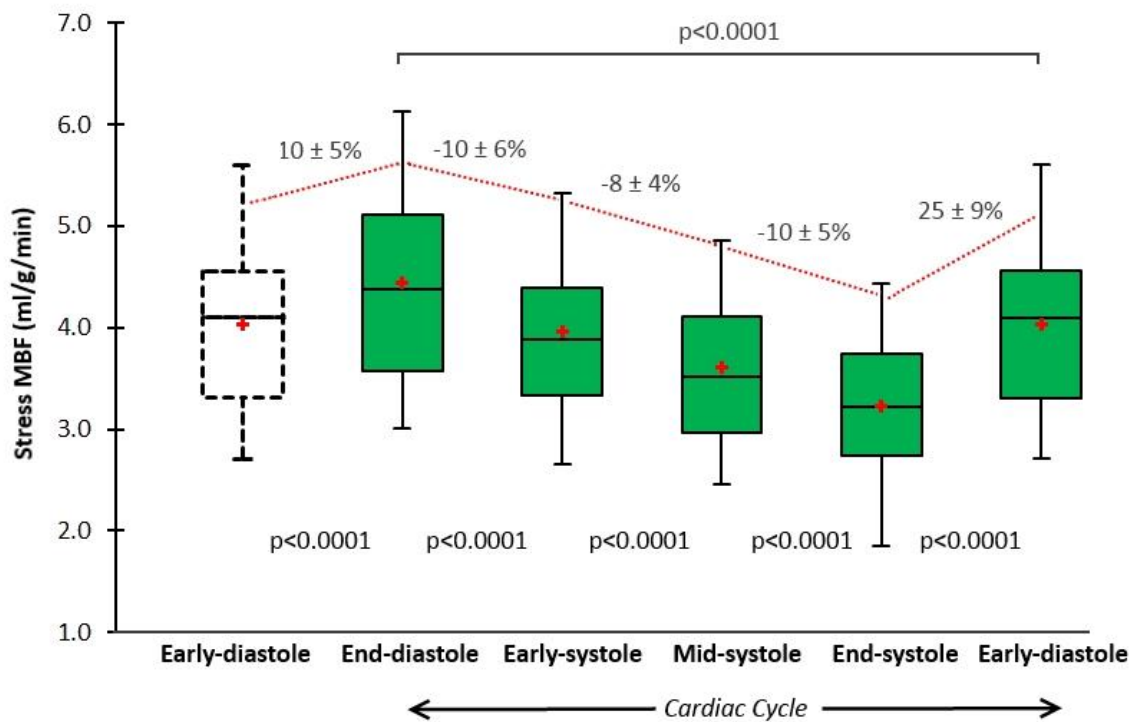


**Figure 7.2 Cyclic Variation in Stress MBF**

Mean stress MBF in healthy volunteers (n=30) showed significant cyclic variation throughout the cardiac cycle (p<0.0001). Box plots for stress MBF show the interquartile range (box), median (dividing black line) and mean (red cross) with whiskers extending to 1.5 x interquartile range. There were successive reductions in stress MBF from end-diastole to early-, mid- and end-systole, and a significant increase from early- to end-diastole (all p values <0.0001) (trend shown by red line). The maximal interval change in stress MBF was between end-systole and early-diastole (25% increase). MBF = myocardial blood flow

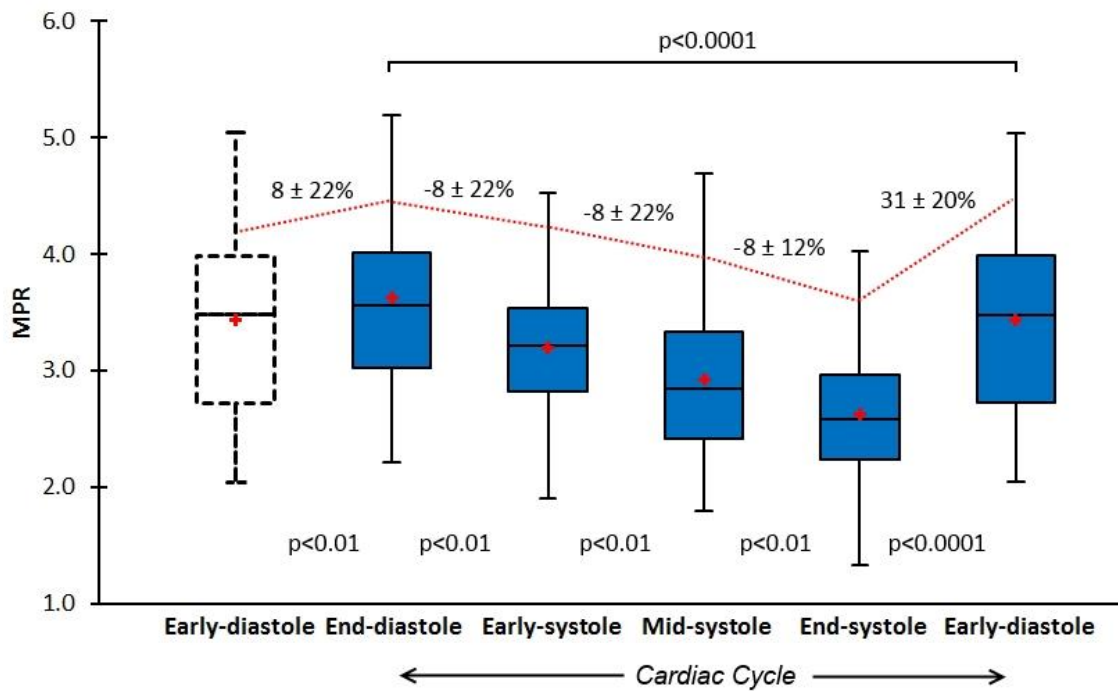


**Figure 7.3 Cyclic Variation in MPR**

Mean MPR in healthy volunteers ( $n=30$ ) showed significant cyclic variation throughout the cardiac cycle ( $p<0.0001$ ). Box plots for MPR show the interquartile range (box), median (dividing black line) and mean (red cross) with whiskers extending to  $1.5 \times$  interquartile range. There were successive reductions from end-diastole to early-, mid- and end-systole, and a significant increase from early- to end-diastole (all  $p$  values  $<0.01$ ) (trend shown by red line). The maximal interval change in MPR was between end-systole and early diastole (31% increase). MPR = myocardial perfusion reserve

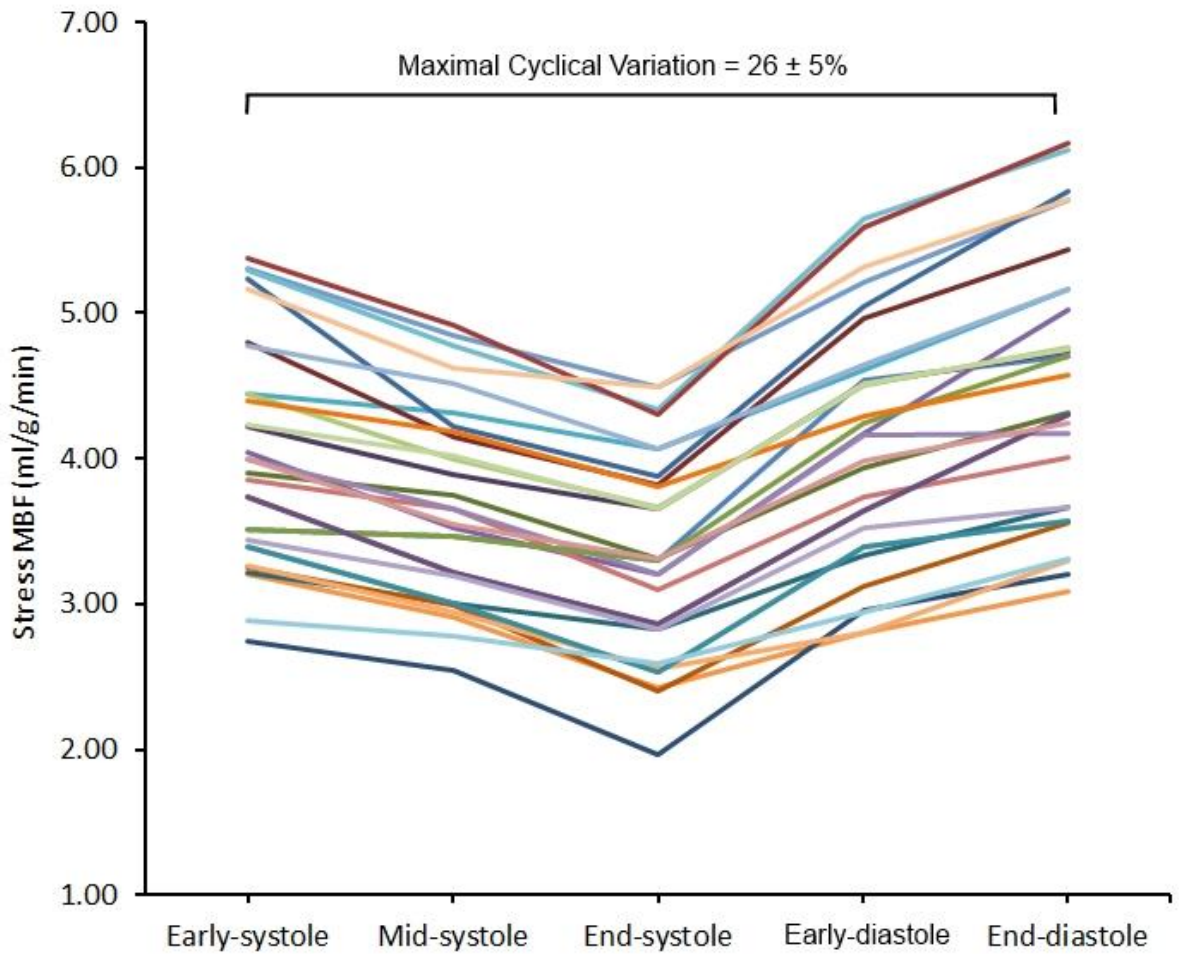


**Figure 7.4 Individual Stress MBF estimates in Healthy Volunteers**

*There was significant cyclic variation in stress MBF in all volunteers (n=30). In all cases the peak MBF occurred at end-diastole and the minimum at end-systole. The mean maximal cyclic variation in stress MBF was 26%. MBF = myocardial blood flow*

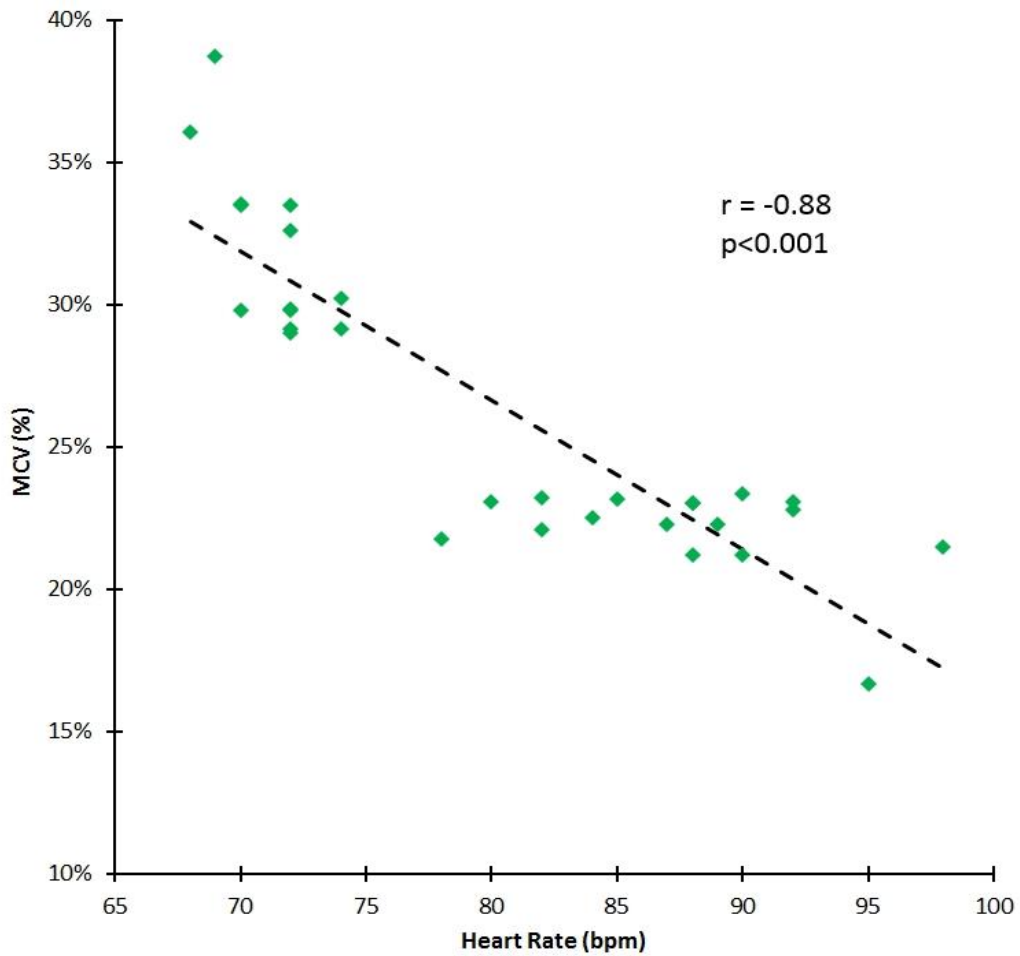


**Figure 7.5 Correlation between MCV and Peak Heart Rate at Stress**

*There was a strong linear negative correlation between the maximal cyclic variation (MCV) in stress MBF and the peak heart rate during adenosine-induced maximal hyperaemia in healthy volunteers (n=30). MBF = myocardial blood flow*

### **7.4.2.3 Reproducibility**

Intra-observer CoVs for stress MBF, rest MBF, MPR and MCV in stress MBF were 9%, 11%, 15% and 10%, respectively. Corresponding CoVs for inter-observer reproducibility were 14%, 16%, 18% and 12% respectively.

## **7.5 Discussion**

The main findings of this study are 1) quantitative perfusion CMR can track physiological changes in myocardial perfusion throughout the cardiac cycle; 2) estimates of stress MBF and MPR in healthy volunteers show significant cyclic variation with successive reductions throughout systole and an increase in diastole; 3) the greatest interval change in stress MBF and MPR occurs between end-systole and early-diastole; 4) there is no significant cyclic variation in rest MBF estimates.

The finding of significant cyclic variation in stress MBF and MPR is consistent with the expected physiology relating to phasic changes in myocardial tension. In vivo animal studies directly visualising the microcirculation with angiography show significant compression of intramyocardial vessels during systole (Yada et al., 1993)(15). In humans, coronary flow patterns across the cardiac cycle have been directly measured with intracoronary pressure wires. Davies *et al* showed that blood flow in the left coronary artery (LCA) is predominantly diastolic i.e. when myocardial tension is low (2006). During systole, they found a dominant forward-travelling pushing wave, which is reflected when reaching the microvascular bed because of the higher myocardial tension, and this results in virtually no forward flow, or even retrograde flow. Therefore, our observation that MBF estimates successively fall

throughout systole and increase in diastole is consistent with these described coronary flow patterns.

The greatest interval change in stress MBF and MPR was seen between end-systole and early-diastole (Table 7.2, Figures 7.1-7.3). This is in keeping with invasive studies that show LCA inflow velocity peaks in early-diastole (Davies et al., 2006). It is also consistent with an observation by Davies *et al* that there is a transient secondary forward-travelling pushing wave in early diastole seen in LCA waveforms. This secondary wave coincides with closure of the aortic valve and accelerates blood further towards the myocardium.

Heller *et al* showed that arterial waveforms in the proximal RCA have significantly less phasic variation because right ventricular peak systolic pressure is much lower than aortic peak systolic pressure and because the right ventricular wall offers less mechanical compressive resistance (Heller et al., 1994). However, they also showed that distal RCA branches (posterior descending and posterolateral coronary arteries) show the same diastolic dominance as the left coronary system as they subtend LV myocardial segments subjected to the same phasic changes in myocardial tension as the rest of the LV. Consistent with this observation, we found no significant differences in MCV in stress MBF between the left coronary (LAD and LCX) and RCA perfusion territories - and they showed the same pattern of phasic variation across the 5 time points (Table 7.2).

Three previous quantitative perfusion CMR studies (including 1 utilising 3D data acquisition) have also shown significant differences in stress MBF and MPR according to phase, with significantly higher values in diastole (Radjenovic et al., 2010;

Motwani et al., 2012b, 2014b). A recent semi-quantitative study also found steeper myocardial time-intensity curves in diastole compared to systole (Nchimi et al., 2014). However, all of these previous studies have been limited to the assessment of myocardial perfusion at only two different time points in the cardiac cycle. The current study is the first to assess variation in MBF estimates *throughout* the cardiac cycle in humans and determine the overall trend between 5 selected time points. Recently, cyclic changes in myocardial perfusion have also been examined in rats (n=6) by Troalen *et al* using a novel steady-pulsed arterial spin labelling (ASL) approach to map MBF (2014). Dynamic MBF maps were obtained with an extremely high temporal resolution (6ms) offering even more comprehensive coverage throughout the cardiac cycle than in our study. However, the acquisition time using this technique in rats was approximately 12min (at a heart rate of 400 bpm), preventing application of this method to humans where even longer acquisition times would be required. Furthermore, the use of myocardial ASL in humans to quantify MBF remains limited by inadequate signal-to-noise ratio (SNR) efficiency, high physiological noise, and timing restrictions related to cardiac and respiratory motion (Zun et al., 2009). Nonetheless, this small study in rats showed a similar phasic variation in stress MBF estimates, which peaked in diastole and steadily fell in systole with an overall mean MCV of  $18 \pm 8\%$ .

In our study, there was no significant cyclic variation in rest MBF estimates (Table 7.2, Figure 7.1). This is in keeping with the result of the 3 previous volunteer and patient studies, which also showed no significant difference between rest MBF estimates in systole and diastole (Radjenovic et al., 2010; Motwani et al., 2012b,

2014b). A fourth study assessing semi-quantitative measures of resting myocardial perfusion also found no significant difference between systole and diastole (Shin et al., 2010). A possible explanation for a lack of cyclic variation in resting MBF is sufficient autoregulation in the microvascular network at rest, which is only overcome in the stress state by adenosine-induced maximal hyperaemia or significant tachycardia. Only the recent study in rats utilising ASL showed a significant cyclic variation in resting MBF, but this was under the influence of isoflurane anaesthesia which is known to induce coronary vasodilatation and therefore not representative of a true physiological resting state (Troalen et al., 2014; Iltis et al., 2005). Additionally, the resting heart rate in rats is significantly higher than in humans ( $322\pm 43$  bpm in the study by Troalen *et al*) and therefore these findings are not necessarily translatable to human physiology (Troalen et al., 2014).

Finally, we found a strong negative linear correlation between MCV and peak heart rate during stress (Figure 7.5). Notably, this observation was also seen in the aforementioned study in rats by Troalen *et al* (2014). A possible explanation is the capacitive property of the myocardial vascular system due to an abundant capillary network. The latter serves to dampen the rapid fluctuations in pressure seen with increasing heart rates in order to maintain a steady downstream blood flow – the so-called ‘windkessel’ effect (Frank, 1990). At lower heart rates the effects of phasic myocardial tension are relatively unopposed by capacitance and thus a greater MCV is seen which is in keeping with our findings.

In summary, we have demonstrated that significant phasic differences in MBF estimates quantified with CMR are seen not only at polar ends of the cardiac cycle

but also *throughout* the cardiac cycle. Considering the nature of coronary haemodynamics, cyclic MBF changes may reveal new physiological information because they are a function of coronary flow, myocardial contraction and microvascular condition. Therefore, using CMR to assess MBF throughout the cardiac cycle and determine parameters such as MCV, may be useful in the future assessment of diseases known to alter microvascular function such as diabetes or atherosclerosis - but further studies in these disease states are needed.

## **7.6 Study Limitations**

The spatio-temporal undersampling method required to accelerate perfusion data acquisition is sensitive to respiratory motion, cardiac arrhythmia and low-pass temporal filtering - all of which pose challenges to quantitative assessment. Low-pass temporal filtering in particular may have led to underestimation of MBF.

To obtain systolic and diastolic perfusion data in the same location and within the same acquisition, this study was limited to the assessment of a single mid-ventricular section. This was a technical necessity and meant we could not assess phasic differences in apical and basal myocardial segments, which may behave differently from the mid-ventricle. Future studies with more advanced acceleration and 3D perfusion data acquisition are needed to address these issues - but these strategies also come with additional challenges for absolute MBF quantitation.

Finally, the model used for estimating MBF assumes a linear relationship between signal and contrast agent concentration i.e. ignoring saturation effects in the LV blood pool, which can lead to underestimation of MBF (Sourbron, 2010). Proposed

solutions include the use of a non-linear signal model combined with pre-contrast T1-mapping and/or the use of a small pre-bolus to measure the AIF. However, such methods add further complexity to data acquisition and post-processing - and therefore neither was used in this study. Furthermore, there is currently no evidence that either of these potential solutions actually leads to improved diagnostic accuracy in the clinical setting (e.g. for the detection of CAD). In fact the only study directly addressing this question came to the opposite conclusion i.e. the use of a pre-bolus AIF was found to reduce diagnostic accuracy compared to a single-bolus approach (Groothuis et al., 2010). Additionally, our findings are based on intra-individual comparisons and the relative changes in perfusion values throughout the cardiac cycle, and therefore underestimation in absolute MBF due to saturation effects is less relevant.

## **7.7 Conclusions**

Quantitative perfusion CMR can be used to non-invasively track cyclical variations in MBF *throughout* the cardiac cycle. In this study, estimates of MBF followed the expected physiological trend, peaking at end-diastole and falling steadily through to end-systole. This technique may be useful in future physiological or pathological studies of coronary flow and microvascular function.

## 8 Final Conclusions

The evidence for the use of perfusion CMR in the assessment of CAD, both as a clinical and cardiovascular research tool, continues to grow rapidly. Many important perfusion CMR studies have been published over the last 5 years—some providing large-scale clinical validation and prognostic data, and others describing more technical advances in acquisition and quantitation.

In this thesis we have focused on recent advances in accelerating perfusion data acquisition. Advanced acceleration techniques have been used to improve spatial resolution, or alternatively achieve 3D whole-heart coverage – but at the initiation of this thesis, it was not clear if either strategy offered any incremental benefit over standard techniques or how they compared to each other.

Acceleration (or sacrifice of spatial coverage) can also be used to simultaneously acquire perfusion data at different time-points in the cardiac cycle. This is important as the impact of a variable cardiac phase of acquisition on quantitative estimates of MBF with CMR was also poorly understood at the outset of this research.

Accordingly, this thesis included studies that manipulated the standard approach to perfusion CMR using advanced acceleration techniques, in order to investigate the relative impact of spatial resolution, spatial coverage and cardiac phase of acquisition on both qualitative and quantitative assessment of ischaemia. Our main findings were as follows:

## 8.1 Spatial Resolution

- i. High spatial resolution perfusion CMR has greater overall diagnostic accuracy than standard-resolution acquisition for the detection of CAD in both single and multi-vessel disease, and also detects more subendocardial ischaemia.
- ii. High-resolution perfusion CMR increases the observed MIB and distribution of ischaemia detected in angiographic 3VD compared to standard-resolution acquisition due to better detection of subendocardial ischaemia. However, the incremental value of high-resolution acquisition for correctly identifying, stratifying and managing this high-risk group has to be determined in further clinical studies.
- iii. There is significantly less dark rim artefact with high-resolution compared to standard-resolution perfusion CMR. The high-resolution technique is however more prone to respiratory and *k-t* reconstruction artefacts. Overall therefore, image quality scores are similar between high-resolution and standard-resolution techniques.

## 8.2 Spatial coverage

- i. Image quality, artefact and diagnostic confidence scores are similar for both 2D high-resolution and 3D perfusion CMR
- ii. There is strong correlation and broad agreement between estimates of MIB from both 2D high-resolution and 3D whole-heart perfusion CMR techniques. However, the 95% limits of agreement are relatively wide and therefore a larger

comparative study is needed before they can be considered interchangeable - particularly around the clinically relevant 10% MIB threshold.

### 8.3 Cardiac Phase

- i. In both 2D and 3D quantitative perfusion CMR studies, systolic estimates of MBF are significantly lower than diastolic estimates, but both phases can be used to detect CAD with high diagnostic accuracy.
- ii. The phase of acquisition should ideally be stated in future quantitative perfusion CMR studies
- iii. For both 2D and 3D perfusion CMR, there was significantly higher image quality and less dark rim artefact with systolic acquisition compared to diastolic – but similar diagnostic accuracy for detecting CAD. Therefore, where open to choice, such as with 3D techniques, perfusion data acquisition in systole is preferable.
- iv. Quantitative perfusion CMR can be used to non-invasively track cyclical variations in MBF *throughout* the cardiac cycle, and estimates of MBF appear to follow the expected physiological trend, peaking at end-diastole and falling steadily through to end-systole. This technique may be useful in future pathophysiological studies of coronary blood flow and microvascular function.

## 9 References

- Al-Saadi, N. et al. (2000). Noninvasive detection of myocardial ischemia from perfusion reserve based on cardiovascular magnetic resonance. *Circulation*. **101** (12), pp. 1379–1383
- Araoz, P.A. et al. (2005). 3 Tesla MR imaging provides improved contrast in first-pass myocardial perfusion imaging over a range of gadolinium doses. *Journal of Cardiovascular Magnetic Resonance*. **7** (3), pp. 559–564
- Atkinson, D.J. et al. (1990). First-pass cardiac perfusion: evaluation with ultrafast MR imaging. *Radiology*. **174** (3), pp. 757–762
- Bache, R.J. and Schwartz, J.S. (1982). Effect of perfusion pressure distal to a coronary stenosis on transmural myocardial blood flow. *Circulation*. **65** (5), pp. 928–935
- Beanlands, R.S. et al. (1995). Noninvasive quantification of regional myocardial flow reserve in patients with coronary atherosclerosis using nitrogen-13 ammonia positron emission tomography. Determination of extent of altered vascular reactivity. *Journal of the American College of Cardiology*. **26** (6), pp. 1465–1475
- Di Bella, E.V.R. et al. (2005). On the dark rim artifact in dynamic contrast-enhanced MRI myocardial perfusion studies. *Magnetic resonance in medicine*. **54** (5), pp. 1295–1299
- Bernstein, M.A. et al. (2006). Imaging artifacts at 3.0T. *Journal of magnetic resonance imaging*. **24** (4), pp. 735–746
- Biglands, J. et al. (2011). Evaluation of the effect of myocardial segmentation errors on myocardial blood flow estimates from DCE-MRI. *Physics in Medicine and Biology*. **56**, pp. 2423–2443
- Bingham, S.E. and Hachamovitch, R. (2011). Incremental prognostic significance of combined cardiac magnetic resonance imaging, adenosine stress perfusion, delayed enhancement, and left ventricular function over preimaging information for the prediction of adverse events. *Circulation*. **123** (14), pp. 1509–1518

- Bodi, V. et al. (2005). Usefulness of a comprehensive cardiovascular magnetic resonance imaging assessment for predicting recovery of left ventricular wall motion in the setting of myocardial stunning. *Journal of the American College of Cardiology*. **46** (9), pp. 1747–1752
- British Heart Foundation (2010). *Coronary Heart Disease Statistics 2010*. [Online]. 2010. Available from: [www.heartstats.org](http://www.heartstats.org). [Accessed: 10 July 2014].
- Brown, K.A. et al. (1983). Prognostic value of exercise thallium-201 imaging in patients presenting for evaluation of chest pain. *Journal of the American College of Cardiology*. **1** (4), pp. 994–1001
- Carew, T.E. and Covell, J.W. (1976). Effect of intramyocardial pressure on the phasic flow in the intraventricular septal artery. *Cardiovascular research*. **10** (1), pp. 56–64
- Cerqueira, M.D. et al. (2002). Standardized myocardial segmentation and nomenclature for tomographic imaging of the heart: a statement for healthcare professionals from the Cardiac Imaging Committee of the Council on Clinical Cardiology of the American Heart Association. *Circulation*. **105** (4), pp. 539–542
- Chareonthaitawee, P. et al. (2001). Heterogeneity of resting and hyperemic myocardial blood flow in healthy humans. *Cardiovascular research*. **50** (1), pp. 151–161
- Chen, G. et al. (2008). Prior image constrained compressed sensing (PICCS): a method to accurately reconstruct dynamic CT images from highly undersampled projection data sets. *Medical Physics*. **35** (2), pp. 660–663
- Chen, L. et al. (2012). Myocardial perfusion MRI with an undersampled 3D stack-of-stars sequence. *Medical Physics*. **39** (8), pp. 5204–5211
- Cheng, A.S.H. et al. (2007). Cardiovascular magnetic resonance perfusion imaging at 3-tesla for the detection of coronary artery disease: a comparison with 1.5-tesla. *Journal of the American College of Cardiology*. **49** (25), pp. 2440–2449
- Chilian, W.M. and Marcus, M.L. (1985). Effects of coronary and extravascular pressure on intramyocardial and epicardial blood velocity. *American Journal of Physiology-Heart and Circulatory Physiology*. **248** (2), p. H170

- Chilian, W.M. and Marcus, M.L. (1982). Phasic coronary blood flow velocity in intramural and epicardial coronary arteries. *Circulation Research*. **50** (6), pp. 775–781
- Christian, B.T. et al. (2010). Dynamic PET denoising with HYPR processing. *Journal of nuclear medicine*. **51** (7), pp. 1147–1154
- Christian, T.F. et al. (2004). Absolute Myocardial Perfusion in Canines Measured by Using Dual-Bolus First-Pass MR Imaging. *Radiology*. **232** (3), pp. 677–684
- Christian, T.F. et al. (1992). Noninvasive identification of severe coronary artery disease using exercise tomographic thallium-201 imaging. *American journal of Cardiology*. **70** (1), pp. 14–20
- Chung, S.-Y. et al. (2010). Comparison of stress perfusion MRI and SPECT for detection of myocardial ischemia in patients with angiographically proven three-vessel coronary artery disease. *AJR. American journal of roentgenology*. **195** (2), pp. 356–362
- Costa, M.A. et al. (2007). Quantitative magnetic resonance perfusion imaging detects anatomic and physiologic coronary artery disease as measured by coronary angiography and fractional flow reserve. *Journal of the American College of Cardiology*. **50** (6), pp. 514–522
- Davies, J.E. et al. (2006). Evidence of a dominant backward-propagating “suction” wave responsible for diastolic coronary filling in humans, attenuated in left ventricular hypertrophy. *Circulation*. **113** (14), pp. 1768–1778
- DeLong, E.R. et al. (1988). Comparing the areas under two or more correlated receiver operating characteristic curves: a nonparametric approach. *Biometrics*. **44** (3), pp. 837–845
- DePasquale, E.E. et al. (1988). Quantitative rotational thallium-201 tomography for identifying and localizing coronary artery disease. *Circulation*. **77** (2), pp. 316–327
- Diamond, G.A. and Forrester, J.S. (1979). Analysis of probability as an aid in the clinical diagnosis of coronary-artery disease. *New England Journal of Medicine*. **300** (24), pp. 1350–1358

- Ebersberger, U. et al. (2013). Magnetic Resonance Myocardial Perfusion Imaging at 3.0 Tesla for the Identification of Myocardial Ischemia : Comparison with Coronary Catheter Angiography and Fractional Flow Reserve Measurements. *European heart journal cardiovascular Imaging*. **14** (12), pp. 1174–1180
- Eckstein, R.W. et al. (1963). Phasic and mean blood flow in the canine septal artery and an estimate of systolic resistance in deep myocardial vessels. *Circulation Research*. **12** (2), pp. 203–211
- Elkington, A.G. et al. (2004). Combined long-and short-axis myocardial perfusion cardiovascular magnetic resonance. *Journal of Cardiovascular Magnetic Resonance*. **6** (4), pp. 811–816
- Emond, M. et al. (1994). Long-term survival of medically treated patients in the Coronary Artery Surgery Study (CASS) Registry. *Circulation*. **90** (6), pp. 2645–2657
- Eng, J. (2003). Sample Size Estimation: How Many Individuals Should Be Studied? *Radiology*. **227** (2), pp. 309–313
- Fihn, S.D. et al. (2012). 2012 ACCF/AHA/ACP/AATS/PCNA/SCAI/STS guideline for the diagnosis and management of patients with stable ischemic heart disease: a report of the American College of Cardiology Foundation/American Heart Association task force on practice guidelines, and the. *Circulation*. **126** (25), pp. e354–471
- Frank, O. (1990). The basic shape of the arterial pulse. First treatise: Mathematical analysis. *Journal of Molecular and Cellular Cardiology*. **22** (3), pp. 255–277
- Futamatsu, H. et al. (2007). Evaluation of cardiac magnetic resonance imaging parameters to detect anatomically and hemodynamically significant coronary artery disease. *American heart journal*. **154** (2), pp. 298–305
- Gargiulo, P. et al. (2013). The Prognostic Value of Normal Stress Cardiac Magnetic Resonance in Patients With Known or Suspected Coronary Artery Disease: A Meta-analysis. *Circulation: Cardiovascular Imaging*. **6** (4), pp. 574–582
- Ge, L. et al. (2009). Myocardial perfusion MRI with sliding-window conjugate-gradient HYPR. *Magnetic Resonance in Medicine*. **62** (4), pp. 835–839

- Gebker, R. et al. (2007a). How we perform myocardial perfusion with cardiovascular magnetic resonance. *Journal of cardiovascular magnetic resonance*. **9** (3), pp. 539–547
- Gebker, R. et al. (2007b). MR Myocardial Perfusion Imaging with k-Space and Time Broad-Use Linear Acquisition Speed-up Technique: Feasibility Study<sup>1</sup>. *Radiology*. **245** (3), pp. 863–871
- Gerber, B.L. (2008). MR perfusion imaging. What will be its impact for detection of coronary disease in the future? *European heart journal*. **29** (4), pp. 434–435
- Gharib, A.M. et al. (2007). Coronary MR angiography at 3T during diastole and systole. *Journal of Magnetic Resonance Imaging*. **26** (4), pp. 921–926
- Goto, M. et al. (1991). Cardiac contraction affects deep myocardial vessels predominantly. *The American journal of physiology*. **261** (5 Pt 2), pp. H1417–29
- Greenwood, J.P. et al. (2012). Cardiovascular magnetic resonance and single-photon emission computed tomography for diagnosis of coronary heart disease (CE-MARC): a prospective trial. *The Lancet*. **379** (9814), pp. 453–460
- Griswold, M.A. et al. (2002). Generalized autocalibrating partially parallel acquisitions (GRAPPA). *Magnetic Resonance in Medicine*. **47** (6), pp. 1202–1210
- Groothuis, J.G.J. et al. (2010). Comparison of dual to single contrast bolus magnetic resonance myocardial perfusion imaging for detection of significant coronary artery disease. *Journal of Magnetic Resonance Imaging*. **32** (1), pp. 88–93
- Gutberlet, M. et al. (2006). Comprehensive cardiac magnetic resonance imaging at 3.0 Tesla: feasibility and implications for clinical applications. *Investigative radiology*. **41** (2), pp. 154–167
- Hachamovitch, R. et al. (2003a). Comparison of the short-term survival benefit associated with revascularization compared with medical therapy in patients with no prior coronary artery disease undergoing stress myocardial perfusion single photon emission computed tomography. *Circulation*. **107** (23), pp. 2900–2907

- Hachamovitch, R. et al. (2003b). Determinants of risk and its temporal variation in patients with normal stress myocardial perfusion scans\* 1:: What is the warranty period of a normal scan? *Journal of the American College of Cardiology*. **41** (8), pp. 1329–1340
- Hachamovitch, R. et al. (1998). Incremental prognostic value of myocardial perfusion single photon emission computed tomography for the prediction of cardiac death: differential stratification for risk of cardiac death and myocardial infarction. *Circulation*. **97** (6), pp. 535–543
- Hamon, M. et al. (2010). Meta-analysis of the diagnostic performance of stress perfusion cardiovascular magnetic resonance for detection of coronary artery disease. *Journal of cardiovascular magnetic resonance*. **12** (1), p. 29
- Hanley, J.A. and McNeil, B.J. (1983). A method of comparing the areas under receiver operating characteristic curves derived from the same cases. *Radiology*. **148** (3), pp. 839–843
- Hautvast, G.L.T.F. et al. (2011). Quantitative analysis of transmural gradients in myocardial perfusion magnetic resonance images. *Magnetic resonance in medicine*. **1487**, pp. 1477–1487
- Heller, L.I. et al. (1994). Blood flow velocity in the right coronary artery: assessment before and after angioplasty. *Journal of the American College of Cardiology*. **24** (4), pp. 1012–1017
- Hiramatsu, O. et al. (1998). In vivo observations of the intramural arterioles and venules in beating canine hearts. *The Journal of Physiology*. **509** (2), pp. 619–628
- Hsu, L.-Y. et al. (2012). A Quantitative Pixel-Wise Measurement of Myocardial Blood Flow by Contrast-Enhanced First-Pass CMR Perfusion Imaging: Microsphere Validation in Dogs and Feasibility Study in Humans. *JACC: Cardiovascular Imaging*. **5** (2), pp. 154–166
- Huber, A. et al. (2012). Magnetic resonance perfusion of the myocardium: semiquantitative and quantitative evaluation in comparison with coronary angiography and fractional flow reserve. *Investigative radiology*. **47** (6), pp. 332–338

- Iltis, I. et al. (2005). In vivo assessment of myocardial blood flow in rat heart using magnetic resonance imaging: Effect of anesthesia. *Journal of Magnetic Resonance Imaging*. **22** (2), pp. 242–247
- Ishida, N. et al. (2003). Noninfarcted Myocardium: Correlation between Dynamic First-Pass Contrast-enhanced Myocardial MR Imaging and Quantitative Coronary Angiography. *Radiology*. **229** (1), pp. 209–216
- Iskandrian, A.S. et al. (1993). Independent and incremental prognostic value of exercise single-photon emission computed tomographic (SPECT) thallium imaging in coronary artery disease. *Journal of the American College of Cardiology*. **22** (3), pp. 665–670
- Jaarsma, C. et al. (2012). Diagnostic Performance of Noninvasive Myocardial Perfusion Imaging Using Single-Photon Emission Computed Tomography, Cardiac Magnetic Resonance, and Positron Emission Tomography Imaging for the Detection of Obstructive Coronary Artery Disease: A Meta-Anal. *Journal of the American College of Cardiology*. **59** (19), pp. 1719–1728
- Jahnke, C. et al. (2007). Prognostic value of cardiac magnetic resonance stress tests: adenosine stress perfusion and dobutamine stress wall motion imaging. *Circulation*. **115** (13), pp. 1769–1776
- Jerosch-Herold, M. et al. (1998). Magnetic resonance quantification of the myocardial perfusion reserve with a Fermi function model for constrained deconvolution. *Medical Physics*. **25**, pp. 73–84
- Jerosch-Herold, M. et al. (2002). Myocardial blood flow quantification with MRI by model-independent deconvolution. *Medical Physics*. **29** (5), pp. 886–897
- Jerosch-Herold, M. (2010). Quantification of myocardial perfusion by cardiovascular magnetic resonance. *Journal of cardiovascular magnetic resonance : official journal of the Society for Cardiovascular Magnetic Resonance*. **12**, p. 57
- Jogiya, R. et al. (2014). Ischemic Burden by Three-dimensional Myocardial Perfusion Cardiovascular Magnetic Resonance: Comparison with Myocardial Perfusion Scintigraphy. *Circulation: Cardiovascular Imaging*. p. CIRCIMAGING–113

- Jogiya, R. et al. (2012). Validation of Dynamic 3-Dimensional Whole Heart Magnetic Resonance Myocardial Perfusion Imaging Against Fractional Flow Reserve for the Detection of Significant Coronary Artery Disease. *Journal of the American College of Cardiology*. **68** (8), pp. 756–765
- Kajander, S.A. et al. (2011). Clinical Value of Absolute Quantification of Myocardial Perfusion With 15O-Water in Coronary Artery Disease Clinical Perspective. *Circulation: Cardiovascular Imaging*. **4** (6), pp. 678–684
- Kajiya, F. et al. (1985). Evaluation of local blood flow velocity in proximal and distal coronary arteries by laser Doppler method. *Journal of biomechanical engineering*. **107**, pp. 10–15
- Kassab, G.S. et al. (1993). Morphometry of pig coronary arterial trees. *American Journal of Physiology-Heart and Circulatory Physiology*. **265** (1), pp. H350–H365
- Keijer, J.T. et al. (2000a). Magnetic resonance imaging of myocardial perfusion in single-vessel coronary artery disease: implications for transmural assessment of myocardial perfusion. *Journal of cardiovascular magnetic resonance*. **2** (3), pp. 189–200
- Keijer, J.T. et al. (2000b). Magnetic resonance imaging of regional myocardial perfusion in patients with single-vessel coronary artery disease: quantitative comparison with (201)Thallium-SPECT and coronary angiography. *Journal of magnetic resonance imaging*. **11** (6), pp. 607–15
- Kellman, P. et al. (2001). Adaptive sensitivity encoding incorporating temporal filtering (TSENSE). *Magnetic Resonance in medicine*. **45** (5), pp. 846–852
- Kellman, P. and Arai, A.E. (2007). Imaging sequences for first pass perfusion --a review. *Journal of cardiovascular magnetic resonance*. **9** (3), pp. 525–537
- Kidambi, A. et al. (2013). Relationship between Myocardial Edema and Regional Myocardial Function after Reperfused Acute Myocardial Infarction: An MR Imaging Study. *Radiology*. **267** (3), pp. 701–708

- Kim, R.J.J. et al. (2000). The use of contrast-enhanced magnetic resonance imaging to identify reversible myocardial dysfunction. *New England Journal of Medicine*. **343** (20), pp. 1445–1453
- Klem, I. et al. (2006). Improved detection of coronary artery disease by stress perfusion cardiovascular magnetic resonance with the use of delayed enhancement infarction imaging. *Journal of the American College of Cardiology*. **47** (8), pp. 1630–1638
- Klocke, F.J. et al. (2003). ACC/AHA/ASNC guidelines for the clinical use of cardiac radionuclide imaging--executive summary: a report of the American College of Cardiology/American Heart Association Task Force on Practice Guidelines (ACC/AHA/ASNC Committee to Revise the 1995 Guideli. *Journal of the American College of Cardiology*. **42** (7), pp. 1318–1333
- Knuuti, J. et al. (2009). Quantification of myocardial blood flow will reform the detection of CAD. *Journal of nuclear cardiology*. **16** (4), pp. 497–506
- Kozerke, S. and Plein, S. (2008). Accelerated CMR using zonal, parallel and prior knowledge driven imaging methods. *Journal of Cardiovascular Magnetic Resonance*. **18**, pp. 1–18
- Kramer, C.M. et al. (2013). Standardized cardiovascular magnetic resonance (CMR) protocols 2013 update. *Journal of Cardiovascular Magnetic Resonance*. **15** (1), p. 91
- Kramer, C.M. et al. (2008). *Standardized cardiovascular magnetic resonance imaging ( CMR ) protocols, society for cardiovascular magnetic resonance: board of trustees task force on standardized protocols*. **10**, pp. 1–10
- Larghat, A.M. et al. (2013). Reproducibility of first-pass cardiovascular magnetic resonance myocardial perfusion. *Journal of magnetic resonance imaging*. **874**, pp. 865–874
- Leongpoi, H. et al. (2001). Quantification of myocardial perfusion and determination of coronary stenosis severity during hyperemia using real-time myocardial contrast echocardiography. *Journal of the American Society of Echocardiography*. **14** (12), pp. 1173–1182

- Lipinski, M.J. et al. (2013). Prognostic Value of Stress Cardiac Magnetic Resonance Imaging in Patients with Known or Suspected Coronary Artery Disease: A Systematic Review and Meta-Analysis. *Journal of the American College of Cardiology*. **62** (9), pp. 826–838
- Lockie, T. et al. (2011). High-resolution magnetic resonance myocardial perfusion imaging at 3.0-Tesla to detect hemodynamically significant coronary stenoses as determined by fractional flow reserve. *Journal of the American College of Cardiology*. **57** (1), pp. 70–75
- Ma, H. et al. (2012). Myocardial perfusion magnetic resonance imaging using sliding-window conjugate-gradient highly constrained back-projection reconstruction for detection of coronary artery disease. *The American journal of cardiology*. **109** (8), pp. 1137–1141
- Mahmariyan, J.J. et al. (1990). Quantitative exercise thallium-201 single photon emission computed tomography for the enhanced diagnosis of ischemic heart disease. *Journal of the American College of Cardiology*. **15** (2), pp. 318–329
- Manka, R. et al. (2010). Clinical feasibility of accelerated, high spatial resolution myocardial perfusion imaging. *JACC. Cardiovascular imaging*. **3** (7), pp. 710–717
- Manka, R. et al. (2011). Dynamic 3-dimensional stress cardiac magnetic resonance perfusion imaging: detection of coronary artery disease and volumetry of myocardial hypoenhancement before and after coronary stenting. *Journal of the American College of Cardiology*. **57** (4), pp. 437–444
- Manka, R. et al. (2012). Whole-heart dynamic three-dimensional magnetic resonance perfusion imaging for the detection of coronary artery disease defined by fractional flow reserve: determination of volumetric myocardial ischaemic burden and coronary lesion location. *European heart journal*. **33** (16), pp. 2016–2024
- Mansfield, P. (1984). Real-time echo-planar imaging by NMR. *British medical bulletin*. **40** (2), pp. 187–190
- Maredia, N. et al. (2010). Effect of improving spatial or temporal resolution on image quality and quantitative perfusion assessment with k-t SENSE acceleration in first-

pass CMR myocardial perfusion imaging. *Magnetic resonance in medicine*. **64** (6), pp. 1616–1624

Marie, P.Y. et al. (1993). Usefulness of exercise SPECT-thallium to detect asymptomatic restenosis in patients who had angina before coronary angioplasty. *American heart journal*. **126** (3 Pt 1), pp. 571–577

Martin Bland, J. and Altman, D.G. (1986). Statistical methods for assessing agreement between two methods of clinical measurement. *The Lancet*. **327** (8476), pp. 307–310

Martin, W. et al. (1992). Balanced triple-vessel disease: enhanced detection by estimated myocardial thallium uptake. *Nuclear medicine communications*. **13** (3), pp. 149–153

Matsumoto, T. and Kajiya, F. (2005). Coronary microcirculation: Physiology and mechanics. *Fluid Dynamics Research*. **37** (1-2), pp. 60–81

Meyer, C.H. et al. (1992). Fast spiral coronary artery imaging. *Magnetic Resonance in Medicine*. **28** (2), pp. 202–213

Mistretta, C.A. et al. (2006). Highly constrained backprojection for time-resolved MRI. *Magnetic resonance in medicine*. **55** (1), pp. 30–40

Montalescot, G. et al. (2013). 2013 ESC guidelines on the management of stable coronary artery disease: the Task Force on the management of stable coronary artery disease of the European Society of Cardiology. *European heart journal*. **34** (38), pp. 2949–3003

Morton, G. et al. (2012). Quantification of absolute myocardial perfusion in patients with coronary artery disease: comparison between cardiovascular magnetic resonance and positron emission tomography. *Journal of the American College of Cardiology*. **60** (16), pp. 1546–1555

Motwani, M. et al. (2011). Accelerated, high spatial resolution cardiovascular magnetic resonance myocardial perfusion imaging. *Journal of nuclear cardiology*. **18** (5), pp. 952–958

- Motwani, M. et al. (2013). Advanced cardiovascular magnetic resonance myocardial perfusion imaging: high-spatial resolution versus 3-dimensional whole-heart coverage. *Circulation. Cardiovascular imaging*. **6** (2), pp. 339–348
- Motwani, M. et al. (2014a). Assessment of ischaemic burden in angiographic three-vessel coronary artery disease with high-resolution myocardial perfusion cardiovascular magnetic resonance imaging. *European Heart Journal Cardiovascular Imaging*. **15** (6), pp. 701–708
- Motwani, M. et al. (2012a). High-resolution versus standard-resolution cardiovascular MR myocardial perfusion imaging for the detection of coronary artery disease. *Circulation. Cardiovascular imaging*. **5** (3), pp. 306–313
- Motwani, M. et al. (2014b). Quantitative three-dimensional cardiovascular magnetic resonance myocardial perfusion imaging in systole and diastole. *Journal of Cardiovascular Magnetic Resonance*. **16** (1), p. 19
- Motwani, M. et al. (2012b). Systolic Versus Diastolic Acquisition in Myocardial Perfusion MR Imaging. *Radiology*. **262** (3), pp. 816–823
- Muzik PhD, O. and Duvernoy, M.D. (1998). Assessment of diagnostic performance of quantitative flow measurements in normal subjects and patients with angiographically documented coronary artery disease by means of nitrogen-13 ammonia and positron emission tomography. *Journal of the American College of Cardiology*. **31** (3), pp. 534–540
- Nagel, E. and Shaw, L.J. (2014). The assessment of ischaemic burden: thoughts on definition and quantification. *European heart journal cardiovascular Imaging*. **15** (6), pp. 610–611
- Nchimi, A. et al. (2014). Influence of the cardiac cycle on time–intensity curves using multislice dynamic magnetic resonance perfusion. *The international journal of cardiovascular imaging*. pp. 1–9

- Panting, J.R. et al. (2002). Abnormal subendocardial perfusion in cardiac syndrome X detected by cardiovascular magnetic resonance imaging. *New England Journal of Medicine*. **346** (25), pp. 1948–1953
- Parkash, R. et al. (2004). Potential utility of rubidium 82 PET quantification in patients with 3-vessel coronary artery disease. *Journal of nuclear cardiology*. **11** (4), pp. 440–449
- Patel, A.R. et al. (2010). Assessment of Advanced Coronary Artery Disease Advantages of Quantitative Cardiac Magnetic Resonance Perfusion Analysis. *Journal of the American College of Cardiology*. **56** (7), pp. 561–569
- Pedersen, H. et al. (2009). k t PCA: Temporally constrained k t BLAST reconstruction using principal component analysis. *Magnetic Resonance in Medicine*. **62** (3), pp. 706–716
- Pedersen, H. and Kelle, S. (2008). Quantification of myocardial perfusion using free-breathing MRI and prospective slice tracking. *Magnetic Resonance in Medicine*. **61** (3), pp. 734–8
- Plein, S. et al. (2004). Assessment of non-ST-segment elevation acute coronary syndromes with cardiac magnetic resonance imaging. *Journal of the American College of Cardiology*. **44** (11), pp. 2173–2181
- Plein, S. et al. (2007). Dynamic contrast-enhanced myocardial perfusion MRI accelerated with k-t sense. *Magnetic resonance in medicine*. **58** (4), pp. 777–785
- Plein, S. et al. (2008a). High spatial resolution myocardial perfusion cardiac magnetic resonance for the detection of coronary artery disease. *European heart journal*. **29** (17), pp. 2148–2155
- Plein, S. et al. (2008b). k-Space and Time Sensitivity Encoding–accelerated Myocardial Perfusion MR Imaging at 3.0 T: Comparison with 1.5 T1. *Radiology*. **249** (2), pp. 493–500
- Pruessmann, K.P. et al. (2001). Sensitivity encoded cardiac MRI. *Journal of Cardiovascular Magnetic Resonance*. **3** (1), pp. 1–9

- Radjenovic, A. et al. (2010). Estimates of systolic and diastolic myocardial blood flow by dynamic contrast-enhanced MRI. *Magnetic resonance in medicine*. **1703**, pp. 1696–1703
- Rakowski, H. and Carasso, S. (2007). Quantifying diastolic function in hypertrophic cardiomyopathy: the ongoing search for the holy grail. *Circulation*. [Online]. **116** (23), pp. 2662–2665 Available from: <http://www.ncbi.nlm.nih.gov/pubmed/18056537>. [Accessed: 6 October 2012].
- Rentrop, P.K. et al. (1985). Changes in collateral channel filling immediately after controlled coronary artery occlusion by an angioplasty balloon in human subjects. *Journal of the American College of Cardiology*. **5** (3), pp. 587–592
- Rieber, J. et al. (2006). Cardiac magnetic resonance perfusion imaging for the functional assessment of coronary artery disease: a comparison with coronary angiography and fractional flow reserve. *European heart journal*. **27** (12), pp. 1465–1471
- Sabsiton Jr, D.C. and Gregg, D.E. (1957). Effect of cardiac contraction on coronary blood flow. *Circulation*. **15** (1), pp. 14–20
- Sakuma, H. et al. (2005). Diagnostic accuracy of stress first-pass contrast-enhanced myocardial perfusion MRI compared with stress myocardial perfusion scintigraphy. *American Journal of Roentgenology*. **185** (1), pp. 95–102
- Salerno, M. et al. (2011). Optimization of spiral-based pulse sequences for first-pass myocardial perfusion imaging. *Magnetic Resonance in Medicine*. **65** (6), pp. 1602–1610
- Salerno, M. and Kramer, C.M. (2013). Advances in parametric mapping with CMR imaging. *JACC. Cardiovascular imaging*. **6** (7), pp. 806–22
- Schaefer, D.J. (1998). Safety aspects of radiofrequency power deposition in magnetic resonance. *Magnetic resonance imaging clinics of North America*. **6** (4), pp. 775–789
- Schulz-Menger, J. et al. (2013). Standardized image interpretation and post processing in cardiovascular magnetic resonance: Society for Cardiovascular Magnetic Resonance

(SCMR) Board of Trustees Task Force on Standardized Post Processing. *Journal of Cardiovascular Magnetic Resonance*. **15** (1), p. 35

Schwitzer, J. et al. (2001). Assessment of myocardial perfusion in coronary artery disease by magnetic resonance: a comparison with positron emission tomography and coronary angiography. *Circulation*. **103** (18), pp. 2230–2235

Schwitzer, J. et al. (2013). MR-IMPACT II: Magnetic Resonance Imaging for Myocardial Perfusion Assessment in Coronary artery disease Trial: perfusion-cardiac magnetic resonance vs. single-photon emission computed tomography for the detection of coronary artery disease: a comparative. *European heart journal*. **34** (10), pp. 775–781

Schwitzer, J. et al. (2008). MR-IMPACT: comparison of perfusion-cardiac magnetic resonance with single-photon emission computed tomography for the detection of coronary artery disease in a multicentre, multivendor, randomized trial. *European heart journal*. **29** (4), pp. 480–489

Schwitzer, J. et al. (2012). Superior diagnostic performance of perfusion-cardiovascular magnetic resonance versus SPECT to detect coronary artery disease: The secondary endpoints of the multicenter multivendor MR-IMPACT II (Magnetic Resonance Imaging for Myocardial Perfusion Assessm. *Journal of cardiovascular magnetic resonance*. **14** (1), p. 61

Sdringola, S. et al. (2011). Impact of Unexpected Factors on Quantitative Myocardial Perfusion and Coronary Flow Reserve in Young, Asymptomatic Volunteers. *JACC: Cardiovascular Imaging*. **4** (4), pp. 402–412

Segal, J. et al. (1992). Alterations of phasic coronary artery flow velocity humans during percutaneous coronary angioplasty. *Journal of the American College of Cardiology*. **20** (2), pp. 276–286

Shaw, L.J. et al. (2008). Optimal medical therapy with or without percutaneous coronary intervention to reduce ischemic burden results from the Clinical Outcomes Utilizing Revascularization and Aggressive Drug Evaluation (COURAGE) trial nuclear substudy. *Circulation*. **117** (10), pp. 1283–1291

- Shin, T. et al. (2010). Systolic 3D first-pass myocardial perfusion MRI: Comparison with diastolic imaging in healthy subjects. *Magnetic resonance in medicine*. **63** (4), pp. 858–864
- Shin, T. et al. (2008). Three dimensional first-pass myocardial perfusion imaging at 3T: feasibility study. *Journal of cardiovascular magnetic resonance*. **10** (1), p. 57
- Shin, T. et al. (2013). Three-dimensional first-pass myocardial perfusion MRI using a stack-of-spirals acquisition. *Magnetic Resonance in Medicine*. **69**, pp. 839–844
- Slavin, G. et al. (2001). First-Pass Myocardial Perfusion MR Imaging with Interleaved Notched Saturation: Feasibility Study. *Radiology*. **219** (1), pp. 258–263
- Sourbron, S. (2010). Technical aspects of MR perfusion. *European journal of radiology*. **76** (3), pp. 304–313
- Spaan, J.A. et al. (1981). Diastolic-systolic coronary flow differences are caused by intramyocardial pump action in the anesthetized dog. *Circulation Research*. **49** (3), pp. 584–593
- Stanton, T. and Marwick, T.H. (2010). Assessment of subendocardial structure and function. *JACC. Cardiovascular imaging*. **3** (8), pp. 867–875
- Tonino, P.A.L. et al. (2010). Angiographic Versus Functional Severity of Coronary Artery Stenoses in the FAME Study Fractional Flow Reserve Versus Angiography in Multivessel Evaluation. *Journal of the American College of Cardiology*. **55** (25), pp. 2816–2821
- Troalen, T. et al. (2014). In vivo characterization of rodent cyclic myocardial perfusion variation at rest and during adenosine-induced stress using cine-ASL cardiovascular magnetic resonance. *Journal of cardiovascular magnetic resonance*. **16** (1), p. 18
- Tsao, J. et al. (2003). k-t BLAST and k-t SENSE: dynamic MRI with high frame rate exploiting spatiotemporal correlations. *Magnetic resonance in medicine*. **50** (5), pp. 1031–1042
- Tsao, J. and Kozerke, S. (2012). MRI temporal acceleration techniques. *Journal of Magnetic Resonance Imaging*. **36** (3), pp. 543–560

- Uren, N.G. et al. (1994). Relation between myocardial blood flow and the severity of coronary-artery stenosis. *New England Journal of Medicine*. **330** (25), pp. 1782–1788
- Utz, W. et al. (2008). Single- or dual-bolus approach for the assessment of myocardial perfusion reserve in quantitative MR perfusion imaging. *Magnetic resonance in medicine*. **59** (6), pp. 1373–1377
- Vitanis, V. et al. (2011). High resolution three-dimensional cardiac perfusion imaging using compartment-based k-t principal component analysis. *Magnetic resonance in medicine*. **65** (2), pp. 575–587
- Walker, S. et al. (2013). Cost-effectiveness of cardiovascular magnetic resonance in the diagnosis of coronary heart disease: an economic evaluation using data from the CE-MARC study. *Heart*. **99** (12), pp. 873–881
- Wang, L. et al. (2006). Coronary Risk Factors and Myocardial Perfusion in Asymptomatic Adults:: The Multi-Ethnic Study of Atherosclerosis (MESA). *Journal of the American College of Cardiology*. **47** (3), pp. 565–572
- Watkins, S. et al. (2009). Validation of magnetic resonance myocardial perfusion imaging with fractional flow reserve for the detection of significant coronary heart disease. *Circulation*. **120** (22), pp. 2207–2213
- Wijns, W. et al. (2010). Guidelines on myocardial revascularization: The Task Force on Myocardial Revascularization of the European Society of Cardiology (ESC) and the European Association for Cardio-Thoracic Surgery (EACTS). *European Heart Journal*. **31** (20), pp. 2501–2555
- Wilke, N. et al. (1997). Myocardial perfusion reserve: assessment with multisection, quantitative, first-pass MR imaging. *Radiology*. **204** (2), pp. 373–384
- Willinek, W.A. et al. (2010). Dual-source parallel radiofrequency excitation body MR imaging compared with standard MR imaging at 3.0 T: initial clinical experience 1. *Radiology*. **256** (3), pp. 966–975
- Wolff, S.D. et al. (2004). Myocardial first-pass perfusion magnetic resonance imaging: a multicenter dose-ranging study. *Circulation*. **110** (6), pp. 732–737

Yada, T. et al. (1993). In vivo observation of subendocardial microvessels of the beating porcine heart using a needle-probe videomicroscope with a CCD camera. *Circulation research*. **72** (5), pp. 939–946

Zun, Z. et al. (2009). Assessment of myocardial blood flow (MBF) in humans using arterial spin labeling (ASL): feasibility and noise analysis. *Magnetic Resonance in Medicine*. **62** (4), pp. 975–983

## 10 Appendix

### 10.1 Ethics Approval Form: Study 1 and 2

REC / 8

**NHS**

Research Ethics Administration Office  
50 Lancaster Park Road  
Harrogate  
HG2 7Sx

28 July 2006

Professor Stephen G. Ball  
Professor of Cardiology  
Academic Unit of Cardiovascular Medicine  
Level G, Jubilee Wing  
Yorkshire Heart Centre  
The General Infirmary,  
Leeds  
LS1 3EX

Telephone: (01423) 554450  
Facsimile: (01423) 553392  
e-mail: [Christine.Garrett@hdf.nhs.uk](mailto:Christine.Garrett@hdf.nhs.uk)

Dear Professor Ball

Full title of study: Assessment of myocardial perfusion by Magnetic Resonance Imaging: Evaluation of accelerated acquisition techniques  
REC reference number: 061Q1107145

The REC gave a favourable ethical opinion to this study on 18 July 2006.

Further notification has been received from local site assessor following site-specific assessment. On behalf of the Committee, I am pleased to confirm the extension of the favourable opinion to the site. I attach an updated version of the site approval form, listing all sites with a favourable ethical opinion to conduct the research.

Research governance approval

The research should not commence at any NHS site until research governance approval from the relevant NHS care organisation has been confirmed.

Statement of compliance

The Committee is constituted in accordance with the Governance Arrangements for Research Ethics Committees (July 2001) and complies fully with the Standard Operating Procedures for Research Ethics Committees in the UK.

061Q1107/45 Please quote this number on all correspondence.

Yours sincerely

 G w-0e

Mrs Christine Garrett  
Committee Co-ordinator

Enclosure: Site approval form

Copy to: Dr Jonathan Gower, Department of Research and Development  
University of Leeds.

HARROGATE LOCAL RESEARCH ETHICS COMMITTEE  
An advisory committee to North and East Yorkshire and Northern Lincolnshire Strategic Health Authority

**Harrogate Local Research Ethics Committee**  
LIST OF SITES WITH A FAVOURABLE ETHICAL OPINION

*For all studies requiring site-specific assessment, this form is issued by the main REC to the Chief Investigator and sponsor with the favourable opinion letter and following subsequent notifications from site assessors. For issue 2 onwards, all sites with a favourable opinion are listed, adding the new sites approved.*

REC reference number: 06/Q1 107/45 Issue number: Date of issue: 28 July 2006

Chief Investigator: Professor Stephen G. Ball

Full title of study: Assessment of myocardial perfusion by Magnetic Resonance Imaging: Evaluation of accelerated acquisition techniques

*This study was given a favourable ethical opinion by Harrogate Local Research Ethics Committee on 18 July 2006. The favourable opinion is extended to each of the sites listed below. The research may commence at each NHS site when management approval from the relevant NHS care organisation has been confirmed.*

Principal Investigator	Post	Research site	Site assessor	Date of favourable opinion for this site	Notes
Professor Stephen Ball	Professor of Cardiology	Leeds Teaching Hosp Leeds NHS Trust	Leeds (West) Research Ethics Committee	28/07/2006	

Approved by the Chair on behalf of the REC:

 (Signature of CWR/Administrator)  
(delete as applicable)  
Name

<sup>(1)</sup> The notes column may be used by the main REC to record the early closure or withdrawal of a site (where notified by the Chief Investigator or sponsor), the suspension of termination of the favourable opinion for an individual site, or any other relevant development. The date should be recorded.

## 10.2 Ethics Approval Form: Study 3



### **National Research Ethics Service**

**Leeds (West) Research Ethics Committee**

First Floor  
Millside  
Mill Pond Lane  
Leeds  
LS6 4RA

Telephone: 0113 3050122  
Facsimile:

05 October 2010

Dr Sven Plein  
Consultant Cardiologist, Wellcome Intermediate Clinical Fellow  
University of Leeds  
Academic Unit of Cardiovascular Medicine  
G floor, Jubilee Wing  
Leeds General Infirmary  
LS1 3EX

Dear Dr Plein

**Study Title:** Assessment of myocardial perfusion by Magnetic Resonance Imaging: 3T Optimization of acquisition and analysis methods in patients with heart disease.  
**REC reference number:** 10/H1307/103

Thank you for your letter of 29 September 2010, responding to the Committee's request for further information on the above research and submitting revised documentation.

The further information was considered in correspondence by a sub-committee of the REC. A list of the sub-committee members is attached.

#### **Confirmation of ethical opinion**

On behalf of the Committee, I am pleased to confirm a favourable ethical opinion for the above research on the basis described in the application form, protocol and supporting documentation as revised, subject to the conditions specified below.

#### **Ethical review of research sites**

The favourable opinion applies to all NHS sites taking part in the study, subject to management permission being obtained from the NHS/HSC R&D office prior to the start of the study (see "Conditions of the favourable opinion" below).

The Committee has not yet been notified of the outcome of any site-specific assessment (SSA) for the non-NHS research site(s) taking part in this study. The favourable opinion does not therefore apply to any non-NHS site at present. I will write to you again as soon as one Research Ethics Committee has notified the outcome of a SSA. In the meantime no study procedures should be initiated at non-NHS sites.

#### **Conditions of the favourable opinion**

The favourable opinion is subject to the following conditions being met prior to the start of the study.

This Research Ethics Committee is an advisory committee to Yorkshire and The Humber Strategic Health Authority  
*The National Research Ethics Service (NRES) represents the NRES Directorate within the National Patient Safety Agency and Research Ethics Committees in England*

Management permission or approval must be obtained from each host organisation prior to the start of the study at the site concerned.

For NHS research sites only, management permission for research ("R&D approval") should be obtained from the relevant care organisation(s) in accordance with NHS research governance arrangements. Guidance on applying for NHS permission for research is available in the Integrated Research Application System or at <http://www.rdforum.nhs.uk>.

*Where the only involvement of the NHS organisation is as a Participant Identification Centre (PIC), management permission for research is not required but the R&D office should be notified of the study and agree to the organisation's involvement. Guidance on procedures for PICs is available in IRAS. Further advice should be sought from the R&D office where necessary.*

*Sponsors are not required to notify the Committee of approvals from host organisations.*

**It is the responsibility of the sponsor to ensure that all the conditions are complied with before the start of the study or its initiation at a particular site (as applicable).**

#### **Approved documents**

The final list of documents reviewed and approved by the Committee is as follows:

<i>Document</i>	<i>Version</i>	<i>Date</i>
Investigator CV		15 July 2010
Protocol	1.1	01 September 2010
REC application		19 July 2010
Letter of invitation to participant		
Participant Information Sheet	1.1	01 September 2010
Response to Request for Further Information		29 September 2010
Participant Consent Form	1.1	01 September 2010
Evidence of insurance or indemnity		08 October 2009

#### **Statement of compliance**

The Committee is constituted in accordance with the Governance Arrangements for Research Ethics Committees (July 2001) and complies fully with the Standard Operating Procedures for Research Ethics Committees in the UK.

#### **After ethical review**

Now that you have completed the application process please visit the National Research Ethics Service website > After Review

You are invited to give your view of the service that you have received from the National Research Ethics Service and the application procedure. If you wish to make your views known please use the feedback form available on the website.

The attached document "*After ethical review – guidance for researchers*" gives detailed guidance on reporting requirements for studies with a favourable opinion, including:

- Notifying substantial amendments
- Adding new sites and investigators

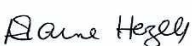
- Progress and safety reports
- Notifying the end of the study

The NRES website also provides guidance on these topics, which is updated in the light of changes in reporting requirements or procedures.

We would also like to inform you that we consult regularly with stakeholders to improve our service. If you would like to join our Reference Group please email [referencegroup@nres.npsa.nhs.uk](mailto:referencegroup@nres.npsa.nhs.uk).

**10/H1307/103** **Please quote this number on all correspondence**

Yours sincerely

  
**Dr Rhona Bratt**  
Chair

Email: [Elaine.hazell@leedsth.nhs.uk](mailto:Elaine.hazell@leedsth.nhs.uk)

*Enclosures: List of names and professions of members who were present at the meeting and those who submitted written comments*

*"After ethical review – guidance for researchers"*

*Copy to: Mrs Rachel E de Souza*

*R&D, Leeds Teaching Hospitals NHS Trust*

*Petra Bijsterveld*

## 10.3 Ethics Approval Form: Study 4 and 6

recb/g

**NHS**

Leeds (West) Research Ethics Committee  
6th Floor, Wellcome Wing  
Leeds General Infirmary  
Great George Street  
Leeds  
LS1 3EX

Telephone: 0113 392 6788  
Facsimile: 0113 392 2863

05 September 2005

Professor Stephen Ball  
Professor of Cardiology  
Leeds Teaching Hospitals NHS Trust  
Institute of Cardiovascular Research  
G Floor, Jubilee Building  
Leeds General Infirmary  
Leeds  
LS1 3EX

Dear Professor Ball

Full title of study: Assessment of myocardial perfusion by Magnetic Resonance Imaging: Optimisation of acquisition and analysis methods  
REC reference number: 05/Q1205/142

Thank you for your letter of 14 August 2005, responding to the Committee's request for further information on the above research and submitting revised documentation.

The further information has been considered on behalf of the Committee by the Chair.

Confirmation of ethical opinion

On behalf of the Committee, I am pleased to confirm a favourable ethical opinion for the above research on the basis described in the application form, protocol and supporting documentation as revised.

The favourable opinion applies to the research sites listed on the attached form.

Conditions of approval

The favourable opinion is given provided that you comply with the conditions set out in the attached document. You are advised to study the conditions carefully.

Approved documents

The final list of documents reviewed and approved by the Committee is as follows:

<u>Documents</u>	<u>Version</u>	<u>Date</u>
Application		13 June 2005
Investigator CV		(None Specified)
Protocol	1	(None Specified)
Copies of Advertisements	1	None Specified)
GP/Consultant Information Sheets	1.5	13 June 2005

An advisory committee to West Yorkshire Strategic Health Authority

<u>Participant</u> Information Sheet	2	None Specified
<u>Participant</u> Consent Form	2	(None Specified)
Response to Request for Further Information		14 August 2005

#### Management approval

The study should not commence at any NHS site until the local Principal Investigator has obtained final management approval from the R&D Department for the relevant NHS care organisation.

#### Notification of other bodies

The Committee Administrator will notify the research sponsor and the R&D Department for NHS care organisation(s) that the study has a favourable ethical opinion.

#### Statement of compliance

The Committee is constituted in accordance with the Governance Arrangements for Research Ethics Committees (July 2001) and complies fully with the Standard Operating Procedures for Research Ethics Committees in the UK.

05/Q1205/142                      Please quote this number on all correspondence

With the Committee's best wishes for the success of this project,

Yours sincerely



Lucy Enever  
Assistant Administrator  
On Behalf Of  
Dr John Puntis  
Chairman

[Email: Lucy.Enever@leedsth.nhs.uk](mailto:Lucy.Enever@leedsth.nhs.uk)

#### Enclosures:

Standard approval conditions  
Site approval form (SF1)

SF1 list of approved sites

Leeds (West) Research Ethics Committee  
**LIST OF SITES WITH A FAVOURABLE ETHICAL OPINION**

For all studies requiring site-specific assessment, this form is issued by the main REC to the Chief Investigator and sponsor with the favourable opinion letter and following subsequent notifications from site assessors. For Issue 2 onwards, all sites with a favourable opinion are listed, adding the new sites approved.

REC reference number: 05/Q1205/142      Issue number: 1      Date of issue: 05 September 2005

Chief Investigator: | Professor Stephen Ball

Full title of study: | Assessment of myocardial perfusion by Magnetic Resonance Imaging: Optimisation of acquisition and analysis methods

This study was given a favourable ethical opinion by Leeds (West) Research Ethics Committee on 01 September 2005. The favourable opinion is extended to each of the sites listed below. The research may commence at each NHS site when management approval from the relevant NHS care organisation has been confirmed.

Principal Investigator	Post	Research site	Site assessor	Date of favourable opinion for this site	Notes (*)
Professor Stephen Ball	Professor of Cardiology	LEEDS TEACHING HOSPITALS NHS TRUST	Leeds (West) Research Ethics Committee	05/09/2005	

Approved by the Chair on behalf of the REC:

..... (Signature) /Administrator  
 (delete as applicable)

## 10.4 Ethics Approval Form: Study 5

The Leeds Teaching Hospitals   
NHS Trust

Ref: Josephine Dominic

Research & Development

22/09/2011

Leeds Teaching Hospitals NHS Trust  
34 Hyde Terrace  
Leeds  
LS2 9LN

Dr Sven Plein

Consultant Cardiologist, British Heart Foundation Senior Clinical Research Fellow  
University of Leeds

Tel: 0113 392 2878

Fax: 0113 392 6397

Academic Unit of Cardiovascular Medicine

G floor, Jubilee Wing

Leeds General Infirmary

LS1 3EX

r@d@leedsth.nhs.uk  
www.leedsth.nhs.uk

Dear Dr Sven Plein

**Re: NHS Permission at LTHT for: Systolic Versus Diastolic Myocardial Perfusion Imaging: A Three-Dimensional Cardiovascular Magnetic Resonance Study.**  
LTHT R&D Number: CD11/9960  
REC: 11/YH/0309

I confirm that *NHS Permission for research* has been granted for this project at The Leeds Teaching Hospitals NHS Trust (LTHT). NHS Permission is granted based on the information provided in the documents listed below. All amendments (including changes to the research team) must be submitted in accordance with guidance in IRAS. Any change to the status of the project must be notified to the R&D Department.

Permission is granted on the understanding that the study is conducted in accordance with the *Research Governance Framework for Health and Social Care*, ICH GCP (if applicable) and NHS Trust policies and procedures available at [http://www.leedsth.nhs.uk/sites/research\\_and\\_development/](http://www.leedsth.nhs.uk/sites/research_and_development/).

This permission is granted only on the understanding that you comply with the requirements of the *Framework* as listed in the attached sheet "Conditions of Approval".

If you have any queries about this approval please do not hesitate to contact the R&D Department on telephone 0113 392 2878.

### Indemnity Arrangements

The Leeds Teaching Hospitals NHS Trust participates in the NHS risk pooling scheme administered by the NHS Litigation Authority 'Clinical Negligence Scheme for NHS Trusts' for: (i) medical professional and/or medical malpractice liability; and

Chairman Mike Collier CBE Chief Executive Maggie Boyle

The Leeds Teaching Hospitals incorporating:

Chapel Allerton Hospital Leeds Dental Institute Seacroft Hospital

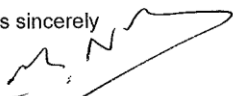
St James's University Hospital The General Infirmary at Leeds Wharfedale Hospital



(ii) general liability. NHS Indemnity for negligent harm is extended to researchers with an employment contract (substantive or honorary) with the Trust. The Trust only accepts liability for research activity that has been managerially approved by the R&D Department.

The Trust therefore accepts liability for the above research project and extends indemnity for negligent harm to cover you as investigator and the researchers listed on the Site Specific Information form. Should there be any changes to the research team please ensure that you inform the R&D Department and that s/he obtains an appropriate contract, or letter of access, with the Trust if required.

Yours sincerely



**Dr D R Norfolk**  
**Associate Director of R&D**

**Approved documents**

The documents reviewed and approved are listed as follows

<i>Document</i>	<i>Version</i>	<i>Date of document</i>
NHS R&D Form	3.1	21/07/11
SSI Form	3.1	12/07/11
Directorate Approval		08/08/11
Protocol	1.0	July 2011
REC Letter confirming favourable opinion		19/09/11
Patient information sheet (REC Approved)	1.1	July 2011
Consent form (REC Approved)	1.1	July 2011
Letter of invitation (REC Approved)	1.0	July 2011
GP letter (REC Approved)	1.0	July 2011